Characterising the small RNA-regulatory architecture of *Acinetobacter baumannii*

A thesis submitted to Trinity College Dublin, the

University of Dublin

in partial fulfilment of the requirements for the degree of

DOCTOR OF PHILOSOPHY

by

Fergal Hamrock

2025

Moyne Institute of Preventive Medicine
Department of Microbiology
Trinity College Dublin,
The University of Dublin

Declaration

I declare that this thesis has not been submitted as an exercise for a degree at this or any other university and it is entirely my own work.

I agree to deposit this thesis in the University's open access institutional repository or allow the Library to do so on my behalf, subject to Irish Copyright Legislation and Trinity College Library conditions of use and acknowledgement.

I consent to the examiner retaining a copy of the thesis beyond the examining period, should they so wish (EU GDPR May 2018).

Fergal Hamrock

Summary:

The Gram-negative bacterium *Acinetobacter baumannii* is a significant opportunistic pathogen in critically ill and hospitalised patients. It exhibits a remarkable ability to survive under harsh environmental conditions, resisting desiccation, oxidative stress, and exposure to disinfectants. Clinical isolates frequently form biofilms and employ micronutrient acquisition strategies, allowing colonisation of surfaces in clinical settings and facilitating propagation within hosts. Moreover, many *A. baumannii* strains are acquiring multidrug resistance (MDR), limiting the efficacy of antimicrobial treatments and underscoring the urgent need to understand the genetic regulators underpinning its environmental persistence and MDR mechanisms. While much attention has been given to transcriptional regulators, the role of bacterial small RNAs (sRNAs) in *A. baumannii* remains poorly characterised. sRNAs are known to regulate gene expression in other bacteria through direct, imperfect antisense base-pairing. This study sought to elucidate *A. baumannii* sRNA interactions by identifying their RNA partners using Hi-GRIL-seq, a high-throughput RNA proximity ligation and sequencing technique applied under several experimental conditions. We identified forty sRNAs forming sRNA-RNA chimeras, suggesting their involvement in gene regulation in *A. baumannii*. One sRNA, Aar, was found to regulate four mRNA targets, including the outer membrane protein CarO. Aar binds the translational initiation regions of these targets via a conserved seed region, as demonstrated through both in vitro and in vivo approaches. This binding inhibits translation without inducing mRNA degradation. Overexpression of Aar led to reduced CarO levels, highlighting its role in fine-tuning outer membrane protein expression. Another sRNA, Arp, was found to regulate the major type IV pilin subunit PilA, crucial for DNA uptake in *A. baumannii*. Arp sequesters the translational initiation region of *pilA* mRNA, preventing ribosome binding in a heterologous reporter system. While further work is needed to fully understand Arp's function, it may shed light on the mechanisms controlling horizontal gene transfer in this pathogen. This study provides the first mechanistic insights into post-transcriptional regulation in *A. baumannii* and serves as a valuable resource for future RNA-centred investigations in this organism.

Acknowledgments:

Completing this PhD thesis has been a long and exciting – if sometimes challenging – journey. This PhD really granted me the opportunity to hone my skills and further expand my interest in molecular microbiology, an area that I will likely always be passionate about. It really was an unforgettable way to challenge myself academically, and it would have been impossible if not for the support, guidance and encouragement of so many people in my life. I would like to express my gratitude to those people who made it possible here.

First and foremost, I would like to express my deepest gratitude to my advisor, Dr Carsten Kröger. When I first contacted you five years ago to inquire about a masters project in your research group, I did not expect that we would develop such a harmonious working relationship. Your invaluable guidance, insightful feedback, and unwavering support over these five years have been instrumental in shaping my research and academic growth. Your encouragement to conduct research in Würzburg allowed me to further expand my horizons. Your patience and dedication to my development as a scholar have been deeply appreciated, and I am forever grateful for your mentorship. It was an honour exploring post-transcriptional gene regulation in *Acinetobacter baumannii* under your stewardship.

I am also grateful to the members of my thesis committee, Dr Marta Martins and Dr Alastair Fleming, for their time, expertise and constructive criticism. Your diverse perspectives and thorough evaluations have greatly enriched the quality of this thesis. Thank you for listening to my research outcomes and plans over these years. I also thank Dr Anna Ershova and Dr Karsten Hokamp for sharing their expertise and wisdom with me. I would also like to thank Dr Alex Westermann in the Helmholtz Institute for RNA-based infection biology and the entire Westermann research group, particularly Daniel Ryan, for accepting me into their laboratory and helping me generate first class research.

I would also like to thank my colleagues and fellow graduate students in the Moyne Institute. The camaraderie, discussions, and shared laughs have made this journey more manageable and enjoyable. A special thanks to all those in the Kröger group for their

advice and encouragements. There are many students in the Moyne, past and present, that I would like to thank for their comraderie in particular, including; Ali, Maha, Orlaith, Rebecca, Eoghan, Kevin, Brian, Kate, Sarah, Mary, Jorge, Bin, Amy, Filza, Candida, Zoe, German, Marty, James, Sadhbh, Stephen, Brenda, Reham and Hadeel. It truly feels like we are one big family after spending so much time together.

I am deeply indebted to the administrative and technical staff in the department, whose assistance and support have been invaluable. I would like to thank Dee for her support and guidance. I would like to thank Stephen and Ronan for making me laugh all the time and keeping me company in the mornings. I would like to thank Connie and Miriam for being great office conversation friends. I would like to thank Noreen and Jayne for their administrative support. I would like to thank Ciaran, Dave and Margaret for keeping the building running and for their continued help over the years.

My deepest thanks go to my family, especially my parents, Deirdre and John, and my siblings, Aedán and Marie, for their unconditional love and encouragement. I must also thank Eoin and Brendan for their friendship. To my partner, Özge, your patience, understanding, and support have been my source of strength throughout this journey.

Finally, I would like to acknowledge the financial support provided by Trinity College Dublin, the Irish Research Council and EMBO, which made this research possible.

To everyone who has been a part of this journey, your contributions have been invaluable, and I am forever grateful. Thank you.

Publications:

- **Hamrock, F. J.**, Ryan, D., Shaibah, A., Ershova, A. S., Mogre, A., Sulimani, M. M., Ben Taarit, S., Hokamp, K., Westermann, A. J., & Kröger, C. (2024). Global analysis of the RNA–RNA interactome in *Acinetobacter baumannii* AB5075 uncovers a small regulatory RNA repressing the virulence-related outer membrane protein CarO. *Nucleic Acids Research*, 1–18.
- Shaban, L., Ershova, A. S., **Hamrock, F. J.**, Shaibah, A., Sulimani, M. M., Amin, M. R., Russell, J. N., Ravichandran, R., Schaffer, K., Martins, M., Cameron, A. D. S., & Kröger, C. (2021). Draft Genome Sequence and Annotation of *Acinetobacter soli*. *Microbiology Resource Announcements*, *10*(40), 1–2.

Conference presentations:

- **Hamrock F. J.**, Ryan D, Shaibah A, Ershova A, Mogre A, Reichardt S, Hokamp K, Westermann AJ, Kröger C, GRIL-seq uncovers a posttranscriptional regulator of CarO and BfnH in *Acinetobacter baumannii* AB5075, DAPI 2023, 2023. Oral presentation.
- **Hamrock F. J.**, Ryan D, Hokamp K, Westermann AJ and Kröger, C, Functional Characterisation of small RNAs in *Acinetobacter baumannii*, "AcinetoVibes" Conference, 2022. Oral presentation.
- **Hamrock F. J.**, Ryan D, Westermann AJ, Hokamp K, Kröger C, Functional Characterisation of small RNAs in *Acinetobacter baumannii*, DAPI 2024, 2024. Poster presentation.
- **Hamrock F. J.**, Ryan D, Shaibah A, Ershova A, Mogre A, Reichardt S, Hokamp K, Westermann AJ, Kröger C, GRIL-seq uncovers a posttranscriptional regulator of CarO and BfnH in *Acinetobacter baumannii* AB5075, 13th Symposium on the Biology of *Acinetobacter*, Coimbra, Portugal, 2023. Poster presentation.
- **Hamrock F. J.**, Ryan D, Hokamp K, Westermann AJ and Kröger, C, Functional Characterisation of small RNAs in *Acinetobacter baumannii*, Molecular Microbiology Conference, Birmingham, 2022, 2022. Poster presentation.

Table of Contents

List of Tables

List of Figures

Chapter 1 – Introduction

1.1 *Acinetobacter baumannii* is a nosocomial pathogen of global concern

In recent decades, the Gram-negative bacterium *Acinetobacter baumannii* has gained global prominence as a major source of difficult to treat infections (Harding et al., 2018). These organisms are aerobic coccobacilli and are members of the *Acinetobacter* genus within the *Moraxellaceae* family of microorganisms (Ma et al., 2021). Historically, *Acinetobacter* species were regarded as harmless organisms that degrade recalcitrant, aromatic compounds in soil or aquatic environments (Towner, 2009). While most *Acinetobacter* species are non-pathogenic, five *Acinetobacter* species predominantly act as opportunistic pathogens; *A. baumannii*, *Acinetobacter dijkshoorniae*, *Acinetobacter pittii*, *Acinetobacter seifertii* and *Acinetobacter nosocomialis* (Bouvet et al., 1986; Cosgaya et al., 2016; Nemec et al., 2011, 2015). *A. baumannii* is of particular concern as it infects ~ 1,000,000 people every year (Spellberg et al., 2013). Different *A. baumannii* strains exhibit varying levels of pathogenesis, highlighting the heterogenous nature of these organisms (Maure et al., 2023). The antibiotic susceptible *A. baumannii* ATCC17978 strain was first isolated in 1951 and acted as the primary *A. baumannii* model for many decades, along with others including ATCC19606 and AYE (Antunes et al., 2011). However, they are less reflective of clinically relevant *A. baumannii* and were replaced by the AB5075 strain, a highly virulent and genetically pliable isolate (Jacobs et al., 2014). *A. baumannii* invades epithelial cells, endothelial cells, neutrophils and macrophages (Choi et al., 2008; Kamoshida et al., 2016; Qin et al., 2020). Recently, *A. baumannii* clinical isolates capable of intracellular replication were documented (Distel et al., 2023; Rubio et al., 2022; Sycz et al., 2021). This demonstrates that circulating *A. baumannii* strains are constantly evolving to optimise host colonisation (Maure et al., 2023).

Unlike other *Acinetobacter* species, *A. baumannii* is more abundant in hospitals than in natural environments (Towner, 2009). Deforestation and the availability of nutrient-rich, urban habitats have facilitated the proliferation of *A. baumannii* in human environments (Wilharm et al., 2024). This pathogen likely suffered through a population bottleneck event prior to undergoing rapid genomic expansion which resulted in the emergence of six international clonal lineages (ICL 1-6) (Diancourt et al., 2010). Two of these lineages (ICL1 and ICL2) are responsible for causing the majority of multidrug resistant (MDR) and extensively drug resistant (XDR) infections (Antunes et al., 2014; Karah et al., 2012).

Approximately ~45% of global *A. baumannii* infections are MDR and can even reach >70% in certain regions (Antunes et al., 2014; Kempf et al., 2012). Due to the lack of effective therapeutics, major public health agencies have classified carbapenem-resistant *A. baumannii* (CRAB) strains as a priority pathogen warranting greater attention (Centers for Disease Control and Prevention, 2019; Tacconelli et al., 2018). The abundance of CRAB infections in Asian, American, Middle Eastern and North African countries are particularly devastating (Ma et al., 2021). Infections caused by MDR strains of *A. baumannii* have high mortality rates that are up to 20% (Antunes et al., 2014). These strains are burdens on the health care systems of many countries, they cost the US economy $1.6 billion annually alone (Butler et al., 2019; Cornejo-Juárez et al., 2020; Nelson et al., 2016). This has catastrophic consequences on the economies of developing countries, which often exhibit the highest levels of MDR infections.

A. baumannii typically infects hospitalised, immunocompromised hosts (Wong et al., 2017). This afflicts older aged persons, patients in intensive care units (ICUs), patients that underwent recent surgery and those on dialysis in particular (Mahgoub et al., 2002). Infections are associated with the use intrusive medical devices, such as catheters, ventilators and nasogastric tubes (Jung et al., 2015). *A. baumannii* infects skin and soft tissue by accessing burn wounds or sites of trauma following military combat or natural disasters (Johnson et al., 2007; Zhang, Liu, et al., 2012). Poor infection management in these scenarios exacerbates the spread of this pathogen. Soldiers involved in combat in Iraq and Afghanistan witnessed a dramatic increase in MDR *A. baumannii* wound infections (Keen et al., 2010). *A. baumannii* causes bloodstream infections, through intravenous catheters, causing mortality rates up to 40% (Wisplinghoff et al., 2012). This pathogen is a major cause of ventilator-associated pneumonia (VAP) within ICUs (Jaruratanasirikul et al., 2019). These infections are incredibly serious, with mortality rates reaching up to 50% (Weiner et al., 2016). Community acquired *A. baumannii* infections pose a growing threat to health security, particularly among countries with humid climates (Anstey et al., 1992; Dexter et al., 2015; Wang et al., 2002). They cause fulminant pneumonia, septic shock and multi organ failure, resulting in high mortality rates (Dexter et al., 2015). Community acquired infections are rare and are associated with pre-existing risk factors including alcoholism, diabetes, nephrotic damage and lung disease (Chen et al., 2001; Leung et al., 2006). The severe nature of *A. baumannii* infections has created an urgent need to deepen our understanding of its biology.

1.2 Survival of *Acinetobacter baumannii* in inhospitable environments

A. baumannii has gained the ability to withstand harsh clinical environments and evade antimicrobial treatments, enabling it to thrive under unfavourable growth conditions. To do so, *A. baumannii* strains have evolved sophisticated survival mechanisms that promote growth in extreme environments and resist antibiotic exposure (Harding et al., 2018). These mechanisms, often referred to as 'persist and resist' strategies in the literature, set *A. baumannii* apart from other nosocomial pathogens and are key factors behind its emergence as a significant threat. In this section, we will explore the primary strategies employed by *A. baumannii* to survive in adverse conditions.

1. Antimicrobial resistance in *A. baumannii*

The innate ability of *A. baumannii* to acquire antimicrobial resistance (AMR) has sparked global interest into this microorganism (Touchon et al., 2014). This bacterium's genetic plasticity facilitates both intrinsic modifications, through rapid mutations and chromosomal rearrangements, and extrinsic adaptations, through the incorporation of foreign mobile genetic elements (Kyriakidis et al., 2021). The development of AMR is frequently driven by horizontal gene transfer (HGT), as *A. baumannii* readily acquires and integrates environmental DNA into its genome (Touchon et al., 2014). This organism can lyse other bacterial species through the use contact dependent type VI secretion systems, releasing genetic material from competing species which serve as a source of antimicrobial resistance genes (ARGs) (Borgeaud et al., 2015; Cooper et al., 2017; Schwarz et al., 2010). Additionally, many *A. baumannii* isolates are naturally competent, efficiently acquiring ARGs from their surroundings (Ramirez et al., 2010). This uptake occurs during twitching motility on wet surfaces, suggesting that DNA uptake is mediated by type IV pili (Wilharm et al., 2013). These appendages bind foreign DNA and retract, allowing DNA access to the periplasm (Vesel et al., 2021). Foreign DNA is then translocated into the cytoplasm by the ComA/ComEC system where it is integrated into the genome through homologous recombination (Marie et al., 2017; Nero et al., 2018). This model of DNA uptake is shown in **Figure 1.1A**. The incorporation of ARG into *A. baumannii* strains has equipped them new AMR strategies.

The major molecular mechanisms that confer AMR within *A. baumannii* are well described (Kyriakidis et al., 2021). AMR is achieved primarily through three mechanisms; reducing the intracellular concentration of the antibiotic in the cell (by preventing uptake or increasing efflux of the antibiotic), modifying the antibiotic target or by enzymatically inactivating the antibiotic (Rangel et al., 2021). The most prominent strategies used to mediate AMR in *A. baumannii* are represent in in **Figure 1.1B**.

A. baumannii strains have endogenous resistance to β-lactam antibiotics, compounds that inactivate penicillin binding proteins (PBPs) preventing transpeptidation resulting in imbalanced peptidoglycan levels and cell death (Green, 2002). These organisms produce β-lactamase enzymes to hydrolyse this class of antibiotics (Tooke et al., 2019). Outer membrane proteins (OMPs) are suggested to be involved in the efflux and uptake of β-lactam antibiotics (Iyer et al., 2018; Srinivasan et al., 2015; Tomás et al., 2005; Zhong et al., 2020). One such OMP, referred to as the carbapenem-associated resistance protein (CarO) was thought to be involved in the uptake of carbapenem in this pathogen (Mussi et al., 2005, 2007; Siroy et al., 2005). This view has come under scrutiny in recent years (Uppalapati et al., 2020; Zahn et al., 2015). *A. baumannii* employs the resistance–nodulation–division (RND) family of efflux pumps, such as the AdeABC, to remove intracellular β-lactam antibiotics (Hawkey et al., 2018; Huang et al., 2008). These efflux pumps are regulated by the AdeRS two-component regulatory system (Leus et al., 2018; Marchand, Marchand, et al., 2004). *A. baumannii* also modifies the structure of PBP active sites to develop β-lactam antibiotic resistance (Cayô et al., 2011).

This organism has also developed resistance to aminoglycosides, a class of antibiotics that bind to 16S ribosomal RNA (rRNA) on the 30S subunit of ribosomes, creating errors in protein biosynthesis (Krause et al., 2016). This is achieved by producing aminoglycoside modifying enzymes (AMEs) to reduce aminoglycoside binding affinity, by altering aminoglycoside target sites (using 16S rRNA methyltransferases) and by reducing antibiotic uptake or increasing antibiotic efflux (Kyriakidis et al., 2021). The AdeABC and AbeM efflux pumps are involved in the removal of aminoglycoside antibiotics from this pathogen (De Silva et al., 2019; Xu et al., 2019).

A. baumannii can develop resistance to tetracyclines, a class of antibiotics that bind to 30S ribosomal subunits preventing binding of aminoacyl-transfer RNAs and halting

protein biosynthesis (Chukwudi, 2016). Tetracyclines are removed by RND-family efflux pumps, including AdeIJK and AdeABC, and the major facilitator superfamily (MFS) efflux pumps TetA and TetB in this pathogen (Huys et al., 2005; Yuhan et al., 2016). *A. baumannii* also inactivates tetracyclines using plasmid-encoded monooxygenases Tet(X3), Tet(X4) and Tet(X5) (He et al., 2019; Wang et al., 2020). Additionally, this pathogen produces ribosomal protection proteins, such as TetM and TetO, that modify the ribosome, blocking activity of tetracyclines (Dönhöfer et al., 2012).

This pathogen modulates resistance to fluoroquinolones, antibiotics that inhibit the activity of DNA gyrase and topoisomerase reducing chromosomal supercoiling, causing breaks in double stranded DNA (Correia et al., 2017). *A. baumannii* adjusts to fluoroquinolone exposure by downregulating porins involved in uptake of these antibiotics and upregulating efflux pumps that extrude these compounds (Coyne et al., 2011). Many strains of this pathogen carry plasmids that encode Qnr proteins, AMEs and efflux pumps that inactivate fluoroquinolones or remove them from the bacteria (Robicsek et al., 2006).

Polymyxin antibiotics, including colistin, bind to the lipid A portion of lipo-oligosaccharides (LOS) of *A. baumannii* outer membranes, destabilising the inner and outer membranes (Mohapatra et al., 2021). The complete LOS within clinical isolates of *A. baumannii* enables colistin resistance (Moffatt et al., 2010). *A. baumannii* develops resistance to polymyxins by accumulating mutations that remove the negative charge of lipid A in LOS which prevents polymyxins binding (Sun et al., 2020). Alternatively, *A. baumannii* mutates genes involved in the biosynthesis of lipid A or induces expression of efflux pumps (Hood et al., 2013).

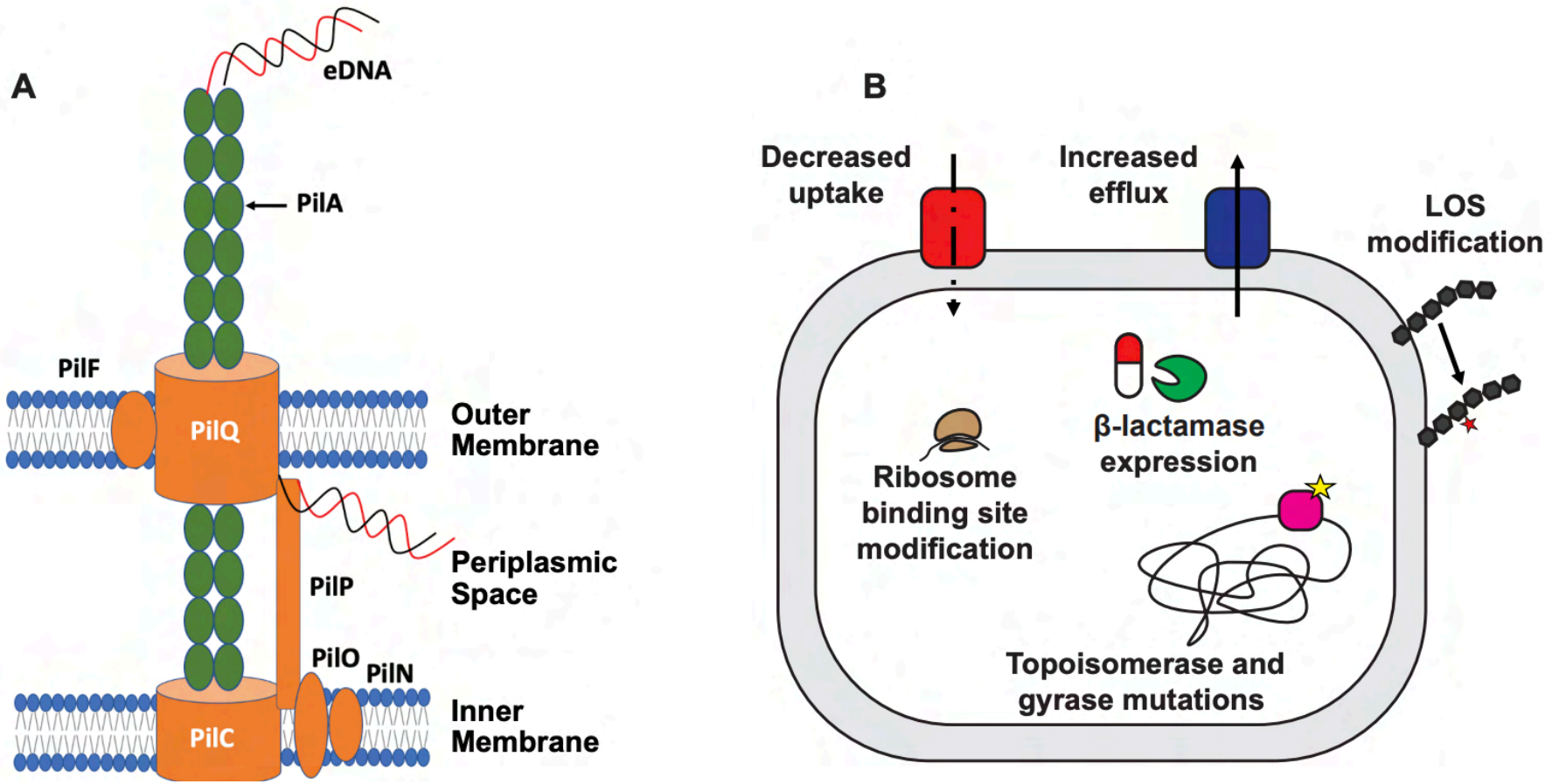

Figure 1.1 Antimicrobial resistance strategies in *A. baumannii*.

(A) DNA uptake is mediate through type IV pili. Environmental DNA (eDNA) first binds PilA before the pilus retracts, granting eDNA access to the periplasmic space. The DNA is then integrated into the *A. baumannii* genome. (B) Major antibiotic resistance strategies in *A. baumannii*. This pathogen reduces uptake and increases efflux of antibiotics. It modifies molecules, including ribosomes, lipooligosaccharides (LOS), DNA topoisomerase and DNA gyrase to prevent antibiotic activity. It also produces enzymes that degrade the antibiotic i.e. β-lactmases.

2. *A. baumannii* environmental persistence strategies

In addition to its resistance to antimicrobial therapies, *A. baumannii* can replicate in unfavourable environments, enabling it to effectively colonize hospital settings (Harding et al., 2018). This pathogen is capable of surviving harsh conditions encountered in healthcare facilities, including prolonged desiccation, exposure to oxidative agents, and disinfectants. Moreover, it forms biofilms and exhibits exceptional micronutrient acquisition abilities, allowing it to thrive both in hospital environments and within hosts.

The innate desiccation resistance of *A. baumannii* is a critical adaptation to survival in hospitals (Wendt et al., 1997). This pathogen survives for long periods of water deprivation, even after months of drying. The polysaccharide capsule retains water in *Acinetobacter baylyi*, a non-pathogenic relative of *A. baumannii* (Espinal et al., 2012; Scott et al., 2014). Functional *A. baumannii* LOS also maintains the integrity of the outer membrane and prevents leakage of hydrophilic compounds from the cell (Boll et al., 2015). Many desiccation strategies used by *A. baumannii* are linked to oxidate stress responses. The disruption of BfmR, the response regulator of the BfmRS two-component regulatory system results in increased *A. baumannii* sensitivity to desiccation stress (Farrow et al., 2018). BfmR induces the KatE catalase that decomposes the reactive oxygen species (ROS) hydrogen peroxide (Mulvey et al., 1990). When deprived of water, *A. baumannii* is more resistant to hydrogen peroxide and has improved survival within macrophages (where ROS are used to kill bacteria) exhibiting the cross-resistance strategies used (Farrow et al., 2018; Green et al., 2022). *A. baumannii* also produces two hydrophilins (DtpA and DtpB) that contribute to desiccation resistance (Green et al., 2022). Furthermore, the RecA recombination protein repairs the breaks in the DNA that are created when dried *A. baumannii* is rehydrated (Aranda et al., 2011; Norton et al., 2013). The disinfectant chlorohexidine is frequently used within hospitals, it is used to disinfect skin and decontaminate medical devices prior to surgery (McDonnell et al., 1999). *A. baumannii* acquires chlorohexidine resistance by removing intracellular molecules by using AceI efflux pumps (Hassan et al., 2013). *A. baumannii* is proposed to enter a viable but non-culturable (VBNC) state upon desiccation, among other conditions, allowing survival in unfavourable environments (König et al., 2023).

A. baumannii also forms biofilms on medical device surfaces and on skin allowing it to colonise new hosts and withstand antimicrobial treatments (Harding et al., 2018). In biofilms, large clumps of cells are bound together in extracellular polymeric substances. *A. baumannii* expresses adhesins, OMPs, secretion systems and capsular polysaccharides to establish and maintain biofilm formation. Most biofilm forming strains express the type I chaperone-usher (Csu) pilus system to enable biofilm formation on biotic and abiotic surfaces (Tomaras et al., 2008). The Csu pili are transcriptionally regulated by the BfmRS and GacSA two-component regulatory systems (Cerqueira et al., 2014; Tomaras et al., 2008). The maturation of biofilms in *A. baumannii* is mediated by the biofilm associated protein (Bap), a large outer-membrane bound appendage (Loehfelm et al., 2008). This protein promotes cell-cell adhesion and growth on plastic surfaces. Bap is secreted by the same type I secretion system that also secretes RTX-domain containing proteins that also assist in biofilm maturation (Harding et al., 2017; Satchell, 2011).

During *A. baumannii* infections, the hosts attempts to deprive the pathogen of essential metals, including iron, zinc and manganese, to limit the growth of this pathogen *in vivo* (Murdoch et al., 2022). To overcome host nutritional immunity, *A. baumannii* has developed strategies to scavenges these metals from the host. This bacterium secretes siderophores that chelate iron with high affinity. *A. baumannii* has adapted several siderophore production cluster of genes, to create acinetobactin, baumannoferrin and fimsbactin siderophores (Gaddy et al., 2012; Penwell et al., 2015; Proschak et al., 2013). Scavenging of zinc in *A. baumannii* is achieved through the production of the ZnuABC transporter that is itself regulated by the Zur transcriptional regulator (Hood et al., 2012; Moore et al., 2014; Mortensen et al., 2014).

1.3 Post-transcriptional regulation in bacteria

To effectively respond to antibiotic exposure and stressful environmental conditions, *A. baumannii* tightly regulates gene expression (Kröger et al., 2017). The role of transcriptional regulators in modulating gene expression in this organism is well-documented, with many examples discussed in **Section 1.2**. However, the influence of regulatory small RNAs (sRNAs) on gene expression in *A. baumannii* has not been as thoroughly established (Kröger et al., 2017; Sarshar et al., 2022). In this section, the

significance of sRNAs in other bacterial species will be highlighted, their role in *A. baumannii* physiology will be explored, and various methods for profiling sRNA interaction networks will be discovered.

1. Bacterial sRNAs are key genetic regulators

Bacterial small RNAs (sRNAs) are short RNA molecules, typically 50-250 nucleotides in length, that serve as critical post-transcriptional regulators in many species (Storz et al., 2011). The expression of sRNAs is often dependent on specific growth conditions and is frequently induced by changing environmental conditions (Gottesman et al., 2006). This enables bacteria to quickly coordinate gene expression and adapt to environmental changes. Bacterial sRNAs can influence protein levels either directly or by regulating mRNA expression through imperfect antisense base-pairing (Guillier et al., 2006). These molecules are generally categorized into two groups: *cis*-encoded sRNAs and *trans*-encoded sRNAs. *Cis*-encoded sRNAs are transcribed from the complementary strand of their mRNA targets, while trans-encoded sRNAs are transcribed from separate locations, often at a distance from their mRNA targets. *Trans*-encoded sRNAs have garnered significant interest from the RNA research community due to their potential role as global regulators of gene expression. These sRNAs are typically transcribed from intergenic regions (IGRs) or from the 5′- or 3′-untranslated regions (UTRs) of protein-coding genes (Waters et al., 2009). Although most research has focused on the regulatory functions of sRNAs in *Enterobacteriaceae*, there is growing interest in characterising sRNAs in other bacterial models.

Trans-encoded sRNAs, which regulate the expression of mRNA targets through antisense base-pairing, utilise a contiguous stretch of nucleotides known as a "seed region" to initiate binding (Matera et al., 2022). The seed region binds to complementary motifs in the mRNA targets, ensuring the specificity of sRNA-mRNA interactions and allowing the sRNA to modulate multiple pathways simultaneously. Productive sRNA-mRNA interactions form duplex structures that can either enhance or repress the expression of the mRNA targets; the main mechanisms involved are summarised in **Figure 1.2**. Typically, sRNAs bind to the ribosome binding site (RBS) or the first five codons of the target transcript, referred to as the five-codon window, blocking access of the 30S ribosomal subunit to the translation initiation site and thereby reducing the

steady-state levels of the target protein (Bouvier et al., 2008). Alternatively, the sRNA-mRNA interaction complex can recruit RNases to degrade both interaction partners, destabilising the transcript. Binding of sRNAs can also induce structural remodelling in the target transcript, sequestering or exposing translational initiation sites, which can either repress or activate the expression of the target gene (Storz et al., 2011).

Most sRNAs fine-tune gene expression, however, many others have broad and important physiological consequences in bacteria (Michaux et al., 2014). Some sRNAs modulate AMR and antibiotic tolerance pathways, allowing certain species to evade antibiotic therapies (Dersch et al., 2017). Transcriptome analyses reveal that certain sRNAs are induced by sublethal concentrations of antibiotics, suggesting that they are integral responders that enable survival in such conditions (Howden et al., 2013). So far, sRNAs are known to regulate AMR by controlling genes involved in; antibiotic uptake, antibiotic efflux, lipopolysaccharides (LPS) modification, biofilm formation and DNA mutagenesis (Dersch et al., 2017). The sRNAs RyhB and MicF modulate expression of the outer membrane proteins (OMPs) CirA and OmpF, respectively, that are responsible for uptake of the bacteriocin colicin Ia (CirA) and β-lactam antibiotics (OmpF) in *Escherichia coli* (Kim et al., 2015; Salvail et al., 2013). The sRNAs SdsR and DsrR control the expression of antibiotic efflux pumps TolC and MdtEF, respectively (Nishino et al., 2011; Parker et al., 2016). The sRNA MgrR represses P-ethanolamine transfer, an enzyme that modifies lipopolysaccharides and conferring sensitivity to polymyxin antibiotics (Moon et al., 2009).

Additionally, many sRNAs modulate genes associated with virulence and pathogenesis. For instance, the *Staphylococcus aureus* sRNA, RNAIII, modulates α-haemolysin expression and represses virulence factor production (Waters et al., 2009). The sRNA PinT co-ordinates the transition from host cells invasion to intracellular replication of *Salmonella* strains (Westermann et al., 2016). Interestingly, certain pathogenic species, such as *Legionella pneumophila*, can transfer sRNAs to the host to modulate host immune responses (Sahr et al., 2022). Other sRNAs modulate iron starvation response genes, for instance the sRNA RyhB prevents *E. coli* from expressing non-essential iron-utilising genes (Richards et al., 2011). OMP-regulating sRNAs are typically integrated into extracytoplasmic function sigma factor regulons, allowing them to provide an immediate response following membrane damage (Heimann, 2002). In *E. coli*, the sigma factor σ^E

is induced when deleterious misfolded OMPs accumulate, activating expression of the sRNAs RybB, MicA and MicL (Nitzan et al., 2017). These sRNAs regulate envelope homeostasis by repressing OMPs which allows enables envelope repair systems to act without being overwhelmed by newly synthesised OMPs (Fröhlich et al., 2018).

Many bacterial species, particularly among *Enterobacteriaceae*, require the presence of RNA binding proteins (RBPs) to mediate sRNA-mRNA base-pairing (Pichon et al., 2007). A classic example of this is the RBP Hfq which mediates sRNA-based regulation in most Gram-negative species. Hfq was not believed to promote sRNA-mRNA interactions in Gram-positive species, however work in *Listeria monocytogenes* and *Clostridioides difficile* has challenged this perspective (Fuchs et al., 2021; Nielsen et al., 2009). Hfq acts as a molecular platform for sRNAs and mRNAs by bringing them in close proximity for base-pairing and protecting them from degradation (Hoekzema et al., 2019). It can directly cause structural rearrangements of these RNAs that expose the seed region of sRNAs or the sRNA binding regions of target mRNAs to facilitate interactions. Hfq is composed of six monomers that polymerise to form a hexameric disk structure (Santiago-Frangos et al., 2018). Individual monomers contain a Sm-like domain and a disordered C-terminal domain. In the hexamer, the Sm-domains create two RNA binding surfaces; a proximal face and a distal face. The proximal face binds mRNA poly-A rich tails and particular motifs (AAN) of type II sRNAs while the distal face binds sRNA terminator sequences (Schu et al., 2015). In *E. coli*, sRNAs compete for access to Hfq for regulation, the C-terminal domain mediates RNA binding and enables release of double stranded RNA (Santiago-Frangos et al., 2017, 2018).

Other RBPs, including ProQ, are also involved in regulating sRNA-mRNA in bacteria (Ng Kwan Lim et al., 2021). The sedimentation of RNAs and proteins in a glycerol gradient (GRAD-seq) identified that ProQ is another important RNA chaperone that controls sRNA activity (Smirnov et al., 2016, 2017). ProQ, unlike Hfq, recognises sRNAs based on structure rather than specific sequences within these molecules (Liao et al., 2023). Since then, GRAD-seq experiments have uncovered novel RBPs in other species, including KhpB in *C. difficile*, and the exoribonuclease Cbf1 in *Streptococcus pneumoniae* (Hör et al., 2020; Lamm-Schmidt et al., 2021). The RBPs CsrA and CspC/E are other known sRNA-regulators in Gram-negative species (Holmqvist et al., 2018). CsrA typically represses mRNA transcripts associated with entry into stationary phase

while promoting those that enable exponential growth (Potts et al., 2017). In *Pseudomonas aeruginosa*, RsmA (the CsrA homologue) is inhibited by several RsmA-regulating sRNAs (Janssen et al., 2018).

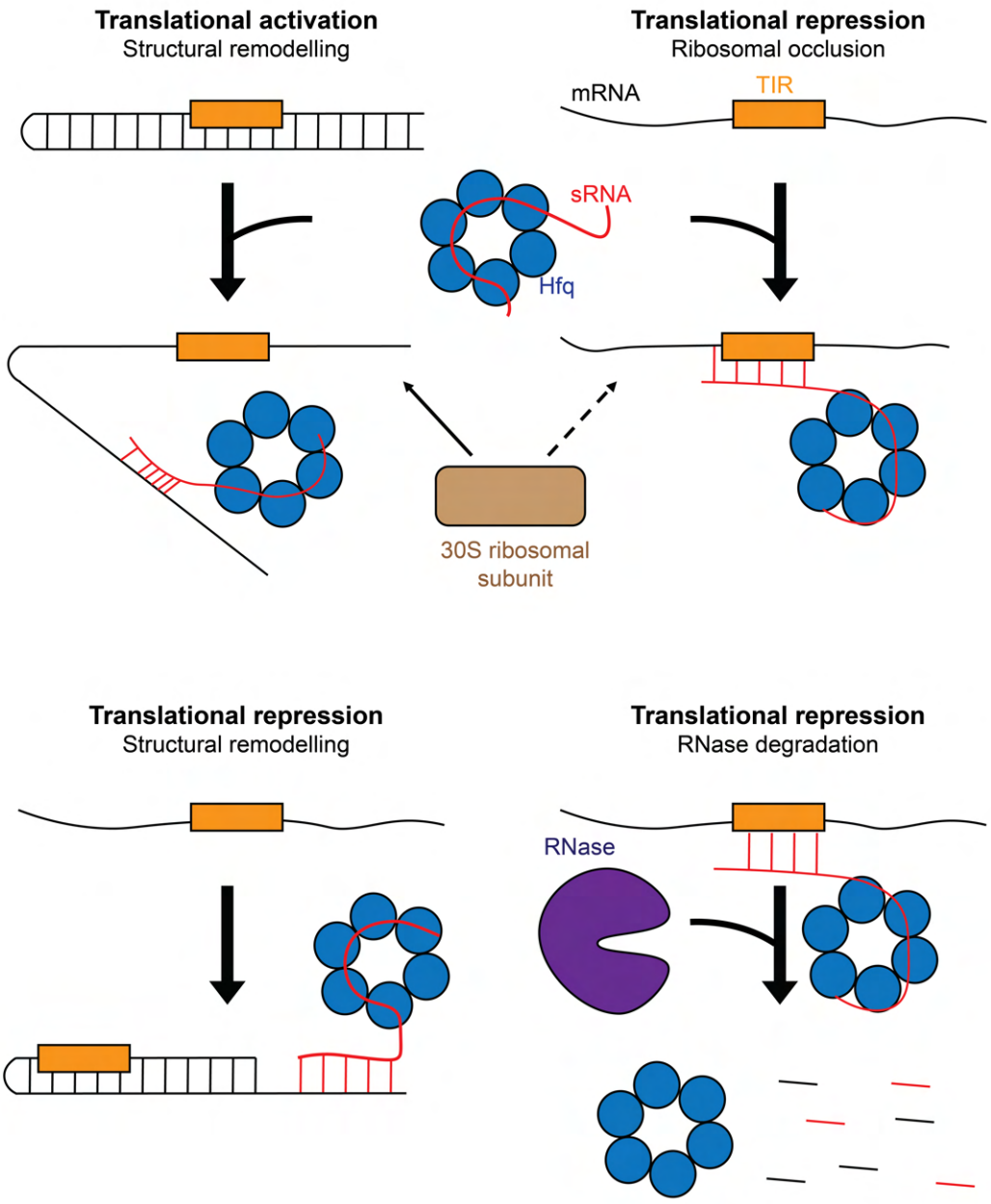

Figure 1.2 Bacterial sRNAs can activate or repress the expression of target mRNAs through antisense base-pairing.

The sRNAs can bind to a highly structured mRNA molecule, causing structural rearrangements that expose a sequestered translational initiation region (TIR), activating that molecule. Alternatively, sRNAs can directly block the TIR or cause structural rearrangements that block this site, repressing the target. Many sRNAs recruit RNases that recognise and bind double stranded RNAs. The RNA chaperone Hfq is often needed to mediate such interactions.

2. Role of sRNAs in *A. baumannii*

Despite its clinical importance, the RNA biology of *A. baumannii* was cryptic prior to the undertaking of this project (Sarshar et al., 2022). A sRNA referred to as the amino acid regulator (Aar) was the first sRNA identified in an *Acinetobacter* species. Aar was first identified in the non-pathogenic *A. baylyi* ADP1 (Schilling et al., 2010). It was more abundant in stationary phase than in exponential phase and was induced by iron limitation and salt shock in this organism. The overexpression of Aar in *A. baylyi* ADP1 resulted in the upregulation of six amino acid metabolic genes, as determined by northern blotting, however no base-pairing interactions were confirmed. Later, 31 potential sRNA candidates were uncovered in *A. baumannii* ATCC17978 (Sharma et al., 2014). Northern blotting confirmed the expression of 3 of these putative sRNAs in the *A. baumannii* MTCC1425 strain. One of them, called AbsR25, was transcriptionally repressed by ethidium bromide, indicating that it might be involved in efflux. Overexpression of AbsR25 correlated with a decrease in expression of AbaF, a MFS transporter, however, it is unclear if this results from base-pairing interactions (Sarshar et al., 2022). Transcriptomic analyses by the Kröger and Shaw research groups identified numerous putative sRNAs in *A. baumannii* AB5075 and ATCC17978, respectively (Kröger et al., 2018; Weiss et al., 2016). The Shaw group used RNA-seq to identify 78 sRNA candidates in the AB5075 strain, 6 of which were validated by northern blotting. The Kröger group used differential RNA-sequencing (dRNA-seq) to predict the exact transcriptional start sites (TSSs) of sRNAs (Kröger et al., 2018). They identified 110 sRNAs in *A. baumannii* ATCC17978, 88 of these are conserved in the AB5075 strain. Other studies identified potential *A. baumannii* sRNAs that impact biofilm formation, however the mechanisms behind such phenotypes were not explored (Álvarez-Fraga et al., 2017; Shenkutie et al., 2023). Anderson and colleagues suggested that a plasmid-encoded sRNA, SrvS, is responsible for the phase switching of *A. baumannii* AB5075 from a virulent, opaque form (VIR-O) to an avirulent, translucent form (Anderson et al., 2020). They later proposed that SrvS, acts as "rheostat", allowing phase switching by controlling TetR type transcriptional regulators through yet unexplained means (Pérez-Varela et al., 2022). Regulatory sRNAs involved in colistin resistance were computationally predicted by comparing colistin resistant and sensitive clinical strains of *A. baumannii* (Cafiso et al., 2020). This led to the identification of 6 *cis*-encoded and 2 microRNAs that may participate in colistin survival.

The role of RBPs in modulating sRNA activity is also poorly understood in *Acinetobacter* species compared to *Enterobacteriaceae* species. *Acinetobacter* members encode a Hfq homologue that is structurally distinct from Hfq in other Gram-negatives (Kröger et al., 2017). Analysis of Hfq in *A. baylyi* and *A. baumannii* ATCC17978 revealed that it produces an unusually long C-terminal containing glycine rich repeats (Schilling et al., 2009; Sharma et al., 2018). The expression of *A. baylyi* Hfq in a Hfq-deficient *E. coli* reversed growth impairments (Schilling et al., 2009). Similarly, the loss of *A. baylyi hfq* slowed growth and its restoration restored this growth to wildtype levels. Later work demonstrated that recombinant *A. baumannii* ATCC17978 interacts with AbsR25 and the *E. coli* sRNAs DsrA and MicA (Sharma et al., 2018). In this study, full length ATCC17978 Hfq enabled RyhB-*sodB* interactions in *E. coli*. These interactions were affected when using truncated Hfq variants. Hfq is important for carbon metabolism, pathogenesis and stress response mechanisms including desiccation tolerance in *A. baumannii* ATCC17978 (Kuo et al., 2017; Sharma et al., 2018). To our knowledge, no deletion mutants of Hfq were constructed in the AB5075 strain. Furthermore, the targeted knockdown of *hfq* mRNA by CRISPR-interference in the AB5075 strain was lethal, indicating that it is essential in this strain (Intorcia et al., 2024). While it is clear that Hfq is an important regulator in *A. baumannii*, the role that it plays in sRNA-mRNA annealing is unknown.

3. Identification of sRNA-mRNA interactions in bacteria

To elucidate the molecular mechanisms underlying sRNA-mediated regulation, numerous studies have aimed to identify their mRNA targets (Wagner et al., 2015). This can be achieved through either bioinformatic or experimental approaches. The bioinformatic characterisation of sRNA-mRNA interactions in bacterial species is well-established and cost-effective (Georg et al., 2020). *In silico* prediction tools, such as IntaRNA and RNAhybrid, identify mRNA targets that exhibit sequence complementarity to the sRNA under investigation (Busch et al., 2008; Krüger et al., 2006). These tools take into account the secondary structure and the intermolecular base-pairing potential of sRNA-mRNA candidates. Although they reliably predict known sRNA-mRNA interactions, they are significantly limited in identifying novel ones. The development of comparative prediction tools, such as CopraRNA, has facilitated the rudimentary

characterisation of entire sRNA-RNA interactions (sRNA "targetome") within individual bacterial species (Wright et al., 2013, 2014). CopraRNA considers the phylogenetic conservation of sRNA and mRNA homologue sequences across closely related species or strains, thereby reducing the number of false-positive interactions. However, CopraRNA may still produce incorrect predictions (false positives) or fail to predict genuine interactions (false negatives) (Georg et al., 2020). False positives may arise from "sponging" interactions between mRNAs and sRNAs that lack a clear physiological role (Grüll et al., 2019). False negatives are often the result of interactions occurring outside the preset CopraRNA search space, which is typically within 300 nucleotides upstream or downstream of the start codon, or due to differences in RNA structure in vivo influenced by RBPs. A combined approach, utilising both computational and experimental methods, appears to be the most effective strategy for characterising sRNA targetomes (Georg et al., 2020).

The first genome-wide experiments for sRNA target identification were conducted by profiling the transcriptomes of wild-type and sRNA-deletion bacterial strains, enabling researchers to explore the roles of specific sRNAs (Hör et al., 2018). Initially, this was achieved using DNA microarrays, which were later superseded by RNA sequencing (Douchin et al., 2006; Papenfort et al., 2008, 2009). Through the analysis of differentially expressed genes, these studies were able to identify and validate potential sRNA targets. These methods were further refined by incorporating pulse overexpression, where the sRNA is transiently overexpressed in the sRNA-deletion strain before the transcriptome is assessed via RNA-seq (Massé et al., 2005; Papenfort et al., 2006). While both approaches facilitated early characterisation of sRNA-mRNA interactions, including investigations into the role of RyhB, they also had notable limitations. These approaches relied on the sRNA affecting the stability of its mRNA targets, meaning that sRNAs which repressed translation without influencing mRNA degradation were often overlooked. Additionally, the high levels of sRNA expression in pulse overexpression experiments could lead to off-target effects, unintentionally modulating transcripts that are not typical targets (Hör et al., 2018). This issue can be partially mitigated by incorporating sRNA seed region mutant controls in the experiment (Gebhardt et al., 2023; Sharma et al., 2011).

The challenges associated with the aforementioned techniques inspired the creation of new sRNA target identification systems. Pulldown experiments combined with transcriptomics purify individual sRNAs with their bound mRNA interaction partners enable convenient characterisation. The interaction networks of specific sRNAs is accomplished sing MS2-affinity purification coupled with RNA-sequencing (MAPS) and global sRNA target identification by ligation and sequencing (GRIL-Seq), these methods are shown in **Figure 1.3**. MAPS depends on an MS2-aptamer, a short RNA that binds with high affinity to the MS2 coat protein (Carrier et al., 2016). MS2-sRNA fusions are induced *in vivo* before lysates are passed through an affinity column coated with MS2-maltose binding protein. This captures sRNA-RNA complexes that can subsequently by eluted and profiled by RNA-sequencing. MAPS helped characterise addition PinT mRNA targets (Correia Santos et al., 2021). GRIL-seq depends on the ligation of RNA molecules to create sRNA-RNA chimeras that are enriched and sequenced (Han et al., 2016). To accomplish this, the sRNA and T4 RNA ligase are ectopically expressed from separate plasmids *in vivo* generating chimeras. The sRNA-target chimeras are bound to oligo dT tails that are complementary the poly(A) tails of the sRNA on magnetic beads. The sequenced RNA is then mapped to the genome and sRNA-containing reads that map to another locus are considered chimeric and representative of potential interactions. This helped functionally characterise the iron regulated sRNA PrrF1 in *P. aeruginosa* (Han et al., 2016).

While MAPS and GRIL-seq have facilitated the characterisation of certain sRNAs, it is onerous to do this for all sRNAs on an individual basis. This led to innovation of myriad *in vivo* sRNA interactome discovery systems (Hör et al., 2018). All techniques to date are reliant on proximity ligations of sRNAs to their RNA targets, these techniques are shown in **Figure 1.3**. The most widely used system to capture interactions is RNA interaction by ligation and sequencing (RIL-seq) (Melamed et al., 2016). RIL-seq is an intricate experiment; first RNA-RBP complexes are UV-crosslinked *in vivo* before being the chromosomally-tagged RBPs (typically Hfq) are co-immunoprecipitated (Melamed et al., 2018). The bound RNAs are then then trimmed and ligated into RNA-RNA chimeras, while the RBPs are depleted. RNA sequencing of resulting chimeras is performed and statistical tests are performed to detect likely sRNA-RNA interactions. RIL-seq has revolutionised the characterisation of sRNA regulatory networks in many pathogenic species, including *Salmonella enterica*, *P. aeruginosa*, *Vibrio cholera* and

C. difficile (Fuchs et al., 2023; Gebhardt et al., 2023; Huber et al., 2022; Matera et al., 2022). A recent derivative of RIL-seq called intracellular RIL-seq (iRIL-seq) uses T4 RNA ligase to ligate interacting RNAs prior to Hfq co-immunoprecipitation, simplifying this experiment (Liu et al., 2023; Wu et al., 2024). UV-crosslinking, ligation and sequencing of hybrids (CLASH) is another technique used to capture sRNA-RNA interactions in bacteria (Waters et al., 2017). It bears striking resemblance to RIL-seq as is shown in **Figure 1.3**. Briefly, RNA-RBP complexes are UV-crosslinked *in vivo* and co-immunoprecipitated using FLAG-tags. RNAs are then trimmed and the RNA-RBP complexes are further purified using His-tags. Interacting RNAs are then ligated together and to linkers and RNA-RBP complexes are selected based on size. The resulting RNA is sequenced and this enables identification of likely sRNA-RNA interactions. This method was used to capture interactions bound to RNase E in pathogenic *E. coli*, showing that certain sRNAs mediate recruit RNases to degrade their mRNA targets (Waters et al., 2017). Further work established the Hfq-bound interactome in non-pathogenic *E. coli* (Iosub et al., 2020).

RIL-seq and CLASH rely on prior understanding of the role that RBPs mediate in the desired organism to profile the interactome. This limits the utility of these strategies in species like *A. baumannii* with understudied RBPs. The proximity ligation protocol high-throughput global sRNA target identification by ligation and sequencing (Hi-GRIL-seq) overcomes this challenge (Zhang et al., 2017). Hi-GRIL-seq modifies GRIL-seq by omitting the enrichment step and using deeper sequencing resolution to enable global understanding of sRNA regulation. In Hi-GRIL-seq, interacting RNA molecules are ligated into RNA-RNA chimeras by inducing the ectopic expression of T4 RNA ligase (**Figure 1.3**). Sequencing reads that map to two different genetic loci, and contain a sRNA-sequence, are considered chimeric and are potential interaction pairs. Hi-GRIL-seq was used to identify novel sRNA-mRNA interactions in *P. aeruginosa* and to probe sRNA-RNA interactions between a phage and its satellite in *V. cholerae* (Dunham et al., 2023; Zhang et al., 2017).

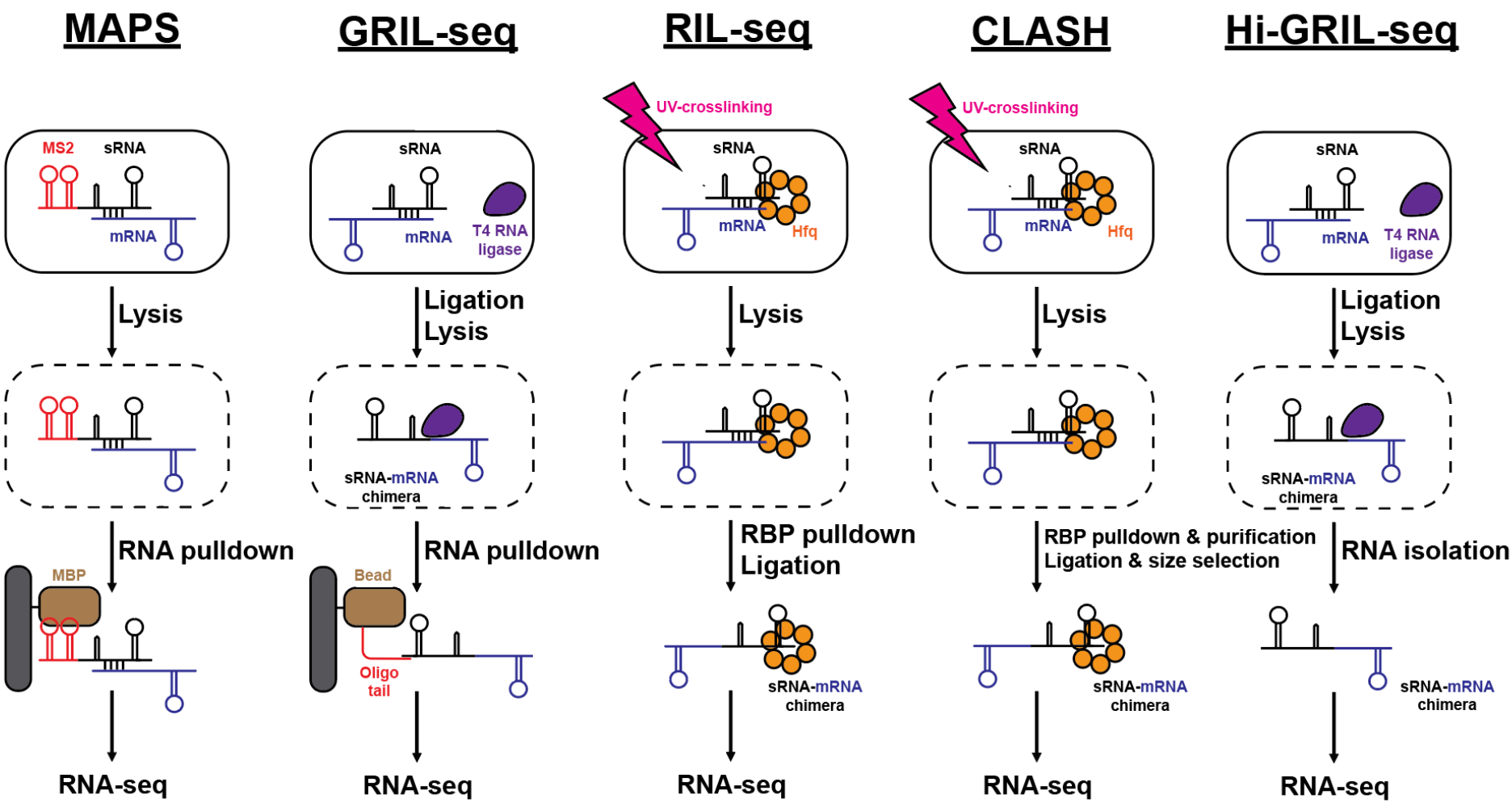

Figure 1.3 Bacterial sRNA target identification systems.

In vivo strategies used to detect sRNA targets in bacteria are shown, including; MAPS, GRIL-seq, RIL-seq, CLASH and Hi-GRIL-seq. While MAPS and GRIL-seq are based on RNA pulldowns and can consequently only functionally characterise one sRNA at a time, RIL-seq, CLASH and Hi-GRIL-seq can characterise all sRNAs simultaneously. RIL-seq and CLASH depend on pulldowns of RNA binding proteins (RBPs), while Hi-GRIL-seq is independent of them.

1. 4 Aims of this study

The overarching goal of this study was to capture the entire RNA-RNA interactome in *A. baumannii* and to mechanistically characterise sRNA-mRNA interactions. To this end, Hi-GRIL-seq was employed to uncover the *A. baumannii* RNA-RNA interactome. Hi-GRIL-seq enabled this without depending on RBPs, which as previously mentioned, are poorly characterised in *A. baumannii*. Hi-GRIL-seq was performed in *A. baumannii* AB5075, due to the genetic malleability and clinical relevance of this strain (Jacobs et al., 2014). The Hi-GRIL-seq experiment itself was carried out by Dr Carsten Kröger prior to commencing my Master's thesis (Hamrock, 2021). Analysis of the Hi-GRIL-seq output at that time was incomplete and yielded no clear interaction pairs. This analysis was optimised during this PhD to uncover the role of regulatory sRNAs in this organism.

Our main priorities were to:

- Optimise analysis of Hi-GRIL-seq in *A. baumannii*.
- Identify novel sRNA-mRNA interactions in *A. baumannii*.
- Consider the role of Hfq in mediating these interactions.
- Further our mechanistic understanding of these interactions.
- Consider the biological importance of these interactions.

Hi-GRIL-seq identified multiple potential sRNA-RNA interactions in *A. baumannii*, providing the first insight into post-transcriptional regulation in this pathogen (**Chapter 3**). In this work, we paid particular to the sRNAs Aar (**Chapter 4**) and Arp (**Chapter 5**).

Chapter 2 – Materials and methods

2.1 Microbial culturing

1. Media

All media used in this study are summarised in **Table 2.1**. Media was prepared using deionised water and was sterilised prior to bacterial cultivation, either through autoclaving or through filtration with 0.2 µm Polyethersulfone (PES) filters (Fisher Scientific). Agar plates were stored at 4ºC for long term storage.

Table 2.1 Media used in the study

Medium	Reagent	Concentration
Lysogeny broth (Lennox, L-broth)	Tryptone	10 g/L
	NaCl	5 g/L
	Yeast extract	5 g/L
Lennox agar (Lennox, L-agar)	L-broth	N/A
	Agar	1.5% (w/v) agar
Transformation medium	Agarose – D3	20 g/L
	Tryptone	2.5 g/L
	NaCl	2.5 g/L

2. Bacterial strains

All bacterial strains used in this study are summarised in **Table 2.2**. For long term storage, overnight bacterial strains, grown in L-broth, were resuspended in 30% (v/v) glycerol at -80ºC. To obtain single colonies, bacterial cryo-stocks were streaked on L-plates containing the desired antibiotic and were grown at 30ºC or 37ºC overnight for 16-18 h in a Memmert incubator to obtain single colonies. These plates were used within 2 weeks of being streaked.

3. Plasmids

The plasmids used in this study are summarised in **Table 2.3**. Plasmids were routinely stored in bacterial cryo-stocks that contained the corresponding antibiotic.

Table 2.2 Bacterial strains used in the study

Species	Strain	Genotype	Resistance	Source
E. coli	TOP10	F– *mcrA* Δ(*mrr-hsdRMSmcrBC*) φ80*lacZ*Δ*M15*Δ*lacX74 nupG recA1 araD139* Δ*(ara-leu)7697 galE15 galK16 rpsL*(StrR) *endA1* λ–	-	Invitrogen
A. baumannii	AB5075	Wildtype	-	S. Salcedo (Jacobs et al., 2014)
A. baumannii	AB5075	Δ*aar*	-	This study
A. baumannii	AB5075	Δ*baeR*	-	M. Suleimani (Kröger lab)
A. baumannii	AB5075	Δ*adeR*	-	M. Suleimani (Kröger lab)
A. baumannii	AB5075	Δ*gacS*	-	M. Suleimani (Kröger lab)
A. baumannii	AB5075	*aar**	-	This study
A. baumannii	AB5075	*carO::3×FLAG-Apra*	$Apra^R$	This study
A. baumannii	AB5075	Δ*aar carO::3×FLAG-Apra*	$Apra^R$	This study
A. baumannii	AB5075	Δ*arp*	-	This study
Salmonella enterica Typhimurium	4/74	Wildtype	-	Kröger lab
Salmonella enterica Typhimurium	4/74	Δ*hfq*::*kan*	Kan^R	Kröger lab

Table 2.3 Plasmids used in the study

Plasmid name	Description	Resistance	Reference
pVRL2Z	P_{BAD} promoter encoding plasmid capable of replicating in *A. baumannii*	Zeo^R	Lucidi et al., 2018
pVRL2Z-*t4rnlI*	T4 RNA ligase placed under transcriptional control of P_{BAD}	Zeo^R	This study. Created by C. Kröger
pVRL2Z-Aar-sfGFP	Transcriptional reporter of the Aar promoter. Superfolder GFP (sfGFP) was placed under control of it	Zeo^R	This study. Created by S. Ben Taarit
pVRL2Z-Aar	Aar was placed under control of the L-arabinose inducible P_{BAD} promoter	Zeo^R	This study
pJV300	Control plasmid for use in an *E. coli* translational reporter system	Amp^R	Urban and Vogel, 2007
pP_L-Aar	Aar overexpression vector for use in an *E. coli* translational reporter system	Amp^R	This study. Urban and Vogel, 2007
pP_L-Aar*	Aar* overexpression vector for use in an *E. coli* translational reporter system	Amp^R	This study. Urban and Vogel, 2007
pP_L-Arp	Arp overexpression vector for use in an *E. coli* translational reporter system	Amp^R	This study. Urban and Vogel, 2007
pXG10-CarO	CarO-sfGFP expression vector for use in an *E. coli* translational reporter system	Cm^R	This study. Urban and Vogel, 2007
pXG10-BfnH	BfnH-sfGFP expression vector for use in an *E. coli* translational reporter system	Cm^R	This study. Urban and Vogel, 2007
pXG10-ABUW_RS07310	ABUW_RS07310-sfGFP expression vector for use in an *E. coli* translational reporter system	Cm^R	This study. Urban and Vogel, 2007
pWH1266	*E. coli-A. baumannii* shuttle vector	Tet^R, Amp^R	Hunger et al., 1990
pWH1266-CarO	CarO-sfGFP expression vector for use in an *A. baumannii* translational reporter system	Tet^R	This study
pWH1266-BfnH	BfnH-sfGFP expression vector for use in an *A. baumannii* translational reporter system	Tet^R	This study
pWH1266-PilA	PilA-sfGFP expression vector for use in an *A. baumannii* translational reporter system	Tet^R	This study
cAar	Aar overexpression vector	Tet^R	This study

4. Bacterial culture conditions

Typically, bacteria were grown in liquid culture at 37°C in the presence of the antibiotic required for selection. Single colonies were inoculated in 5 ml L-broth in glass tubes to set up overnight cultures. These were grown in a shaking incubator (Labwit) at 200 rpm for 16 h. Larger volumes of culture (25 ml) were prepared by sub-inoculating a 1:1,000 dilution (25 µl) of overnight cultures in L-broth. Cells were grown in 250 ml Erlenmeyer flasks to the desired growth phase in a shaking incubator (Labwit, 220 rpm agitation). Growth of bacteria in liquid culture was monitored spectrophotometrically by measuring optical density at a wavelength of 600nm (OD_{600}) using a GENESYS 10 spectrophotometer (Thermo Spectronic). To measure cell survival, the number of colony forming units in the culture (CFU/ml) was assessed. This was accomplished by preparing 10-fold serial dilutions of bacterial cultures in L-broth. These dilutions were then plated on L-agar and the number of colonies was recorded and used to measure the CFU/ml. To investigate the impact that environmental stressors have on Aar expression, *A. baumannii* was grown to late exponential phase (OD_{600} = 1.0) at either 37°C or 25°C. These samples were "shocked" for 15 min prior to RNA isolation and Northern blotting (**sections 2.5 and 2.5**). The cells grown at 25°C were transferred to 37°C as a heat-shock. The cells grown at 37°C were either osmo-shocked through the addition of NaCl (0.3), iron starved through the addition of 2, 2′-dipyridyl (2 mM) or treated with the antibiotic polymyxin B (1 µg/mL). Negative controls, where cells were grown at 37°C or 25°C before being returned to their respective temperature for 15 min, were also included.

5. Antibiotics

The details regarding the antibiotics used for selection in this study are outlined in **Table 2.4**. Antibiotics were either prepared (as a 1000× stock solution) in deionised water, and filter sterilised, or in 70% ethanol. Antibiotics were diluted 1:1,000 in L-broth or in molten L-agar (cooled to ~55°C prior to pouring).

2.2 General molecular techniques

1. Isolation of genomic DNA for use in PCRs

Genomic DNA (gDNA) was isolated from *A. baumannii* for use as a PCR template. Briefly, an aliquot (400 µl) of an overnight culture was collected by centrifugation (21,100 × g for 1 min). The pellet was resuspended in sterile, deionised water (200 µl). This mixture was boiled (100°C) for 10 min prior to being vortexed. This sample was subsequently centrifuged (21,100 × g for 5 min) and the supernatant was removed and mixed with an equal volume of chloroform, before being centrifuged again (21,100 × g for 10 min). The resulting aqueous phase was separated from the organic phase and DNA concentration was measured using the Nanodrop™ (Thermo Scientific). The extracted gDNA was adjusted to 100 ng/µl in sterile, deionised water and stored at -20°C for use a PCR template.

2. Isolation of plasmids from bacterial strains

Plasmids were isolated from overnight cultures, supplemented with the antibiotics required for selection, using the E.Z.N.A.® Plasmid DNA Mini Kit 1 (Omega Bio-Tek). Approximately 4 ml of *E. coli* and *A. baumannii* cultures were first collected by centrifugation (13000 × g) and the pellet was processed as outlined by the manufacturer's specifications (Omega Bio-Tek). The concentration of purified plasmids was measured using the Nanodrop™ (Thermo Scientific) before being stored at -20°C for further use.

3. Polymerase Chain Reaction (PCR)

Polymerase chain reactions (PCRs) were routinely used to amplify gDNA and plasmid DNA throughout this study. PCR reactions were performed using template DNA (100 ng/ µl gDNA or 1-20 ng/µl plasmid DNA), primers and polymerase mixes, the volumes used in each reaction are listed in **Table 2.4**. The entire list of primers used in this study is outlined in **Appendix I**. Both MangoTaq™ DNA polymerase (Bioline) and VeriFi™ polymerase (PCR Biosystems) were used in this study. MangoTaq™ DNA polymerase

was used to amplify PCR products > 1 kbp, while VeriFi™ polymerase was used to amplify PCR products < 1 kbp.

Table 2.4 Components for PCRs

Component	Volume (µl)
Polymerase mix (MangoTaq™ or VeriFi™)	25
Template DNA (100 ng/µl)	1
Forward primer	1
Reverse primer	1
Water	22
Total	**50**

The cycling conditions for conventional PCRs are listed in **Table 2.5**:

Table 2.5 Conventional PCR cycling conditions

Step	Temperature	Time	Cycles
Denaturation	95°C	2 min	1
Denaturation	95°C	15 s	35
Annealing	Variable	30 s	
Extension	72°C	Variable	
Extension	72°C	2 min	1

Single colonies were used for PCR-based detection of specific DNA sequences. This involved resuspending individual colonies in sterile, deionised water (20 µl) before boiling them (95°C, 15 min). The cells were pelleted (maximum speed, 1 min) and the resulting supernatant (1 µl) was used as the DNA template for amplification. The cycling conditions used for these "colony PCRs" are listed in **Table 2.6**:

Table 2.6 Colony PCR cycling conditions

Step	Temperature	Time	Cycles
Denaturation	95°C	15 min	1
Denaturation	95°C	15 s	35
Annealing	Variable	30 s	
Extension	72°C	Variable	
Extension	72°C	2 min	1

4. Agarose gel electrophoresis

PCR products were analysed on 1-2% (w/v) agarose gels to ensure that the amplicon sizes matched the predicted size. Agarose gels were prepared by melting agarose powder in 1×TAE (40 mM Tris-acetate, 1 mM EDTA). Aliquots (5 µl) of PCR products were mixed with 6×DNA loading dye (1 µl, 40 % (v/v) Glycerol, 60 mM EDTA, 10 mM Tris-HCl (pH 7.6), 0.25 % (w/v) Bromphenol blue (pH 8.0), 0.25 % Xylene cyanol FF and 0.25 % Orange G) prior to loading. Agarose gels were routinely run in 1×TAE buffer (100 V, 30 min) to enable size separation of DNA molecules. CSL-MDNA-1KBPLUS (Cleaver Scientific) and Hyperladder IV (Bioline) were used as comparators to determine amplicon sizes. Agarose gels were stained with SYBR™ Safe DNA gel stain (Thermo Fisher Scientific) to visualise amplicons. Gels were imaged using either the ImageQuant™ LAS 4000 (GE Healthcare Life Sciences) or the safeVIEW-MINI2 Blue Light Transilluminator (Cleaver Scientific).

5. Purification of PCR products

PCR products, that were validated by electrophoresis, were routinely purified using PCR purification kits to remove excess primers and other PCR reactants. This was accomplished using the E.Z.N.A.® Cycle Pure Kit (Omega Bio-Tek). Two replicates of each reaction were pooled together to improve the yield of purified DNA. These samples were processed as outlined by the manufacturer's specifications (Omega Bio-Tek). The concentration of purified PCR products was measured using the Nanodrop™ (Thermo Scientific) before being stored at -20°C for further use.

6. *Dpn*I restriction digestions

The purified and linearised, PCR-amplified backbones of plasmids used for SLiCE cloning (**section 2.2**) were digested with Anza™ 10 *Dpn*I restriction enzyme (Thermo Fisher Scientific) to remove template plasmids. This involved incubating purified backbone PCR products (1 µg) with Anza™ 10× Buffer (1 µl), Anza™ 10 *Dpn*I (1 µl) and water (up to 10 µl) at 37°C for 2 h.

7. SLiCE cloning

The construction of plasmids used in this study was accomplished using the SLiCE cloning procedure (Zhang et al., 2014; Zhang, Werling, et al., 2012). Briefly, this involved recombination of PCR-amplified insert DNA fragments into linearised plasmid backbones. This was accomplished using ~20 bp of homology between the ends of the insert fragments and the plasmid backbone DNA. A control sample lacking insert DNA was included in each SLiCE reaction to ensure that template plasmids were fully digested by *Dpn*I. The reaction setup for this procedure is depicted in **Table 2.7**. These reaction mixtures were incubated at 37°C for 1 h and subsequently transformed into calcium competent *E. coli*.

Table 2.7 SLiCE reaction setup

Component	SLiCE reaction	SLiCE control
T4 DNA Ligase buffer (10×)	1 µl	1 µl
SLiC extract	1 µl	1 µl
PCR-amplified linearised plasmid	100 ng	100 ng
PCR-amplified insert DNA	100 ng	0 ng
Water	To 10 µl	To 10 µl
Total	**10 µl**	**10 µl**

8. Transformations of calcium competent *E. coli*

To prepare calcium competent *E. coli* TOP10 for transformations with plasmid DNA, a single colony of the desired *E. coli* strain was used to prepare an overnight culture tube. From this, a 1:1,000 dilution of the overnight culture (50 µl) was used to inoculate a 50 ml flask of L-broth. This culture was grown at 37°C until it reached the exponential phase of growth (OD_{600} = 0.4 – 0.8). The culture was centrifuged (4,000 rpm for 8 min at 4°C), and the pellet was resuspended in 40 ml ice-cold 0.1 M $CaCl_2$. The resuspended culture was kept on ice for 20 min before being centrifuged again under the same conditions. The pellet was resuspended in 10 ml ice-cold 0.1 M $CaCl_2$ and 1.15 ml of 87% (v/v) glycerol was added. This mixture was aliquoted (100 µl) in 1.5 ml Eppendorf tubes and stored at -80°C for later use. The aliquots of cells were thawed on ice, mixed with either plasmid DNA (~10 ng) or SLiCE cloning products (10 µl) and kept on ice for 10 min. After this,

these samples were heat-shocked in a water bath at 42°C for 2 min and placed back on ice for 2 min. The transformed cells were resuspended in 800 µl L-broth and incubated at 37°C for 90 min. These cells were subsequently centrifuged (11,000 × g for 1 min) and most of the supernatant was removed. The pellet was resuspended in the remaining supernatant and this was plated on L-agar plates containing the desired antibiotics. These samples were grown at 37°C overnight.

9. Transformations of electrocompetent *S.* Typhimurium

To prepare electrocompetent *S.* Typhimurium 4/74 for transformations with plasmid DNA, a single colony of the designated strain was used to inoculate an overnight culture tube of L-broth. From this, a 1:1,000 dilution of the overnight culture (25 µl) was used to inoculate a 25 ml flask of L-broth. This culture was grown at 37°C until it reached the exponential phase of growth (OD_{600} = 0.5). The culture was centrifuged (4,000 rpm, 8 min, 4°C). The resulting pellet was washed in 25 ml ice-cold sterile, deionised water and centrifuged again under the same conditions. This washing step was repeated, and the pellet was washed again in 10 ml ice-cold sterile, deionised water. The pellet was then resuspended in 300 µl sterile, ice-cold, 10% (v/v) glycerol and stored at -80°C for later use. Electrocompetent cells were thawed on ice, aliquoted (40 µl) and mixed with pP_L-Aar and pXG10-BfnH or pJV300 and pXG10-BfnH. These mixtures were transferred to electroporation cuvettes and electroporated in a Biorad GenePulser Xcell electroporator (2.5 kV, 25 µF, 200 Ω). The cells were resuspended in 1 ml of prewarmed L-broth (37°C) and transferred to 1.5 ml Eppendorf tubes. These tubes were incubated at 37°C for 1 h and plated on L-plates containing the desired antibiotics. These samples were grown at 37°C overnight.

10. Natural transformation of *A. baumannii*

To transform *A. baumannii* with plasmid DNA or chimeric PCR products (**section 2.4**), a previously described natural transformation protocol was employed (Godeux et al., 2020). Briefly, a single, opaque colony of the desired *A. baumannii* AB5075 strain was used to inoculate 2 ml L-broth in a test tube. This was grown at 37°C until it reached an

OD_{600} of ~1.0. This culture was then diluted to an OD_{600} of 0.01 in PBS. An aliquot (5 µl) of this dilution was mixed with plasmid DNA (~10 ng) or purified chimeric PCR products (5 µl). This mixture (2.5 µl) was used to inoculate 1 ml of *A. baumannii* transformation medium (2% Euromedex agarose D3, 5 g/L tryptone and 2.5 g/L NaCl), and this was incubated at 37°C overnight. The following day, *A. baumannii* cells were resuspended in PBS (100 µl) and plated on L-agar containing the required antibiotic. For the creation of clean deletion mutants (**section 2.4**), the transformation medium was incubated at 37°C for 6 h before cells were resuspended and plated on 20% (w/v) sucrose containing L-agar plates. These samples were grown at 30°C overnight.

11. Measurement of fluorescence

The fluorescence (arbitrary units) and optical density at a wavelength of 600 nm (OD_{600}) of cultures were measured in a Synergy H1™ Hybrid Multi-Mode microplate fluorometer. The fluorescence was measured using continuous orbital shaking and excitation at 485 nm and emission at 508 nm. The relative fluorescence of strains was calculated as follows:

$$Relative\ fluorescence = \frac{Fluorescence\ of\ sample}{Optical\ density\ of\ sample}$$

2.3 Hi-GRIL-seq in *A. baumannii* AB5075

1. Hi-GRIL-seq experiment

The Hi-GRIL-seq experiment used in this study was previously outlined (Hamrock et al., 2024). In short, single, opaque colonies of *A. baumannii* pVRL2Z-*t4rnlI* were used to prepare overnight cultures in L-broth. From this, a 1:1,000 dilution of the overnight culture (25 µl) was used to inoculate a 25 ml flask of L-broth. These cultures were grown at 37°C until they reached early stationary phase (OD_{600} = 2.0). After this, the cultures were incubated with 100 mM L-arabinose for 1 h to induce expression of T4 RNA ligase from pVRL2Z-*tr4rnlI*. RNA was isolated as outlined in **section 2.5**. Imipenem and

dipyridyl shocks were conducted by adding 16 μg/mL imipenem and 0.2 mM 2,2′-dipyridyl for 10 min before T4 RNA ligase induction. A T4 RNA ligase "non-induced" control was included. This involved growing cells to OD_{600} = 2.0 before incubating them for an hour without adding L-arabinose. Each condition was performed in biological duplicate.

2. Bioinformatic analysis of Hi-GRIL-seq

The library preparation for RNA-seq and the sequencing of RNA was conducted at Vertis Biotechnologie AG (Germany) as previously outlined (Hamrock, 2021). The assessment of sequencing read quality, mapping and visualisation was performed by Karsten Hokamp (Genetics Department, Trinity College Dublin). Briefly, the quality of sequencing reads was assessed using FastQC and short reads were trimmed using trim_galore and mapped against the *A. baumannii* reference genome, including three plasmids (NZ_CP008706.1, NZ_CP008707.1, NZ_CP008708.1, NZ_CP008709.1) using bowtie2 version 2.4.2 (Kröger et al., 2018; Langmead et al., 2012). The unaligned reads were used for detection of chimeric RNA molecules. This involved extracting 20 bp sequences from the start and end of the unaligned reads and mapping them against the genome using bowtie2. The chimeric RNA reads where one of the ends encoded a candidate sRNA and the other was a different annotated feature were selected. The steps involved in this analysis is available as a set of Perl scripts at: https://figshare.com/articles/software/chimera/24746625. Transcripts per million (TPM) values were calculated as previously described (Li et al., 2010). Chimeric RNA reads from all conditions were combined and sRNA-containing chimeras with under 10 sequencing reads were excluded from the analysis to reduce identification of transient or spurious sRNA-RNA interactions. The sRNA-containing chimeras with >10% of sequencing reads derived from the non-induced control group was also excluded from analysis. Figures describing the Hi-GRIL-seq results were prepared using Integrated Genomics Viewer (IGV, (Robinson et al., 2011)) and circlize package on R (Gu et al., 2014).

2.4 Genetic manipulations in *A. baumannii* AB5075

1. Generating deletion mutants

To functionally characterise the biological function of several genes, markerless deletion mutant strains were constructed in *A. baumannii* AB5075. These genes were deleted using a homologous recombination strategy (Godeux et al., 2020). Briefly, 2,000 nucleotides upstream and downstream of the target gene were amplified from gDNA. These upstream and downstream regions were fused to a *sacB-aacC4* cassette using overlap extension PCR. This cassette was previously amplified from the pMHL2 plasmid, it encodes SacB, a sucrose sensitive gene that acts as a counterselection marker, and AacC4, an apramycin resistance selection marker. Using natural transformation, this chimeric PCR fragment (~8 kbp) was transformed into *A. baumannii* AB5075. These transformants were plated on apramycin-containing L-plates to select for colonies containing the insertion mutant product. To obtain a markerless deletion, another chimeric PCR product (~4,000 bp) composed of only 2,000 nucleotides upstream and downstream of the target gene, was amplified by overlap extension PCR (primers P1 & P7 and P4 & P8). This chimeric PCR product was transformed into the corresponding insertion mutant strain through natural transformation and plated on 20% (v/v) sucrose-containing L-plates. The resulting colonies were screened for apramycin sensitivity and loss of the gene was confirmed by colony PCR and by Nanopore sequencing or Illumina sequencing (MicrobesNG).

2. Generating a chromosomal Aar seed region mutant (Aar*)

A seed region mutant strain of *A. baumannii* AB5075 (Aar*) was created by incorporating point mutations into the nucleotides responsible for Aar-mediated base-pairing on the chromosome using homologous recombination (Godeux et al., 2020). Briefly, a ~2,000 nucleotides amplicon composed of the upstream region of *aar* and a portion of *aar* containing the seed region was amplified with a primer that contained the *aar* seed region point mutation. Similarly, a ~2000 nucleotides amplicon composed of the downstream region and the *aar* gene was amplified with primers that contained the

aar seed region mutation. The upstream and downstream regions were fused by overlap extension PCR to create a ~4,000 nucleotide chimeric PCR product containing the *aar* seed region mutation (5′-CTCC-3′ → 5′-GTGG-3′). This chimeric PCR fragment was transformed into the Aar-insertion mutant deletion strain (*A. baumannii ΔaarC::sacB_aacC4*) by natural transformation. The transformants were plated on sucrose-containing L-plates as before and screened for apramycin sensitivity. The reintegration of the *aar* encoding locus with the seed region mutation was confirmed by colony PCR and by Sanger sequencing (Eurofins Genomics).

3. Generating chromosomal 3×FLAG fusions

Throughout this study, we constructed several chromosomal gene fusions to investigate the impact of sRNAs on protein steady state levels. This involved replacing stop codon of genes under investigation with a sequence encoding 3×FLAG. To create these strains, 3×*FLAG* from the pSUB11 plasmid was first amplified and cloned into the pMHL2 plasmid to create pMHL2-3×FLAG. The 3×*FLAG-sacB-aacC4* cassette was subsequently amplified from pMHL2-3×FLAG. Approximately 2,000 nucleotides upstream and downstream of the stop codon of the gene of interest were amplified from gDNA. A chimeric PCR product composed of 3×*FLAG-sacB-aacC4* cassette and the upstream and downstream regions of the gene of interest was created through overlap extension PCR. This chimeric PCR product was transformed into *A. baumannii* AB5075 and transformants were plated on apramycin-containing L-plates to select for colonies containing the insertion mutant product. Resulting colonies were subsequently screened for apramycin resistance and verified by colony PCR and Sanger sequencing (Eurofins Genomics). Positive colonies were screened by western blotting (**section 2.6**) to confirm that the 3×FLAG fusions were detectable.

2.5 Analysis of RNA

1. Isolation of RNA from *A. baumannii* AB5075

RNA was isolated from *A. baumannii* AB5075 using a TRIzol®-based approach (Kröger et al., 2013). Briefly, *A. baumannii* was grown to the desired growth phase (as determined by optical density). *A. baumannii* cells were routinely grown to mid exponential phase (OD_{600} = 0.3), late exponential phase (OD_{600} = 1.0), early stationary phase (OD_{600} = 2.0) and late stationary phase (growth after 16 h) in 25 ml L-broth prior to RNA isolation. Aliquots of *A. baumannii* cultures (equivalent to OD_{600} = 4.0) were taken and transcription was halted by addition of 2/5 of the culture volume of ice-cold "stop solution" (95% ethanol, 5% phenol) (Tedin et al., 1996). This mixture was incubated on ice for 30 min before centrifugation (3220 × g, 4°C, 10 min). Most of the supernatant was discarded, and the pellet was resuspended in the remained and transferred to a fresh 1.5 ml Eppendorf tube. After this, the tube was centrifuged (maximum speed, 4°C, 1 min). The supernatant was discarded, and the pellet was stored at -80°C for further processing. After thawing, the pellet was resuspended in 1 ml TRIzol® (Invitrogen) on ice, before being transferred to a 2 ml phase-lock gel tube (VWR). This was vigorously mixed with methanol (400 µl), incubated at room temperature for 5 min before being centrifuged at maximum speed for 15 min. The aqueous phase of the phase-lock tube was transferred to a new Eppendorf tube, mixed with isopropanol (400 µl) and incubated at room temperature for 30 min. The mixture was centrifuged (maximum speed, 30 min) and the pellet was washed in 70% (v/v) ethanol (350 µl). This was centrifuged (maximum speed, 10 min) and the RNA precipitate pellet was dried and covered in DEPC-treated water (20 µl). This tube was heated at 65°C for 5 min, and vortexed, to resuspend the RNA. The concentration of RNA was measured using the Nanodrop™ (Thermo Scientific) and quality was assessed using a Bioanalyser 2100 (Agilent) before being stored at -80°C for further use.

2. Generation of Digoxigenin-labelled riboprobes

Digoxigenin (DIG)-labelled, single-stranded RNA "riboprobes" were prepared for use in Northern blotting. These riboprobes were prepared by *in vitro* transcription using the DIG Northern Starter Kit (Roche) according to the manufacturer's specifications. A T7 RNA polymerase sequence was incorporated downstream of the designated sRNA to create DIG-labelled RNA complementary to the sRNA. This was accomplished by amplifying the sRNA encoding genes from gDNA using primers encoding the T7 RNA polymerase sequence (5′-GAATTAATACGACTCACTATA-3′). The purified PCR product (200 ng) was mixed with 10× labelling buffer (2 µl), 10× transcription buffer (2 µl), T7 RNA polymerase (2 µl) and DEPC-treated water (to 20 µl) and incubated 42°C for 1 h before addition of DNase I (2 µl) at 37°C for 15 min to remove template DNA. DNase I activity was halted with the addition of 17 mM EDTA pH 8.0. The riboprobe labelling efficiency was tested after this to determine the amount of riboprobe needed for Northern blotting. First, 10-fold dilutions of the riboprobe were made in DEPC-treated water and aliquots of each dilution (1 µl) were pipetted onto a Nylon membrane (Roche). This membrane was crosslinked in a BIO-LINK® crosslinker (Vilber Lourmat) at 120 mJ. The membrane was first washed in washing buffer for 5 min, blocked in 1× blocking buffer for 2 h and incubated with a 1:10,000 dilution of antidigoxigenin-AP Fab in 1× blocking buffer for 30 min. The membrane was then incubated in washing buffer for 5 min, twice, and detection buffer for 5 min before being covered in CDP-star (Applied Biosystems). Chemiluminescent imaging was performed using an ImageQuant LAS4000 imager (GE Healthcare). The decision to use diluted or undiluted riboprobe was made depending on the signal intensity of the serial dilutions.

3. Northern blotting

Northern blotting was performed using the DIG Northern Starter Kit (Roche) according to the manufacturer's specifications as previously described (Kröger et al., 2018). This involved heating 5 – 10 µg RNA at 65°C prior to loading on a denaturing, 7% v/v polyacrylamide gel (7.3 M urea, 1× TBE) along with RiboRuler LowRange RNA ladder (ThermoFisher Scientific) as a comparator. These RNA molecules were electrophoresed at 100 V for 2 h using 1× TBE buffer. The RNA was blotted onto a Nylon membrane

(Roche) using Biometra Fastblot B43 semi-dry blotting apparatus (Analytik Jena) at 125 mA for 30 min at 4°C. RNA was fixed to the membrane by using a BIO-LINK® crosslinker (Vilber Lourmat) at 120 mJ. The RNA ladder was cut from the rest of the membrane, stained in 2% methylene blue and washed in deionised water to visualise the ladder. The remainder of the membrane was prehybridised at 62°C for 1 h in an Enviro-Genie hybridisation oven (Scientific Industries) in pre-warmed DIG Easy Hyb buffer (Roche). Following this, 5 µl of undiluted riboprobe was boiled at 95°C for 5 min, placed on ice for 5 min, before being incubated with the membrane in DIG Easy Hyb buffer at 62°C overnight. The membrane was processed on an orbital shaker at room temperature. It was then washed in Stringency Wash Buffer I (5 min, twice) and in Stringency Wash Buffer II (15 min, twice) that were preheated to 65°C. After this, the membrane was washed in washing buffer (5 min), blocked in 1× blocking buffer (2 h) and incubated antidigoxigenin-AP Fab (1:10,000 dilution) containing 1× blocking buffer (30 min). The membrane was subsequently incubated in washing buffer (5 min, twice) and detection buffer (5 min) before being covered in CDP-star (Applied Biosystems) in plastic. The ladder was reattached to the membrane prior chemiluminescent imaging using an ImageQuant LAS4000 imager (GE Healthcare). A 5S rRNA riboprobe was used as a loading control (5 µl of 1:10 diluted riboprobe). The composition of all Northern buffers and solutions is listed in **Table 2.8**.

Table 2.8 Northern blotting buffers

Solution	Reagent	Concentration
Maleic acid buffer pH 7.5	Maleic acid	0.1 M
	NaCl	0.15 M
Washing buffer	Maleic acid buffer pH 7.5	1×
	Tween-20	0.3% (v/v)
20× SSC	Sodium citrate	0.3 M
	NaCl	3 M
Stringency wash buffer I	SSC	2×
	SDS	0.1 % (v/v)
Stringency wash buffer II	SSC	0.5×
	SDS	0.1 % (v/v)
Blocking buffer	Casein Blocking Solution (Roche)	1×
	Maleic acid buffer pH 7.5	1×
Detection buffer pH 9.5	Tris-HCl	0.1 M
	NaCl	0.1 M

4. Northern blotting quantification

The band intensities observed in the Northern blotting experiments were quantified using ImageJ (Schneider et al., 2012). The average pixel intensity of the sRNA samples and the average pixel intensity of the background (membrane with no sample) were measured. The adjusted pixel intensity of the sRNA samples was calculated by subtracting the background intensity from the sample, as detailed in the following equation:

$$Adjusted\ sRNA\ intensity = sRNA\ intensity - background\ intensity$$

The adjusted 5S rRNA band intensity was measured in the same manner. The expression of the sRNA relative to the 5S rRNA loading control was calculated, as detailed in the following equation:

$$Relative\ sRNA\ expression = \frac{Adjusted\ sRNA\ intensity}{Adjusted\ 5S\ rRNA\ intensity}$$

The fold change in sRNA expression was then calculated in a target sample relative to a control sample (generally the wildtype strain). The control sample is indicated in each experiment. A value greater than 1.0 indicates that the target sample was upregulated compared to the control sample, while conversely, a value less than 1.0 indicates that the target sample was downregulated compared to the control sample. The fold change in expression was calculated as detailed in the following equation:

$$Fold\ change = \frac{Relative\ expression_{target}}{Relative\ expression_{control}}$$

5. *In vitro* transcription and radiolabelling of RNA

In vitro transcription was used to create templates of Aar/Aar* that were used for radiolabelling with phosphorus-32 (^{32}P). This was performed as previously described (Ryan et al., 2020). First, T7 promoter encoding primers were used to amplify the *aar*/*aar** loci from gDNA. The Aar* mutant was constructed using overlap extension PCRs to create point mutations in the predicted seed region (CUCC → GUGG, positions 29-32). After this, *in vitro* transcription was performed using the MEGAscript™ T7 kit (Invitrogen). Template DNA was removed with DNase I (1 U, 37°C, 15 min). The *in vitro* transcription products were separated by electrophoresis on a 6% (v/v) polyacrylamide gel (7M urea, 1× TBE) along with a LowRange RNA ladder (ThermoFisher Scientific) for size comparison. The bands at anticipated sizes were excised from the gel and segmented before being suspended overnight in RNA elution buffer (0.1 M NaOAc, 0.1% SDS, 10 mM EDTA) at 8°C and shaking at 1,400 rpm. The RNA was precipitated in in ethanol:NaOAc (30:1), before being washed with 75% ethanol and eluted in 20 µl DEPC-treated water (Fisher). For radiolabelling, the *in vitro* transcribed Aar/Aar* (50 pmol) was first dephosphorylated with 25 U of calf intestine alkaline phosphatase (Invitrogen) at 37°C for 1 h and extracted with phenol:cholorform:isoamylalcohol (P:C:I, 25:24:1). The dephosphorylated RNA (20 pmol) was 5′-labelled (20 µCi of 32P-γATP) with 1 U of polynucleotide kinase (NEB) for 1 h at 37 °C. Radiolabelled RNA was run on a G-50 column (GE Healthcare) and extracted from a polyacrylamide gel as above.

6. Electrophoretic motility shift assays

Electrophoretic motility shift assays (EMSAs) were performed as previously described (Ryan et al., 2020). This involved incubating 5′-radiolabelled Aar/Aar* RNA (4 nM) with 1× structure buffer (Ambion), 1 µg yeast RNA and putative mRNA interaction partners at the following concentrations: 0 nM, 16 nM, 32 nM, 62.5 nM, 125 nM, 250 nM, 500 nM and 1000 nM, for 1 h at 37°C. Following this, 3 µl of 5× native loading dye (0.5× TBE, 0.2% (w/v) bromophenol blue, 50% (v/v) glycerol) was added to each reaction and the entire volume of each sample was loaded on a 6% (v/v) native polyacrylamide gel and electrophoresed in 0.5× TBE buffer (4°C, 3 hours, 300V). Following this, the native gels were dried on 3 mm filter paper (Whatman) using a vacuum pump and exposed to a phosphor screen overnight. The phosphor screens were imaged using a phosphorimager (Typhoon™ FLA 7000, GE Healthcare).

7. In-line probing

In-line probing was performed by incubating 0.2 pmol 5′-radiolabelled Aar/Aar* RNA in 1× in-line probing buffer (50 mM Tris-HCl, pH 8.3, 100 mM KCl, 20 mM MgCl2) with the following concentrations of putative mRNA targets; 0 pmol, 0.2 pmol and 2 pmol, at room temperature for 40 h as previously described (Ryan et al., 2020; Sharma et al., 2007). The reactions were mixed with 10 µl 2× colourless gel-loading solution (10 M urea, 1.5 mM EDTA, pH 8.0). The uncleaved Aar/Aar* control ladders were prepared by mixing 0.2 pmol of their respective radiolabelled RNA with 10 µl 2× colourless gel-loading solution. To prepare the RNase T1 ladder, 0.4 pmol of the radiolabelled Aar/Aar* molecules were first denatured with 8 µl of 1× sequencing buffer (Ambion) at 95°C for 1 min. After being cooled at 37°C for 5 min, 1 µl of RNase T1 (0.1 U/µl) was added and samples were incubated at 37°C for 5 min. The alkaline hydrolysis ladder was prepared by incubating 0.4 pmol of radiolabelled Aar/Aar* with 9 µl alkaline hydrolysis buffer (Ambion) and this was incubated at 95°C for 5 min. These ladders were also mixed with colourless gel-loading solution prior to loading. All the samples and ladders were subsequently loaded and ran on a 10% (v/v) polyacrylamide gel (7M urea). Following this, the in-line probing gels were dried on 3 mm filter paper (Whatman) using a vacuum

pump and exposed to a phosphor screen overnight. The phosphor screens were imaged using a phosphorimager (Typhoon™ FLA 7000, GE Healthcare) as before.

2.6 Analysis of proteins

1. Preparation of whole cell lysates

Protein whole cell lysates were isolated from *A. baumannii* AB5075 by growing 25 ml cultures at 37°C to the desired growth phase. *A. baumannii* cells were routinely grown to late stationary phase (growth after 16 h) prior to isolating whole cell lysates. To prepare whole cell lysates, *A. baumannii* cells (equivalent to OD_{600} = 0.1) were collected by centrifugation in Eppendorf tubes (1.5 ml), this was performed at 2,500 x g for 5 min at 4°C. The resulting pellets were washed twice in PBS and collected by centrifugation again using the same conditions. The pellets were resuspended in 1× Lämmli buffer and heated at 95°C for 10 min. These tubes were centrifuged again at maximum speed at 4°C for 1 min. The whole cell lysates were used directly for western blotting or stored at -20°C for later use.

2. Western blotting

Western blotting was performed as previously described (Reference). This involved separating whole lysates (0.03 OD_{600} units per lane) on a discontinuous SDS-polyacrylamide gel. The gel was composed of a stacking layer (5% polyacrylamide) and a separating layer (15% polyacrylamide). The whole cell lysates were electrophoresed along with EZ-Run™ Prestained Rec Protein Ladder (Fisher Scientific) to act as a comparator. The gels were run at 80 V until the dye front entered the separating layer. After this, the gels were run at 120 V until the dye front reached the bottom of the separating layer. The gels were subsequently washed with deionised water and equilibrated in 1× transfer buffer (25 mM Tris, 0.19 M glycine) for 10 min along with 0.45 µm Amersham™ Protran® nitrocellulose membranes (Merck) and 3 mm filter paper (Whatman). These components were assembled into sandwiches" in gel holder cassettes and proteins were blotted (300 mA, 90 min) onto the nitrocellulose membranes using a

Mini Trans-Blot Electrophoretic Transfer Cell (Bio-Rad) with an ice pack. Following blotting, even transfer of proteins on membranes was routinely assessed by staining the membranes in Ponceau S (Sigma) until bands became visible. After this, membranes were washed in deionised water to remove Ponceau S staining, the membranes were then blocked (2 h) in blocking buffer (5% (w/v) skimmed milk powder, 0.9% (w/v) NaCl and 10 mM Tris/HCl pH 7.5) to prevent non-specific binding of antibodies. The membranes were also washed (10 min, twice) in antibody buffer (0.5% (w/v) skimmed milk powder, 0.9% (w/v) NaCl, 0.1% (v/v) Tween-20 and 10 mM Tris/HCl pH 7.5). The membranes were washed in antibody buffer containing primary antibodies (anti-FLAG (Sigma), diluted 1:10,000; anti-DnaK (*E. coli*, Enzo), diluted 1:5,000) at 4°C overnight. Membranes were subsequently washed (10 min, four times) in PBST (PBS and 0.05 % (v/v) Tween-20). Following this, membranes were washed (90 min) in antibody wash containing the secondary antibody (anti-Mouse IgG Fc, horseradish-peroxidase (Thermo Fisher Scientific), diluted 1:10,000). Membranes were washed (10 min, three times) in PBST, covered in ECL chemiluminescent HRP substrate (Pierce). Chemiluminescent imaging was performed using an ImageQuant LAS4000 imager (GE Healthcare) as before.

3. Western blotting quantification

The band intensities observed in the western blotting experiments were quantified using ImageJ (Schneider et al., 2012). The average pixel intensity of the 3×FLAG fusion bands and the average pixel intensity of the background (membrane with no sample) were measured. The adjusted pixel intensity of the 3×FLAG fusion samples was calculated by subtracting the background intensity from the sample, as detailed in the following equation:

$$Adjusted\ 3 \times FLAG\ intensity = 3 \times FLAG\ intensity - background\ intensity$$

The adjusted DnaK loading control band intensity was measured in the same manner. The expression of the 3×FLAG protein relative to DnaK was calculated, as detailed in the following equation:

$$Relative\ 3 \times FLAG\ expression = \frac{Adjusted\ 3 \times FLAG\ intensity}{Adjusted\ DnaK\ intensity}$$

The fold change in 3×FLAG protein expression was then calculated in a target sample relative to a control sample (generally the wildtype strain). The control sample is indicated in each experiment. A value greater than 1.0 indicates that the target sample was upregulated compared to the control sample, while conversely, a value less than 1.0 indicates that the target sample was downregulated compared to the control sample. The fold change in expression was calculated as detailed in the following equation:

$$Fold\ change = \frac{Relative\ expression_{target}}{Relative\ expression_{control}}$$

Chapter 3 – Hi-GRIL-seq enables global analysis of the *A. baumannii* AB5075 RNA-RNA interactome

3.1 Introduction:

The characterisation of bacterial sRNAs and their targets is a notoriously laborious and painstaking process (Ahmed et al., 2018). Identification of functional regulatory sRNAs was accomplished by linking a phenotypic observation to overexpression an sRNA under investigation (Argaman et al., 2001). This allowed researchers to infer their mRNA interaction partners. While this strategy vastly improved our understanding of bacterial gene expression, it was serendipitous and did not consider the toxicity or the unclear phenotypes that sRNA overexpression may have. The advent of high throughput RNA sequencing has streamlined the identification of sRNA-mRNA interactions in prokaryotic species (Carrier et al., 2016; Lalaouna et al., 2015; Waters et al., 2017). The ligation of sRNAs to their cognate mRNA targets to form sRNA-mRNA chimeric RNA coupled with RNA-seq has, in particular, facilitated discovery of these interactions (Fuchs et al., 2023; Gebhardt et al., 2023; Melamed et al., 2016). While most of these proximity ligation procedures are reliant on the co-immunoprecipitation of RNA molecules with the corresponding RBPs, **hi**gh throughput **g**lobal s**R**NA target **i**dentification by **l**igation and **seq**uencing (Hi-GRIL-seq) has enabled identification of sRNA-mRNA interactions independently of RBPs (Zhang et al., 2017). Hi-GRIL-seq involves inducing expression of T4 RNA ligase *in vivo* to ligate sRNA molecules to interacting RNAs. By sequencing the resulting RNA-RNA chimeras, the sRNAs. "interactome" can be determined. Hi-GRIL-seq was successfully used to investigate RNA-RNA interactions in *P. aeruginosa* and in *Vibrio cholera* (Dunham et al., 2023; Zhang et al., 2017). We employed Hi-GRIL-seq to perform a genome-wide analysis of the *A. baumannii* AB5075 sRNA interactome. This allowed us to circumvent the uncertain role that the RBP Hfq mediates in sRNA-mRNA annealing in *Acinetobacter* species (Schilling et al., 2009). In this chapter, I outline how the Hi-GRIL-seq experiment was conducted and how the resulting chimeric sequencing reads were processed to find novel sRNA interactions. The Hi-GRIL-seq experiment was first analysed in my master's thesis, however, this analysis was improved and extended for my PhD (Hamrock, 2021). This chapter marks the first characterisation of sRNA-mRNA interactions in *A. baumannii*.

3.2 Induction of *A. baumannii* with 100 mM L-arabinose is sufficient for RNA-RNA ligations:

Prior to performing the Hi-GRIL-seq experiment, the impact of T4 RNA ligase expression on *A. baumannii* cell survival was determined. Since the accumulation of RNA-RNA ligations is lethal to bacterial cells, a reduction of *A. baumannii* growth is reflective of the expression of T4 RNA ligase. Carsten Kröger placed expression of the T4 RNA ligase encoding gene (*t4rnlI*) under control of the L-arabinose inducible P_{BAD} promoter on the pVRL2Z plasmid (pVRL2Z-*t4rnlI*) (Lucidi et al., 2018). He then measured impact of different concentrations of L-arabinose on *A. baumannii* viability. This was accomplished by measuring the optical density of overnight cultures of *A. baumannii* expressing the control plasmid (pVRL2Z) or pVRL2Z-*t4rnlI* that were incubated with L-arabinose (Hamrock, 2021). This allowed him to identify that 100 mM L-arabinose was a concentration sufficient for T4 RNA ligase induction. To ensure that induction with this concentration L-arabinose could reliably reduce cell survival, I measured *A. baumannii* cell survival. This involved calculating the colony forming units per ml (CFU/ml) of the culture that could be recovered after induction. This was performed by imitating the Hi-GRIL-seq experiment setup (**section 3.2**). *A. baumannii* cultures expressing pVRL2Z and pVRL2Z-*t4rnlI* were grown to early stationary phase (ESP, OD_{600}=2.0). They were then induced without (0 mM) or with (100 mM) L-arabinose for 1 hour. The induction of *A. baumannii* AB5075 carrying the pVRL2Z-*t4rnlI* plasmid with 100 mM L-arabinose significantly reduced viability compared to non-induced version ($p=0.01$) and to induced and non-induced cultures of *A. baumannii* AB5075 carrying the pVRL2Z plasmid ($p<0.05$). This is shown in **Figure 3.1**. This demonstrated that 100 mM L-arabinose minimises lethality of *A. baumannii* AB5075 while still being sufficient for RNA-RNA ligation.

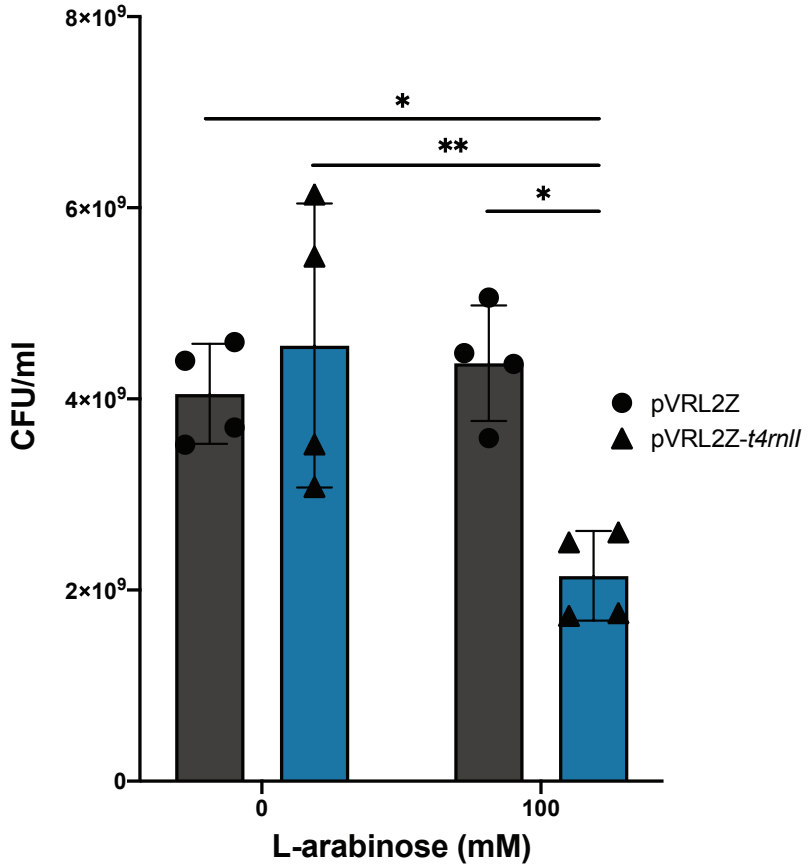

Figure 3.1 Viability experiment identifies that 100 mM L-arabinose reduces *A. baumannii* cell density without causing excessive cell death.

Colony forming units (CFU/ml) of strains carrying the pVRL2Z-*t4rnlI* plasmid and strains carrying the empty control vector (pVRL2Z) plasmid were measured following 1 h induction with 100 mM L-arabinose once the cultures reached ESP. Error bars represent the standard deviation from four independent biological replicates. Statistical comparisons were performed using Two-way ANOVA followed by Tukey's multiple comparisons test. Differences were considered statistically significant where * denotes P<0.05, ** denotes P<0.01, *** denotes P<0.001 and **** denotes P<0.0001.

3.3 Hi-GRIL-seq experimental setup:

To identify the *A. baumannii* AB5075 sRNA interactome and to characterise biologically important sRNA-mRNA interactions in this pathogen, we performed the Hi-GRIL-seq experiment. This sequencing experiment was performed by Carsten Kröger prior to the commencement of my Masters project and the full details regarding this experimental setup were first described in my master's thesis (Hamrock, 2021). The experimental procedures used for Hi-GRIL-seq are depicted as a schematic in **Figure 3.2**. Briefly, cultures of *A. baumannii* expressing pVRL2Z-*t4rnlI* were grown to ESP and ectopic expression of T4 RNA ligase was induced through incubation with 100 mM L-arabinose

for 1 hour. A control where cells were grown to ESP and incubated for 1 hour without L-arabinose ("non-induced control", NI) was included. Since sRNAs are frequently activated when the bacteria encounters stressful environmental conditions, we also subjected cultures to brief 10 minute stress conditions prior to T4 RNA ligase induction (Holmqvist et al., 2017). As carbapenem-resistant *A. baumannii* pose a significant threat to global health, we subjected *A. baumannii* to the beta-lactam antibiotic imipenem (IMIP) for 10 minutes prior to addition of L-arabinose (Hamidian et al., 2019; Tacconelli et al., 2018). As *A. baumannii* must overcome host driven iron limitation during infection, we mimicked the deprivation of iron in the culture by adding the iron chelator 2,2′-dipyridyl (DIP) prior to induction. An unshocked, L-arabinose induced culture (IND) was also included as a positive control. These experimental treatments were performed in biological duplicate (n=2). All the conditions used in the Hi-GRIL-seq experiment are summarised in **Table 3.1**:

Table 3.1 Conditions used in Hi-GRIL-seq

Name	Abbrev.	Stressor	Induced with 100 mM L-arabinose?
Non-induced control	NI	None	No
Induced sample	IND	None	Yes
Iron starvation	DIP	0.2 mM 2,2′-dipyridyl	Yes
Imipenem shock	IMIP	16 μg/mL imipenem	Yes

Following this, the *A. baumannii* cultures were lysed and the total RNA from the samples was isolated and used to construct cDNA libraries for RNA-sequencing.

3.4 Analysis of Hi-GRIL-seq derived RNA-RNA chimeras:

A prior Hi-GRIL-seq analysis of *P. aeruginosa* suggested that only a small fraction of the sequencing reads would be chimeric (Zhang et al., 2017). To improve detection of chimeric sequencing reads, we increased the sequencing depth beyond typical bacterial transcriptomic experiments. This enabled us to obtain >77 million sequencing reads per library. Trimmed the sequencing reads were mapped to the *A. baumannii* AB5075

genome to calculate the abundance of reads mapping to and outside of annotated features (**Figure 3.3**).

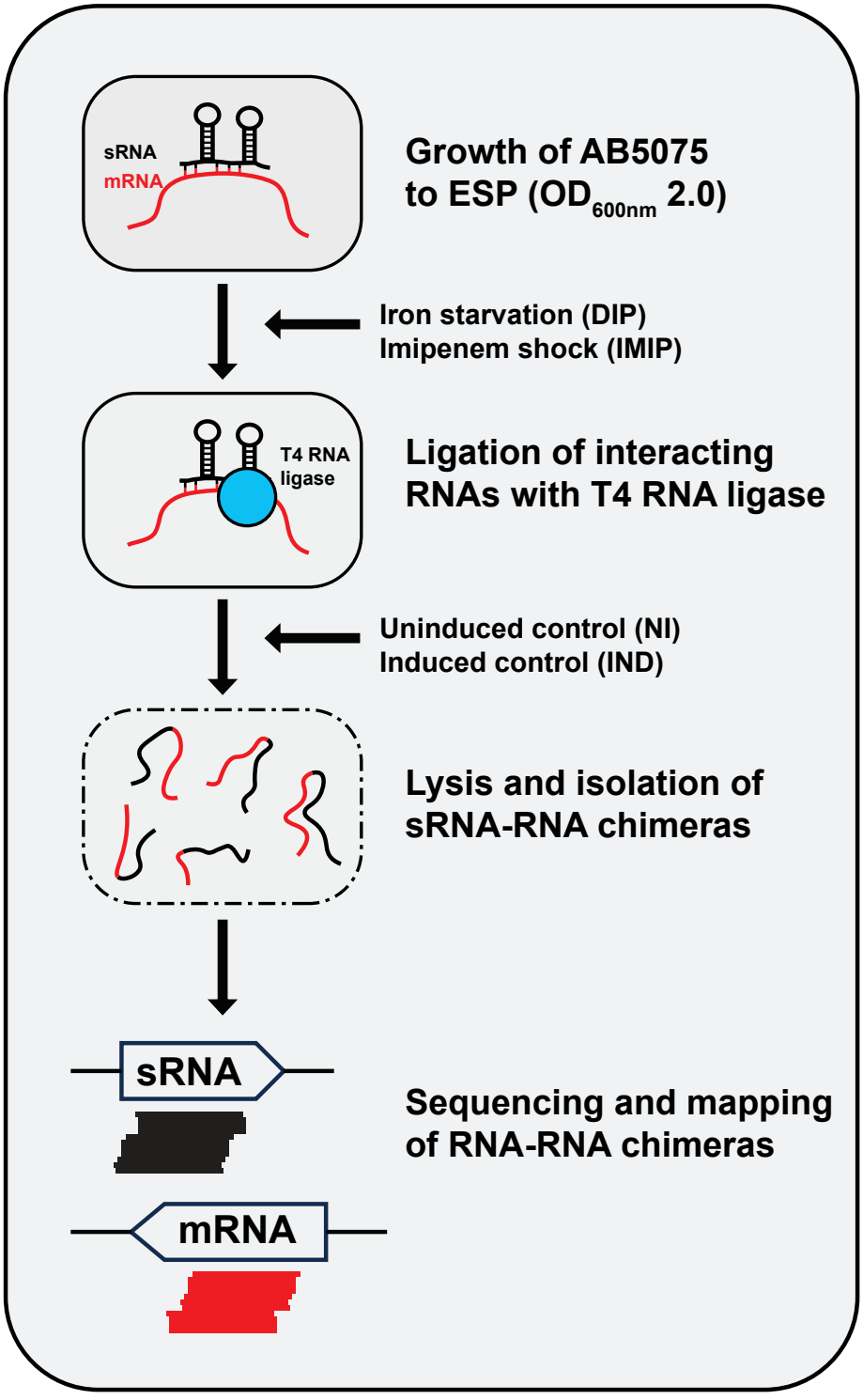

Figure 3.2 Schematic outlining the Hi-GRIL-seq protocol.

A. baumannii cells at early stationary phase (ESP) were shocked with 2,2′-dipyridyl (iron starvation, DIP) or imipenem (IMIP). T4 RNA ligase was induced in these samples by addition of L-arabinose. Both induced and uninduced control samples were also included. The *A. baumannii* cells were then lysed and RNA molecules were isolated and sequenced. Chimeric RNA-RNA sequences containing sRNAs were then identified.

Table 3.2 Number of RNA species sequencing reads detected in Hi-GRIL-seq

RNA species	DIP-1	DIP-2	IMIP-1	IMIP-2	IND-1	IND-2	NI-1	NI-2
mRNA	52,025,041	56,916,042	55,102,716	57,939,373	56,419,452	57,620,063	49,574,560	49,904,086
Rnase P RNA	128,558	195,476	137,562	148,273	182,167	216,948	114,691	163,784
CRISPR	5,542	6,049	5,735	5,909	6,676	6,624	6,726	7,365
Pseudogene	68,864	70,601	78,848	72,990	83,433	82,262	57,716	83,864
rRNA	323,179	210,949	111,165	101,692	191,425	184,889	82,233	172,098
Riboswitch	18,820	21,327	14,849	14,385	21,293	18,000	17,134	16,403
sRNA	4,012,086	4,632,735	5,700,008	5,643,120	6,336,995	5,798,985	10,722,923	18,985,097
tRNA	323,971	372,754	784,193	582,403	743,796	703,106	280,502	619,125
Unmapped	13,686,065	12,194,835	11,742,835	11,534,914	14,651,194	13,549,949	8,060,235	8,446,076
Antisense	3,645,026	3,150,220	2,686,941	2,489,675	3,016,083	2,670,149	2,447,638	3,574,547
Intergenic	5,881,929	6,262,108	4,855,523	5,755,835	6,827,144	6,635,011	6,149,214	5,611,515
Total	**80,119,081**	**84,033,096**	**81,220,375**	**84,288,569**	**88,479,658**	**87,485,986**	**77,513,572**	**87,583,960**

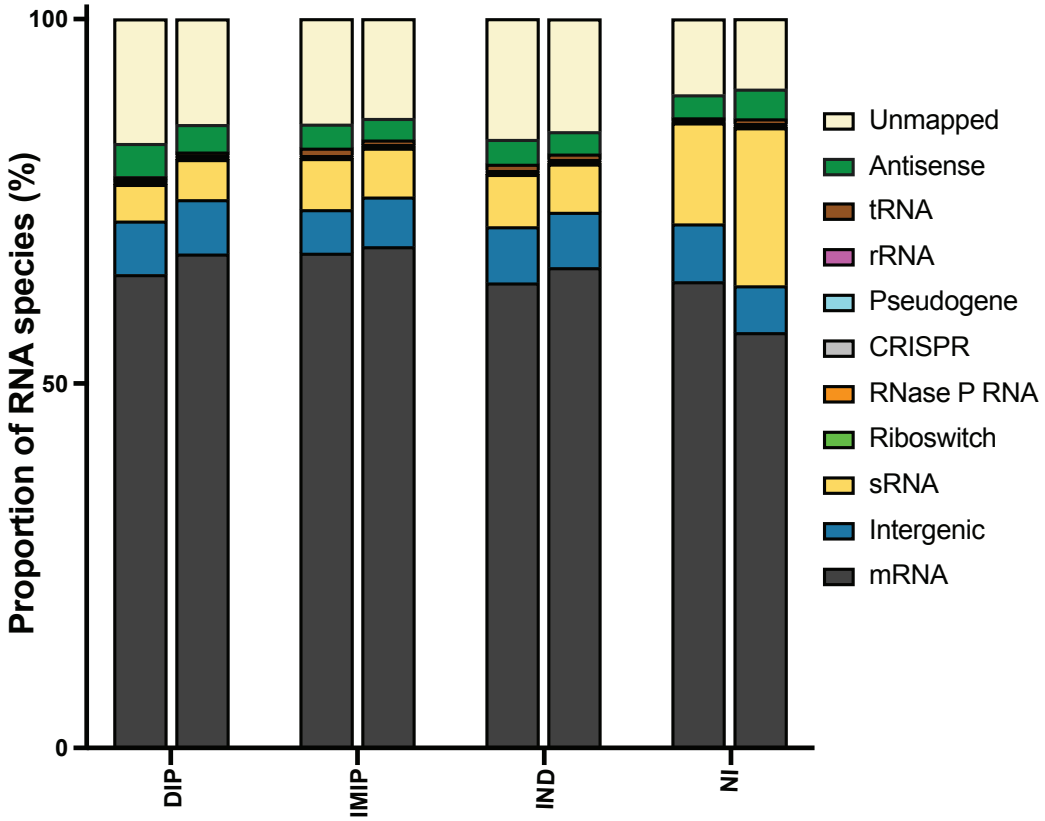

Figure 3.3 The percentage of RNA species identified by Hi-GRIL-seq in iron starvation (DIP), imipenem shock (IMIP), the induced sample (IND) and the uninduced negative control (NI) treatment conditions.

Results from independent biological duplicates of each treatment condition is visualised as adjacent bars. The sum of the RNA species percentage is >100% due to the presence of sequencing reads derived from regions with overlapping annotations.

More than 82% of the reads in each Hi-GRIL-seq condition mapped to the genome, suggesting that these reads were non-chimeric. To identify the chimeric reads, the first and last 20 nucleotides of unmapped reads were separately aligned to the *A. baumannii* AB5075 genome. On average, that there was a slightly higher number of chimeric reads in the induced samples (IND, DIP, IMIP, 0.9-1.4%) than in the non-induced control (0.8-0.9%) suggesting that the induction of T4 RNA ligase did improve RNA-RNA ligation. It should be noted that the identification of chimeric molecules in the negative control group indicates that basal expression of T4 RNA ligase was driven from P_{BAD} even in the absence of L-arabinose. The total number of trimmed, mapped, unmapped and chimeric sequencing reads are depicted in **Table 3.3**:

Table 3.3 Number of Hi-GRIL-seq sequencing reads

Sample	Trimmed reads	Mapped reads	Unmapped reads	Chimeric reads
DIP-1 (iron starvation, rep 1)	80,066,010	66,379,944	13,686,065	1,055,475
DIP-2 (iron starvation, rep 2)	83,974,370	71,779,534	12,194,835	882,759
IMIP-1 (imipenem shock, rep 1)	81,151,404	69,408,568	11,742,835	799,707
IMIP-2 (imipenem shock, rep 2)	84,224,000	72,689,085	11,534,914	767,536
IND-1 (induced control, rep 1)	88,400,835	73,749,640	14,651,194	1,148,934
IND-2 (induced control, rep 2)	87,412,204	73,862,254	13,549,949	1,189,429
NI-1 (uninduced control, rep 1)	77,471,916	69,411,680	8,060,235	600,895
NI-2 (uninduced control, rep 2)	87,519,423	79,073,346	8,446,076	781,147

The proportion of these sequencing reads is shown in **Figure 3.4**. To identify likely sRNA-mRNA interactions, we identified the chimeric sequencing reads that contained an annotated sRNA on one end and another genomic feature on the other. Between 3.5-5.5% chimeric sequencing reads derived from the IND, DIP and IMIP conditions contained a sRNA-encoding sequence. The number of total sRNA-containing chimeric sequencing reads in each conditions is listed in **Table 3.4**. In total, we detected that 86 sRNAs identified in *A. baumannii* AB5075 in sRNA-containing chimeras.

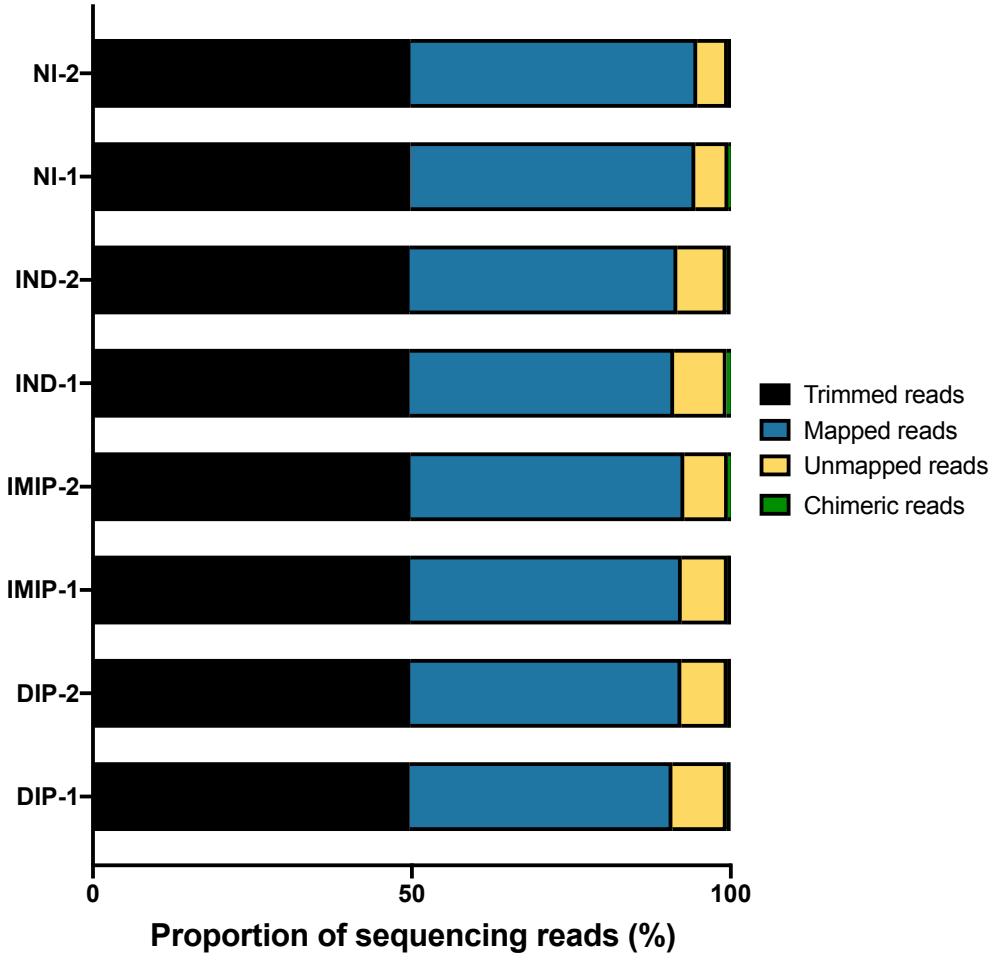

Figure 3.4 The percentage of RNA sequencing reads identified by Hi-GRIL-seq in iron starvation (DIP), imipenem shock (IMIP), the induced sample (IND) and the uninduced negative control (NI) treatment conditions.

Results from independent biological duplicates of each treatment condition are visualised as bars. The percentages of trimmed reads, mapped reads, unmapped reads and chimeric sequencing reads identified in each treatment condition are shown.

Table 3.4 Number of sRNA-containing chimeric sequencing reads

Sample	sRNA-containing chimeric reads
DIP-1 (iron starvation, rep 1)	37,333
DIP-2 (iron starvation, rep 2)	38,138
IMIP-1 (imipenem shock, rep 1)	30,292
IMIP-2 (imipenem shock, rep 2)	31,761
IND-1 (induced control, rep 1)	60,702
IND-2 (induced control, rep 2)	65,820
NI-1 (uninduced control, rep 1)	57,581
NI-2 (uninduced control, rep 2)	64,730

To help visualise global sRNA-RNA interactions in *A. baumannii* AB5075, the genomic locations of sRNA-containing chimeric reads with ≥50 sequencing reads were mapped to the chromosome as shown in **Figure 3.5**. Each individual sRNA-containing chimera is represented as a dot where the 5′ end of each chimeric fragment was mapped to the x-axis, while the 3′ end of each chimeric fragment was mapped to the y-axis. This is shown separately for each Hi-GRIL-seq treatment condition.

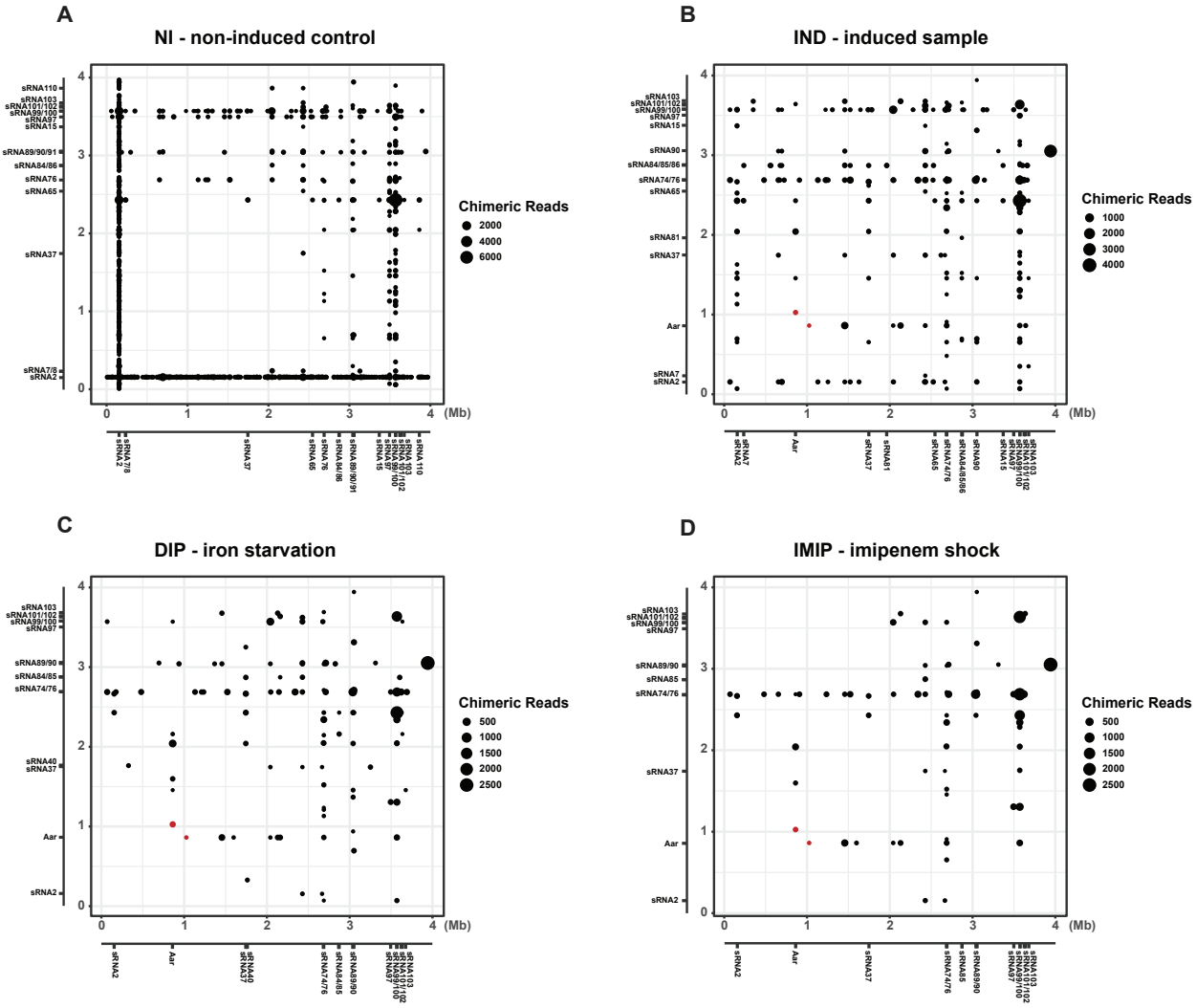

Figure 3.5 Global identification of sRNA-RNA interactions identified by Hi-GRIL-seq in *A. baumannii* AB5075 in different conditions.

The genomic locations of sRNA-containing chimeric reads ≥50 sequencing reads were mapped to the AB5075 chromosome in the (A) T4 RNA ligase uninduced (NI) control condition, (B) T4 RNA ligase induced (IND) condition, (C) iron starvation (DIP) condition and (D) imipenem shock (IMIP) condition. The x-axis represents the 5′ end of each chimeric fragment while the y-axis represents the 3′ end of the fragment. Each dot represents the exact genomic coordinate of these fragments. The size of the dot is proportional to the number of sequencing reads observed. The location of all sRNA candidates contained within RNA-RNA chimeras are shown.

Some sRNAs, particularly sRNA2, were overrepresented in the non-induced control condition (NI) compared to the induced samples (IND, DIP and IMIP). This could be explained by higher expression of sRNA2 in the NI sample than in the over samples, where it has ~5.5-fold increase in transcript per million (TPM) values (**Table 3.5**). It could also be due to basal expression of T4 RNA ligase driven from the P_{BAD} promoter in the NI condition.

Table 3.5 sRNA2 TPM values per condition

sRNA	DIP-1	DIP-2	IMIP-1	IMIP-2	IND-1	IND-2	NI-1	NI-2
sRNA2	16,666.80	19,424.10	64,203.30	57,942.10	38,614.90	39,019.80	168,002.30	276,490.80

While the high abundance of sRNA2 in the NI condition could explain the detection of numerous chimeras in this control group, the possibility that sRNA2-containing chimeras could represent authentic sRNA2-mRNA interactions cannot be discounted. It is also clear from this that numerous chimeric reads that were not detected in the non-induced control group were detected in the induced samples. Examples of this are shown by Aar (sRNA21) and sRNA40. It is worth noting that a greater diversity of RNA molecules were detected in sRNA-containing chimeric reads in the IND sample than in the DIP or IMIP samples. The sRNA-containing chimeras were broadly distributed across the AB5075 genome. An example of this for Aar (sRNA21) is illustrated in **Figure 3.6**.

3.5 Filtering chimeric Hi-GRIL-seq reads:

It is evident from **Figure 3.5** that there is a large number of sRNA-RNA ligations derived from the non-induced control condition. The basal expression of T4 RNA ligase could be overrepresenting interactions where the sRNA and RNA molecule are only transiently in close physical proximity that may not be interacting or that only temporarily interact. These potential temporary interactions are unlikely to have dramatic physiological consequences in the biology *A. baumannii*. To reduce the impact that such transient events exert on the Hi-GRIL-seq dataset and to improve the chances of identifying *bona fide*, functional base-pairing interactions, the sRNA-containing chimeras were filtered. Prior to filtering, the number of sequence reads for each sRNA-containing chimera was combined between biological replicates and treatment conditions to maximise the total

number of chimeras observed. When filtering, we excluded sRNA-containing chimeras that were scarce or that were overrepresented in the non-induced control condition. The sRNA-containing chimeras with <10 sequencing read and those with >10% of sequencing reads obtained from the non-induced control were removed from further analysis. After applying these cut-off scores, the number of AB5075 sRNAs represented in sRNA-containing chimeras reduced from 86 to 40. Using this approach, 632 distinct chromosomal sRNA-containing chimeras and 74 distinct sRNA-containing chimeras ligated to plasmid RNA were identified. The identities and number of chimeric sequencing reads detected after applying these cut-off scores for both chromosomal and plasmid RNA is listed in **Appendix II**. The entire filtered *A. baumannii* AB5075 chromosomal sRNA interactome is visualised in **Figure 3.7**.

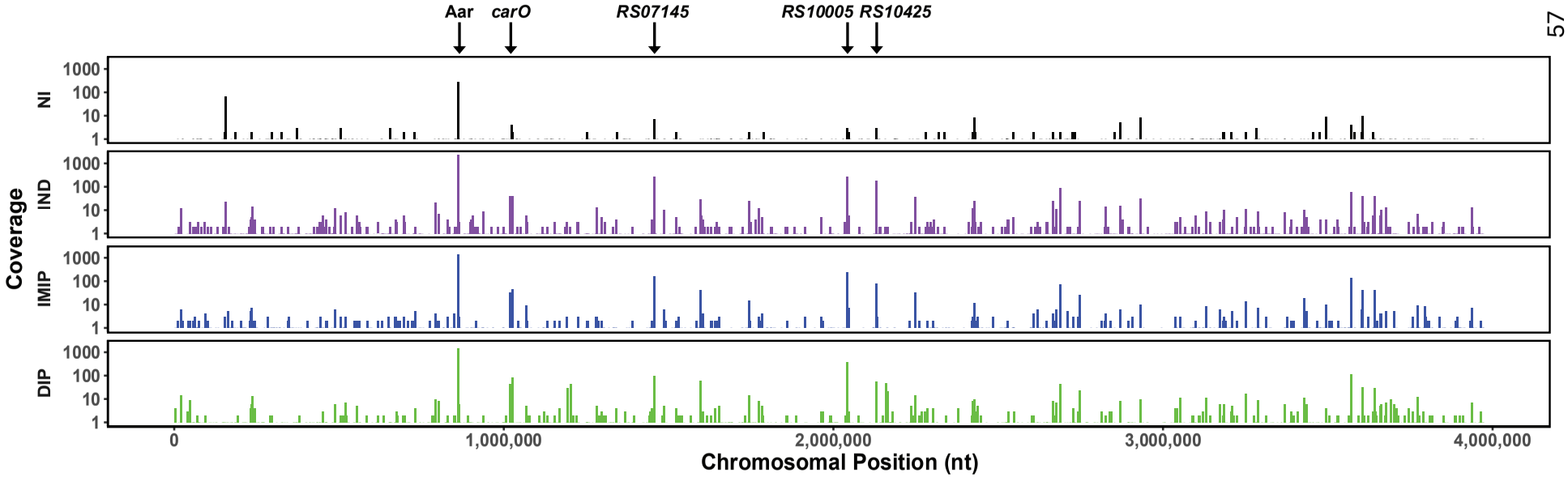

Figure 3.6 Mapped reads of Aar-containing chimeric sequencing reads across the *A. baumannii* AB5075 chromosome.

Mapped reads were prepared by combining the chimeric sequencing reads from treatment condition replicates. Lines indicate the location and abundance of the chimeric junctions. The most abundant mRNA interaction partners ligated within sRNA-containing chimeras are indicated. Figure was prepared by Aalap Mogre.

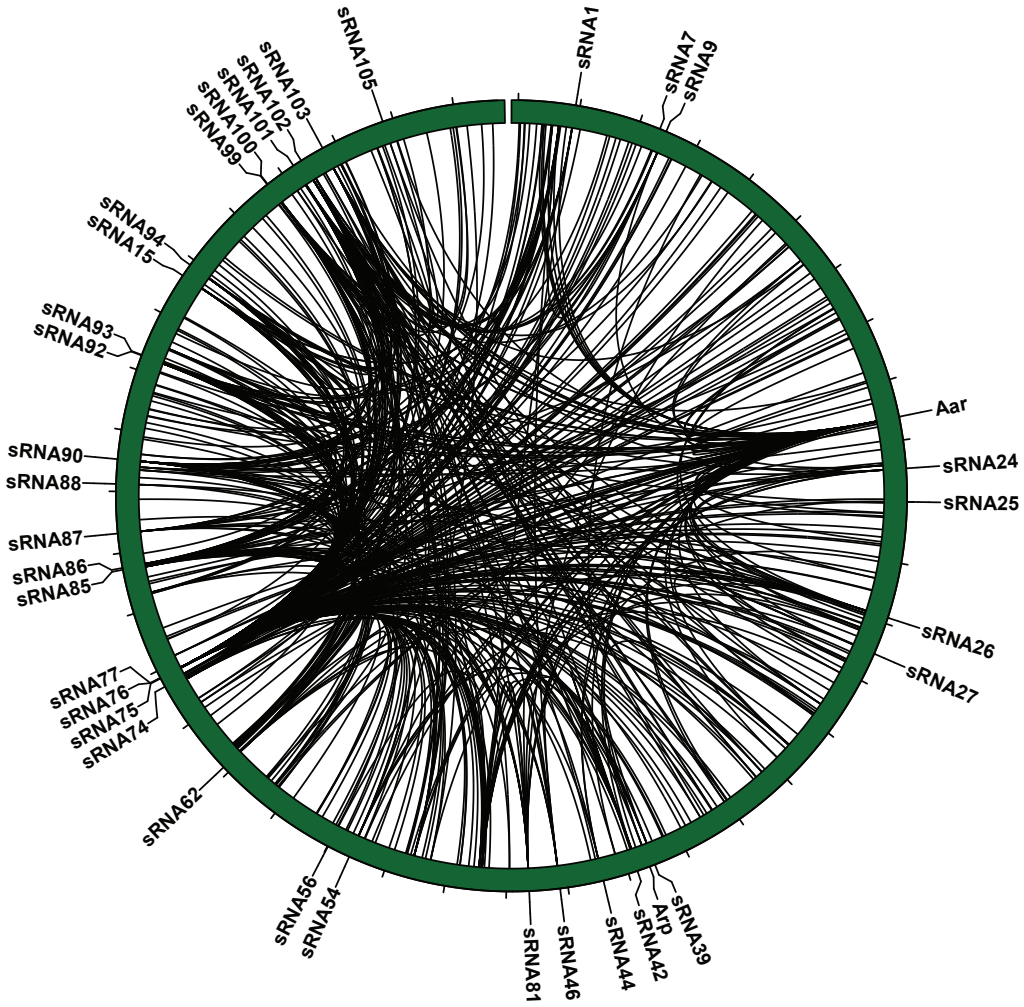

Figure 3.7 Chromosomal sRNA-RNA interactions that are overrepresented in the T4 RNA ligase induced conditions (IND, DIP and IMIP).

Analysis Hi-GRIL-seq revealed that 36 *A. baumannii* AB5075 sRNA candidates were ligated to RNA molecules in other regions of the chromosome. This resulted in the identification of 632 potential chromosomal sRNA-RNA interactions that matched the cut-off scores applied. These interactions are visualised for each sRNA candidate across the AB5075 chromosome.

Important regulatory, non-coding RNAs typically regulate numerous mRNA targets simultaneous, allowing them to modulate gene expression in a global manner (Storz et al., 2011). These sRNA can be referred to as "keystone sRNAs" due to their importance as post-transcriptional regulators (Gebhardt et al., 2023). An analysis of the filtered chimeric Hi-GRIL-seq reads revealed that several sRNAs, including; Aar (sRNA21), sRNA76, sRNA90, sRNA99 and sRNA102 were overrepresented in the sRNA-containing chimera derived from Hi-GRIL-seq (as depicted in **Figure 3.8** and **Table 3.6**). The high abundance of these sRNAs in the filtered chimeric reads suggest that they form regulatory hubs in *A. baumannii*, allowing them to control the expression of numerous mRNA targets.

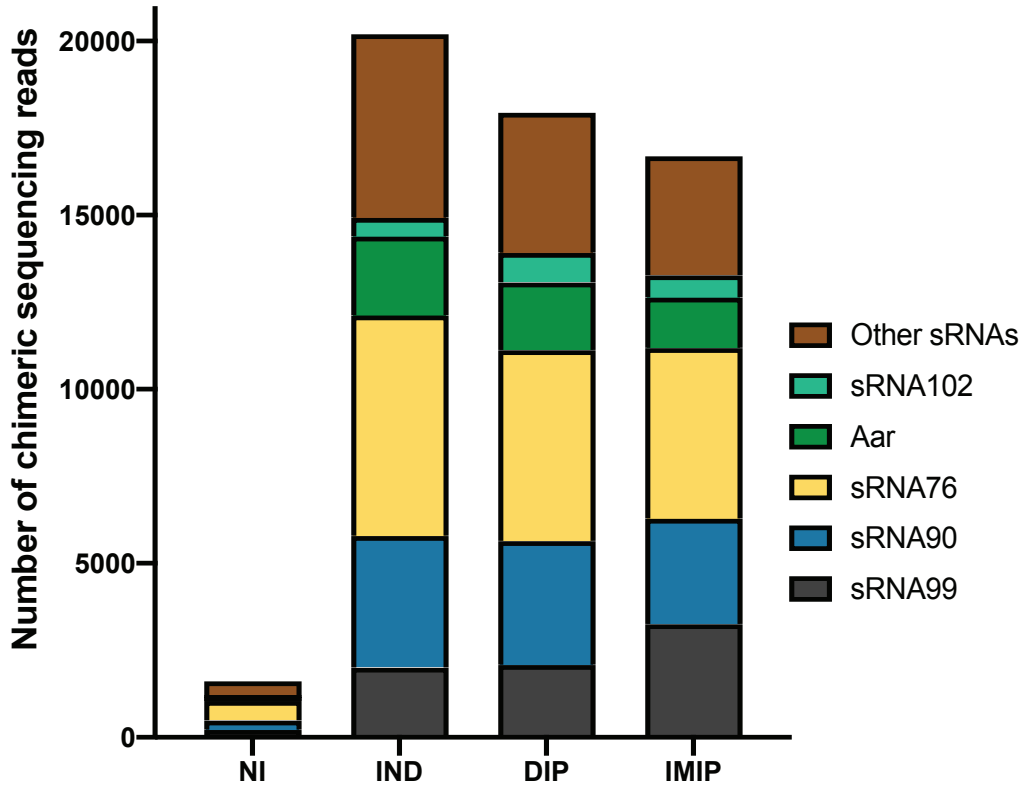

Figure 3.8 Proportion of sRNAs in RNA-RNA chimeras.

The number of chimeric sequencing reads containing sRNA candidate sequences is shown for each condition, including non-induced (NI), induced (IND), iron starvation (DIP) and imipenem shock (IMIP). These chimeric reads are the combination of the biological duplicates of each treatment condition.

Table 3.6 Percentage of sRNAs in sRNA-containing chimeric reads

sRNA	Total chimeric reads (%)	Combined NI chimeric reads (%)	Combined IND chimeric reads (%)	Combined DIP chimeric reads (%)	Combined IMIP chimeric reads (%)
Aar	10.27	6.52	11.26	10.91	8.70
sRNA76	30.66	34.43	31.36	30.54	29.37
sRNA90	18.89	16.15	18.74	19.86	18.18
sRNA99	13.43	13.71	9.92	11.63	19.52
sRNA102	3.71	3.41	2.66	4.77	3.84

Interestingly, the sRNA Aar had relatively low TPM values across all conditions despite accounting for approximately 10.27% of all filtered sRNA-containing chimeric sequencing reads (from all conditions). The TPM values of Aar and the other aforementioned sRNAs are exhibited in **Table 3.7**. The high composition of Aar-containing chimeric sequencing reads despite relatively low TPMs is indicative that it plays a disproportional role in base-pairing compared to its expression level. This suggested that Aar was a likely regulatory sRNA involved in extensive base-pairing interactions in *A. baumannii*. A similar pattern for sRNA90 can be observed, suggesting that it may also be a functional sRNA.

Table 3.7 sRNA TPM values per condition

sRNA	DIP-1	DIP-2	IMIP-1	IMIP-2	IND-1	IND-2	NI-1	NI-2
Aar	1,854.80	1,371.10	1,555.00	1,485.50	3,517.00	3,143.60	2,066.80	1,134.30
sRNA76	43,250.30	37,611.60	74,644.30	45,575.10	59,546.50	43,406.60	17,805.40	38,652.40
sRNA90	3,424.80	3,729.10	1,874.30	2,527.50	3,603.50	3,586.70	4,241.30	1,598.20
sRNA99	21,394.30	21,584.30	8,593.90	21,112.40	17,794.20	15,749.00	26,858.70	29,726.20
sRNA102	2,004.50	1,958.10	3,017.10	2,089.70	1,794.00	1,880.60	712.1	565.2

3.6 Filtered Hi-GRIL-seq chimeras identify potential sRNA-mRNA interactions:

The overrepresentation of Aar in the sRNA-containing chimeric reads in our filtered Hi-GRIL-seq dataset suggests that it is a global regulator of gene expression in *A. baumannii* AB5075. This prompted us to examine the Aar interactome in more detail. Using the Hi-GRIL-seq dataset, we found 95 distinct Aar-containing chimeras. The majority of the

chimeras were derived from chromosome, where 88 potential Aar-RNA interactions were identified. The genomic location of Aar and these potential RNA interaction partners is shown in **Figure 3.9**. Aar formed chimeras with an additional 7 plasmid derived RNA molecules. The ten Aar-containing chimeras with the highest numbers of sequencing reads are shown in **Table 3.8**. The three highest potential mRNA targets encode proteins with domains of unknown function or hypothetical proteins (**Table 3.8**). Aar was also found to be ligated to mRNA encoding outer membrane proteins CarO and OmpW (Catel-Ferreira et al., 2016; Mussi et al., 2007). These outer membrane proteins are suggested to be porins, CarO was thought to be involved in uptake of L-ornithine and carbapenem antibiotics in *A. baumannii*, while OmpW is implicated in the uptake of ferric chloride ($FeCl_3$) (Artuso et al., 2023; Catel-Ferreira et al., 2016; Eijkelkamp et al., 2011; Uppalapati et al., 2020). Genes encoding a rRNA pseudouridine synthase and a 16S rRNA (guanine^{527}-N^7)-methyltransferase RsmG were found among the most abundant Aar-containing Hi-GRIL-seq chimeras. The rRNA pseudouridine synthase (ABUW_RS07825) is a homologue of the 16S rRNA pseudouridine synthase RsuA in *E. coli* that modifies U516 of 16S rRNA to pseudouridine (Jayalath et al., 2020). 16S rRNA (guanine^{527}-N^7)-methyltransferase RsmG catalyses the replacement of guanine with N^7-methylguanine at nucleotide position 527 in 16S rRNA in *A. baumannii*, and it appears to modulate translational efficiency in this pathogen (Zhang et al., 2022). Aar was also ligated to mRNA encoding transfer RNA (tRNA-Leu), an acetyltransferase and a gene of unknown function (NIF3).

Table 3.8 Ten Aar-containing chimeras with highest number of sequencing reads

Interaction partner	Product	Total Merged Chimeric Reads	Merged NI Chimeric Reads	Merged IND Chimeric Reads	Merged DIP Chimeric Reads	Merged IMIP Chimeric Reads
ABUW_RS07145	DUF2171 containing protein	1002	19	493	201	289
ABUW_RS10005	hypothetical protein	916	6	282	383	245
ABUW_RS10425	hypothetical protein	419	4	244	80	91
ABUW_RS04980	ornithine uptake porin CarO type 3	283	4	69	140	70
ABUW_RS07825	rRNA pseudouridine synthase	161	1	40	66	54
ABUW_RS17440	OmpW	141	1	52	39	49
ABUW_RS17255	tRNA-Leu	133	10	42	34	47
ABUW_RS10585	acetyltransferase	99	0	0	99	0
ABUW_RS04930	NIF3	87	0	41	46	0
ABUW_RS11010	16S rRNA (guanine^{527}-N^{7})-methyltransferase	86	0	39	15	32

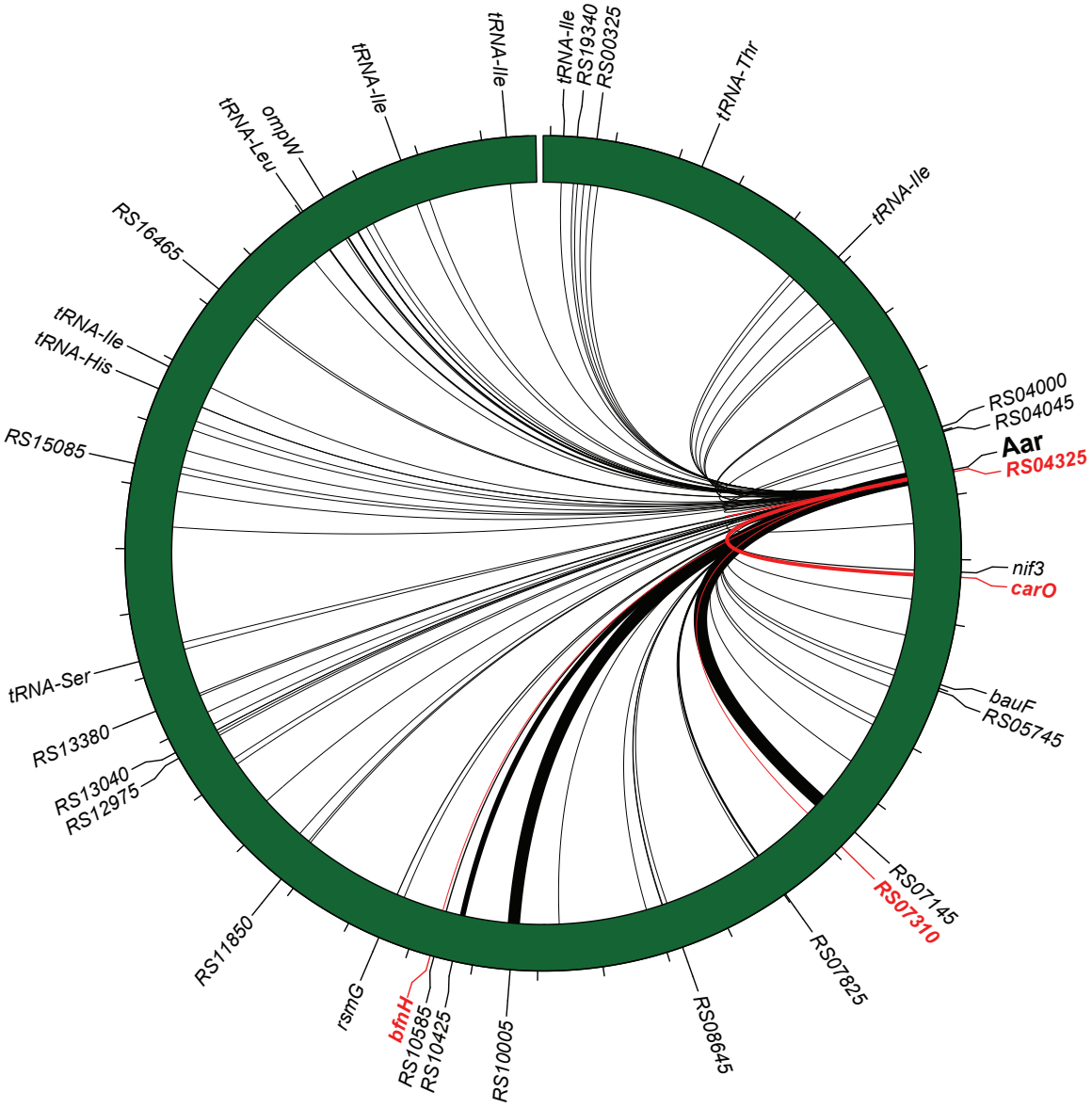

Figure 3.9 Hi-GRIL-seq uncovers the potential Aar interaction partners.

Hi-GRIL-seq revealed that the *A. baumannii* sRNA Aar was found to interact with other RNA molecules (n=88). These interactions are shown across the chromosome where the thickness of the line is proportional to the number of chimeric reads obtained. Aar interaction partners studied in detail are outlined in red.

3.7 Comparing Hi-GRIL-seq to CopraRNA predictions:

By filtering the Hi-GRIL-seq chimeras, I was able to refine the number of potential sRNA-mRNA interactions. To further improve identification of genuine base-pairing interactions, Hi-GRIL-seq chimeras were compared to predictions obtained by CopraRNA (Wright et al., 2013, 2014). CopraRNA is a comparative prediction algorithm that identifies likely sRNA-mRNA interactions based on the conservation of the sRNA and the mRNA target sequences in different bacterial species or strains. CopraRNA (version 2.1.4) was employed to identify potential mRNA interaction partners for 36 sRNA candidates. These sRNA candidates were selected as they were broadly distributed across *A. baumannii* strains and were not strain specific, allowing them to be compared by CopraRNA (Kröger et al., 2018). The following strains were used for these predictions as they are model *A. baumannii* strains and they are reflective of the current circulating infection relevant lineages (Zarrilli et al., 2013). These strains included; *A. baumannii* ATCC17978-mff (NZ_CP012004.1), AB5075-UW (NZ_CP008706.1), AYE (NC_010410.1), A1 (NZ_CP010781.1), LAC-4 (NZ_CP007712.1) and USA15 (NZ_CP020595.1). The exact strains used for each sRNA candidate are listed in **Table 3.9**. CopraRNA was run using the default parameters, with identification of potential interactions within 300 nucleotides upstream or downstream of the start codon. This setting was applied as sRNAs that represses gene expression, canonically bind to the 5′-UTR (particularly within the Shine Dalgarno region) or within the first five codons downstream of the translational start site (referred to as the "5-codon window") to impair ribosome binding and/or translational efficiency (Beyer et al., 1994; Massé et al., 2002; Morita et al., 2006; Storz et al., 2011).

CopraRNA identified a total of 6732 potential mRNA interaction partners for 32 of the sRNA candidates that were tested with ~200 potential targets for each sRNA. To determine whether CopraRNA could be used to help refine the Hi-GRIL-seq results, we compared the filtered chimeras to the CopraRNA predictions. This analysis was performed individually for each sRNA candidate. Overall, I found that 42 of the 632 chimeras identified by Hi-GRIL-seq were shared with the CopraRNA predictions as shown in **Figure 3.10A**. The entire list of potential mRNA targets that were identified by both Hi-GRIL-seq and CopraRNA are detailed in **Appendix III**. By examining the potential RNA targets of Aar in greater detail, 10 of the Hi-GRIL-seq derived chimera

that were found were also predicted by CopraRNA, suggesting that they are high confidence interaction partners (**Figure 3.10B**).

The exact identities of these putative interaction partners are specified in **Table 3.10** where they are listed in order of chimeric sequencing reads obtained by Hi-GRIL-seq. From this, it is evident that Aar formed numerous chimeras with the previously outlined outer membrane protein CarO. CopraRNA suggested that this interaction was statistically significant ($p<0.01$). We also found that CopraRNA suggested that the potential interaction between Aar and mRNA encoding the TonB-dependent receptor BfnH is very statistically significant ($p<0.00001$). BfnH forms part of the baumannoferrin siderophore cluster, where it acts as a receptor for the uptake of the hydroximate siderophore baumannoferrin (Cook-Libin et al., 2022; Sheldon et al., 2020). CopraRNA also suggest that statistically significant ($p<0.05$) interactions occur between Aar and an acyl carrier protein, a hypothetical protein, a drug/metabolite transporter, the response regulator BfmR and a permease. These interactions and the consequences of these interactions are assessed experimentally in **Chapter 4**.

Table 3.9 Strains used for CopraRNA predictions

sRNA candidate	ATCC17978	AB5075	AYE	A1	LAC4	USA15
sRNA1	X	X	X	X	X	X
sRNA7	X	X	X	X	X	X
sRNA9	X	X	X	X	X	X
sRNA15	X	X	X	X	X	X
sRNA21	X	X	X	X	X	X
sRNA24	X	X	X	X		X
sRNA25	X	X	X	X	X	X
sRNA26	X	X	X	X		X
sRNA27	X	X	X	X	X	X
sRNA39	X	X	X	X	X	X
sRNA40	X	X	X	X	X	X
sRNA42	X	X	X	X	X	X
sRNA44	X	X	X	X	X	X
sRNA46	X	X	X	X		X
sRNA54	X	X	X	X	X	X
sRNA56	X	X	X	X	X	X
sRNA62	X	X	X	X	X	X
sRNA74	X	X	X	X	X	X
sRNA75	X	X	X	X	X	X
sRNA76	X	X	X	X	X	X
sRNA77	X	X	X	X	X	X
sRNA81	X	X	X	X	X	X
sRNA85	X	X	X	X	X	X
sRNA86	X	X	X	X	X	X
sRNA87	X	X	X	X	X	X
sRNA88	X	X	X	X	X	X
sRNA90	X	X	X	X	X	X
sRNA92	X	X	X	X		X
sRNA93	X	X	X	X		X
sRNA94	X	X	X	X		X
sRNA99	X	X	X	X	X	X
sRNA100	X	X	X	X	X	X
sRNA101	X	X	X	X	X	X
sRNA102	X	X	X	X	X	X
sRNA103	X	X	X	X	X	X
sRNA105	X	X	X	X	X	X

Table 3.10 Aar interaction partners shared between CopraRNA and Hi-GRIL-seq

Interaction partner	Product	CopraRNA p-value	Hi-GRIL-seq reads
ABUW_RS04980	ornithine uptake porin CarO type 3	0.006586786	283
ABUW_RS15085	acyl carrier protein	0.048226059	40
ABUW_RS04000	amino acid permease	0.01799347	39
ABUW_RS08645	hypothetical protein	0.050870214	39
ABUW_RS13040	hypothetical protein	0.044348082	38
ABUW_RS07310	DMT family transporter	0.02434699	36
ABUW_RS10605	TonB-dependent receptor BfnH	0.000000602	28
ABUW_RS15450	response regulator BfmR	0.030220161	23
ABUW_RS16485	permease	0.040931387	16
ABUW_RS03285	toxin	0.056714319	13

Analysis of the CopraRNA interaction predictions for other sRNAs revealed that a likely interaction occurs between sRNA40 and mRNA encoding PilA, where it is the sole target shared by Hi-GRIL-seq and CopraRNA (**Figure 3.10C**). PilA is the major subunit of type IV pili in *A. baumannii* (Ronish et al., 2019). Type IV pili are vital for mediating twitching motility and for natural transformation in this pathogen. Loss of PilA has completely abrogated uptake of plasmid and chromosomal DNA in this organism (Vesel et al., 2021). Due to the importance that such an interaction would mediate in the development of antimicrobial resistant strains of *A. baumannii*, we decided to further characterise sRNA40 (renamed Arp or **A**cinetobacter **r**egulator of **p**ilin). The number of Hi-GRIL-seq reads and the statistical significance of Arp-*pilA* interactions are outlined in **Table 3.11**.

Table 3.11 Arp interaction partners shared between CopraRNA and Hi-GRIL-seq

Interaction partner	Product	CopraRNA p-value	Hi-GRIL-seq reads
ABUW_RS01495	pilin	0	119

It is clear from this that a large number of chimeric sequencing reads of Arp-*pilA* were detected in the Hi-GRIL-seq analysis. This is notable considering the relatively low expression level of Arp detected (average TPM ~61, TPM values outlined in **Table 3.12**).

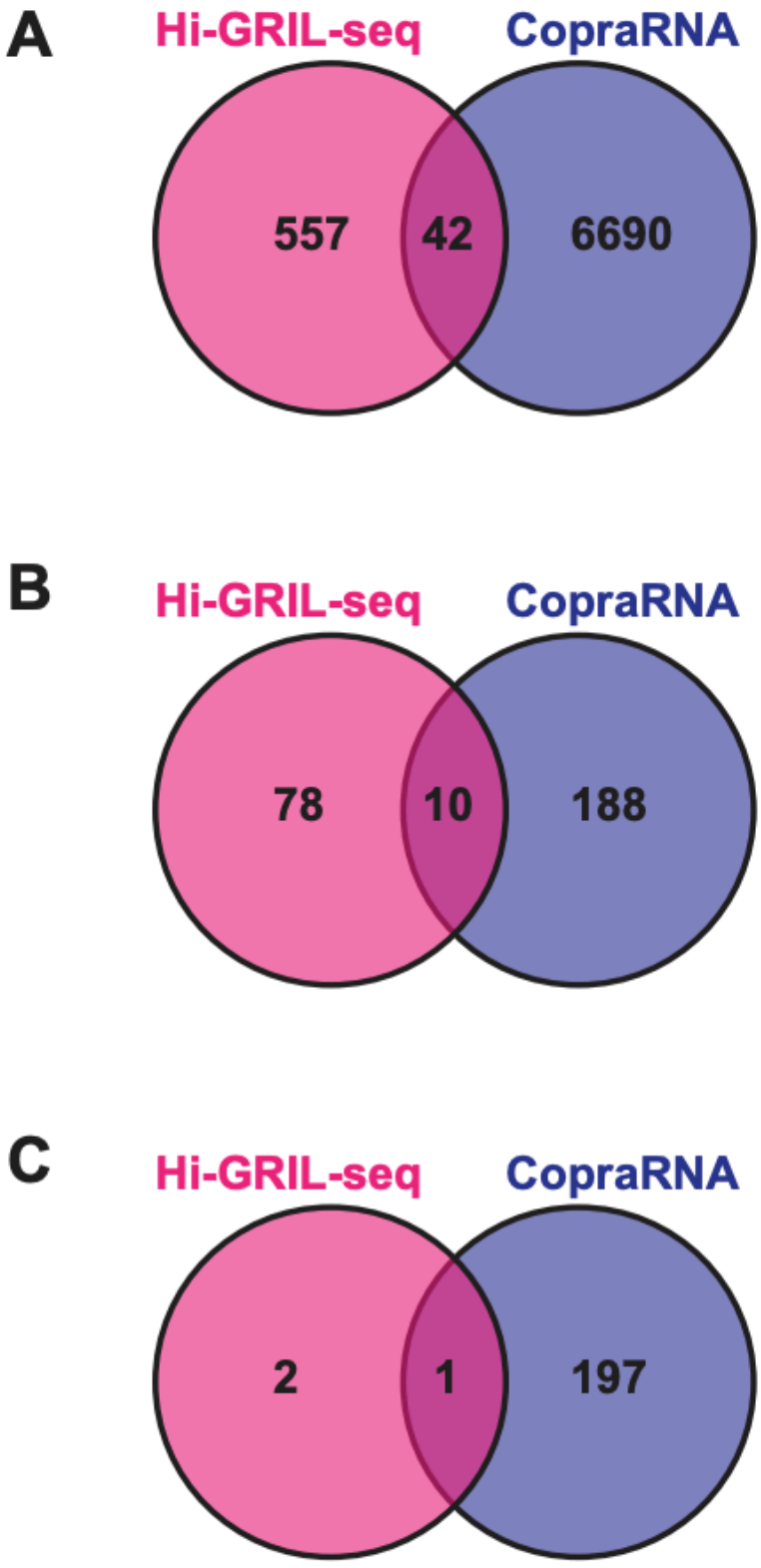

Figure 3.10 CopraRNA enhances use of Hi-GRIL-seq to identify high-confidence sRNA-mRNA interactions.

CopraRNA was used to predict interactions occurring within 300 nucleotides upstream or downstream of start codons for all known *A. baumannii* AB5075 sRNAs. The number of mRNA targets that were shared by both CopraRNA for all sRNAs (A), the sRNA Aar (B) and sRNA40/Arp (C) are shown in Venn diagrams.

Table 3.12 Arp TPM values per condition

sRNA	DIP-1	DIP-2	IMIP-1	IMIP-2	IND-1	IND-2	NI-1	NI-2
Arp	56.7	51.5	62.4	70.3	92.7	70.4	50.5	37.1

Furthermore, a very low p-value was detected ($p<0.000000001$), causing CopraRNA to report the p-value as "0". The disproportionate number of chimeric sequencing reads relative to the low Arp expression levels at the time of the Hi-GRIL-seq experiment suggest that this is a high confidence interaction. The genomic location of Arp and its potential RNA interaction partners are shown in **Figure 3.11**. This interaction and the consequences of this interaction are assessed experimentally in **Chapter 5**.

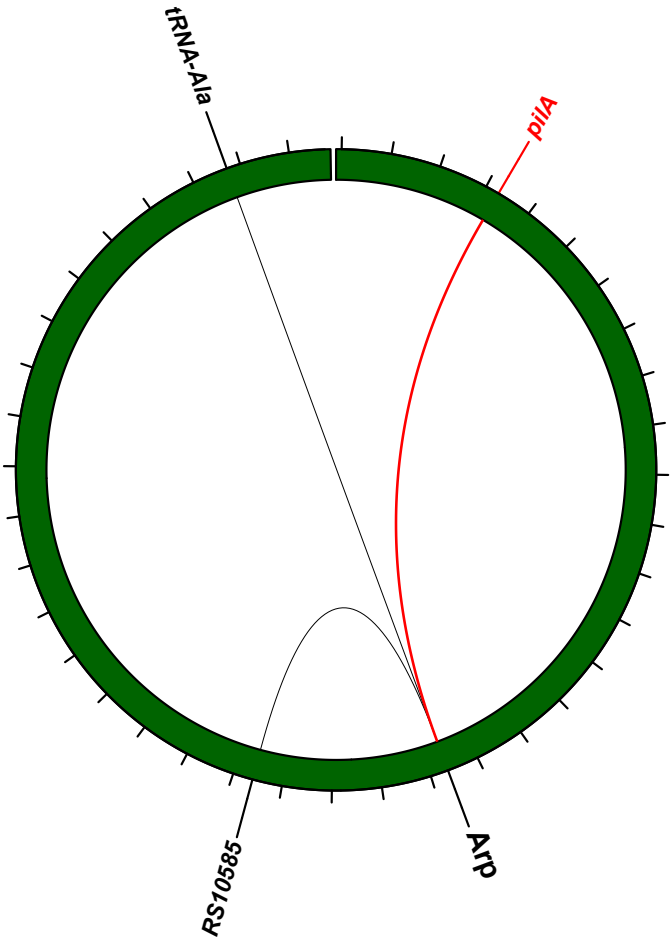

Figure 3.11 Hi-GRIL-seq uncovers the potential Arp interaction partners.

Hi-GRIL-seq revealed that the *A. baumannii* sRNA Arp was found to interact with other RNA molecules (n=3). These interactions are shown across the chromosome where the thickness of the line is proportional to the number of chimeric reads obtained. Arp interaction partners studied in detail are outlined in red.

Chapter 4 – Aar is a global post-transcriptional regulator of gene expression in *A. baumannii*

4.1 Introduction:

The sRNA **a**mino **a**cid **r**egulator (Aar) was identified in *Acinetobacter baylyi*, a non-pathogenic relative of *A. baumannii*, by Schilling and colleagues (Schilling et al., 2010). In this study, they predicted base-pairing interactions between Aar and several mRNA molecules encoding proteins involved in amino acid metabolism *in silico*. They showed that Aar overexpression was associated with the upregulation of these putative mRNA interaction partners. Later transcriptomic studies in *A. baumannii* showed that there is a homologue of Aar in *A. baumannii* (Kröger et al., 2018; Weiss et al., 2016). As outlined in **Chapter 3**, I showed using Hi-GRIL-seq that Aar is a regulator of gene expression in *A. baumannii* with an extensive repertoire of potential mRNA interaction partners. In this chapter, I further our understanding of the physiological importance of Aar in *A. baumannii*. I first examine the dynamics of Aar expression in *A. baumannii* and explore regulation of this sRNA. I then demonstrate that Hi-GRIL-seq uncovers the Aar-mRNA interaction partners, highlighting the Aar interactome in *A. baumannii*. I detail the mechanistic properties of Aar-mediated regulation of mRNA molecules *in vitro*, in heterologous systems and *in vivo* in *A. baumannii*. I identify the Aar nucleotides responsible for initiating antisense base-pairing, offering the first insight of sRNA-mediated gene regulation in this pathogen. With the help of Dr Hokamp (Genetics Dept., TCD), we have made an online genome browser available showing the mapped Hi-GRIL-seq reads and Aar-containing chimeric sequencing reads, allowing others to further characterise Aar using Jbrowse2 (Diesh et al., 2023). This is available at: http://bioinf.gen.tcd.ie/jbrowse2/Hi-GRIL-seq. Pulse overexpression of Aar was also performed in *A. baumannii*, providing greater insight into post-transcriptional regulatory networks in this organism and identifying additional mRNA targets worthy of investigation.

4.2 Aar is a physiologically important sRNA in *A. baumannii*:

1. Aar is conserved in *Acinetobacter* species:

While the identification of an *A. baumannii* homologue of Aar was first reported by Weiss and colleagues, the exact Aar transcriptional start site (TSS) was unknown until Kröger,

and colleagues employed the use of differential RNA-sequencing (dRNA-seq) in *A. baumannii* ATCC17978 (Kröger et al., 2018; Weiss et al., 2016). dRNA-seq can distinguish newly synthesised primary transcripts from processed transcripts due to their distinct biochemical properties (Sharma et al., 2010). Primary transcripts are typically tri-phosphorylated at their 5′ end while mature transcripts are mono-phosphorylated at this site. Mono-phosphorylated RNA, unlike tri-phosphorylated RNA, is susceptible to degradation by a terminator exonuclease (TEX), enriching primary transcripts compared to mature RNA species. Kröger *et al*. isolated RNA from 16 different treatment conditions and pooled them together (Kröger et al., 2018). They then sequenced RNA samples that were treated with (pool dRNA-seq) or without (pool RNA-seq) TEX. As shown in **Figure 4.1**, this strategy enabled identification of the Aar TSS located at position 833,848.

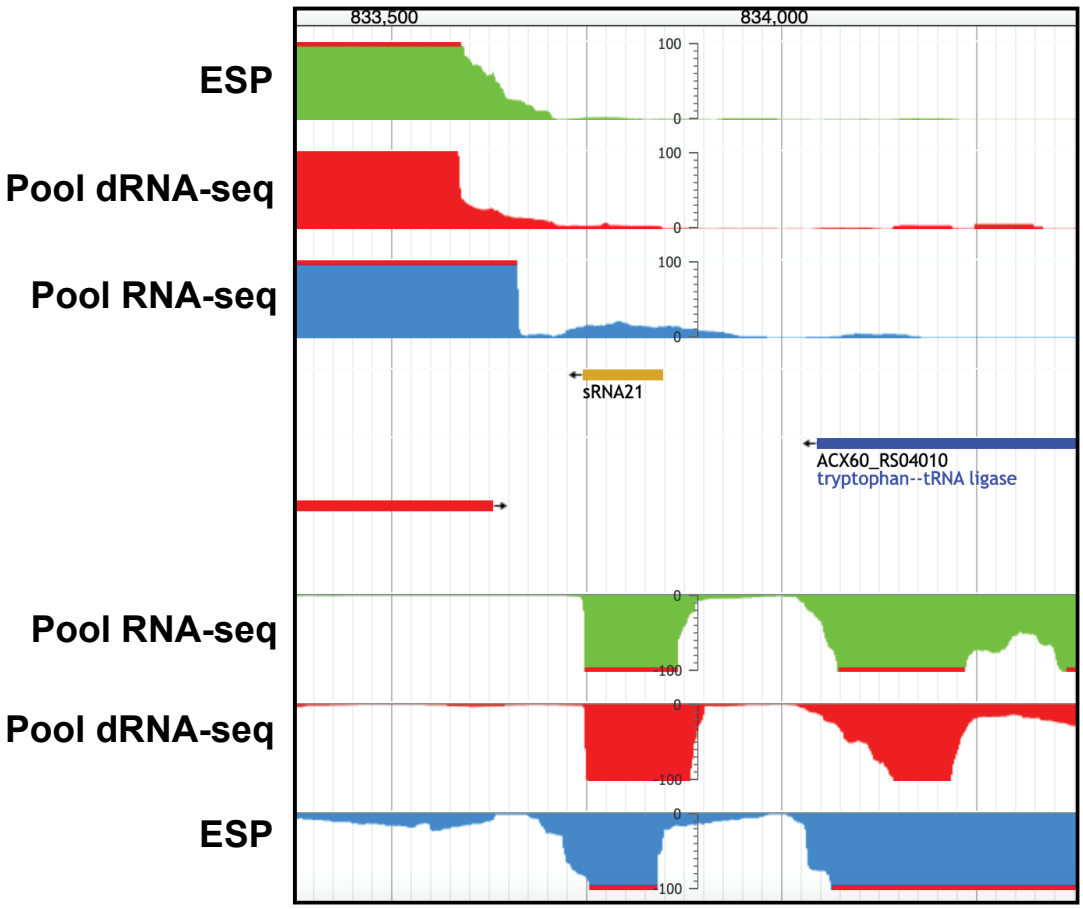

Figure 4.1 Aar expression in *A. baumannii* ATCC17978.

Aar expression (annotated as sRNA21) was identified by RNA-sequencing of RNA obtained from 16 different environmental conditions that were untreated (Pool RNA-seq) or TEX treated (Pool dRNA-seq) using *A. baumannii* ATCC17978 (Kröger et al., 2018). This enabled identification of the Aar TSS.

The *aar* locus from *A. baumannii* ATCC17978, including the TSS, was conserved in the AB5075 strain. Aar has a full-length size of 181 nucleotides in *A. baylyi* ADP1, while it had a full-length size of 103 nucleotides in these *A. baumannii* strains (Kröger et al., 2018; Schilling et al., 2010). To examine this discrepancy, a multiple sequence alignment of *aar* between *A. baylyi* ADP1, *A. nosocomialis* and four model *A. baumannii* strains was performed (**Figure 4.2A**). The upstream region (100 nucleotides) of *aar* in *A. nosocomialis* and *A. baumannii* strains were aligned to the entire ADP1 *aar* to determine the sequence similarity between these regions. There was greater sequence similarity of *A. baylyi* Aar and the other strains at the 3′ end than at the 5′ end. This could be attributed to the use of a separate TSS in *A. baylyi* than in other *Acinetobacter* species. The discrepancy in the size of *A. baylyi* Aar may impact the secondary structure of this sRNA, allowing it to interact with other mRNAs than Aar in *A. baumannii*. Inspection of the *A. baumannii aar* promoter architecture reveals a sequence closely matching the RpoD sigma fact promoter consensus in *A. baumannii* ATCC17978, suggesting that Aar is RpoD-dependent (Kröger et al., 2018).

2. Aar is expressed in a growth phase dependent manner:

To assess the size of Aar in *A. baumannii* AB5075, I generated a markerless Aar-deletion strain (Δ*aar*) using homologous recombination (Godeux et al., 2020). I then employed northern blotting, using a riboprobe spanning the entire length of *aar*, with RNA isolated from wildtype and Δ*aar* strains at late stationary phase (LSP, 16h of growth). As shown **Figure 4.2B**, a full-length Aar with a length of ~103 nucleotides was detected, and smaller bands, in the wildtype strain (Kröger et al., 2018). The smaller bands may represent processed Aar variants or degradation products. All these bands were lost in the Δ*aar* strain indicating that they all emanate from the *aar* locus. The Kröger group previously performed a transcriptomic analysis where RNA was isolated from *A. baumannii* AB5075 at mid exponential phase (MEP, OD_{600} = 0.3), late exponential phase (LEP, OD_{600} = 1.0) early stationary phase (ESP, OD600 = 2.0) and late stationary phase (LSP, 16h of growth) and sequenced at the Core Sequencing Unit Würzburg University in Würzburg, Germany (Bakheet, 2024). The expression of Aar was growth phase dependent, where the sRNA exhibits low expression in exponential phase and higher expression in stationary phase, as shown in **Table 4.1**. To confirm whether Aar

expression is growth phase dependent, I used northern blotting to measure Aar abundance at MEP, LEP, ESP and LSP (**Figure 4.2C**). This revealed that Aar accumulates across growth, with higher signal intensity in stationary phase than in the earlier growth phase.

To better understand the biochemical properties of Aar derived from *A. baumannii* AB5075, we predicted the secondary structure of this sRNA using RNAfold with default parameters (Lorenz et al., 2011). The resulting minimum free energy structure was represented using VARNA (Darty et al., 2009). This suggested that Aar is mostly single stranded with a stem-loop structure at the 5′ end and two more stem-loop structures at the 3′ end followed by a poly(U) tail to promote Rho-independent termination (**Figure 4.3A**). The Aar seed region was in the single strand region and is indicated in this figure, this is discussed in greater detail in **section 4.5**. Analysis of the mapped Hi-GRIL-seq reads uncovered no clear Aar processing sites (**Figure 4.3B**).

Table 4.1 Aar expression (average TPMs) across growth

Mid exponential phase (MEP)	Late exponential phase (LEP)	Early stationary phase (ESP)	Late stationary phase (LSP)
8	52.67	45	383.67

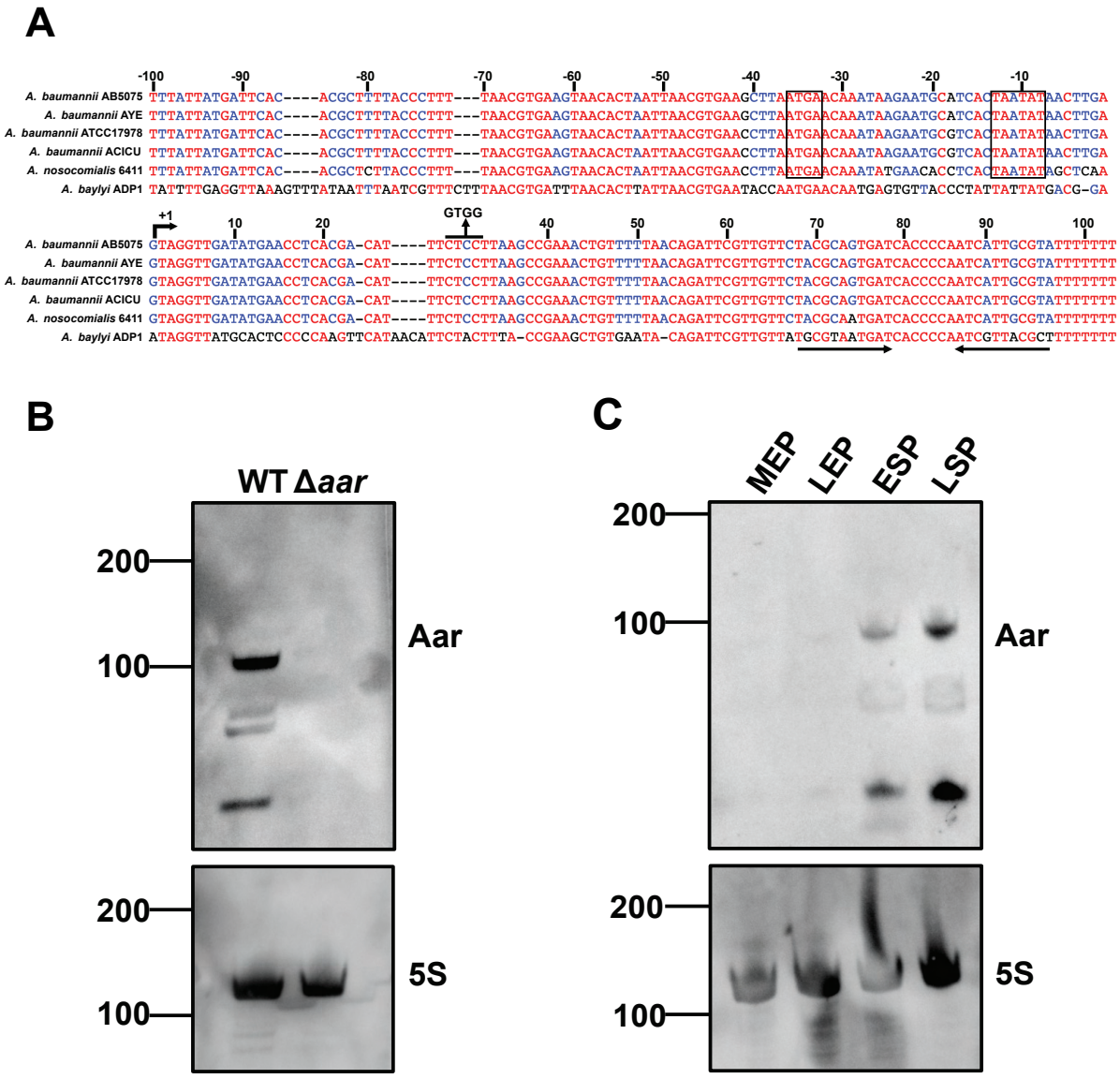

Figure 4.2 Aar is a conserved sRNA that is expressed in a growth phase dependent manner.

(A) A sequence alignment of *aar* in several *Acinetobacter* species was performed using the Multalin tool. The predicted TSS of *aar* is indicated as +1, with the numbers above the sequence reflecting the distance from the TSS. The predicted "seed" region is indicated by a line and the corresponding mutant form is down. The putative -35 and -10 regions are indicated with boxes, while the Rho-independent terminator is visualised with arrows below the sequence. (B) Northern blotting of Aar in wildtype and Δ*aar A. baumannii* AB5075. (C) Expression of Aar across growth as determined by northern blotting, at MEP, LEP, ESP and LSP. 5S rRNA was used as the loading control. The numbers in the northern blots represent the RNA ladder in nucleotides, three biological replicates were carried for each northern blotting experiment and one representative blot is shown.

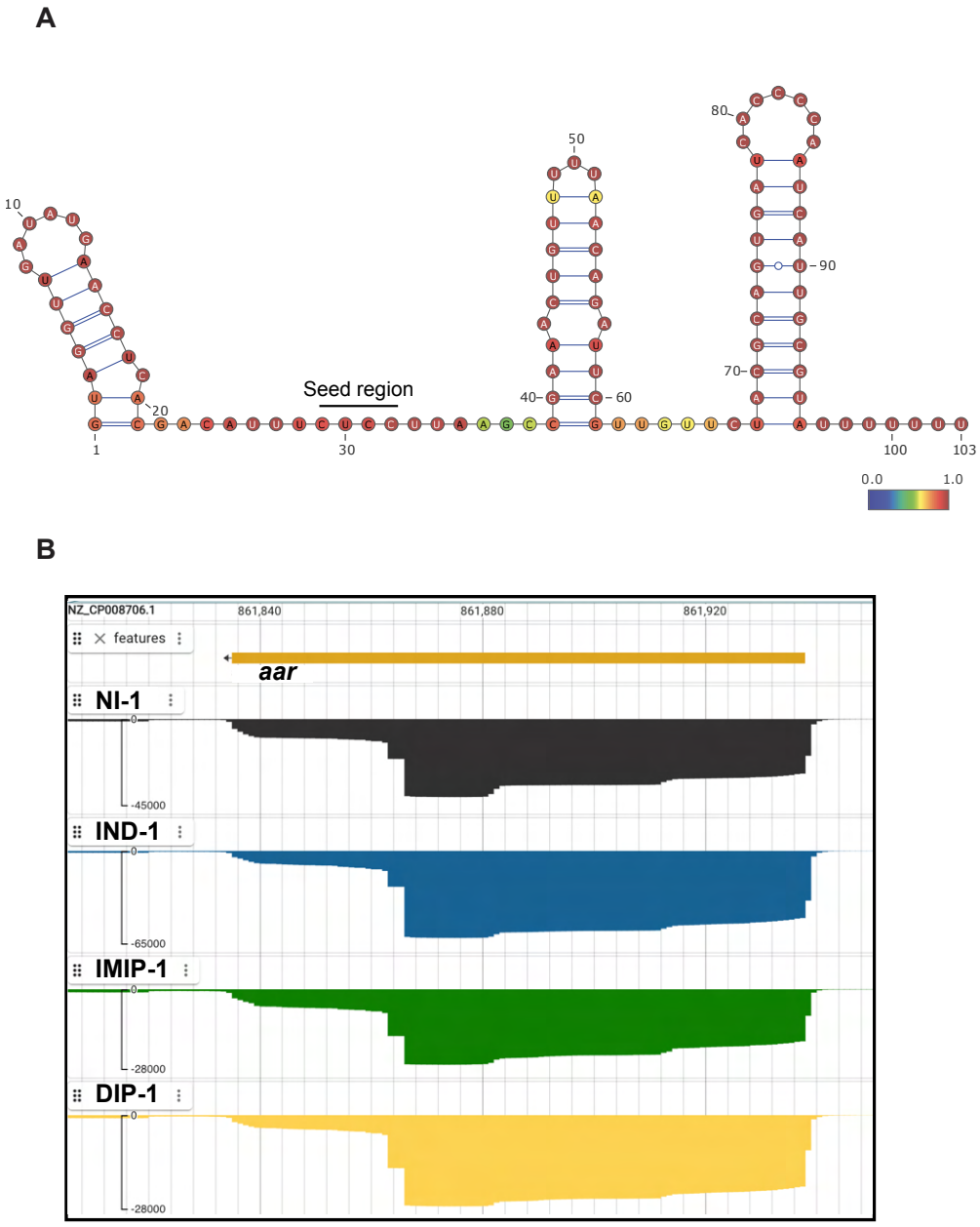

Figure 4.3 Examination of the secondary structure and processing of Aar.
(A) the minimum free energy Aar secondary structure was predicted by RNAfold and represented with VARNA (Darty et al., 2009; Lorenz et al., 2011). The colours of the nucleotides correspond to base-pairing probabilities and the seed region is displayed. (B) The Hi-GRIL-seq mapped reads for the *aar* locus are displayed in JBrowse2, showing one replicate for each Hi-GRIL-seq condition (NI = non-induced control, IND = induced sample, DIP = iron starvation and IMIP = imipenem shock) (Diesh et al., 2023).

3. Aar is induced by environmental shocks:

Bacterial sRNAs are often induced in response to environmental stressors, allowing the organism to survive in rapidly changing environments (Holmqvist et al., 2017). The Kröger group performed transcriptomic analyses in *A. baumannii* AB5075 in different growth conditions to better understand transcriptional responses in this pathogen (Bakheet, 2024). In this study, RNA was isolated from *A. baumannii* that was grown to MEP that was then shocked with environmental stressors or not, prior to RNA sequencing. RNA was isolated from *A. baumannii* that was to MEP at 37°C that was unshocked or that was osmo-shocked (with 0.3 M NaCl) or iron deprived (with 0.22 mM DIP) for 15 min. RNA was also isolated from *A. baumannii* that was to MEP at 25°C that was unshocked or that was temperature shocked (transferred to 37°C for 15 min). Transcriptomic analysis from biological replicates revealed that Aar expression (as measured by TPM) was upregulated in the ambient temperature and temperature shock conditions, compared to the other treatment conditions, as shown in **Figure 4.2**.

Table 4.2 Aar expression (average TPMs) in shock conditions

Mid exponential phase (MEP)	Ambient temperature (22°C)	Temperature shock (22°C→37°C)	Salt shock (0.3 M NaCl)	Iron starvation (0.22 mM DIP)
8	19.33	67.67	11	10.33

To examine differential Aar expression in stressful growth conditions, I performed northern blotting with RNA isolated from *A. baumannii* subjected to several stressors (listed in **Table 4.3**). Briefly, *A. baumannii* AB5075 cultures were grown to LEP at 25°C and 37°C, when Aar expression is low, before shocking them for 15 min and isolating RNA. The samples that were grown at 37°C subjected to either osmotic shock (0.3 M NaCl), iron deprivation (200 µM DIP) or envelope stress (1 µg/mL polymyxin B). The samples that were grown at 25°C were heat shocked by transferring them to a 37°C incubator. Mock treatment controls were included for 25°C and 37°C, where the samples were grown to LEP and returned to their respective temperatures for 15 min prior to RNA isolation.

Table 4.3 Environmental shock conditions

Name	Abbreviation	Description
37°C mock control	37°C	L-broth, grown to LEP at 37°C, returned to 37°C for 15 min
25°C mock control	25°C	L-broth, grown to LEP at 25°C, returned to 25°C for 15 min
Temperature shock	TS	L-broth, grown to LEP at 25°C, shocked at 37°C for 15 min
Osmotic shock	NaCl	L-broth, grown to LEP at 37°C, shocked with 0.3 M NaCl at 37°C for 15 min
Iron deprivation	DIP	L-broth, grown to LEP at 37°C, shocked with 0.2 mM DIP at 37°C for 15 min
Polymyxin B treatment	PB	L-broth, grown to LEP at 37°C, shocked with 1 μg/mL polymyxin B at 37°C for 15 min

Northern blotting revealed that Aar was significantly upregulated following heat shock ($p<0.01$) and osmotic shock ($p<0.05$) compared to the 37°C mock treatment control (**Figure 4.4A and 4.4B**). The average fold changes in Aar expression in each condition are listed in **Table 4.4**.

Table 4.4 Fold-change in Aar expression in each stress condition relative to 37°C

Condition	Average fold-change
37°C	1
25°C	5
TS	14
NaCl	8.6
DIP	6
PB	1.3

Aar was upregulated when grown at ambient (25°C) and physiological (37°C) temperatures as was suggested by the Kröger group's transcriptomic dataset (**Table 4.2**). This was not found to be the case in *A. baylyi* (Schilling et al., 2010). Aar was more abundant following osmotic shock and iron deprivation in *A. baumannii* as was observed

in *A. baylyi* (Schilling et al., 2010). Unexpectedly, Aar was more abundant in the osmotic shock and iron deprivation conditions than when grown at ambient temperature which does not match the transcriptomic dataset provided by the Kröger group (**Table 4.2**). This may be due to poor retention of sRNAs during the RNA-seq library preparation, a phenomenon that has been observed when using commercial kits. Addition of polymyxin B to the *A. baumannii* cultures had no impact on Aar expression levels indicating that Aar is not induced by envelope stress.

4. Transcriptional regulation of Aar:

While the Aar promoter bears a strong resemblance to the *A. baumannii* ATCC17978 RpoD promoter consensus sequence (**Figure 4.1A**), various environmental shocks also induce Aar expression (**Figure 4.4A and 4.4B**). This raises the possibility that Aar is not solely regulated by RpoD but also by other specific transcriptional regulators. To assess the transcriptional regulation of Aar in *A. baumannii* AB5075 by different transcription factors, I created a reporter system where superfolder GFP (sfGFP) was placed under transcriptional control of the *aar* promoter on the pVRL2Z plasmid (pVRL2Z-Aar-sfGFP) as outlined in **Figure 4.4C**. The *A. baumannii* AB5075 wildtype strain and isogenic mutant strains lacking three of the most well-established *A. baumannii* transcription factors, namely BaeR (Δ*baeR*), AdeR (Δ*adeR*) and GacS (Δ*gacS*) were transformed with the reporter plasmid (Cerqueira et al., 2014; Kröger et al., 2017; Lin et al., 2014; Marchand, Damier-piolle, et al., 2004). The relative fluorescent intensity of these strains was measured at LSP where Aar expression levels are at their highest (**Table 4.1**, **Figure 4.4D**). This allowed me to detect a subtle, yet significant increase (1.2-fold, $p<0.05$) in *aar* promoter activity in Δ*adeR*, relative to the wildtype strain. Conversely, there was a significant decrease (1.4-fold, $p<0.01$) in *aar* promoter activity in Δ*gacS*, relative to the wildtype strain. This indicates that AdeR and GacS play opposing roles in Aar expression as repressor and activator, respectively. While the environmental signals sensed by these transcription factors in *A. baumannii* are unknown, AdeR was shown to be upregulated at 30°C and downregulated at higher temperatures, potentially explaining the mechanism of Aar induction following heat shock (Bazyleu et al., 2014).

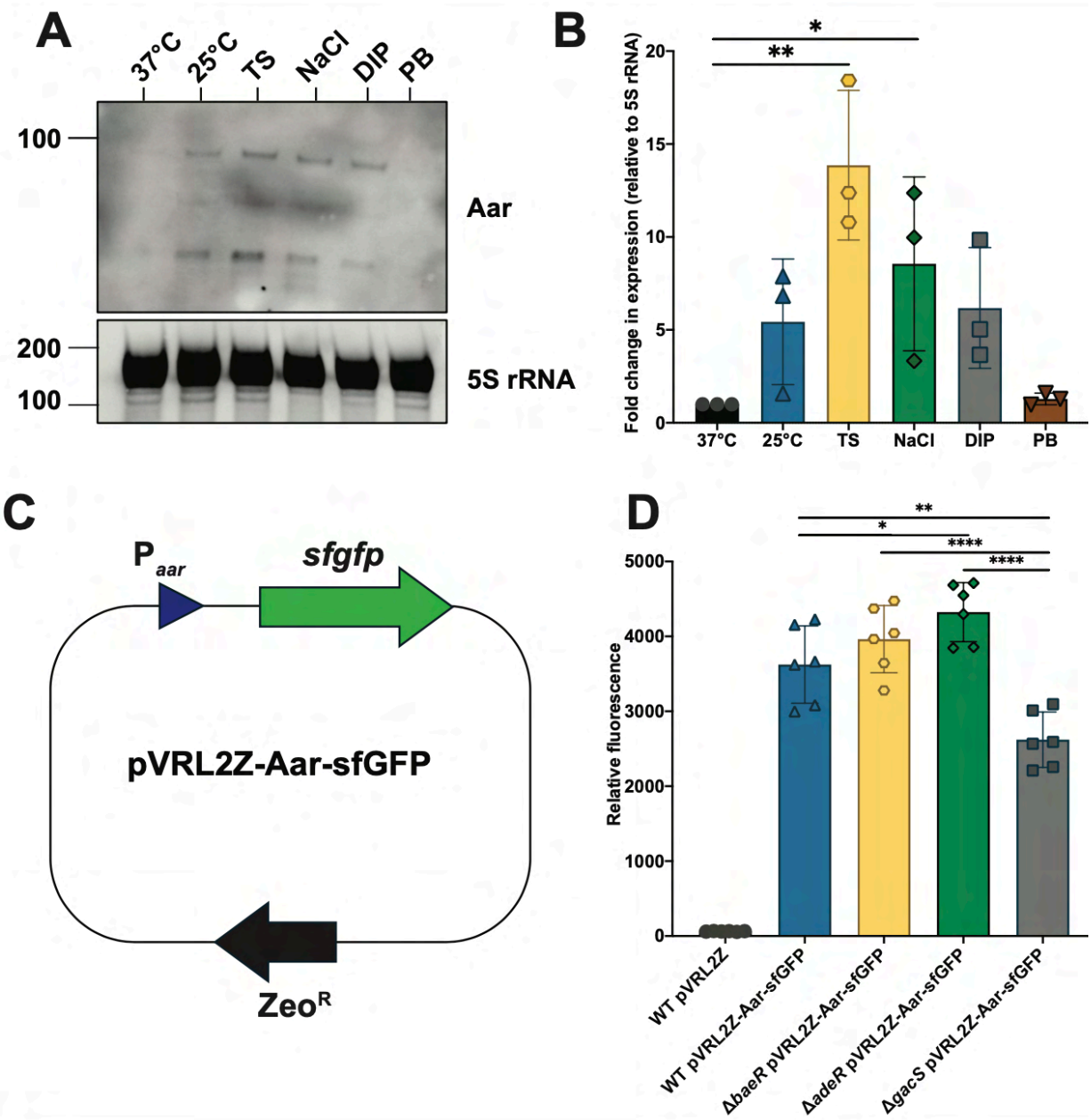

Figure 4.4 Aar is induced by environmental stressors and Aar expression is governed by transcriptional regulators.

(A) Expression of Aar grown to LEP at either 37°C or 25°C, that was heat shocked (25°C to 37°C, TS), shocked with 0.3 M NaCl (NaCl), 200 µM 2,2-dipyridyl (DIP) or 1 µg/ml polymyxin B (PB) for 15 min, as determined by northern blotting. Mock controls at 37°C and 25°C were also included. Northern blotting was performed using three independent biological replicates. (B) Quantification of Aar expression from the shock conditions, calculated as fold changes relative to the 37°C control sample (set to 1). (C) Schematic of an Aar transcriptional reporter plasmid (pVRL2Z-Aar-sfGFP), where sfGFP is placed under transcriptional control of the *aar* promoter (P_{aar}). (D) The *aar* promoter activity was ascertained by measuring fluorescent intensities of *A. baumannii* strains (wildtype, Δ*baeR*, Δ*adeR* and Δ*gacS*) carrying pVRL2Z-Aar-sfGFP at LSP. *A. baumannii* AB5075 carrying the control plasmid (pVRL2Z) was measured as an autofluorescence control. Statistical tests were performed using One-way ANOVA followed by Dunnett's test (B) or Tukey's test (D). Error bars represent the standard deviation from independent biological replicates. Differences were considered statistically significant where * denotes $P<0.05$, ** denotes $P<0.01$, *** denotes $P<0.001$ and **** denotes $P<0.0001$.

4.3 Hi-GRIL-seq enables discovery of Aar-mRNA interactions:

1. Aar does not base-pair with putative *A. baylyi* mRNA targets in *A. baumannii*:

Schilling *et al*. showed that Aar was overexpressed in *A. baylyi* ADP1 when placed under control of its native promoter on the pRK415 plasmid (Schilling et al., 2010). Using northern blotting, they showed that this overexpression of Aar resulted in the upregulation of several mRNA molecules involved in amino acid regulation. To determine whether Aar was capable of base-pairing to these mRNA molecules in *A. baumannii*, I first identified the homologues of these genes in *A. baumannii* AB5075. The identity and locations of these genes are summarised in **Table 4.5**.

Table 4.5 Location of putative A. baylyi mRNA targets in *A. baumannii* AB5075

Gene	Function	Abbr.	Genomic location in AB5075
ABUW_RS05895	Glutamine synthetase	*glnA*	1,247,247-1,248,662
ABUW_RS17390	3-ketoacyl-CoA thiolase	*fadA*	3,632,075-3,633,247
ABUW_RS16310	Acetolactate synthase	*ilvI*	3,394,252-3,395,976
ABUW_RS00155	Phosphoenolpyruvate carboxylase	*ppC*	36,792-39,476
ABUW_RS04755	Phosphoserine aminotransferase	*serC*	980,484-981,563
ABUW_RS16840	3-isopropylmalate dehydratase	*leuC*	3,508,202-3,509,620
ABUW_RS11105	Glycine cleavage system h protein	*gcvH*	2,268,551-2,268,925

I then used our Hi-GRIL-seq genome browser to determine whether these mRNA molecules were present in Aar-containing chimeras. The Hi-GRIL-seq genome browser could only find few chimeras (<10 from all conditions combined) for each of the potential

A. baylyi mRNA targets, suggesting that these mRNA molecules are unlikely to be directly regulated by Aar. The upregulation of these mRNA molecules in *A. baylyi* following Aar overexpression may be due to indirect regulation of these targets or the different regulatory roles of Aar in both species.

2. IntaRNA helps discern Aar-mRNA interactions:

As was previously outlined in **Table 3.10**, CopraRNA refined the Hi-GRIL-seq Aar-mRNA interactions (Wright et al., 2013, 2014). This tool only searches for interactions that are 300 nucleotides upstream/downstream of the mRNA start codon, regardless of actual transcript sizes. To overcome this limitation, the IntaRNA interaction prediction tool was used (version 5.0.10) to individually predict these interactions *in silico* (Busch et al., 2008). The base-pairing between mRNA sequences, from their TSSs (as identified by dRNA-seq in ATCC17978) to their terminator (identified using ARNold), and Aar was predicted using this tool (Kröger et al., 2018; Naville et al., 2011). This allowed me to identify the hybridisation energies and the location of putative Aar-mRNA interactions (**Table 4.6**) for each of the CopraRNA refined mRNA targets. It is clear from this that most of these interactions were predicted to occur in the 5′-UTR, specifically within the Shine Dalgarno (SD) sequence. Bacterial sRNAs typically base-pair to mRNA targets in proximity of the start codon, within the 5′-UTR or the "5-codon window" allowing them to inhibit ribosome binding and impede translation (Bouvier et al., 2008; Storz et al., 2011). This suggested that Aar impairs expression of these mRNA molecules. The locations of base-pairing interactions between Aar and *carO*, *bfnH* and *ABUW_07310* are depicted in **Figure 4.5A, 4.5B and 4.6A,** respectively. To further compare these interaction predictions to the Hi-GRIL-seq dataset, the exact genomic locations of the individual chimeric sequencing reads for each of these putative mRNA targets were examined. The percentages of chimeric reads that mapped to the IntaRNA predictions were calculated and are reported in **Table 4.7**.

Table 4.6 IntaRNA predictions of putative Aar-mRNA interactions

Gene	Product	Interaction in mRNA	Hybridisation energy (kcal/mol)
ABUW_RS04980	CarO	5′-UTR (SD)	-27.4
ABUW_RS15085	acyl carrier protein	5′-UTR (SD)	-11.59
ABUW_RS04000	amino acid permease	Internal	-14.99
ABUW_RS08645	hypothetical protein	5′-UTR (SD)	-13.44
ABUW_RS13040	hypothetical protein	5′-UTR (SD)	-12.97
ABUW_RS07310	DMT family transporter	5′-UTR (SD)	-13.76
ABUW_RS10605	BfnH	5′-UTR (SD)	-32.93
ABUW_RS15450	BfmR	Internal	-22.96
ABUW_RS16485	permease	5′-UTR (SD)	-15.22
ABUW_RS03285	Toxin	5′-UTR (SD)	-11.19

Table 4.7 Hi-GRIL-seq chimeric reads mapping to IntaRNA predictions

Gene	Product	Hi-GRIL-seq reads mapping to predictions (%)
ABUW_RS04980	CarO	86
ABUW_RS15085	acyl carrier protein	15
ABUW_RS04000	amino acid permease	0
ABUW_RS08645	hypothetical protein	10
ABUW_RS13040	hypothetical protein	0
ABUW_RS07310	DMT family transporter	53
ABUW_RS10605	BfnH	86
ABUW_RS15450	BfmR	39
ABUW_RS16485	permease	0
ABUW_RS03285	toxin	0

Eighty-six percent of the identified *carO* (242 chimeras), *bfnH* (24 chimeras) and 53% of *ABUW_RS07310* (19 chimeras) chimeric sequencing reads mapped to their predicted interaction sites, as shown in **Figure 4.5** and **Figure 4.6A**. The high proportion of Aar-

mRNA chimeric reads mapping to these predicted duplex regions indicate that these are interactions in *A. baumannii*. The localisation of the chimeras to the SD sequences further suggest that Aar is a repressor of these genes. The predicted base-pairing duplexes between these putative interaction pairs were compared to identify any commonalities. Four Aar nucleotides (positions 29-33, 5′-CUCC-3′) were involved in base-pairing indicating that these nucleotides are vital for initiating Aar-mediated base-pairing and are the Aar "seed" region. This predicted seed region is located within a single stranded region of Aar (**Figure 4.3A**).

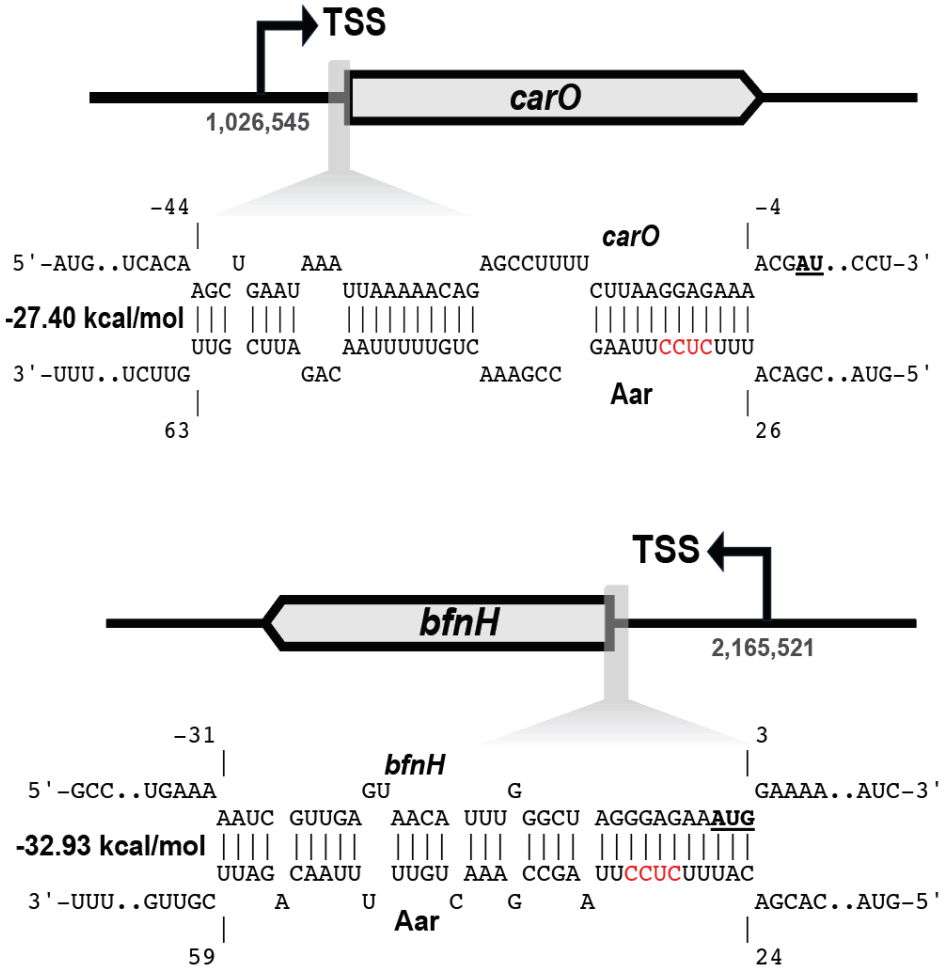

Figure 4.5 IntaRNA predicts likely Aar-mRNA interactions that sequesters *carO* and *bfnH* ribosome binding sites.

IntaRNA identified likely interaction duplexes with (A) *carO* and (B) *bfnH* (Busch et al., 2008). The location of the transcriptional start sites (TSSs, shown as curved arrow), the start codons (bold and underlined) of mRNA targets and the Aar seed region (nucleotides in red) are shown. The locations of predicted interaction duplexes are relative to these start codon.

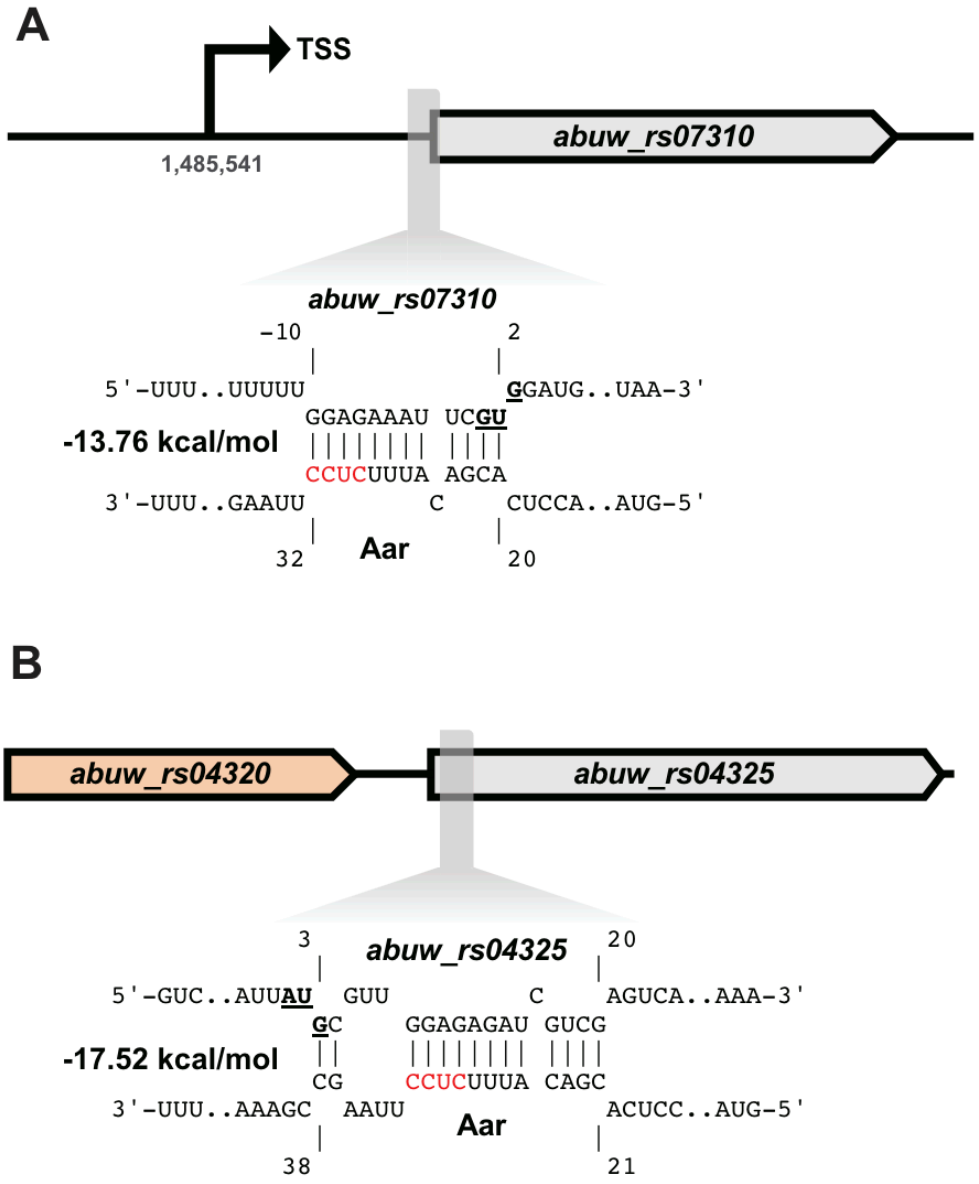

Figure 4.6 IntaRNA predicts likely Aar-mRNA interactions with *ABUW_RS07310* and *ABUW_RS04325* mRNA.

IntaRNA identified likely interaction duplexes with (A) *ABUW_RS07310* and (B) *ABUW_RS04325* (Busch et al., 2008). The location of the transcriptional start sites (TSSs, shown as curved arrow), the start codons (bold and underlined) of mRNA targets and the Aar seed region (nucleotides in red) are shown. The locations of predicted interaction duplexes

IntaRNA was used to predict interactions between Aar and all other filtered interaction pairs that were not outlined by CopraRNA (see **section 3.5**). Aar forms interactions with *ABUW_RS04325* with the predicted seed region, as shown in **Figure 4.6B**. *ABUW_RS04235* encodes a predicted neutral zinc metallopeptidase. The Aar-*ABUW_RS04325* duplex prediction occurs within the 5-codon window of *ABUW_RS04325* and a substantial proportion (92%) of the 12 chimeras mapped to the predicted interaction site (**Figure 4.8B**). The *carO*, *ABUW_RS07310* and *ABUW_RS04325* chimeric sequencing reads were evenly distributed across the IND, DIP and IMIP treatment groups, while the *bfnH* chimeric reads were confined to the DIP treatment group (**Figure 4.9**). The DIP-specific enrichment of Aar-*bfnH* chimeras is consistent with findings from prior studies that suggest that BfnH is only expressed during iron starvation (Eijkelkamp et al., 2011; Nwugo et al., 2011).

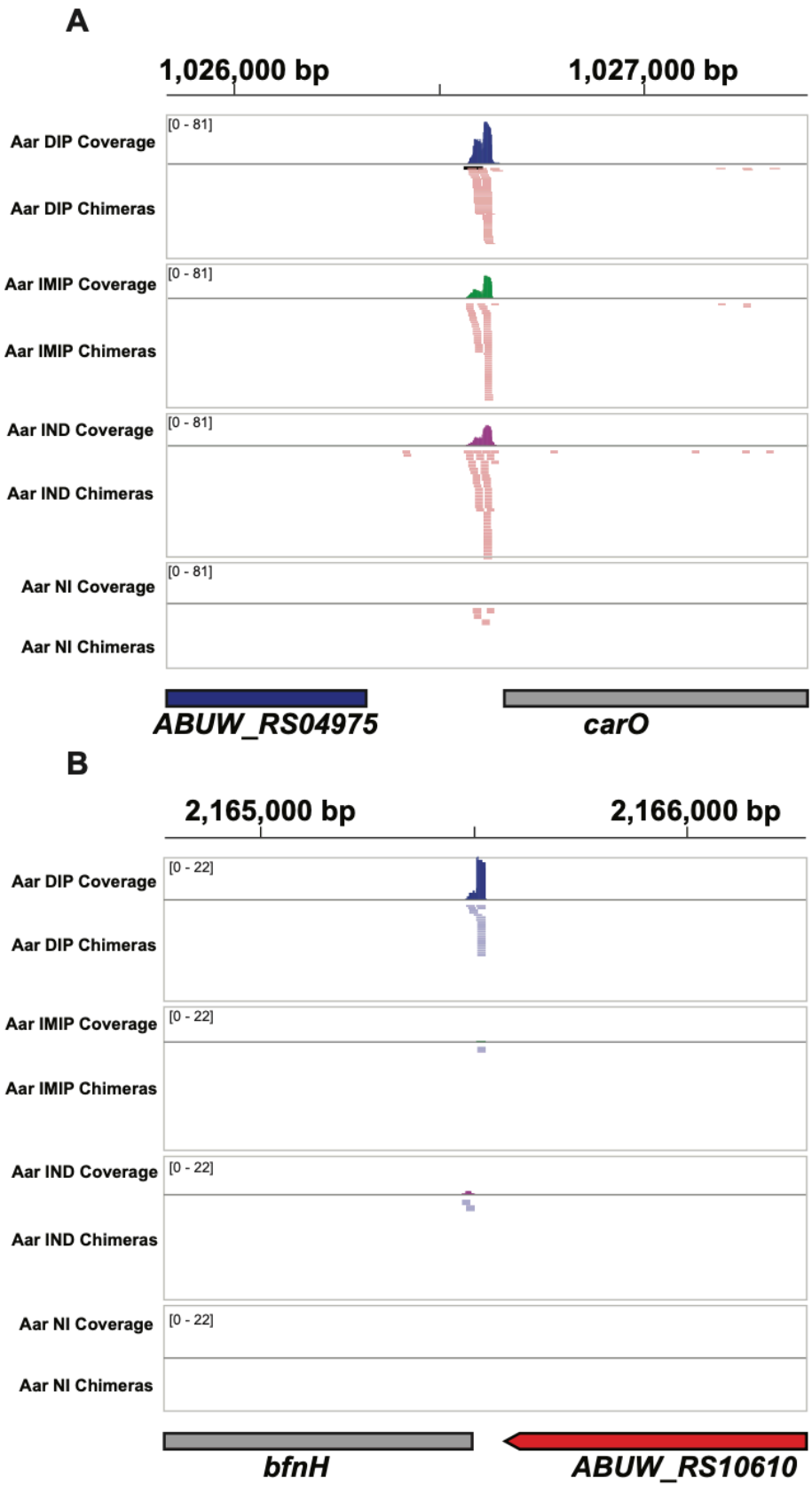

Figure 4.7 Mapping of (A) *carO* and (B) *bfnH* chimeric fragments, of Aar-*carO* and Aar-*bfnH*, respectively, to the AB5075 chromosome.

The chimeric reads for each condition used in Hi-GRIL-seq (NI, IND, DIP and IMIP) was merged and is visualised. A coverage profile of the number of chimeric reads is shown on the upper part of each track. Individual chimeric reads are shown in the lower part of each track.

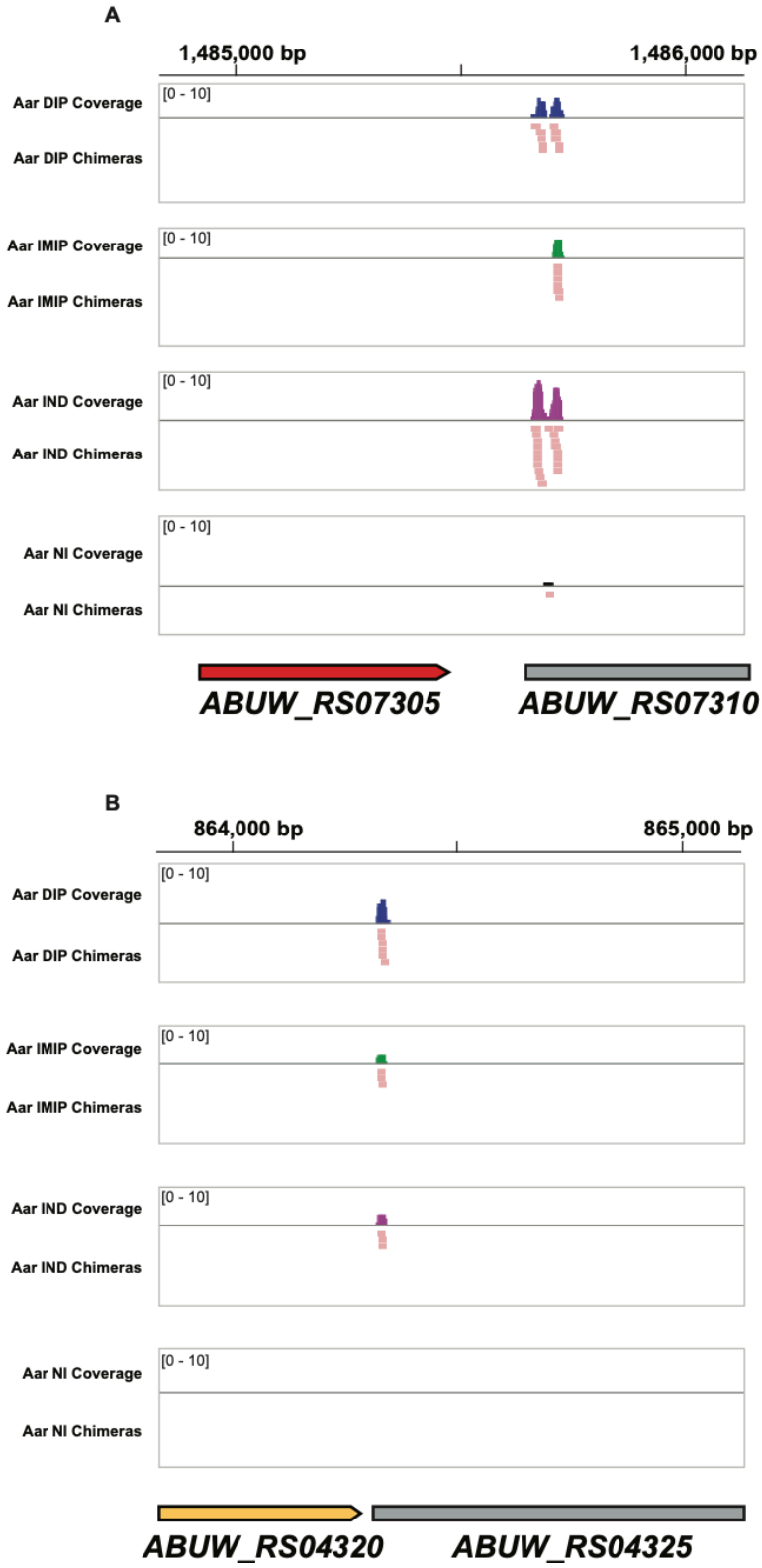

Figure 4.8 Mapping of (A) *ABUW_RS07310* and (B) *ABUW_RS04325* chimeric fragments, of Aar-*ABUW_RS07310* and Aar-*ABUW_RS04325* respectively, to the AB5075 chromosome.

The chimeric reads for each condition used in Hi-GRIL-seq (NI, IND, DIP and IMIP) was merged and is visualised. A coverage profile of the number of chimeric reads is shown on the upper part of each track. Individual chimeric reads are shown in the lower part of each track.

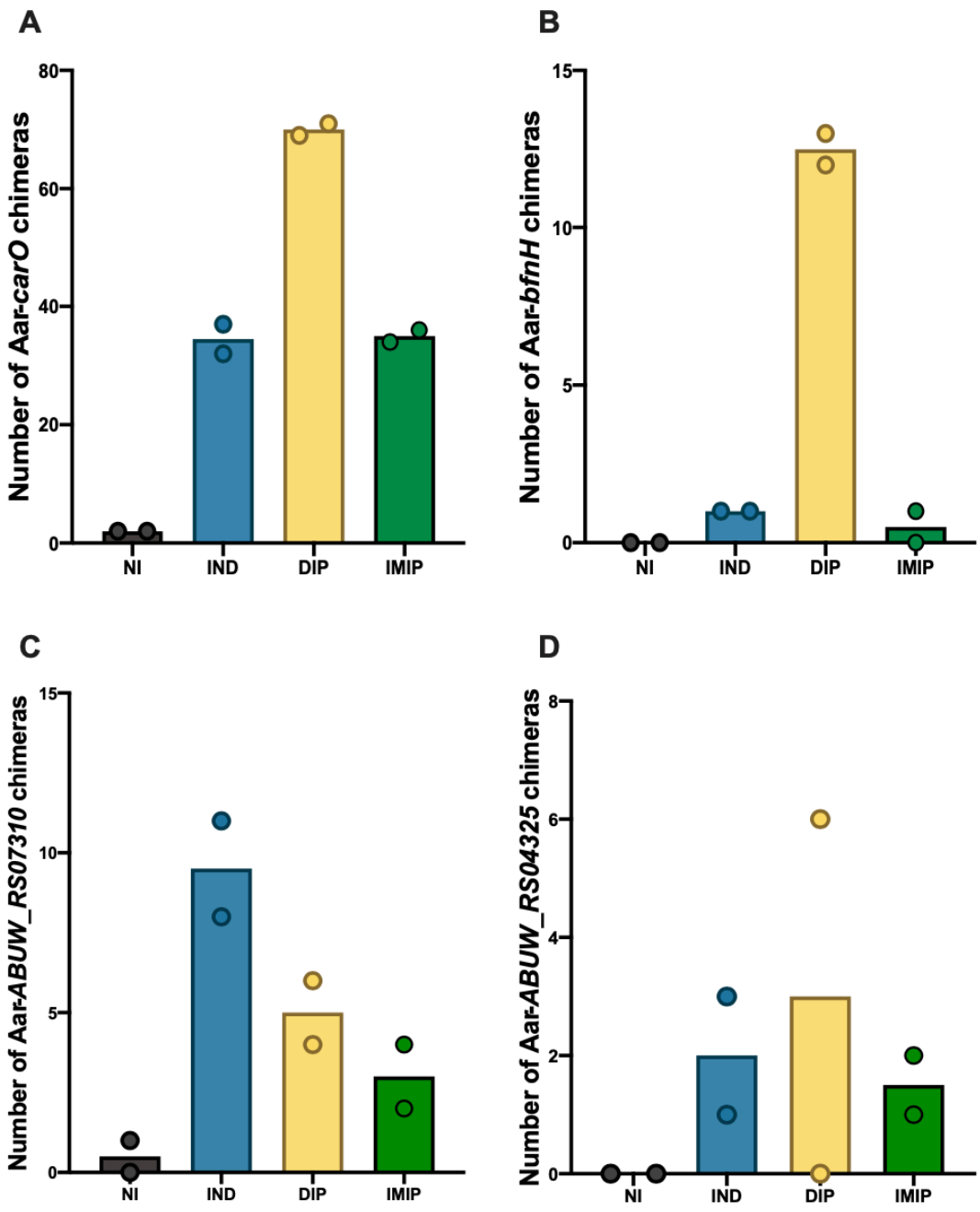

Figure 4.9 Distribution of (A) Aar-*carO*, (B) -*bfnH*, (C) -*ABUW_RS07310* and (D) -*ABUW_RS04325* chimeras among Hi-GRIL-seq conditions.

The average number of chimeras from both biological replicates for each condition (NI, IND, DIP and IMIP) are shown. The exact values of biological replicates are shown as circles for each condition.

4.4 Aar regulates mRNAs target *in vitro* using a conserved seed region:

To investigate whether Aar can interact with *carO*, *bfnH*, *ABUW_RS07310* and *ABUW_RS04325* mRNA *in vitro*, electrophoretic motility shift assays (EMSAs) were performed. This involved incubating 5′ radiolabelled Aar in the absence and the presence of increasing concentrations of these mRNA molecules before resolving these RNA molecules on native polyacrylamide gels. Base-pairing interactions between an sRNA and mRNA interaction partners result in visible band shifting due to retardation of sRNA-mRNA complexes migrating on the gel compared to unbound sRNAs (Bak et al., 2015). Aar and the mRNA molecules were prepared by *in vitro* transcription. The mRNA molecules were approximately 150 nt-long from their TSSs and included the predicted Aar interaction site. Clear band shifting patterns between Aar and higher concentrations of all the mRNA molecules were observed, as shown in **Figure 4.10A-D**. The fraction of complexed Aar did not increase at the highest concentrations of the mRNA targets, indicating that a fraction of Aar is not binding competent. This prevented us from accurately determining the dissociation constants (K_D) of these Aar-mRNA interactions. However, the band-shifting occurred at lower concentrations of *carO* and *bfnH* than for *ABUW_RS07310* and *ABUW_RS04325*. This matched the predicted hybridisation energy of these interactions (**Table 4.6**). This, combined with the presence of more abundant Aar-*carO* and Aar-*bfnH* chimeric sequencing reads, suggests that these interactions may be more physiologically important in *A. baumannii*. To determine whether the predicted Aar seed region was responsible for initiating binding to mRNA targets, Aar was mutated at the seed region from 5′-CUCC-3′ to 5′-GUGG-3′ (Aar*). The EMSAs were repeated for of the mRNA targets and the results are shown in **Figure 4.10E-H**. This completely abolished the formation of Aar-mRNA complexes, validating the vital role of the seed region in base-pairing. To ensure that this abolishment was not caused by alterations in the secondary structure of Aar*, a compensatory mutation in *carO* was created, where the Aar binding site was mutated from 5′-GAGG-3′ to 5′-CACC-3′ (*carO**), to restore base-pairing interaction. Repeating the EMSAs restored band-shifting indicated that Aar*-carO* complexes were formed (**Figure 4.11**).

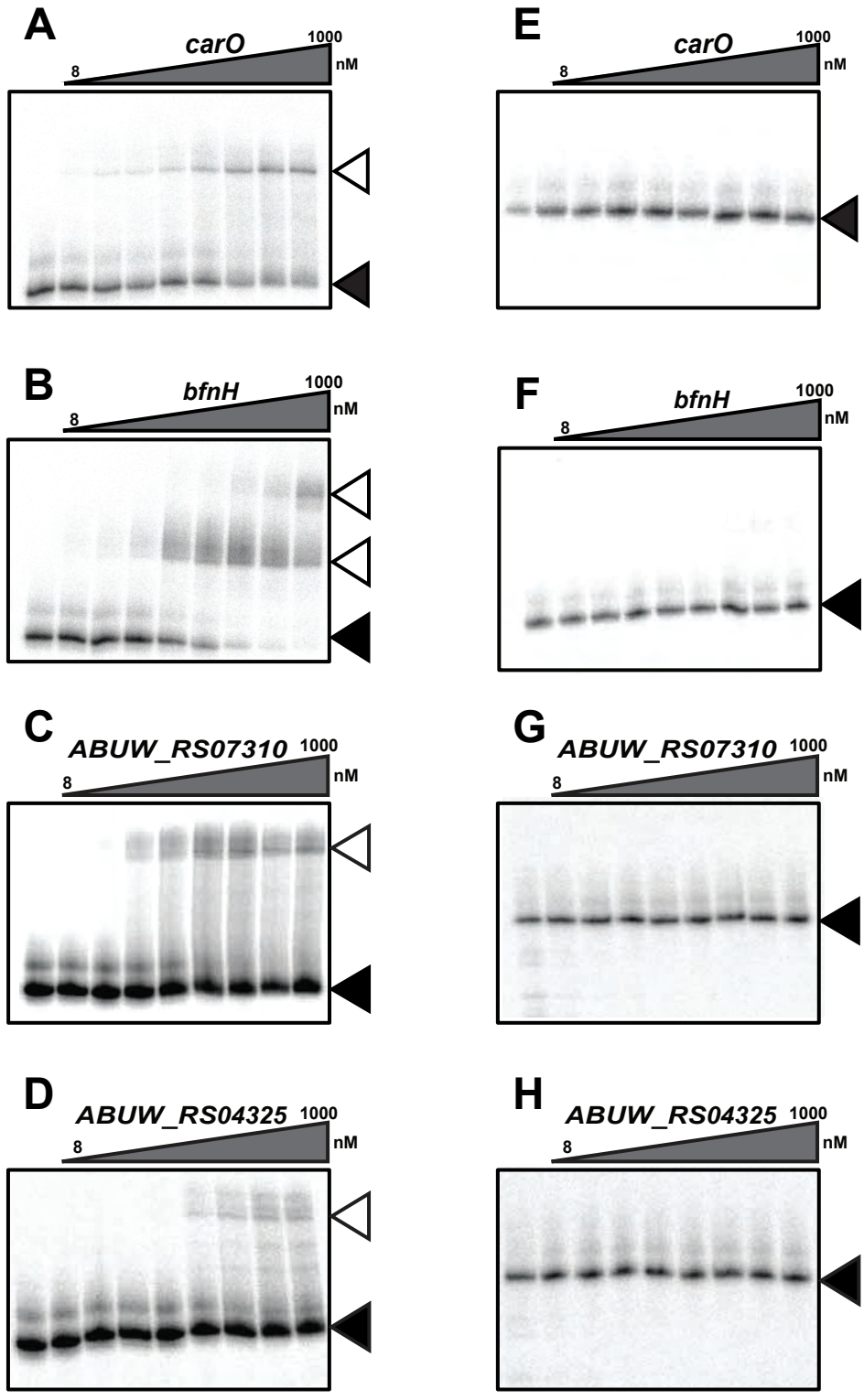

Figure 4.10 EMSAs reveal that Aar base-pair with mRNA molecules using a common seed region.

EMSAs were performed using radiolabelled wildtype Aar in the presence of increasing concentrations (from 8 nM to 1000 nM) of (A) *carO*, (B) *bfnH,* (C) *ABUW_RS07310* and (D) *ABUW_RS04325* mRNA. EMSAs were also performed using radiolabelled Aar with a seed region mutation (Aar*) with increasing concentrations of (E) *carO*, (F) *bfnH*, (G) *ABUW_RS07310* and (H) *ABUW_RS04325* mRNA.

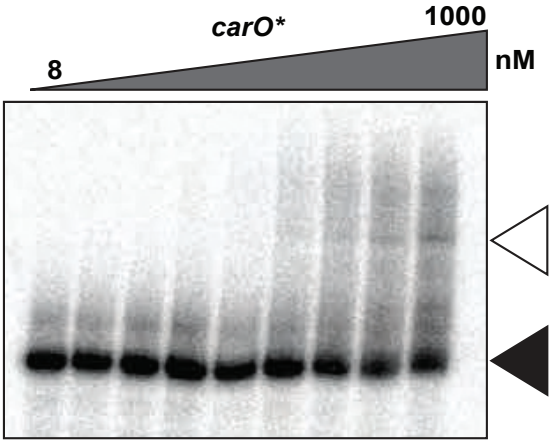

Figure 4.11 Base-pairing interactions between Aar* and *carO* can be restored using compensatory mutations in *carO* mRNA (*carO).**

EMSAs were performed using radiolabelled Aar with a seed region mutation (Aar*) with increasing concentrations of *carO** mRNA.

4.5 In-line probing reveals the exact Aar-*carO* and Aar-*bfnH* duplex structures:

To further explore the mechanistic properties of Aar base-pairing, in-line probing was employed to determine the secondary structure of Aar and the Aar nucleotides involved in base-pairing with *carO* and *bfnH* mRNAs. In-line probing is reliant on the cleavage of single stranded regions of RNA molecules, while RNA-duplexes (such as RNA stems) are protected from cleavage (Soukup et al., 1999). When Aar is incubated in the absence of mRNA interaction partners (-), it is mostly single stranded from the 5′-end until position 38, whereafter it adopts two hairpin loops (**Figure 4.12A**). This matches the *in silico* prediction of the Aar secondary structure, except the predicted stem-loop at the 5′-end is absent in the experimentally inferred secondary structure (**Figure 4.3A**). In-line probing also identified that several regions of Aar were protected in the presence of *bfnH* and *carO* (termed Region 1 to 4), indicating that they are involved in base-pairing with these mRNA molecules (**Figure 12A**). Regions 1 and 2 were protected in the presence of both *carO* and *bfnH*, while Regions 3 and 4 were only protected in the presence of *bfnH*. The exact nucleotides involved in base-pairing in these regions are shown in **Table 4.8**. Disruption of the Aar seed region (Aar*, encompassed within region 2 and visible at positions 29, 31 and 32 of the T4 ladder) resulted in the loss of protection at region 2 (**Figure 12B**). This highlighted the importance of the Aar seed region for driving inter-molecular interactions.

Table 4.8 Location of Aar nucleotides involved in base-pairing

mRNA	Region 1	Region 2	Region 3	Region 4
carO	15-17	25-38	N/A	N/A
bfnH	15-17	25-33	37-43	45-48

Additionally, the first hairpin loop of Aar was unfolded into a single strand when incubated in the presence of *bfnH* mRNA. The impact of *carO* and *bfnH* mRNA on Aar secondary structure is summarised in **Figure 4.13A-D**. This depicts the protected regions involved in base-pairing. The experimentally inferred sRNA-mRNA duplex structures are outlined in **Figure 4.13E and F**. This demonstrates that Aar sequesters the SD sequences of these mRNA molecules, potentially affecting translational efficiency. Taken together, in-line probing demonstrates that the Aar seed region is essential for mediating interactions with *carO* and *bfnH* mRNA. Furthermore, it reveals that Aar-*bfnH* interactions result in extensive rearrangements in Aar secondary structure. This analysis reveals great insight into post-transcriptional regulation by Aar.

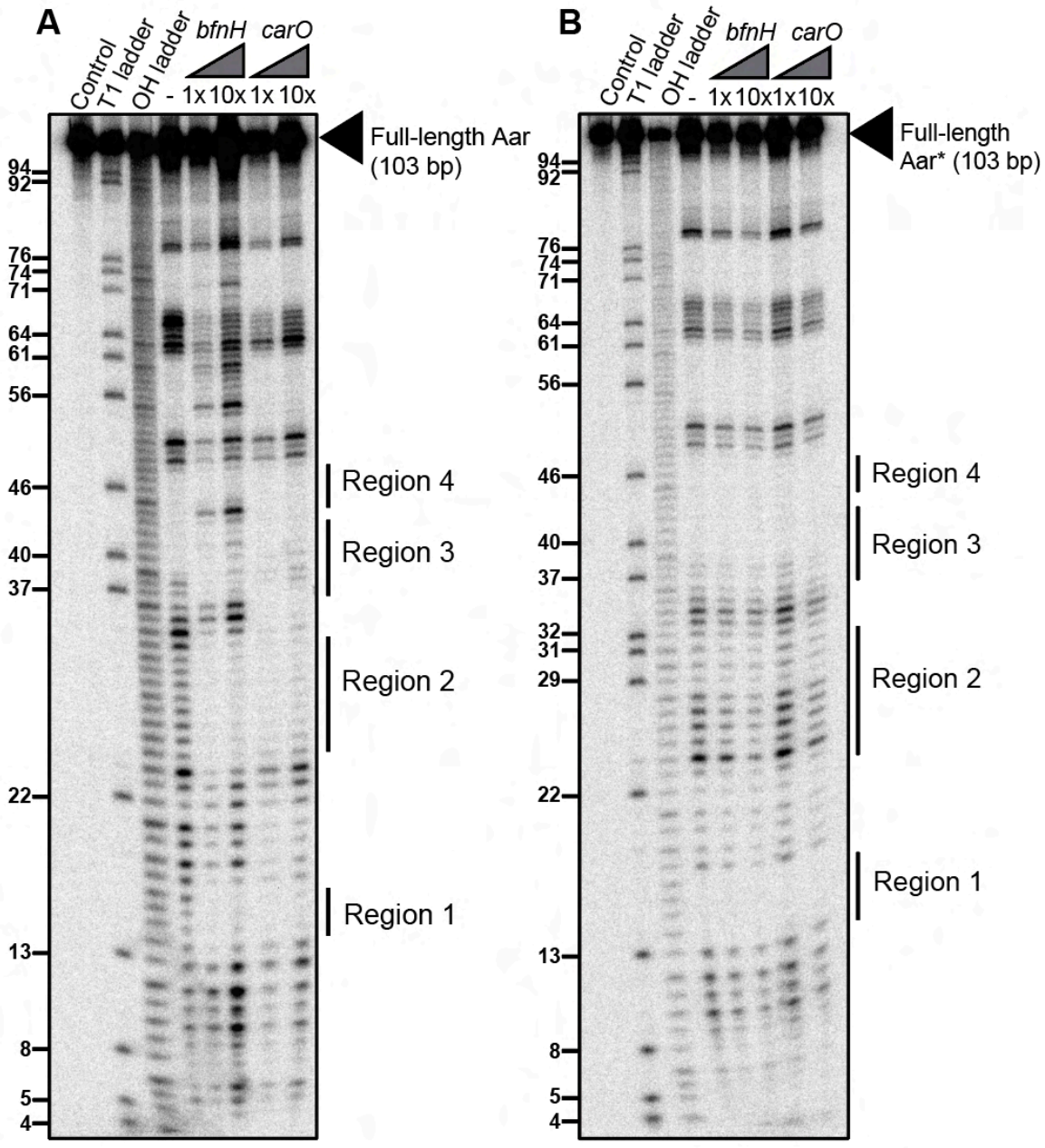

Figure 4.12 In-line probing reveals the exact Aar nucleotides involved in *carO* and *bfnH* base-pairing and disruption of the Aar seed region (Aar*) abolishes interactions.

In-line probing was performed using (A) wildtype Aar and (B) Aar*. This was performed in the absence of mRNA targets and using increasing concentrations of *carO* and *bfnH*. The protected regions (Region 1, Region 2, Region 3 and Region 4) observed using wildtype Aar incubated with *carO* and *bfnH* are indicted. Two ladders were included; a T1 ladder, where the sRNA was cleaved at guanine nucleotides, and a OH ladder, which cleaved the sRNA at the nucleotide level. The Aar seed region nucleotide substitution is visible on the T1 ladder (nucleotides 29, 31 and 32). An uncleaved Aar* control was also included.

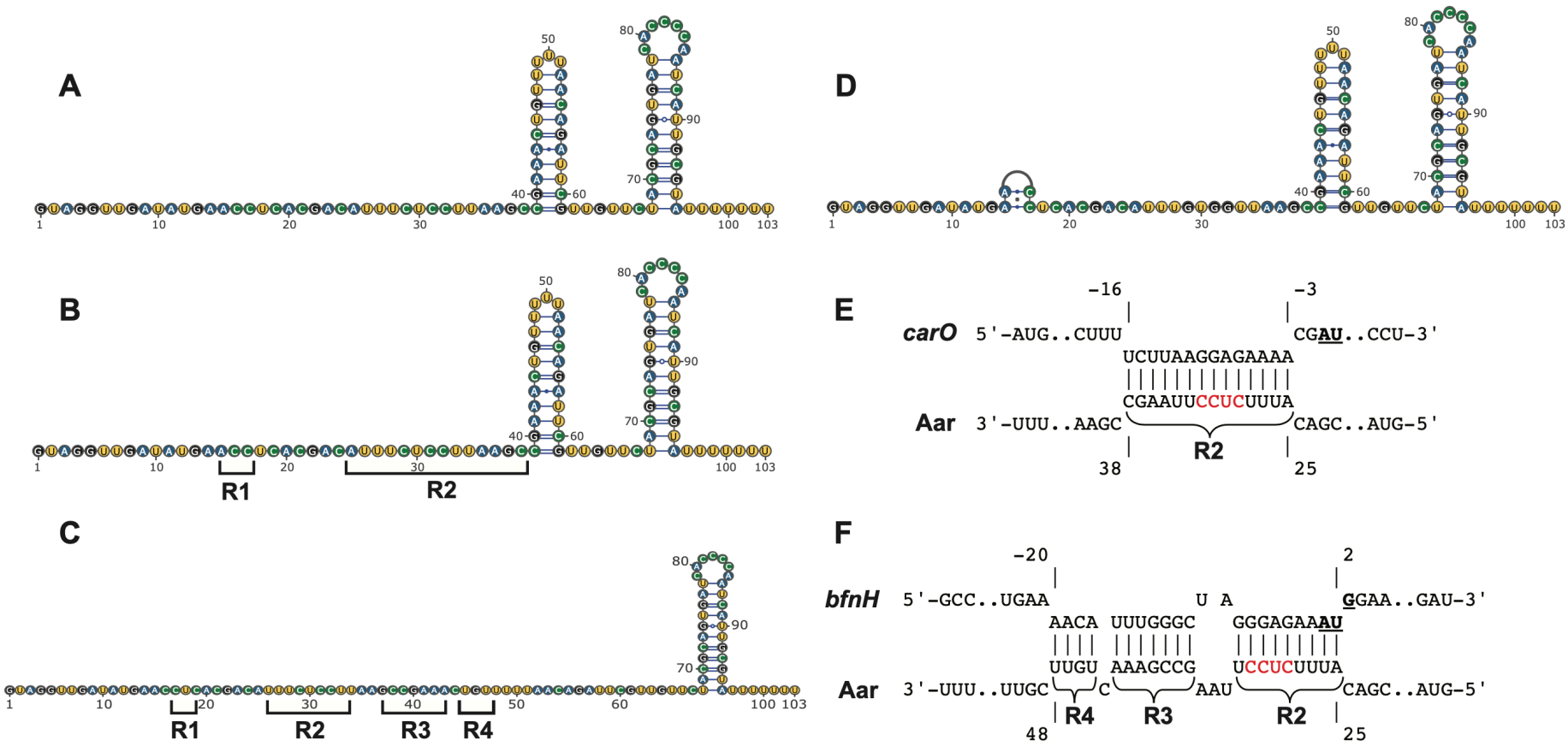

Figure 4.13 Interpretation of in-line probing experiment.

In-line probing allowed determination of the Aar secondary structure in (A) the absence of mRNA molecules, (B) in the presence of *carO* mRNA and (C) in the presence of *bfnH* mRNA. (D) The secondary structure of the Aar* is also shown. The base-pairing (E) Aar-*carO* and (F) Aar-*bfnH* duplexes structures inferred from Hi-GRIL-seq are shown. The start codons of *carO* and *bfnH* are bold and underlined and the predicted Aar seed region is highlighted in red. The location of R1 of Aar is not shown in these duplexes due to uncertainties in where it binds to *carO* and *bfnH* mRNA.

4.6 Aar represses translation of CarO, BfnH and ABUW_RS07310 in heterologous hosts:

To investigate the regulatory role of Aar *in vivo*, an established, two-plasmid based translational reporter system in *E. coli* was employed (Corcoran et al., 2012; Urban et al., 2007). This system was selected as there were no two compatible plasmids capable of co-replicating in *A. baumannii* that were available and was used to characterise sRNA-mRNA interactions in *Vibrio cholerae* (Huber et al., 2022). A schematic outlining the two-plasmid reporter system is detailed in **Figure 4.14**.

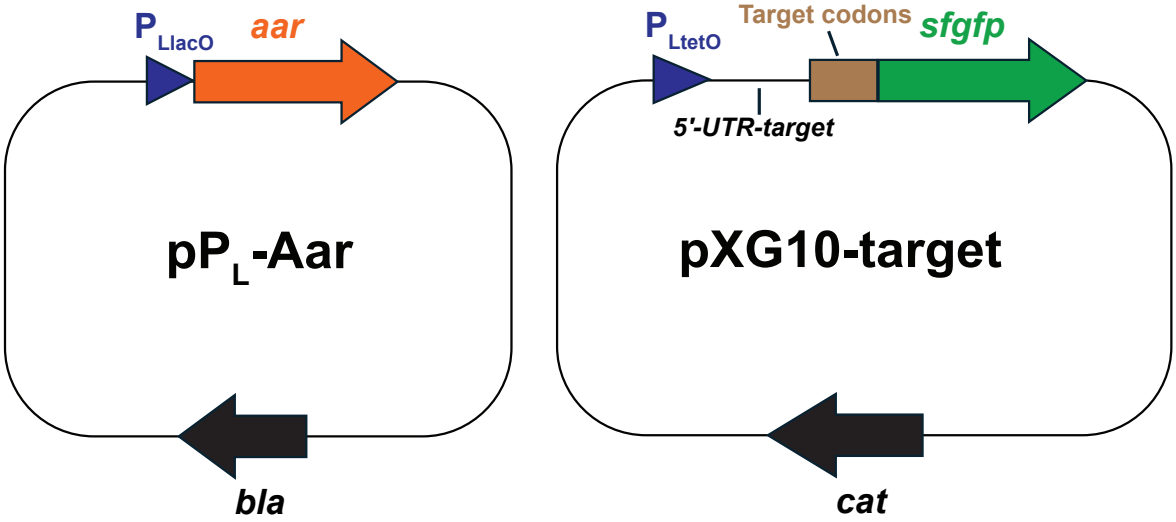

Figure 4.14 Schematic of the heterologous two-plasmid reporter system used to identify Aar-mRNA interactions.

Aar was constitutively overexpressed from the pP_L-Aar, while mRNA-sfGFP translational fusion proteins were constitutively expressed from the pXG10-target plasmid. To determine whether Aar could regulate the mRNA targets, fluorescent measurements were performed using *E. coli* and *S.* Typhimurium strains co-expressing both plasmids and compared to a control strain (expressing pJV300 with pXG10-target).

This involved constitutively overexpressing Aar from the pP_L-Aar plasmid and constitutively expressing target mRNA-sfGFP translational fusion proteins from the pXG10-target plasmid. The 5′-UTRs and first few codons (14, 17 and 6, respectively) of CarO, BfnH and ABUW_RS07310 were cloned into sfGFP (lacking a start codon) on the original pXG10 plasmid. The ABUW_RS04325 target could not be included as it is intergenic and thus lacks the TSS needed for this system. The fluorescent intensity of *E. coli* strains co-expressing these plasmids was compared to strains that co-expressed the pXG10-target plasmid with a control plasmid (pJV300). Expression of Aar significantly reduced the fluorescent intensity of CarO-sfGFP ($p<0.0001$), BfnH-sfGFP ($p<0.0001$) and ABUW_RS07310-sfGFP ($p<0.05$) compared to the control strains as shown in **Figure 4.15**. Furthermore, by introducing the same point mutations into the Aar seed region (Aar*) that were used in EMSAs and in-line probing, the repression of CarO-sfGFP and BnfH-sfGFP expression was abolished (**Figure 4.15A and B**). The fluorescence of CarO-sfGFP in the Aar* strain was restored to levels of the control strain, while the fluorescence of BfnH-sfGFP in the Aar* strain was only partially restored. The partial restoration of BfnH-sfGFP fluorescence levels may be due to more extensive base-pairing interactions outside of region 2 of Aar. These results demonstrate that Aar is a translational repressor of CarO, BfnH and ABUW_RS07310. To elucidate the role of Hfq in mediating Aar-mRNA interactions in heterologous reporter systems, we measured fluorescence of BfnH-sfGFP in wildtype and Hfq-depleted (Δ*hfq*) *Salmonella* Typhimurium ST4/74 as shown in **Figure 4.15D**. As was observed in *E. coli*, the presence of Aar in the wildtype strain significantly impaired the fluorescent intensity of BfnH-sfGFP compared to the control. The overexpression of Aar in the Δ*hfq* strain still led to reduction in fluorescence intensity of BfnH-sfGFP, however, this downregulation was more than 50% impaired compared to the wildtype strain. This suggests that Aar is at least partially dependent on Hfq to mediate translational repression of target mRNAs in this heterologous system. It is not clear from this experiment whether Hfq is needed for mediating sRNA-mRNA annealing or whether it protects Aar from degradation. In summary, using heterologous reporter systems, it was demonstrated that Aar downregulates CarO, BfnH and ABUW_RS07310, by binding to their SD sequences, occluding ribosome binding, and that Hfq assists these interactions.

4.7 Aar represses translation of CarO in *A. baumannii*:

To ensure that Aar also downregulates expression of CarO and BfnH in *A. baumannii*, a plasmid-based translational reporter system was created (**Figure 4.16**). The same CarO-sfGFP and BfnH-sfGFP translational fusions, as were used in the *E. coli* system, including their 5′-UTRs, were placed under control of the β-lactamase promoter (P_{bla}) on the pWH1266 shuttle plasmid to drive constitutive expression of these fusion proteins (Hunger et al., 1990). As there was no other plasmid capable of co-replicating with pWH1266 that could drive Aar overexpression in *A. baumannii*, this system is reliant on endogenous expression levels of Aar.

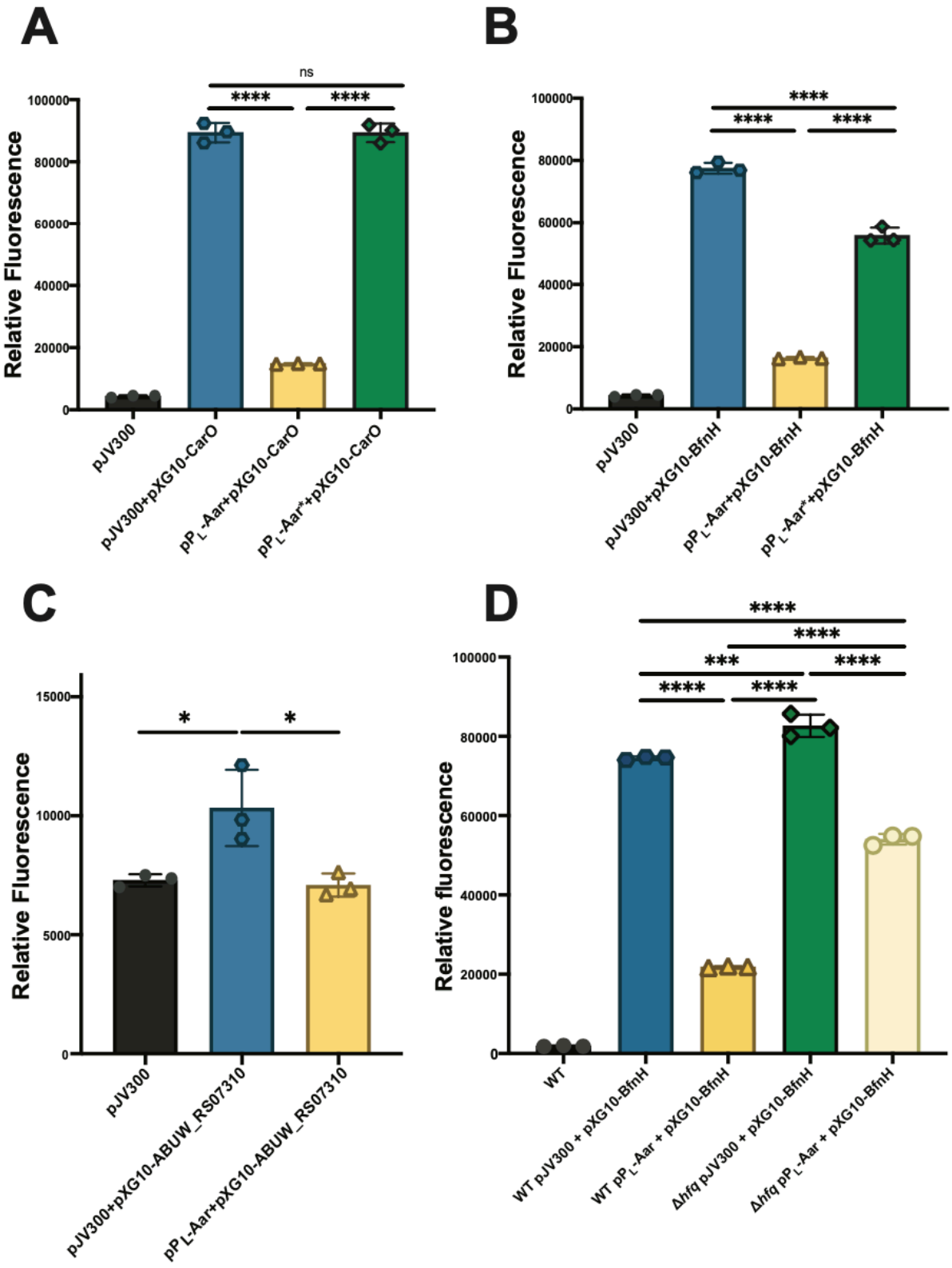

Figure 4.15 Heterologous translational reporters reveal that Aar represses mRNA targets.

The involvement of Aar (and Aar*) in modulating expression of (A) CarO, (B) BfnH and (C) ABUW_RS07310 was assessed using a two-plasmid reporter system in *E. coli*. (D) Hfq contributes to Aar-*bfnH* base-pairing in wildtype and Hfq-deletion (Δ*hfq*) *S.* Typhimurium 4/74 strains. Statistical comparisons were performed using One-way ANOVA followed by Tukey's multiple comparisons test. Differences were considered statistically significant where ns denotes P>0.05, * denotes P<0.05, ** denotes P<0.01, *** denotes P<0.001 and **** denotes P<0.0001.

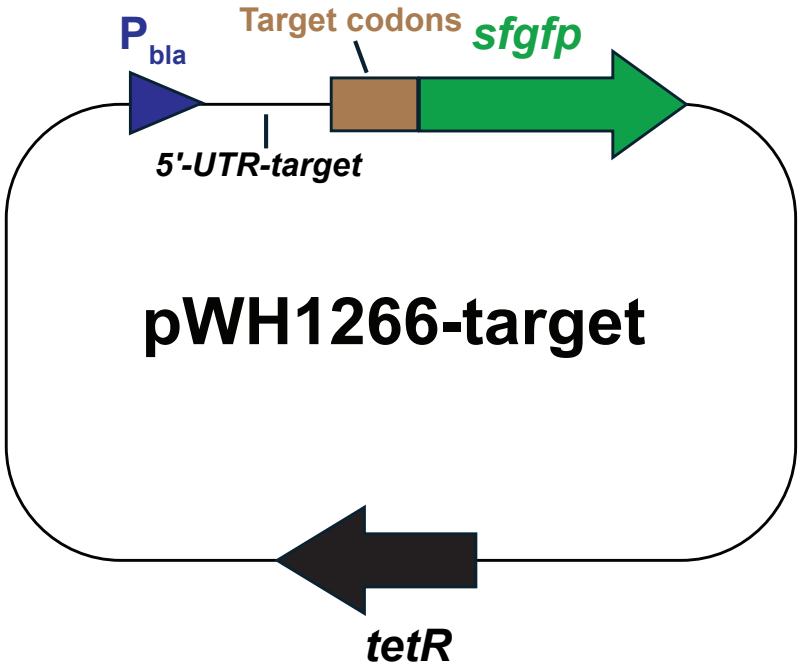

Figure 4.16 Schematic of the plasmid-based reporter system used to identify Aar-mRNA interactions in *A. baumannii* AB5075.

Target mRNA-sfGFP translational fusion proteins were constitutively expressed from β-lactamase promoter (P_{bla}) on the pWH1266-target plasmid. To determine whether endogenous Aar could regulate the mRNA targets, fluorescent measurements were performed using wildtype and Δ*aar* strains expressing this plasmid and compared to a control strain (expressing pWH1266).

To determine whether Aar could downregulate CarO-sfGFP and BfnH-sfGFP, fluorescent measurements of wildtype and Δ*aar* strains carrying these plasmids were conducted at LSP, when endogenous Aar expression levels are highest. To demonstrate that the Aar seed region is vital for mediating these interactions, these experiments were also conducted using an *A. baumannii* AB5075 chromosomal Aar seed region mutant strain (*aar**). This copy of *aar* contained the same substitutions as those used in EMSAs, in-line probing and the heterologous reporter systems. There was no significant change in BfnH-sfGFP fluorescent intensity in either the Δ*aar* nor *aar** the strains compared to the wildtype strain (**Figure 4.17A and B**, respectively). The lack of BfnH repression could be attributed to the low endogenous Aar levels in this condition, only 24 Aar-bfnH chimeras were obtained in the Hi-GRIL-seq experiment (**Figure 4.7**) There was a significant increase in CarO-sfGFP (2-fold; $p<0.0001$) fluorescence intensity in Δ*aar* than in wildtype AB5075 as shown in **Figure 4.17C**. Similarly, CarO-sfGFP fluorescent intensity significantly increased (2.9-fold; $p<0.0001$) in the *aar** strain compared to the wildtype background (**Figure 4.17C**). These results confirm that endogenous levels of Aar are sufficient to impair the CarO

translational efficiency and reveal that the Aar seed region is vital to mediate post-transcriptional regulation of CarO *in vivo* in *A. baumannii*.

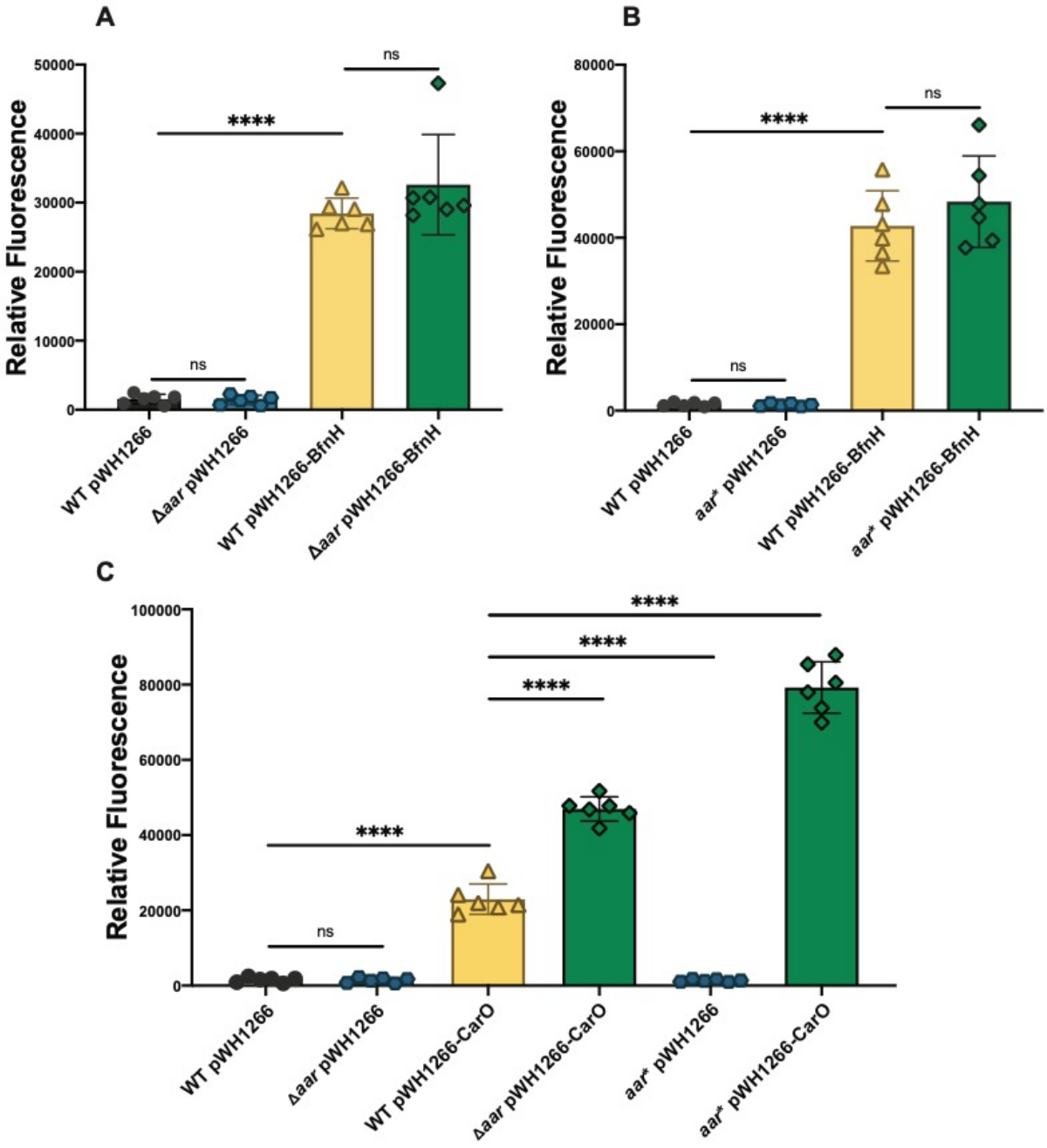

Figure 4.17 Translational reporters reveal that Aar represses *carO* in *A. baumannii* AB5075.

The relative fluorescence intensity of BfnH-sfGFP (A and B) and CarO-sfGFP, from pWH1266-BfnH and pWH1266-CarO respectively, in wildtype (WT), Aar-deletion strains (Δ*aar*) and Aar seed region mutant (Aar*) strains of *A. baumannii* AB5075 at LSP was assessed. Strains carrying the empty vector (pWH1266) were used to measure autofluorescence. Statistical comparisons were performed using One-way ANOVA followed by Tukey's multiple comparisons test. Differences were considered statistically significant where ns denotes P>0.05, * denotes P<0.05, ** denotes P<0.01, *** denotes P<0.001 and **** denotes P<0.0001.

4.8 Aar regulates CarO at the protein level in *A. baumannii*:

To assess the physiological importance of Aar in *A. baumannii*, it was investigated whether Aar could modulate endogenous CarO steady state protein levels in this pathogen. To this end, the impact of Aar overexpression on CarO protein levels was tested.

1. Constructing an Aar overexpression system in *A. baumannii*:

To investigate the impact of Aar on steady state levels of endogenous CarO, pWH1266-Aar, an Aar overexpression plasmid using a similar strategy to Schilling and colleagues was constructed (Schilling et al., 2010). To create this plasmid, the gene encoding Aar and its native promoter were cloned into pWH1266 (**Figure 4.18A**). This plasmid was then expressed in the *A. baumannii* Δ*aar* genetic background (strain cAar). Aar expression levels in cAar were compared to wildtype and Δ*aar A. baumannii* AB5075 carrying the empty control plasmid (pWH1266) using northern blotting at LSP (**Figure 4.18B**). This revealed that Aar expression was ~16-fold more abundant in cAar than in the wildtype strain (**Figure 4.18C**). The high Aar expression levels in cAar enabled investigation of CarO protein levels in AB5075.

2. Constructing *A. baumannii* CarO::3×FLAG strains:

To monitor endogenous levels of CarO in *A. baumannii* AB5075 strains by western blotting, chromosomal *carO::3×FLAG* C-terminal fusion proteins were constructed. The *carO* stop codon (TAA) was replaced with the sequence encoding 3×FLAG using a homologous recombination-based method (Godeux et al., 2020). Chromosomal *carO::3×FLAG* C-terminal fusions were constructed in wildtype and Δ*aar* genetic backgrounds. CarO was previously established to be a heat-modifiable protein that forms two distinct bands when heated at 95°C and analysed on a denaturing gel. These bands include a large “monomeric form” (MF) and a small “faster migration form” (FMF), that are approximately 30 kDa and <20 kDa in *A. baumannii* AB5075, respectively (Mussi et al., 2007; Zahn et al., 2015). Western blotting of *A. baumannii* AB5075 whole cell lysates revealed that both isomers were detectable using our system (**Figure 4.19**). There were no obvious differences in CarO protein levels between the wildtype and Δ*aar* strains,

indicating that use of the pWH1266-Aar overexpression plasmid may be more beneficial in verifying the repressive role of Aar.

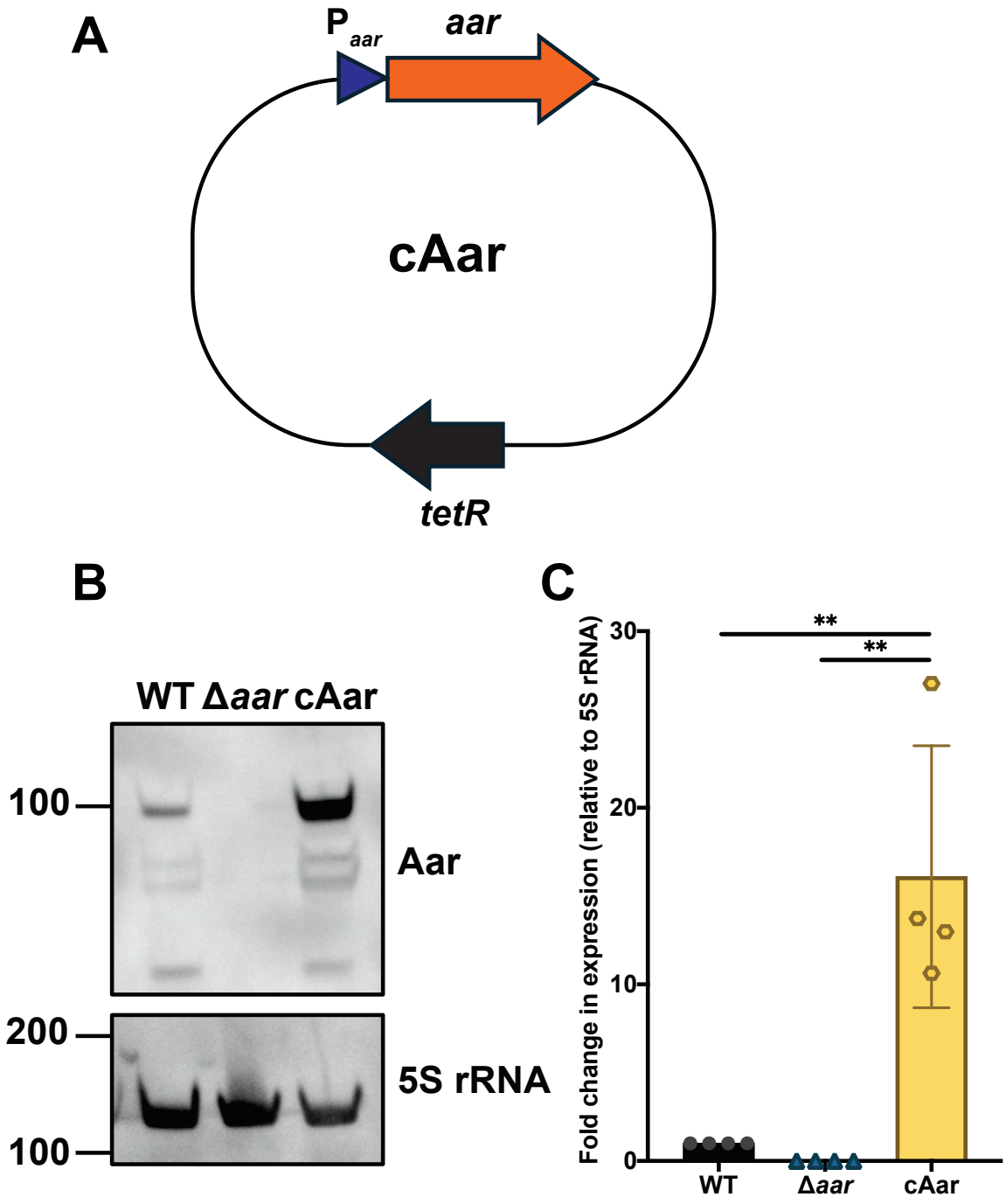

Figure 4.18 Creating an Aar-overexpression vector.

(A) Schematic of an Aar-overexpression vector (pWH1266-Aar/cAar). The *aar* gene was placed under control of its native promoter on the pWH1266 plasmid. (B) Expression of Aar in wildtype (WT), Aar-deletion (Δ*aar*) and Aar-complemented (cAar) *A. baumannii* AB5075 at LSP as determined by northern blotting. 5S rRNA was used as the loading control. The numbers in the northern blots represent the RNA ladder in nucleotides, four biological replicates were used for each northern blotting experiment. (C) Quantification of Aar in WT, Δ*aar* and cAar as determined by northern blotting and calculated as fold changes relative to WT (value set to 1). Statistical tests. Statistical tests were performed using One-way ANOVA followed by Tukey's test. Error bars represent the standard deviation from independent biological replicates. Differences were considered statistically significant where * denotes $P<0.05$ and ** denotes $P<0.01$.

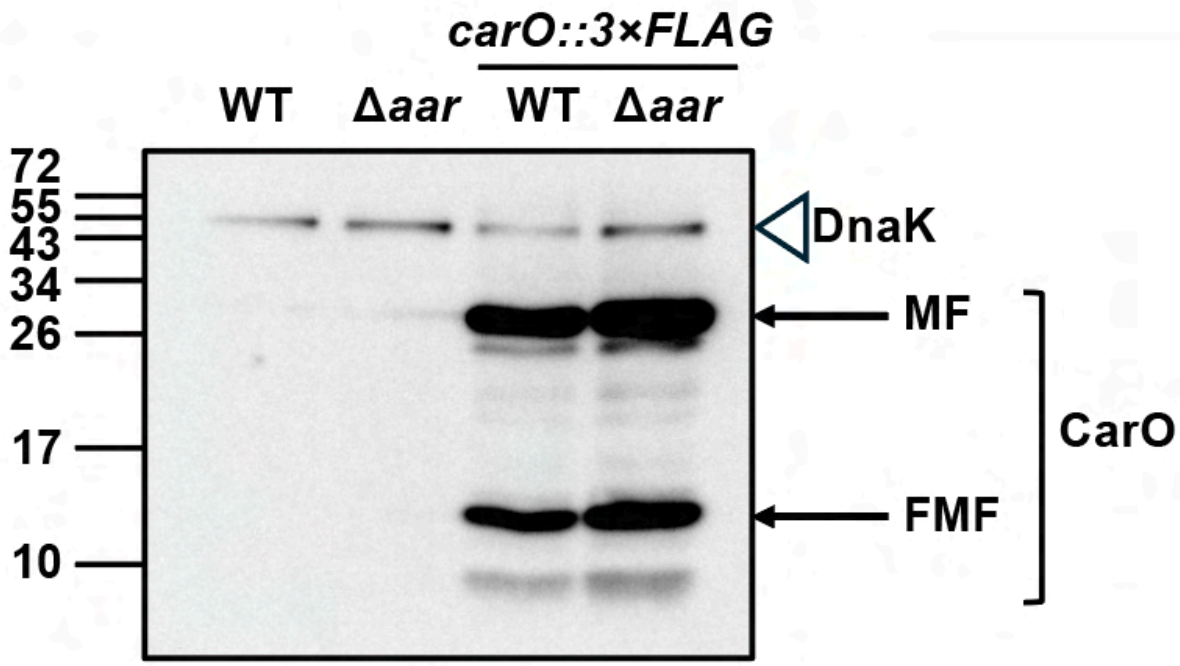

Figure 4.19 Western blotting of *A. baumannii* CarO::3×FLAG chromosomal fusions.

CarO::3×FLAG chromosomal fusions in wildtype (WT) and Aar-deletion (Δ*aar*) *A. baumannii* were tested by western blotting. Western blotting was performed using whole cell lysates of *A. baumannii* at LSP. Additionally, WT and Δ*aar* strains lacking the chromosomal fusions were included as negative controls. DnaK was used as the loading control. Expression of CarO and the loading control DnaK was detected using anti-FLAG and anti-DnaK antibodies respectively. The monomeric form (MF) and faster migration form (FMF) isoforms of CarO are indicated. Western blotting was performed independently using two biological replicates of each strain.

3. Aar overexpression represses CarO::3×FLAG in *A. baumannii*:

To determine whether Aar represses CarO protein levels in *A. baumannii*, CarO::3×FLAG expression levels in wildtype, Δ*aar* and cAar *A. baumannii* AB5075 were compared by western blotting (**Figure 4.20**). These strains were grown to LSP, when Aar expression levels are at their highest, prior to preparation of whole cell lysates. There was a 2.1-fold reduction of CarO::3×FLAG in the cAar strain compared to the wildtype strain (**Figure 4.21**). Similarly, there was a significant reduction (3.5-fold; $p<0.05$) of CarO::3×FLAG in cAar compared to Δ*aar A. baumannii*. From these experiments, it is evident that Aar represses endogenous CarO protein in *A. baumannii*, reflecting the utility of our Hi-GRIL-seq dataset in deciphering physiological important RNA-RNA interactions.

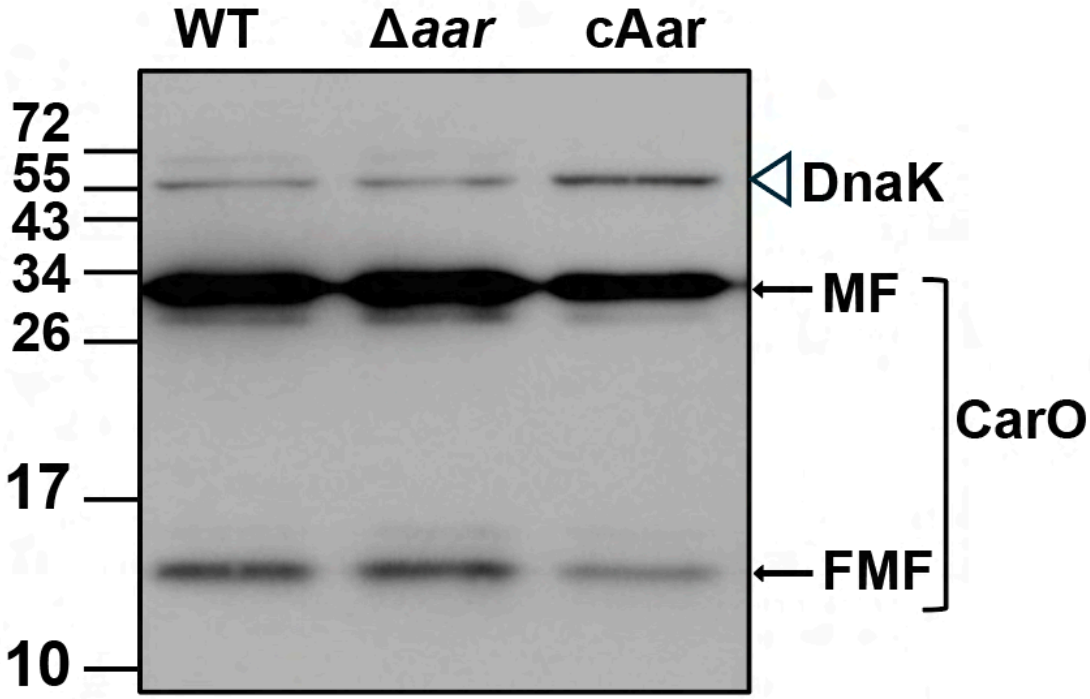

Figure 4.20 Western blotting reveals that Aar-overexpression downregulates CarO in *A. baumannii* AB5075.

Steady state levels of CarO::3×FLAG chromosomal fusions in wildtype (WT), Aar-deletion (Δ*aar*) and Aar-overexpression (cAar) *A. baumannii* AB5075 were tested by western blotting. Western blotting was performed using whole cell lysates of *A. baumannii* at LSP. DnaK served as the loading control. Expression of CarO and the loading control DnaK was detected using anti-FLAG and anti-DnaK antibodies respectively. The monomeric form (MF) and faster migration form (FMF) isoforms of CarO are indicated. Western blotting was performed independently using six biological replicates of each strain.

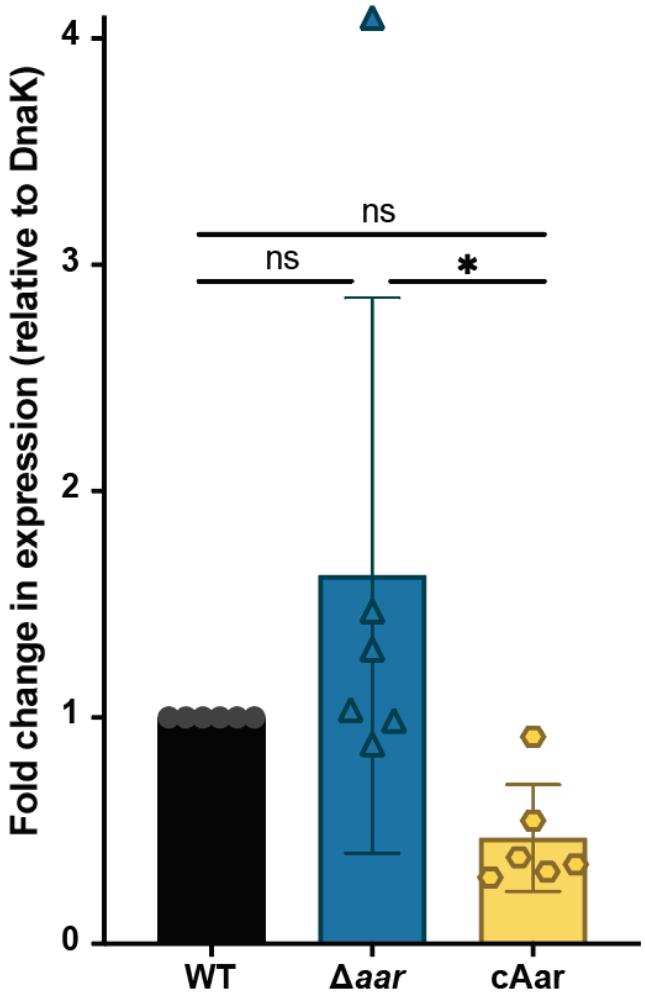

Figure 4.21 Quantification of CarO in wildtype (WT), Aar-deletion (Δ*aar*) and Aar-overexpression (cAar) strains *A. baumannii* AB5075 by western blotting.

CarO expression was calculated as fold changes relative to WT (value set to 1). Statistical tests were performed using One-way ANOVA followed by Tukey's test. Error bars represent the standard deviation from independent biological replicates. Differences were considered statistically significant where ns denotes P>0.05, * denotes P<0.05 and ** denotes P<0.01.

4.9 Target hunt experiments provide greater insight into the Aar mechanism of action:

The previous experiments revealed that Aar binds to the SD sequences of *carO*, *bfnH* and *ABUW_RS07310* mRNAs, repressing their expression. While most sRNAs use this strategy to physically prevent ribosome binding, they can also destabilise mRNA molecules, this is by making them more susceptible to degradation by ribonucleases (Møller et al., 2002; Rice et al., 2011). To investigate whether Aar also destabilises these target mRNAs in *A. baumannii* and to identify other potential mRNA interaction partners, we performed a transient pulse overexpression of the sRNA.

1. Creation of an inducible Aar-overexpression vector:

To perform the pulse overexpression experiment, an inducible Aar-overexpression vector was created. This was accomplished by placing Aar under transcriptional control of the L-arabinose inducible promoter (P_{BAD}) on the pVRL2Z plasmid, creating pVRL2Z-Aar (**Figure 4.22A**). Induction of pVRL2Z-Aar with L-arabinose repressed BfnH-sfGFP, when co-expressed with pXG10-BfnH in *E. coli*, demonstrating that it retained its regulatory ability (**Figure 4.22B**). This plasmid and the control plasmid (pVRL2Z) were transformed into the Δ*aar A. baumannii* AB5075 genetic background for the pulse overexpression experiment. To identify the optical concentration of L-arabinose needed to induce Aar from *A. baumannii* carrying pVRL2Z-Aar, a dose-dependent analysis coupled with northern blotting was performed (**Figure 4.23A**). Aar expression was assessed following induction of the culture with 0 mM, 50 mM or 100 mM L-arabinose for 1 h at LEP. As previously determined, the induction of the culture with 100 mM L-arabinose improved Aar expression. It was also observed that some larger non-specific bands that were induced even in the absence of L-arabinose. It is unclear what they are, but it could be explained by the presence of alternative TSSs within the construct. To ensure that shorter induction times could still yield overexpression in *A. baumannii*, we induced cultures with 100 mM L-arabinose and measured Aar expression following 15 min, 30 min and 1 h intervals using northern blotting (**Figure 4.23B**). It was clear from this that 15 min induction still led to sufficient expression for use in this target hunt experiment. No Aar expression was detected from the negative control (pVRL2Z).

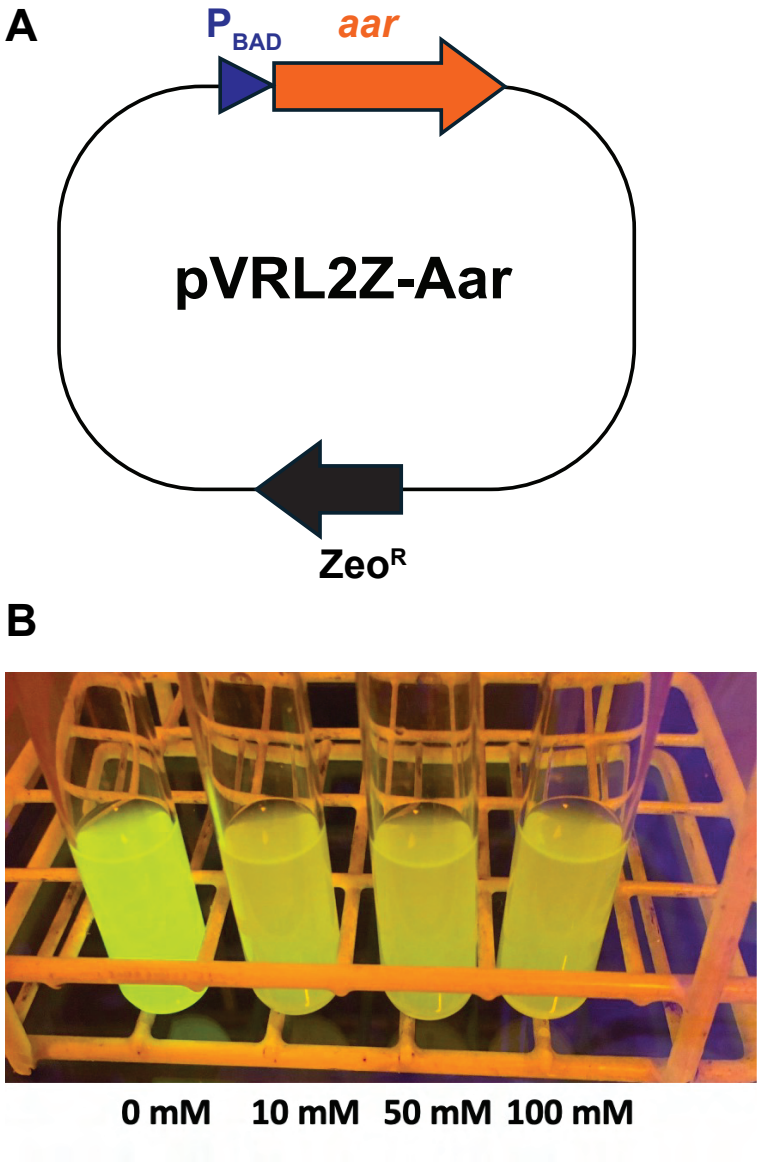

Figure 4.22 Constructing pVRL2Z-Aar.

(A) Schematic of the pVRL2Z-Aar plasmid, *aar* was placed under control of the L-arabinose inducible promoter (P_{BAD}). (B) Aar continues to repress BfnH-sfGFP when *E. coli* co-expressing pVRL2Z-Aar and pXG10-BfnH was induced with L-arabinose (10 mM, 50 mM and 100 mM). Fluorescence was imaged by placing 5 mL overnight cultures under blue light.

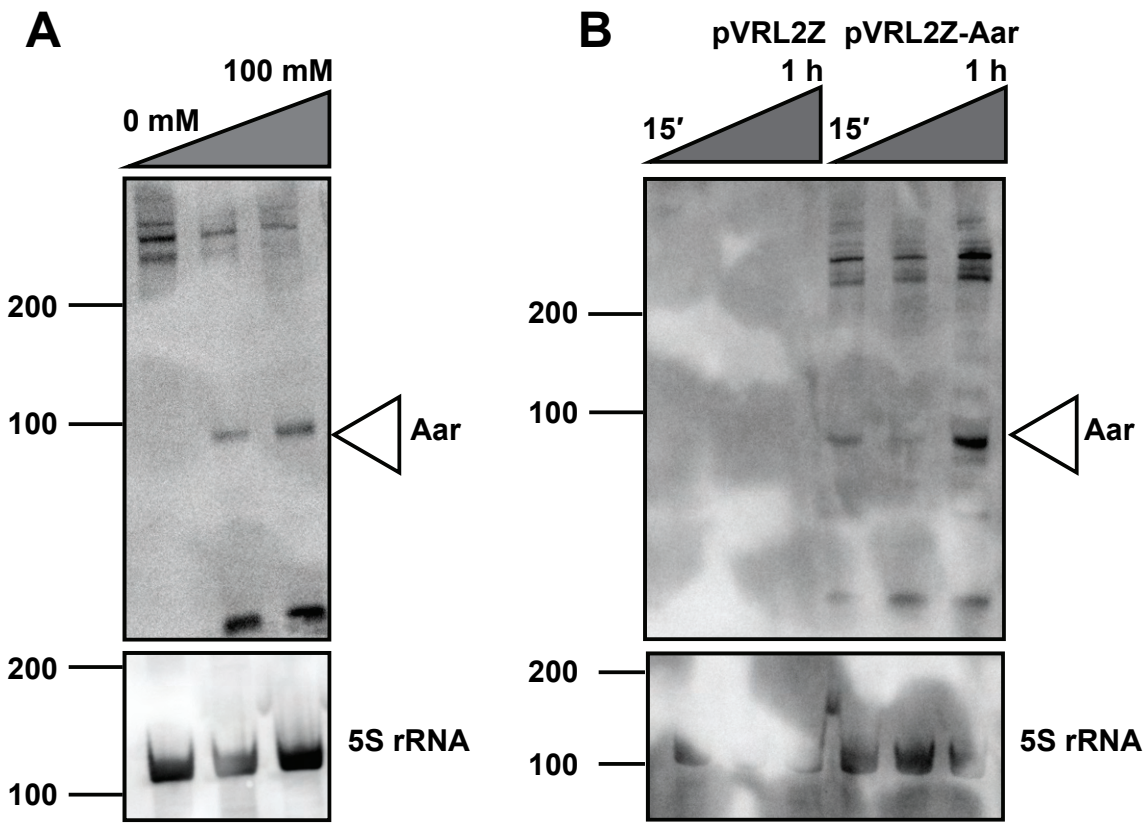

Figure 4.23 Driving Aar expression from pVRL2Z-Aar.

(A) Dose-dependent expression of Aar from pVRL2Z-Aar in *A. baumannii* AB5075 as determined by northern blotting at LEP. Aar expression was induced using different concentrations of L-arabinose (0 mM, 50 mM and 100 mM) after 1 h induction. (B) Expression Aar from pVRL2Z-Aar in *A. baumannii* AB5075 at different time intervals (15 min, 30 min and 1 h) after induction with 100 mM L-arabinose as determined by northern blotting. *A. baumannii* AB5075 expressing the empty vector (pVRL2Z) was included as a control. 5S rRNA was used as the loading control.

2. Pulse overexpression of Aar in *A. baumannii* AB5075:

To perform Aar pulse overexpression, *A. baumannii* cultures expressing pVRL2Z and pVRL2Z-Arp were grown to LEP and incubated with 100 mM L-arabinose for 15 min, prior to RNA isolation and sequencing (GENEWIZ from Azenta Life Science). LEP was selected as this is a growth conditions when endogenous levels of Aar are low (**Figure 4.2C**). This experiment was performed in biological duplicate (n=2) for each strain. To identify mRNA molecules regulated by Aar, we measured the genes that were upregulated (log2(fold change) > 1) or downregulated (log2(fold change) < -1) in the overexpression strain compared to the control strain. The differentially expressed genes are visualised as a volcano plot in **Figure 4.24**.

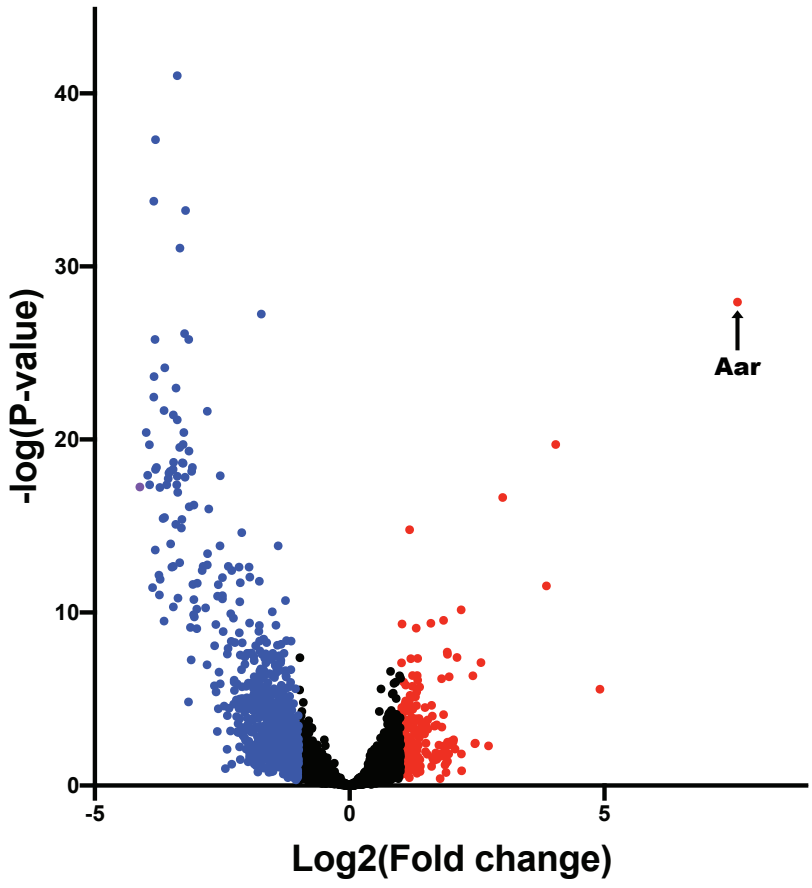

Figure 4.24 Pulse overexpression of Aar leads to differential expression of 1,005 genes.

Volcano plot showing genes upregulated (red) and downregulated (blue) upon Aar overexpression from pVRL2Z-Aar relative to the control strain (pVRL2Z). Points labelled in black failed to meet the required fold change cut off scores. The point corresponding to Aar is indicated, revealing that the pulse-overexpression of this sRNA was successful.

We found that there were 1,005 differentially expressed genes upon Aar overexpression, the majority (78%) of which were downregulated (782 genes) and a smaller fraction (22%) of genes were upregulated (223 genes). This further reinforces the perspective that Aar is a global genetic regulator in *A. baumannii*. The 10 most downregulated and upregulated genes are listed in **Tables 4.9** and **4.10**, respectively. The full list of upregulated and downregulated genes is available in **Appendix IV**.

Table 4.9 Top 10 genes downregulated upon Aar overexpression

Gene	Product	log2(fold change)	p-value
ABUW_RS03690	GntR family transcriptional regulator	-3.82	1.6E-26
ABUW_RS03640	hypothetical protein	-3.84	2.3E-24
ABUW_RS06790	phage protein Bet	-3.84	3.6E-23
ABUW_RS06865	hypothetical protein	-3.84	1.7E-34
ABUW_RS06155	hypothetical protein	-3.87	3.7E-12
ABUW_RS06810	hypothetical protein	-3.93	4.2E-18
ABUW_RS06805	hypothetical protein	-3.93	2.0E-20
ABUW_RS06150	hypothetical protein	-3.96	1.1E-18
ABUW_RS06800	hypothetical protein	-3.99	3.9E-21
ABUW_RS06145	PD-(D/E)XK nuclease-like protein	-4.12	5.5E-18

Unsurprisingly, Aar was the most upregulated gene in the overexpression strain (log2(fold change) = 7.6). Two transcriptional regulators (ABUW_RS00890 and ABUW_RS07305) were also upregulated. ABUW_RS00890 is an orphan response regulator, it is suggested to be a member of the LuxR family, that are involved in quorum sensing in bacterial species (Casella et al., 2017). ABUW_RS07305 is a TetR type transcriptional regulator that is involved in the stochastic phase variation between the virulent, opaque and the non-virulent, translucent subpopulations of *A. baumannii* AB5075 (Chin et al., 2018; Pérez-Varela et al., 2022). Genes involved in chemotaxis, type I fimbriae (FimC) and type IV pili (PilA) were also upregulated upon overexpression of Aar. These genes are involved in

biofilm formation and twitching motility (Pakharukova et al., 2018; Salah Ud-Din et al., 2017; Vesel et al., 2021).

Table 4.10 Top 10 genes upregulated upon Aar overexpression

Gene	Product	log2(fold change)	p-value
Aar	Aar	7.61	1.2E-28
ABUW_RS01495	pilin	4.91	2.7E-06
ABUW_RS20125	hypothetical protein	4.05	1.9E-20
ABUW_RS09960	hypothetical protein	3.86	2.9E-12
ABUW_RS00890	response regulator	3.00	2.3E-17
ABUW_RS07305	TetR/AcrR	2.72	5.1E-03
ABUW_RS05570	EAL domain-containing protein	2.58	7.8E-08
sRNA19	sRNA19	2.47	3.5E-03
ABUW_RS03350	chemotaxis protein	2.46	3.7E-03
ABUW_RS11240	pilus periplasmic chaperone	2.42	4.6E-07

The most downregulated genes included two operons (ABUW_RS06790, ABUW_RS06810, ABUW_RS06805 and ABUW_RS06800 & ABUW_RS06155, ABUW_RS06150 and ABUW_RS06145) that was viral prophages according to BLAST-based searches (Camacho et al., 2009). A GntR family transcriptional regulator (ABUW_RS03690) was also downregulated following Aar overexpression, however, its role in *A. baumannii* gene regulation is currently unknown. Surprisingly, *carO*, *bfnH*, *ABUW_RS07310* and *ABUW_RS04325* were not upregulated or downregulated in the pulse overexpression of Aar. This suggests that Aar is primarily involved in blocking translation of the mRNAs without impacting their stability.

3. Comparing pulse overexpression with Hi-GRIL-seq and CopraRNA:

While pulse overexpression demonstrated that many genes are differentially expressed upon Aar expression, it is uncertain whether these genes are directly regulated by the sRNA through base-pairing or through more indirect mechanisms. To identify Aar-RNA interactions, the results of the pulse-overexpression experiment were compared with the filtered Aar Hi-GRIL-seq chimeras and with CopraRNA predictions (**Figure 4.25**). There were no genes identified by all three approaches, however, 43 putative mRNA targets were

predicted by CopraRNA that were also identified by pulse overexpression as outlined in **Table 4.11**. These genes encode proteins involved in disparate roles in *A. baumannii* including metabolism, antibiotic efflux, and structural proteins with no discernible common pattern of function. The absence of chimeric sequencing reads from the Hi-GRIL-seq experiment undermines the likelihood of potential base-pairing interactions between these RNA molecules.

Nineteen potential Aar targets identified by pulse-overexpression also featured in Hi-GRIL-seq Aar-containing chimeras as outlined in **Table 4.12**. The majority (53%) of these mRNAs were downregulated upon Aar overexpression. The downregulated mRNA molecules are involved in osmolarity regulation, phenylacetic acid degradation and iron starvation responses (Bhuiyan et al., 2016; Hubloher et al., 2020; Zeidler et al., 2017). The upregulated mRNAs included primarily tRNAs and OmpW (Catel-Ferreira et al., 2016). Interestingly, 85% of Aar-*bauF* chimeras (33 chimeras from all conditions) mapped to the predicted interaction duplex of *bauF* as predicted by IntaRNA (**Figure 4.26A and B**) (Busch et al., 2008). BauF is a member of the acinetobactin siderophore cluster of genes, responsible for regulating the biosynthesis and activity of acinetobactin (Sheldon et al., 2020). The chimeric sequencing reads were confined towards the 3′ end of the gene in the iron starvation condition (DIP), suggesting that interaction with Aar may destabilise *bauF* mRNA upon iron starvation. The Aar seed region is predicted to be involved in base-pairing. Therefore, Aar-*bauF* interactions should be investigated further in future experimentation.

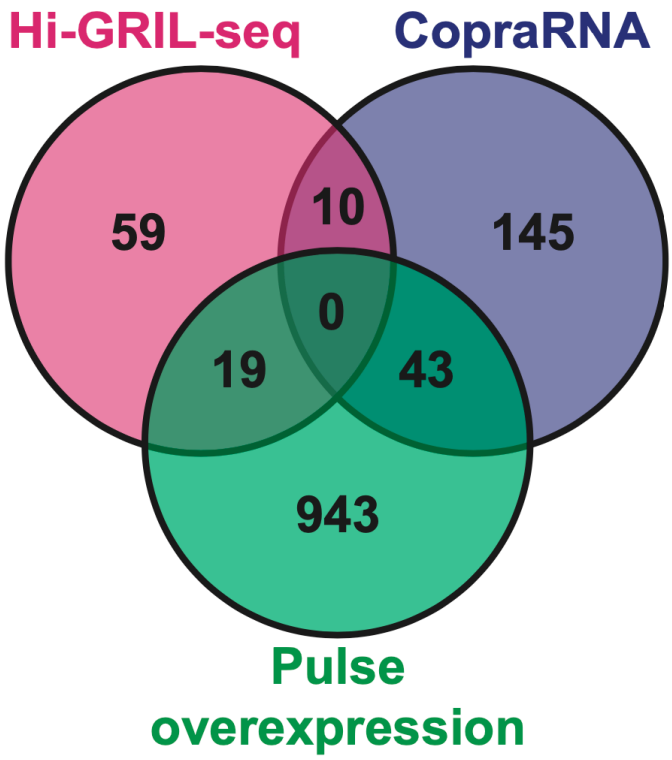

Figure 4.25 Comparing pulse overexpression of Aar with Hi-GRIL-seq and CopraRNA predictions.

Venn diagram showing common, putative mRNA targets identified by pulse overexpression, Hi-GRIL-seq and CopraRNA.

Table 4.11 Potential Aar targets shared by CopraRNA and pulse overexpression

Gene	Product	log2(fold change)	p-value
ABUW_RS09120	CoA transferase subunit B	-1.47	5.62E-04
ABUW_RS11915	methyltransferase	-1.97	2.76E-03
ABUW_RS11360	SfnB sulfur acquisition oxidoreductase	-1.72	2.62E-08
ABUW_RS08280	ABC transporter substrate	-1.00	4.49E-03
ABUW_RS10230	MFS transporter	-1.08	1.88E-01
ABUW_RS08295	nitrite reductase large subunit nirB	-1.63	2.80E-06
ABUW_RS14750	GNAT family N-acetyltransferase	-1.07	3.93E-03
ABUW_RS09050	hypothetical protein	-2.12	2.03E-07
ABUW_RS14405	MarC family protein	-1.52	9.76E-04
ABUW_RS08940	4-carboxymuconolactone decarboxylase	-1.49	3.41E-05
ABUW_RS12440	nucleoside deaminase	-1.14	3.65E-03
ABUW_RS06250	hypothetical protein	-1.02	1.83E-02
ABUW_RS09440	MFS transporter	-1.30	6.55E-02
ABUW_RS03625	hypothetical protein	-2.59	1.13E-11
ABUW_RS11785	amino acid ABC transporter	-1.23	1.21E-01
ABUW_RS09055	nuclear transport factor 2 family protein	-1.84	1.78E-06
ABUW_RS05840	xanthine dehydrogenase	-1.04	6.04E-04
ABUW_RS17120	30S ribosomal protein S15 rpsO	-1.13	2.03E-02
ABUW_RS18350	lipoprotein-sorting protein	-1.24	4.22E-09
ABUW_RS18390	MHS family MFS transporter	-1.50	1.04E-01
ABUW_RS20435	hypothetical protein	-3.34	1.30E-13
ABUW_RS12375	(2Fe-2S)-binding protein	-1.70	1.88E-05
ABUW_RS03505	Asn/Gln amidotransferase subunit GatB	-1.11	2.70E-04
ABUW_RS09110	3-oxoadipate enol-lactonase pcaD	-1.12	1.20E-03
ABUW_RS06510	multidrug efflux RND transporter AdeH	-1.36	1.59E-05

ABUW_RS01595	triacylglycerol lipase	-1.50	2.14E-02
ABUW_RS06285	hypothetical protein	-1.15	9.31E-02
ABUW_RS09065	aromatic-ring-hydroxylating dioxygenase	-1.64	2.91E-04
ABUW_RS09390	DMT family transporter	-1.05	1.87E-02
ABUW_RS10145	dienelactone hydrolase family protein	-1.64	1.09E-05
ABUW_RS00935	excinuclease ABC subunit UvrA	-1.01	4.74E-03
ABUW_RS11380	ATP-binding cassette domain	-1.18	7.03E-06
ABUW_RS08945	protocatechuate 3,4-dioxygenase	-1.74	6.23E-07
ABUW_RS08915	CoA transferase subunit B	-1.76	8.00E-05
ABUW_RS12370	NAD(P)/FAD-dependent oxidoreductase	-1.36	4.37E-05
ABUW_RS01435	type 4a pilus biogenesis protein PilO	1.87	6.40E-02
ABUW_RS17730	Fis transcriptional regulator	1.26	6.42E-02
ABUW_RS09350	DUF2314 domain-containing protein	1.50	3.52E-03
ABUW_RS00855	mechanosensitive ion channel protein	1.04	4.56E-05
ABUW_RS03345	purine-binding chemotaxis protein CheW	2.19	1.51E-02
ABUW_RS11240	fimbria/pilus periplasmic chaperone	2.42	4.56E-07
ABUW_RS14110	SPOR domain-containing protein	1.10	1.19E-02
ABUW_RS01430	PilN domain-containing protein	1.90	4.77E-02

Table 4.12 Potential Aar targets shared by Hi-GRIL-seq and pulse overexpression

Gene	Product	log2(fold change)	p-value
ABUW_RS15160	OtsB	-1.24	1.37E-01
ABUW_RS05445	alpha-keto acid decarboxylase	-1.10	1.16E-01
ABUW_RS14610	hypothetical protein	-1.57	5.27E-03
ABUW_RS05710	BauF	-1.27	1.16E-01
ABUW_RS13120	copper-binding protein	-1.16	1.11E-01
ABUW_RS02150	hypothetical protein	-1.30	5.13E-02
ABUW_RS19340	hypothetical protein	-1.87	5.71E-02
ABUW_RS16465	alpha/beta hydrolase	-1.29	7.31E-03
ABUW_RS02710	hypothetical protein	-1.15	8.49E-02
ABUW_RS12330	PaaZ	-2.01	3.89E-04
ABUW_RS02335	tRNA-Ile	2.00	2.76E-03
ABUW_RS17440	OmpW	2.20	1.42E-01
ABUW_RS18845	tRNA-Ile	1.97	3.54E-03
ABUW_RS18075	tRNA-Ile	1.94	3.93E-03
ABUW_RS00080	tRNA-Ile	2.01	3.53E-03
ABUW_RS15815	tRNA-Ile	1.88	5.90E-03
ABUW_RS02500	tRNA-Ile	2.04	2.25E-03
ABUW_RS12700	hypothetical protein	1.24	3.91E-05
ABUW_RS14905	tRNA-Met	1.92	3.09E-03

A

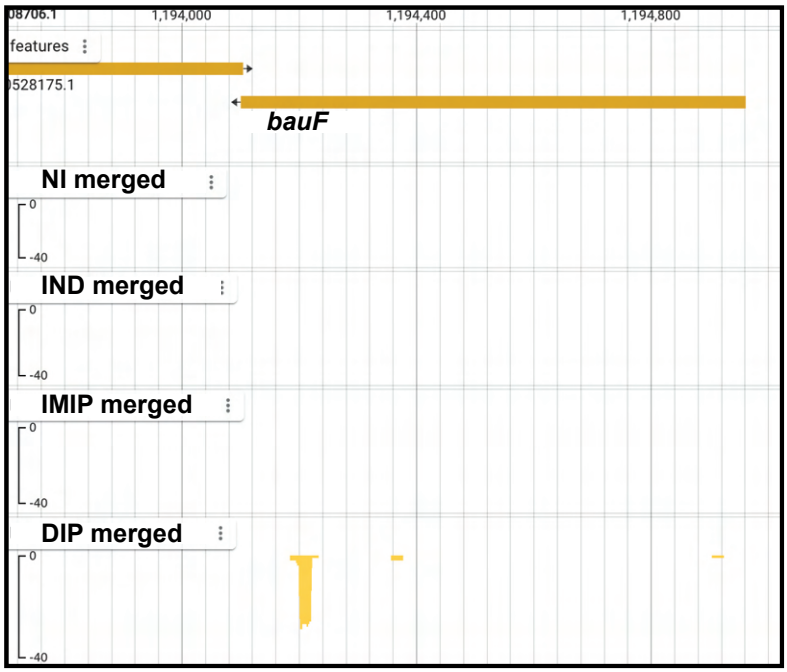

B

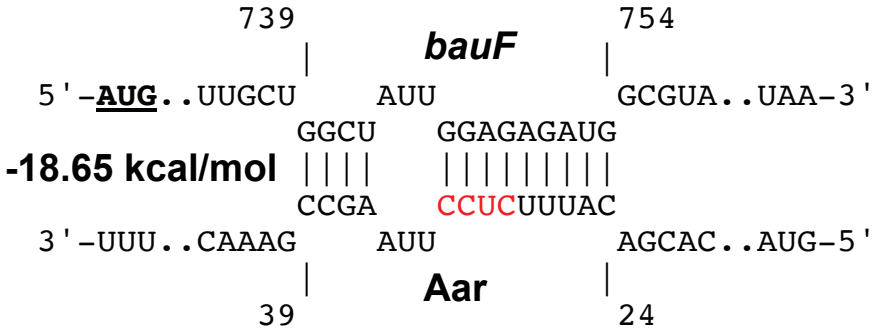

Figure 4.26 Pulse over-expression uncovers another potential Aar interaction partner.

(A) Mapping of *bauF* chimeric fragments from Aar-*bauF* to the AB5075 chromosome. The chimeric reads for each condition used in Hi-GRIL-seq (NI, IND, DIP and IMIP) were merged and are visualised. (B) IntaRNA predicts the likely Aar-*bauF* interaction duplex. The location of the *bauF* start codons (bold and underlined) and the Aar seed region (nucleotides in red) are shown. The location of the predicted interaction duplex are relative to the start codon.

4.10 Overview of Aar:

In this chapter, it was demonstrated that Aar is a conserved sRNA in *Acinetobacter* species, that is expressed in a growth-phase dependent manner in *A. baumannii* AB5075. Aar is induced by several environmental stressors, particularly following heat shock and that it is transcriptionally regulated by AdeR and GacS. Hi-GRIL-seq successfully allowed us to find its mRNA interaction partners including *carO*, *bnfH*, *ABUW_RS07310* and *ABUW_RS04325*. It was demonstrated, *in vitro* and *in vivo*, that Aar forms base-pairing interactions with these mRNA molecules using a conserved seed region and that it may be dependent on Hfq. Aar-*carO* and Aar-*bfnH* interactions were examined in greater detail, showing the precise duplex structures of these interactions. Aar represses CarO translation in *A. baumannii* using a translational reporter system demonstrate that Aar overexpression downregulates the steady state levels of CarO using western blotting. A summary of the post-transcriptional regulation of mRNA molecules by Aar is highlighted in **Figure 4.27**.

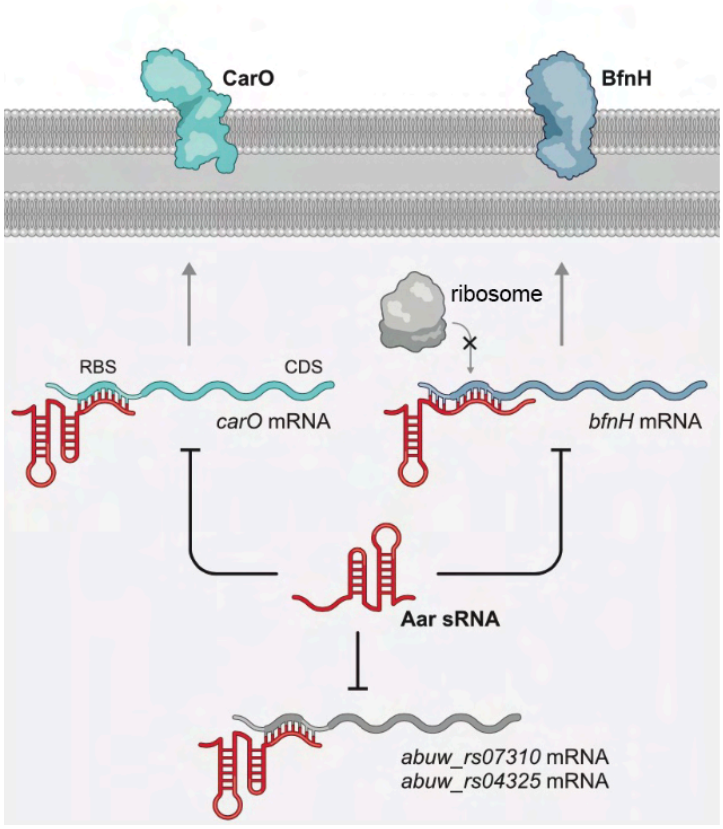

Figure 4.27 Overview of Aar-mediated post-transcriptional regulation in *A. baumannii* AB5075.

Aar binds to *carO*, *bfnH*, *ABUW_RS07310* and *ABUW_RS04325* mRNA at the ribosome binding sites (RBS), blocking translation. Aar does not destabilise these mRNA molecules.

Chapter 5 – The sRNA Arp may act as a potential post-transcriptional regulator of *pilA* mRNA in *A. baumannii*

5.1 Introduction:

The sRNA ***A****cinetobacter* **r**egulator of **p**ilin (Arp) was first identified as an uncharacterised, putative sRNA by the Kröger (referred to as sRNA40) and Shaw (referred to as ABUWs032) research groups (Kröger et al., 2018; Weiss et al., 2016). Weiss and colleagues suggested that Arp and sRNA76 (referred to as ABUWs050) are Group 6 sRNAs and share a high degree of sequence similarity, particularly at their 3′ ends. As outlined in **Chapter 3**, the Hi-GRIL-seq data showed that Arp is a likely regulator of PilA in *A. baumannii* with no other likely potential mRNA interaction partners detected. In this chapter, the dynamics of Arp expression are explored and the role of Arp in modulating PilA expression in heterologous models and *in vivo* in *A. baumannii* is investigated.

5.2 Investigating expression of Arp in *A. baumannii*:

1. Identifying the Arp transcriptional start site:

To identify the exact sRNA transcriptional start sites (TSSs) in the *A. baumannii* ATCC17978, the Kröger group performed dRNA-seq as mentioned in **section 4.2** (Kröger et al., 2018). This allowed them to identify the likely ATCC17978 Arp TSSs as shown in **Figure 5.1A**. Two separate putative TSSs (TSS-1 and TSS-2) were located at positions 1,714,402 and 1,714,426. This may suggest that two separate isoforms of Arp may be produced in this strain or that one of these TSSs is redundant. The expression of Arp was not assessed by northern blotting in this study. To examine differences in sRNA expression between *A. baumannii* strains, Kröger group repeated dRNA-seq in the AB5075 strain (Bakheet, 2024). This revealed a single TSS (TSS-2) located at position 1,763,973, corresponding to the shorter Arp isoform as depicted in **Figure 5.1B**. This implied that only the shorter isoform of Arp in expressed in the *A. baumannii* AB5075 strain. Our attempts to perform northern blotting for Arp were unsuccessful, preventing us from experimentally ascertaining the exact size of this sRNA.

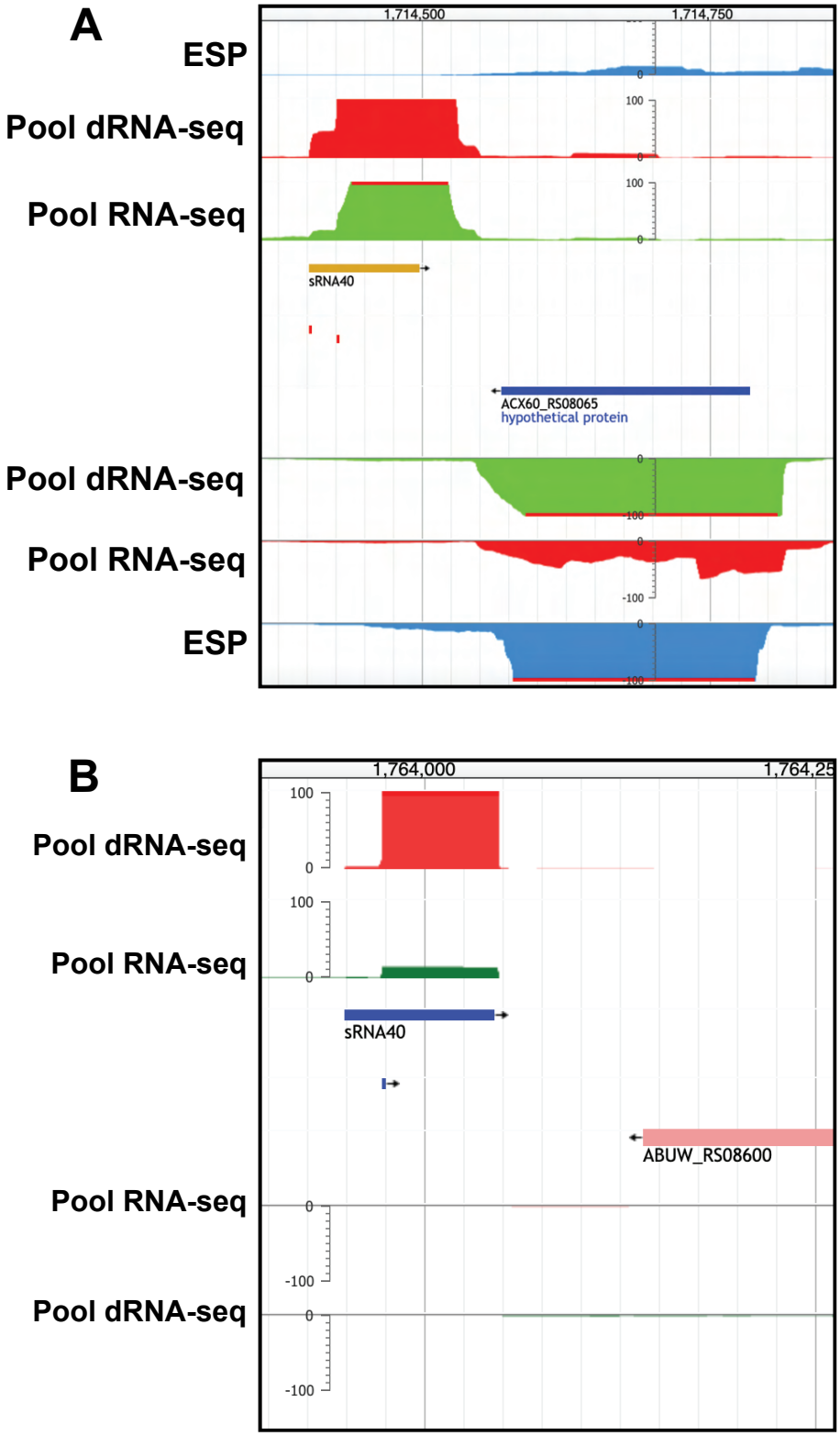

Figure 5.1 Differential RNA-sequencing (dRNA-seq) reveals Arp transcriptional start sites (TSSs).

Arp expression (annotated as sRNA40) was identified in (A) *A. baumannii* ATCC17978 (Kröger et al., 2018) and (B) *A. baumannii* AB5075 (Bakheet, 2024) by RNA-sequencing of untreated (Pool RNA-seq) or TEX treated (Pool dRNA-seq) RNA. This enabled identification of the Arp TSSs.

2. Conservation of Arp among *Acinetobacter* species:

To examine the conservation of Arp among *Acinetobacter* species and determine whether differences in the nucleotide sequence could explain use of separate TSSs, we performed a multiple sequence alignment of *arp* between *A. nosocomialis* and nine model *A. baumannii* strains (**Figure 5.2**). We could not detected a homologue of *arp* in *A. baylyi* ADP1. The upstream region (128 nucleotides) of *arp* in *A. nosocomialis* and *A. baumannii* strains were aligned to determine the sequence similarity between these regions. The exact location of *A. baumannii* TSS-1 and TSS-2 are represented in this alignment. There was high conservation of *arp* and the upstream region, with *A. nosocomialis arp* showing the greatest sequence divergence. We found no differences in the TSS-1 and TSS-2 sequences between the AB5075 and ATCC17978 strains, suggesting that single nucleotide polymorphisms could not account for alternate use of these sites. To better understand the biochemical properties of Arp derived from *A. baumannii* AB5075, we predicted the secondary structure of this sRNA, driven from TSS-2, using RNAfold with default parameters (Lorenz et al., 2011). The resulting minimum free energy structure was represented using VARNA (Darty et al., 2009). This suggested that Arp is single stranded with a stem-loop structure at the 5′ end and a stem-loop structure at the 3′ end followed by a poly(U) tail to promote Rho-independent termination (**Figure 5.3**).

3. Expression of Arp in *A. baumannii* AB5075:

To explore the dynamics of Arp expression in *A. baumannii* AB5075, we examined Arp expression levels (TPM) at MEP, LEP, ESP and LSP using the Kröger group RNA-seq dataset (Bakheet, 2024). We found that Arp expression was too low to be reliably detected as shown in **Table 5.1**. This could be explained by poor retention of sRNAs during library preparation. There were no shock conditions resulted in differential Arp expression in this transcriptomic analysis (Bakheet, 2024).

Table 5.1 Arp expression (average TPMs) across growth

MEP	LEP	ESP	LSP
0.00	3.87	4.42	2.46

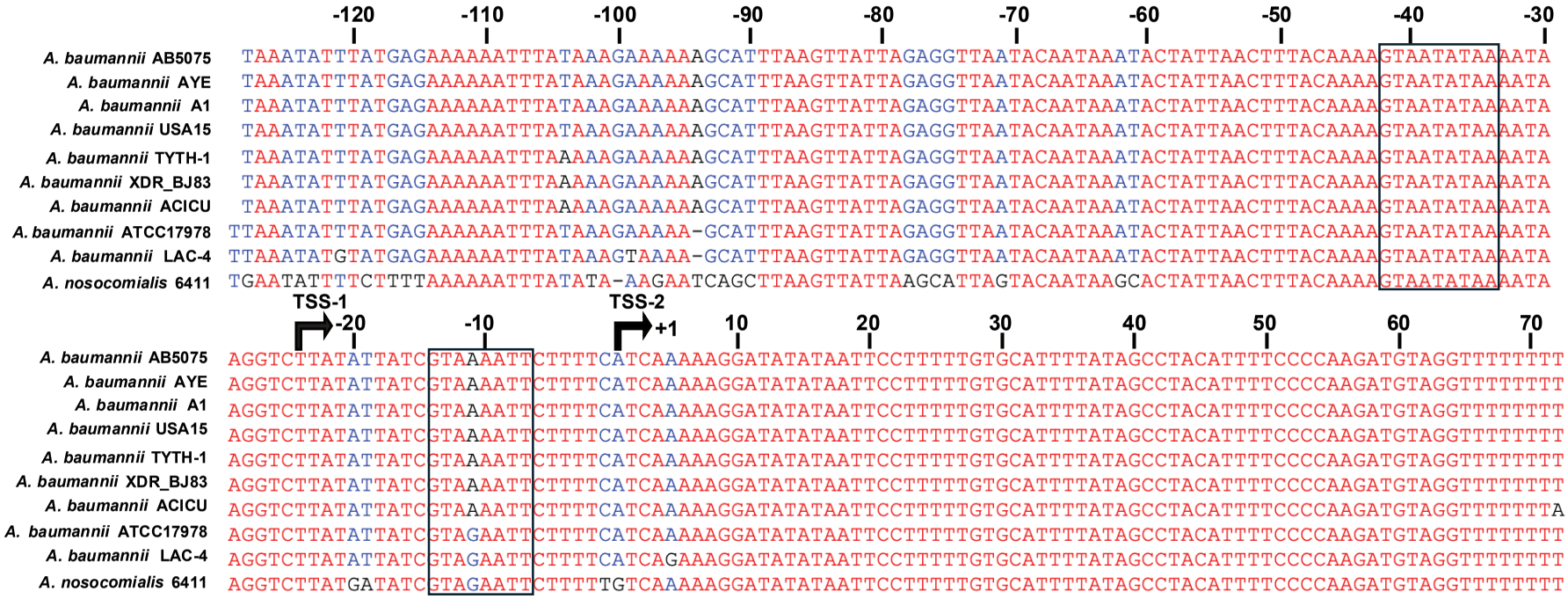

Figure 5.2 Arp is a conserved sRNA in *Acinetobacter* species.

A sequence alignment of *arp* in several *Acinetobacter* species was performed using the Multalin tool. The two potential *A. baumannii* ATCC17978 TSSs (TSS-1 and TSS-2) are shown. TSS-2 of *arp* is indicated as +1, with the numbers above the sequence reflecting the distance from the TSS. The putative -35 and -10 regions are indicated with boxes.

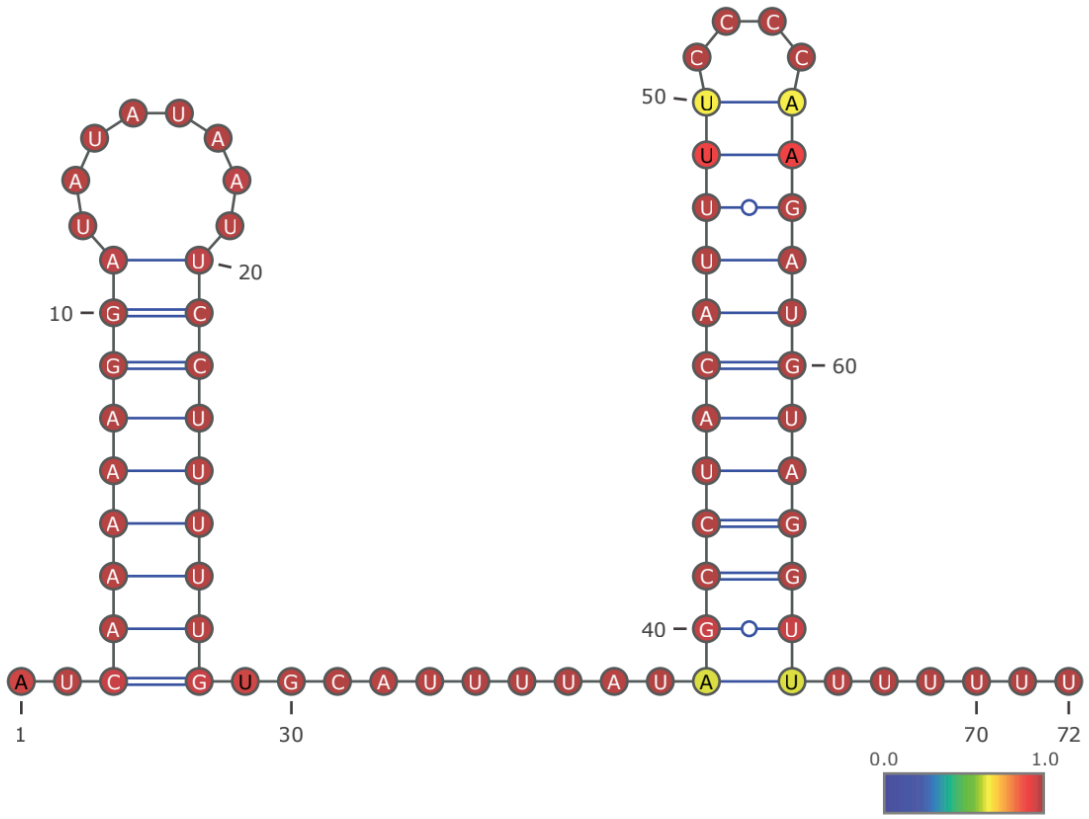

Figure 5.3 Examination of the secondary structure and processing of Arp.

The minimum free energy Arp secondary structure was predicted by RNAfold and represented with VARNA (Darty et al., 2009; Lorenz et al., 2011). The colours of the nucleotides correspond to base-pairing probabilities.

Analysis of the mapped Hi-GRIL-seq reads suggested that Arp was indeed expressed in *A. baumannii*, however, expression is low (**Figure 5.4**). The average expression levels (as determined by TPMs) is outlined in **Table 3.12**. There appeared to be no Hi-GRIL-seq condition where Arp was differentially expressed in particular.

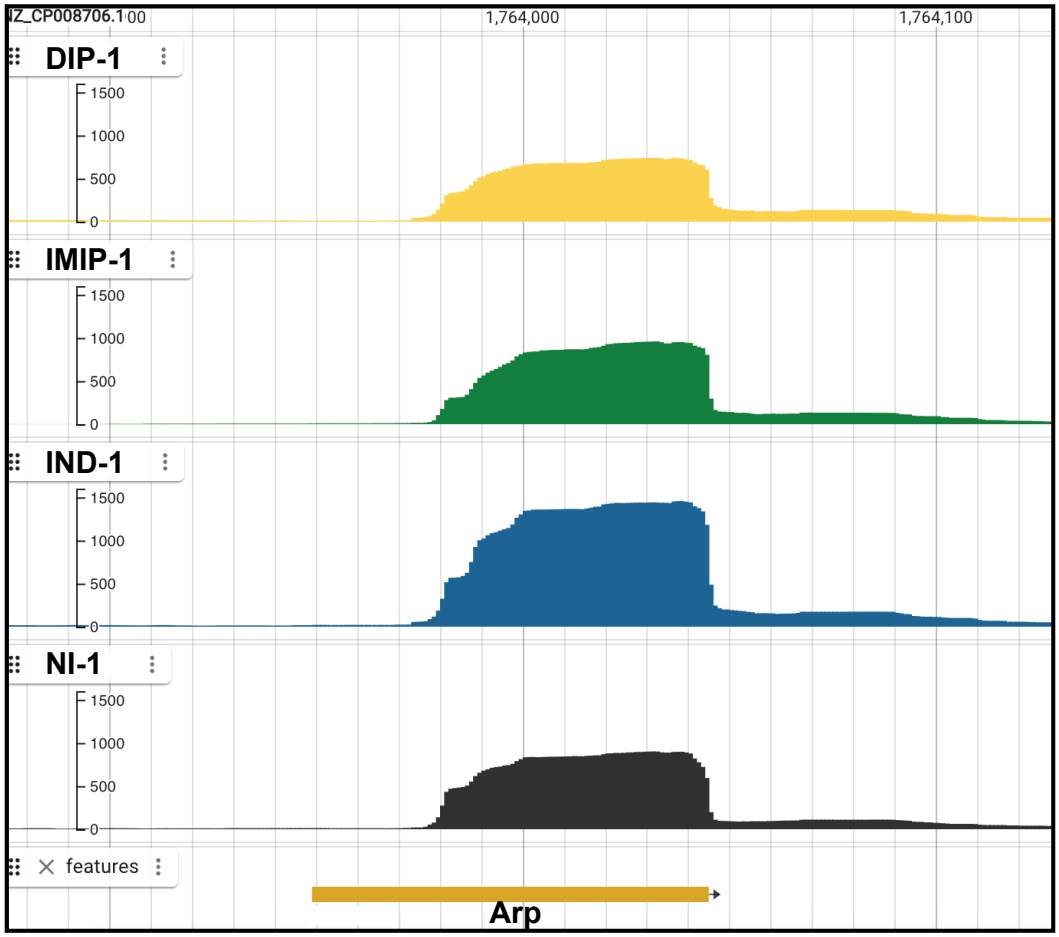

Figure 5.4 Expression of Arp in Hi-GRIL-seq mapped reads.

The Hi-GRIL-seq mapped reads for the *arp* locus are displayed in JBrowse2, showing one replicate for each Hi-GRIL-seq condition (NI = non-induced control, IND = induced sample, DIP = iron starvation and IMIP = imipenem shock) (Diesh et al., 2023).

5.3 Hi-GRIL-seq enables discovery of Arp-*pilA* interactions:

As outlined in Figure 3.10 C, there was only a single mRNA target for Arp that was shared between CopraRNA and Hi-GRIL-seq (Wright et al., 2013, 2014). This the mRNA of *pilA* encoding the major subunit of Type IV pili in *A. baumannii* (Ronish et al., 2019). To determine whether Arp formed a likely base-pairing duplex structure with the *pilA* transcript in *A. baumannii* AB5075, we used IntaRNA to predict interactions *in silico* (Busch et al., 2008). The shorter isoform of Arp driven by TSS-2 was used for this prediction. This revealed that Arp and *pilA* form an extensive interaction at the 5′ end of *pilA* (**Figure 5.5**). This potential duplex extends the 5′-UTR and coding regions of *pilA*, sequestering the SD sequence and the 5-codon, strongly implying that Arp is repressor of PilA translation. Hi-GRIL-seq identified 109 Arp-*pilA* chimeric sequencing reads combined from all conditions. 88% of these chimeric sequencing reads mapped to the predicted interaction duplex, bolstering the perspective that this is a bona fide post-transcriptional regulatory mechanism in *A. baumannii* AB5075.

Furthermore, the Arp-*pilA* chimeric sequencing reads were broadly distributed across the IND, DIP and IMIP Hi-GRIL-seq treatments (**Figure 5.6**). This suggested that Arp-*pilA* interactions are not condition-specific.

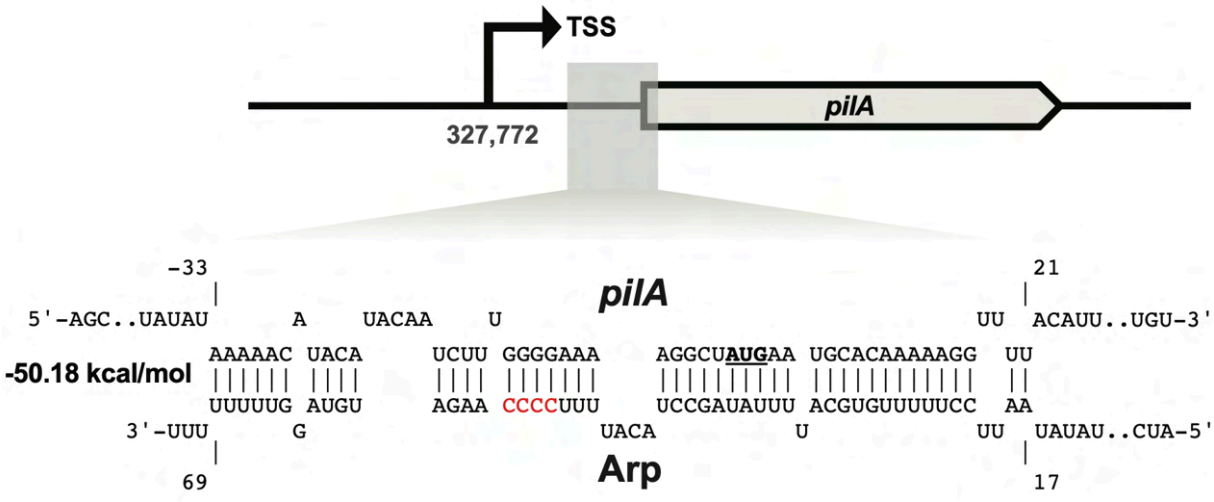

Figure 5.5 IntaRNA predicts likely Arp-*pilA* interaction that sequesters the ribosome binding site.

IntaRNA identified likely interaction duplex with *pilA* (Busch et al., 2008). The location of the transcriptional start site (TSS, shown as curved arrow), the start codon (bold and underlined) of the mRNA target and the potential Arp seed region (nucleotides in red) are shown. The location of predicted interaction duplex is relative to the start codon.

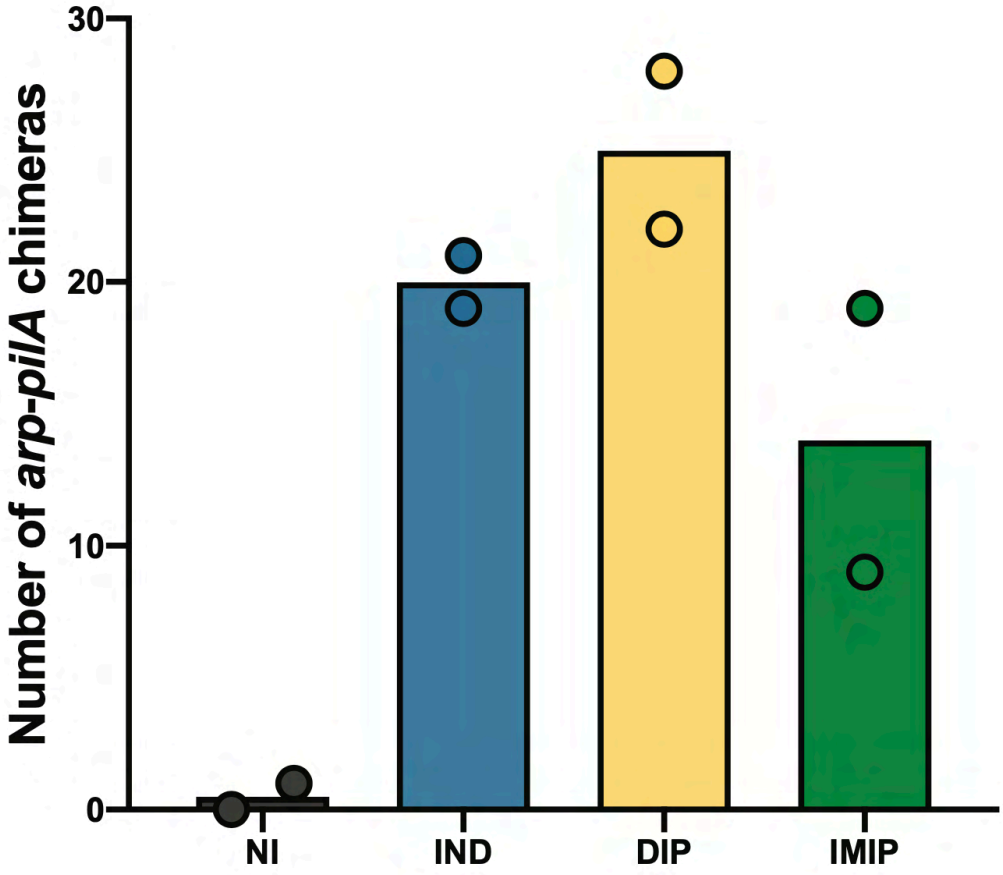

Figure 5.6 Distribution of Aar-*pilA* chimeras among Hi-GRIL-seq conditions.

The average number of chimeras from both biological replicates for each condition (NI, IND, DIP and IMIP) are shown. The exact values of biological replicates are shown as circles for each condition.

5.4 Arp represses PilA translation in a heterologous model:

To determine the regulatory role of Arp, the use the previously described two-plasmid reporter system in *E. coli* as outlined in **section 4.7** was employed (Corcoran et al., 2012; Urban et al., 2007). In this system, Arp was constitutively overexpressed from the pP_L-Arp plasmid, while the 5′-UTRs and first 17 codons of *pilA* were translationally fused to sfGFP and constitutively expressed from the pXG10-PilA plasmid. The fluorescent intensity of *E. coli* strains co-expressing these plasmids was compared to strains that co-expressed the pXG10-PilA plasmid with a control plasmid (pJV300) as shown in **Figure 5.7**. Expression of Arp significantly reduced the fluorescent intensity of PilA-sfGFP ($p<0.0001$) compared to the control strain, validating the repressive role that Arp exerts on PilA expression.

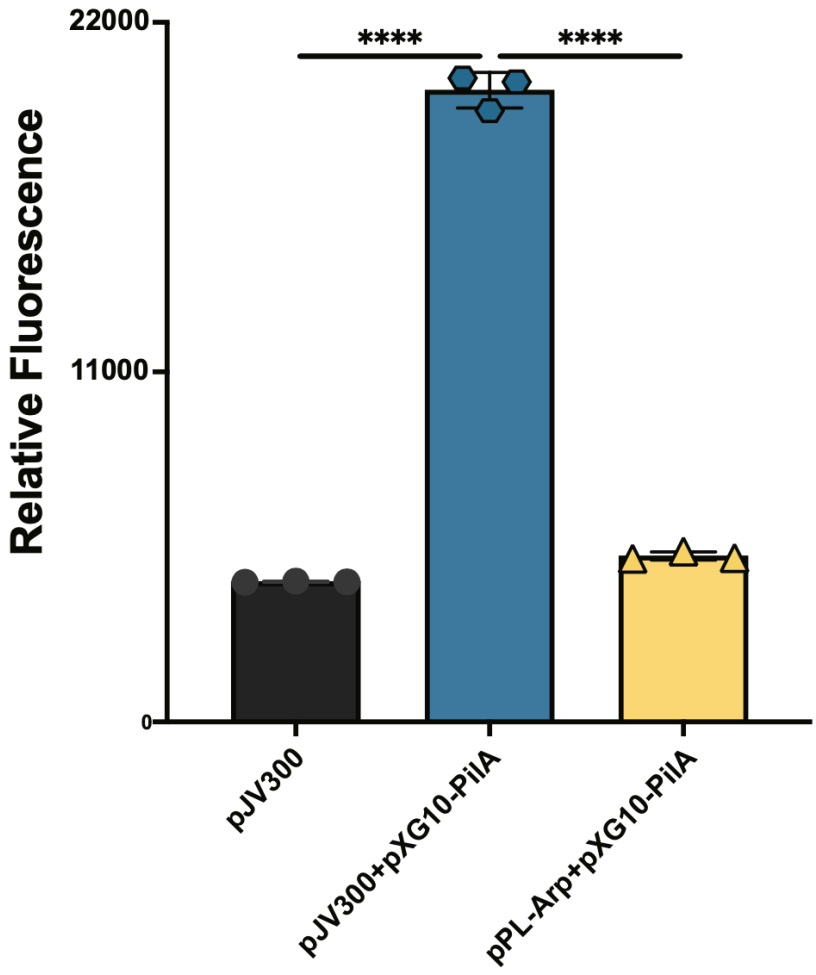

Figure 5.7 Heterologous translational reporter reveal that Arp represses PilA.

The involvement of Aar in modulating expression of PilA was assessed using a two-plasmid reporter system in *E. coli*. Statistical comparisons were performed using One-way ANOVA followed by Tukey's multiple comparisons test. Differences were considered statistically significant where **** denotes P<0.0001.

5.5 Endogenous Arp expression does not repress PilA expression in *A. baumannii*

To confirm that endogenous expression of Arp downregulates the expression of PilA in *A. baumannii* AB5075, a plasmid-based translational reporter system that matched the one described in **section 4.7** was constructed. Briefly, the same PilA-sfGFP translational fusion on pXG10-PilA was placed under control of P_{bla} on pWH1266. The resulting plasmid was referred to as pWH1266-PilA. To determine whether Arp could downregulate PilA-sfGFP, fluorescence measurements of wildtype and Δ*aar* strains carrying this plasmid and the control plasmid (pWH1266) were made. Due to our uncertainty of the Arp expression levels during growth, we measured the relative fluorescent intensity of these strains across 24 h growth in a fluorescent plate reader (**Figure 5.8**). While there was a detectable increase in fluorescent intensity of strains carry pWH1266-PilA compared to the controls, there was no changes in PilA-sfGFP fluorescent intensity in the wildtype and Δ*arp* genetic backgrounds. This may be due to the low endogenous expression of Arp in *A. baumannii* AB5075 (**Table 3.12**).

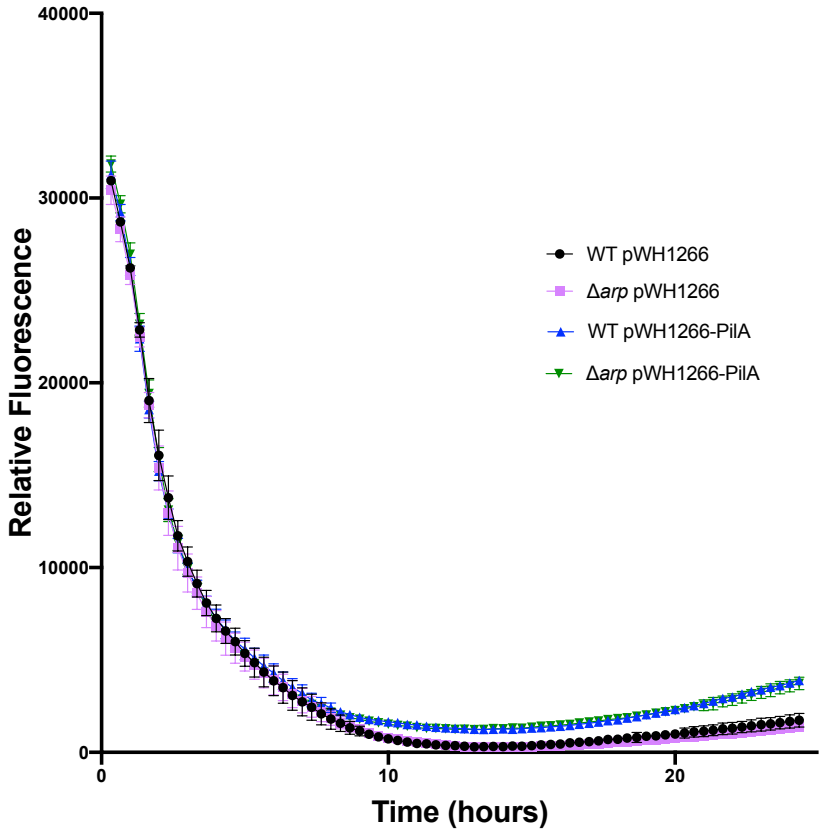

Figure 5.8 Translational reporters could not establish Arp-*pilA* interactions in *A. baumannii* AB5075.

The relative fluorescence intensity of PilA-sfGFP from pWH1266-PilA in wildtype (WT) and Arp-deletion(Δ*arp*) strains of *A. baumannii* AB5075 during 24 h growth was assessed. Strains carrying the empty vector (pWH1266) were used to measure autofluorescence.

5.6 Overview of Arp:

In this chapter, it was demonstrated that Arp is a conserved sRNA in *Acinetobacter* species, that may use two separate TSSs. The expression of Arp in *A. baumannii* AB5075 is low, however, the use of Hi-GRIL-seq identified that *pilA* is a likely mRNA interaction partner. Arp represses PilA expression in a heterologous *E. coli* model, likely by sequestering the SD sequence and 5-codon window of *pilA* mRNA. A condition could not be found where Arp represses translation of PilA in *A. baumannii*, which is most likely attributed to low endogenous expression of Arp in the conditions tested in this organism.

Chapter 6 – Discussion

6.1 Importance of this study:

1. Context of this study:

The emergence of antibiotic-resistant strains of *A. baumannii* has transformed it from an obscure microorganism to a pathogen of global concern (Adams et al., 2008; Hamidian et al., 2019; Perez et al., 2007). This transformation is largely attributed to this organism's ability to readily acquire and develop resistance mechanisms (Antunes et al., 2014; Kröger et al., 2017; Kyriakidis et al., 2021). The development of these resistance mechanisms have rendered antibiotic treatments of infections increasingly ineffective, allowing the organism to fester in immunocompromised hosts (Chen, 2020; Huo et al., 2022). Furthermore, *A. baumannii* exhibits remarkable environmental resilience; it can withstand desiccation, oxidative stress, use of disinfectants and host complement-mediated killing (Coyne et al., 2011; Jawad et al., 1996; Kamuyu et al., 2022; Magda et al., 2022; Monem et al., 2020; Peleg et al., 2008; Wendt et al., 1997). The combination of these strategies have enabled this pathogen to thrive in clinical settings and to operate as a nosocomial pathogen.

The robust nature of *A. baumannii* has launched an effort to better understand the regulatory mechanisms that underly its antibiotic resistance and environmental persistence strategies (Moubareck et al., 2020). *A. baumannii* responds to environmental stress signals in a specific manner, through strict regulation of gene expression. Many studies have focused on the transcriptional regulation of gene expression in *A. baumannii*, establishing the importance of transcriptional regulators in modulating survival mechanisms (Bacon et al., 2024; Farrow et al., 2018; Geisinger et al., 2018; Juttukonda et al., 2019). Conversely, the role of post-transcriptional regulators in modulating gene expression was poorly-establish prior to the undertaking of this study (Kröger et al., 2017, 2018). While several studies did explore the role of Hfq in *A. baumannii* and *A. baylyi*, no studies investigated regulatory role of sRNAs in this pathogen (Intorcia et al., 2024; Kuo et al., 2017; Schilling et al., 2009; Sharma et al., 2018).

In this study, the use of the proximity ligation protocol Hi-GRIL-seq in *A. baumannii* AB5075 was employed to uncover the entire sRNA "interactome" independently of Hfq.

This protocol was originally used in *Pseudomonas aeruginosa*, however, it was adapted and optimised for *A. baumannii* (Hamrock et al., 2024; Zhang et al., 2017). Hi-GRIL-seq was performed in untreated, iron depleted and imipenem shocked conditions, mimicking those conditions encountered within hosts (Fishbain et al., 2010; Marchetti et al., 2020). Hi-GRIL-seq enabled discovery of novel sRNA-mRNA interactions in *A. baumannii* and acts as a valuable resource for understanding post-transcriptional regulation by sRNAs in this organism.

2. Genome-wide analysis of post-transcriptional regulation in *A. baumannii*:

Here, the first global and mechanistic investigation into sRNA-mediated gene regulation in *A. baumannii* was performed, capturing the sRNA interactome of this pathogen. Hi-GRIL-seq in this organism led to the identification of 706 putative sRNA-RNA interactions for future investigation, with comparable efficiency to other proximity ligation based protocols (**Figure 3.5 and 3.7**) (Fuchs et al., 2023; Gebhardt et al., 2023; Huber et al., 2022; Melamed et al., 2016; Waters et al., 2017; Zhang et al., 2017). Analysis of the chimeric sequencing reads revealed that five sRNAs, including Aar, were overrepresented in Hi-GRIL-seq (**Figure 3.8**), suggesting that these "interaction hubs" act as global genetic regulators (Bar et al., 2021; Fuchs et al., 2023; Matera et al., 2022). Furthermore, 7% of the Hi-GRIL-seq derived sRNA interaction partners were also predicted *in silico* using CopraRNA, indicating that such interactions were energetically possible (Wright et al., 2013, 2014) (**Figure 3.10**).

The main focus of this work is on Aar—an sRNA conserved among *Acinetobacter* species, with different isoform sizes in *A. baylyi* and *A. baumannii* (**Figure 4.2**) (Hamrock et al., 2024; Kröger et al., 2018; Schilling et al., 2010). In *A. baumannii*, Aar does not regulate transcripts involved in amino acid metabolism (**Table 4.6**)—as suggested in *A. baylyi*—indicating that Aar isoforms might have divergent roles in both species. Hi-GRIL-seq suggested that Aar formed interactions with the translation initiation regions of *carO*, *bfnH*, *ABUW_RS07310* and *ABUW_RS04325*, using a contiguous sequence of nine nucleotides encompassing the Aar seed region (**Figures 4.5, 4.6, 4.7 and 4.8**). These interactions were confirmed *in vitro*, EMSAs revealed the vital nature of the seed region in mediating base-pairing (**Figures 4.10, 4.11**). In-line probing

revealed that Aar interacts with *carO* and *bfnH* using two and four distinct regions of nucleotides, respectively (**Figure 4.12 and 4.13**).

The use of translational reporter system in *E. coli* and in *A. baumannii* revealed the functional consequences of such interactions providing greater insight into the Aar mechanism of action. The heterologous reporter system revealed that Aar represses translation of *carO*, *bfnH* and *ABUW_RS07310* (**Figure 4.15**) (Corcoran et al., 2012; Urban et al., 2007). This system also suggested that Hfq assists in Aar-mediated repression of these targets. The development of a novel translation reporter system in *A. baumannii* could only capture Aar-*carO* interactions (**Figure 4.17**). This could be due to the possibility that endogenous Aar expression levels were too low to reliably capture Aar-*bfnH* interactions. Alternatively, the post-transcriptional regulation of mRNAs by sRNAs may act differently in *A. baumannii* and *E. coli*. Both reporter systems clarified the importance of the Aar seed region in mediating interactions *in vivo* and disruption of this site impaired base-pairing. These assays revealed that Aar sequesters the SD sequences and five-codon windows of target mRNAs, blocking translation in a manner reminiscent of sRNAs in other bacterial species (Bouvier et al., 2008). The impact of Aar overexpression on CarO steady state levels in *A. baumannii* was mild, with only ~2.1-fold downregulation compared to the wildtype control (**Figures 4.20 and 4.21**). This suggests that Aar primarily fine-tunes targets as was observed for certain sRNAs in other species (Ruhland et al., 2024). It is possible that other *A. baumannii* sRNAs also regulate CarO expression levels or an sRNA sponge might titrate Aar levels in this organism. A previous study in *A. baumannii* ATCC17978 suggested that loss of Hfq was associated with increased *carO* mRNA levels, imply that it acts as a repressor of CarO (Kuo et al., 2017). This may suggest that the post-transcriptional repression of CarO in *A. baumannii* is at least partially driven by Aar. Transient overexpression of Aar in *A. baumannii* could not detect differential expression of *carO*, *bfnH*, *ABUW_RS07310* and *ABUW_RS04325*. This suggests that Aar primarily represses these mRNA targets by blocking ribosome binding rather than by accelerating ribonuclease degradation. Pulse overexpression identified 1,005 differentially expressed genes upon Aar overexpression that warrant further study (**Figure 4.24**). The comparison of the pulse overexpression sequencing results to Hi-GRIL-seq identified that Aar potentially represses *bauF*, a member of the acinetobactin siderophore cluster of genes (**Figure 4.26**) (Sheldon et al., 2020).

As Aar regulates two OMPs that are involved in *A. baumannii* virulence, namely CarO and BfnH, Aar may also be involved contribute to the virulence of this organism. Initially, CarO was predicted to be involved in carbapenem uptake as the loss of *carO* in clinical *A. baumannii* strains was associated with increased resistance to this class of antibiotics (Limansky et al., 2002; Mussi et al., 2005). In recent years, this view has come under increasing challenge (Geisinger et al., 2020; Zahn et al., 2015). CarO is upregulated in *A. baumannii* ATCC17978 biofilms (Cabral et al., 2011). Furthermore, strains lacking this porin have impaired epithelial cell adhesion and reduced killing ability in a murine sepsis model (Labrador-Herrera et al., 2020). Aar is induced by high sodium chloride concentrations in *A. baumannii*, as was also observed in *A. baylyi* (Schilling et al., 2010). Since CarO has cationic affinity and is the second most abundant OM protein in *A. baumannii*, Aar may limit CarO expression levels and prevent excessive sodium uptake (Hood et al., 2010; Labrador-Herrera et al., 2020; Siroy et al., 2005). Additionally, CarO was shown to be involved in the uptake of L-ornithine in *A. baumannii*, a vital precursor of hydroxymate siderophores like baumannoferrin, potentially linking BfnH and CarO targets (Cook-Libin et al., 2022; Mussi et al., 2007; Penwell et al., 2015; Sheldon et al., 2020; Zahn et al., 2015). This may suggest that Aar is involved in iron starvation responses in *A. baumannii*. This is reinforced by the finding that the majority of Aar-*carO* and Aar-*bfnH* chimeras were found in the iron starvation condition (**Figure 4.9**). The identification of *bauF*, another gene involved in siderophore activity in *A. baumannii*, as another potential Aar interaction partner further excites the possibility that Aar fine-tunes the *A. baumannii* response to iron starvation (**Figure 4.26**).

Further investigation into the regulation of Aar expression will provide greater insight into the biological function of this sRNA in *A. baumannii*. Aar is induced when subjected to different environmental stressors—particularly heat and salt shocks—suggesting that it enables *A. baumannii* to adapt to unfavourable conditions (**Figure 4.4**). Aar fine-tunes expression of OMPs including CarO, as OMP-regulating bacterial sRNAs are induced by envelope damage or OMP misfolding, this sRNA may play a vital role in maintaining envelope homeostasis in *A. baumannii* during colonisation (Fröhlich et al., 2018; Geisinger et al., 2019; Hews et al., 2019; Holmqvist et al., 2017; Vogel et al., 2006). By identifying the transcriptional regulators that induce the expression of Aar, its role within the molecular regulatory networks of *A. baumannii* was elucidated. Furthermore, this understanding can help determine whether other sRNAs are part of the same regulatory

network or regulon. By using a novel transcriptional reporter system, it was shown that Aar is transcriptionally induced by GacS and repressed by AdeR (**Figure 4.4**). A recent preprint found that Aar is also transcriptionally activated by BfmR, another *A. baumannii* transcriptional regulator that is involved in biofilm formation, virulence and antibiotic resistance (Geisinger et al., 2018). Together, these results demonstrate that the regulation of Aar is complex, with further investigations required to fully elucidate the biological role of this sRNA.

Chapter 5 focusses on the sRNA Arp—an sRNA conserved among pathogenic *Acinetobacter* species (**Figure 5.2**). Hi-GRIL-seq revealed that Arp interacts with the translation initiation regions of *pilA* (**Figure 5.5**). Arp repressed *pilA* translational fusions in *E. coli* (**Figure 5.7**), however, this could not be re-captured in *A. baumannii* (**Figure 5.8**), likely due to low Arp expression levels (**Table 3.12**). To fully ascertain whether Arp is a true regulator of PilA in *A. baumannii*, the impact of overexpression on PilA-sfGFP expression levels must be assessed. Profiling Arp expression levels in *A. baumannii* subjected to different growth conditions would also offer further insight into the biological role it plays. This could be achieved through the use of a transcriptional reporter as was used for Aar (**Figure 4.4**). As PilA mediates natural competence and twitching motility of *A. baumannii*, the regulation of this appendage by Arp under these conditions must be assessed (Harding et al., 2013; Ronish et al., 2019; Vesel et al., 2021). The transcriptional activity of the Arp promoter should thus be measured in other experimental conditions including during movement on surfaces, during cell-cell contact and within biofilms. The impact of Arp overexpression on PilA steady state levels should also be characterised using a similar strategy as employed in **section 4.8**. If this overexpression alters PilA proteins levels, the impact on DNA uptake must also be considered. This may uncover novel RNA-based strategies to modulate HGT in *A. baumannii*.

The Hi-GRIL-seq dataset has already offered other members of the research community greater insights into post-transcriptional regulation in *A. baumannii*. A recent preprint found that a putative *A. baumannii*-specific σ-factor SigAb upregulated expression of the sRNA *SabS* (also referred to as sRNA90) (Bacon et al., 2024). This transcriptional regulator and *SabS* are induced upon exposure to elevate copper levels, indicating that they are involved in mediating copper tolerance. This study identifies likely interaction

partners for this sRNA, allowing to consider how post-transcriptional regulation by sRNAs is integrated into *A. baumannii* stress response systems.

3. Investigate role of RNA binding proteins in *A. baumannii*:

RNA binding proteins (RBPs) often act as chaperones of sRNA-mediated regulation, enabling sRNA-mRNA annealing and protecting these molecules from degradation (Quendera et al., 2020). Exploring the role that RBPs mediate in sRNA-based gene regulation in *A. baumannii* would improve our understanding of the RNA biology underlying this organism. Hfq is the most well-characterised RBP in Gram-negative organisms, it has an unusual, glycine rich C-terminal domain in *Acinetobacter* species and, while *A. baumannii* Hfq expressed in *E. coli* can mediate sRNA-mRNA base-pairing, its role in its native host is unknown (Schilling et al., 2009; Sharma et al., 2018). In this study, it was shown that Aar is dependent on Hfq to mediate the full repression of BfnH using a heterologous reporter system (**Figure 4.15**) (Corcoran et al., 2012; Urban et al., 2007). It is unclear at this time whether loss of Hfq is vital for mediating base-pairing or whether it makes these RNA molecules more susceptible to degradation. It may be beneficial to repeat the EMSAs in this study with Hfq isolated from *A. baumannii*, this may illuminate whether the unbound fractions of Aar disappear at higher concentrations of mRNA targets (**Figure 4.10**). Loss of Hfq in the *A. baumannii* ATCC17978 strain impairs growth, virulence and survival to environmental stresses (Kuo et al., 2017; Sharma et al., 2018). Similar to other groups, the creation an *A. baumannii* AB5075 *hfq* deletion mutants could not be achieved, leading some to speculate that it is an essential gene in this strain (Bai et al., 2021). This is reinforced by a CRISPR-interference study, that demonstrated that the knockdown of Hfq in *A. baumannii* AB5075 was lethal (Intorcia et al., 2024).

Bacterial sRNA are also modulated by other RBPs including CsrA, cold shock proteins (CSPs) and FinO-domain containing proteins, including ProQ (Quendera et al., 2020). While there are no known FinO domain containing proteins identified in *A. baumannii*, *A. baumannii* expresses homologues of CsrA and CSPs including CspC (Farrow et al., 2020; Hubloher et al., 2021; Oda et al., 2022; Tomlinson et al., 2022). CsrA is critical in modulating amino acid metabolism, virulence, osmolarity and desiccation in *A. baumannii* (Farrow et al., 2020; Hubloher et al., 2021; Oda et al., 2022). CspC

participates in biofilm formation and antibiotic tolerance in this organism (Tomlinson et al., 2022). No work has to this point characterised the involvement in these RBPs in modulating sRNA activity or stability. Experiments such as crosslinking and immunoprecipitation combined with RNA-sequencing (CLIP-seq) may clarify the role these RBPs play in modulating sRNAs in *A. baumannii*, as this has worked in other species (Holmqvist et al., 2016).

6.2 Limitations of the study

While Hi-GRIL-seq was successful at identifying sRNA-RNA interactions in *A. baumannii*, there were several limitations associated with this method that became apparent during this investigation. As evident in **Figure 3.5**, certain sRNAs, particularly sRNA2, were more abundant in chimeras in the non-induced condition than in the induced conditions. While this could be attributed to higher expression of sRNA2 in the non-induced condition than in other conditions (**Table 3.5**) or by basal transcription of T4 RNA ligase from the P_{BAD} promoter, it cannot be discounted that these chimeras may represented true sRNA2-mRNA base-pairing interactions. Furthermore, Hi-GRIL-seq only captures interactions between monophosphorylated sRNAs and their RNA interaction partners (Han et al., 2016). This could exclude all interactions that occur between triphosphorylated sRNAs and their RNA interaction partners. Finally, less sRNA-containing chimeric sequencing reads in our Hi-GRIL-seq study (~0.06%) were observed than were captured by Zhang and colleagues in their Hi-GRIL-seq study (0.26–0.29%) in *P. aeruginosa* (Zhang et al., 2017). This could be explained by differences in the promoters used, Zhang *et al*. used an IPTG inducible system for T4 RNA ligase induction, while we used a P_{BAD} based system or by differences in phosphorylation at the 5′-ends of transcripts of both these species.

6.3 Concluding remarks

In summary, Hi-GRIL-seq was optimised and performed in *A. baumannii*, the first genome-wide investigation into the sRNA interactome of this pathogen. This resulted in the identification of likely interaction partners for many of the sRNA candidates *in A. baumannii*, including the sRNAs Aar and Arp. The Hi-GRIL-seq experiment characterised the role of Aar in detail in *A. baumannii*. It also is the basis of investigating Arp, a previously uncharacterised sRNA. Our Hi-GRIL-seq dataset is an invaluable resource for those profiling post-transcriptional regulation in this organism, several members of the community have already employed this work for such purposes.

Chapter 7 – References

Adams, M. D., Goglin, K., Molyneaux, N., Hujer, K. M., Lavender, H., Jamison, J. J., MacDonald, I. J., Martin, K. M., Russo, T., Campagnari, A. A., Hujer, A. M., Bonomo, R. A., & Gill, S. R. (2008). Comparative genome sequence analysis of multidrug-resistant *Acinetobacter baumannii*. *Journal of Bacteriology*, *190*(24), 8053–8064. https://doi.org/10.1128/JB.00834-08

Ahmed, W., Hafeez, M. A., & Mahmood, S. (2018). Identification and functional characterization of bacterial small non-coding RNAs and their target: A review. *Gene Reports*, *10*(December 2017), 167–176. https://doi.org/10.1016/j.genrep.2018.01.001

Álvarez-Fraga, L., Rumbo-Feal, S., Pérez, A., Gómez, M. J., Gayoso, C., Vallejo, J. A., Ohneck, E. J., Valle, J., Actis, L. A., Beceiro, A., Bou, G., & Poza, M. (2017). Global assessment of small RNAs reveals a non-coding transcript involved in biofilm formation and attachment in *Acinetobacter baumannii* ATCC 17978. *PLoS ONE*, *12*(8), 1–24. https://doi.org/10.1371/journal.pone.0182084

Anderson, S. E., Chin, C. Y., Weiss, D. S., & Rather, P. N. (2020). Copy number of an integron-encoded antibiotic resistance locus regulates a virulence and opacity switch in *Acinetobacter baumannii* AB5075. *MBio*, *11*(5), 1–19. https://doi.org/10.1128/mBio.02338-20

Anstey, N. M., Currie, B. J., & Withnall, K. M. (1992). Community-acquired *Acinetobacter pneumonia* in the Northern Territory of Australia. *Clinical Infectious Diseases*, *14*(1), 83–91. https://doi.org/10.1093/clinids/14.1.83

Antunes, L. C. S., Imperi, F., Carattoli, A., & Visca, P. (2011). Deciphering the multifactorial nature of *Acinetobacter baumannii* pathogenicity. *PLoS ONE*, *6*(8). https://doi.org/10.1371/journal.pone.0022674

Antunes, L. C. S., Visca, P., & Towner, K. J. (2014). *Acinetobacter baumannii*: Evolution of a global pathogen. *Pathogens and Disease*, *71*(3), 292–301. https://doi.org/10.1111/2049-632X.12125

Aranda, J., Bardina, C., Beceiro, A., Rumbo, S., Cabral, M. P., Barbé, J., & Bou, G. (2011). *Acinetobacter baumannii* RecA protein in repair of DNA damage, antimicrobial resistance, general stress response, and virulence. *Journal of Bacteriology*, *193*(15), 3740–3747. https://doi.org/10.1128/JB.00389-11

Argaman, L., Hershberg, R., Vogel, J., Bejerano, G., Wagner, E. G. H., Margalit, H., & Altuvia, S. (2001). Novel small RNA-encoding genes in the intergenic regions of *E. coli*. *Current Biology*, *11*, 941–950. https://doi.org/10.1016/j.gene.2008.09.024

Artuso, I., Poddar, H., Evans, B. A., & Visca, P. (2023). Genomics of *Acinetobacter baumannii* iron uptake. *Microbial Genomics*, *9*(8), 1–18. https://doi.org/10.1099/mgen.0.001080

Bacon, E. E., Myers, K. S., Iruegas-López, R., Banta, A. B., Place, M., Ebersberger, I., & Peters, J. M. (2024). Physiological Roles of an *Acinetobacter*-specific σ Factor. *BioRxiv*.

Bai, J., Dai, Y., Farinha, A., Tang, A. Y., Syal, S., Vargas-Cuebas, G., Opijnen, T. van, Isberg, R. R., & Geisinger, E. (2021). Essential Gene Analysis in *Acinetobacter baumannii* by High- Density Transposon Mutagenesis and CRISPR Interference. *Journal of Bacteriology*, *203*(12), e00565-20.

Bak, G., Han, K., Kim, K., & Lee, Y. (2015). Electrophoretic Mobility Shift Assay of RNA–RNA Complexes. In *Methods in Molecular Biology* (Vol. 1240, pp. 27–37). Humana Press. https://doi.org/10.1007/978-1-4939-1896-6

Bakheet, A. A. (2024). *The transcriptional landscape and small RNAs in Acinetobacter baumannii AB5075 during antibiotic and environmental stress*. Trinity College

Dublin. https://www.tara.tcd.ie/handle/2262/108590
Bar, A., Argaman, L., Altuvia, Y., & Margalit, H. (2021). Prediction of Novel Bacterial Small RNAs From RIL-Seq RNA–RNA Interaction Data. *Frontiers in Microbiology*, *12*(May), 1–16. https://doi.org/10.3389/fmicb.2021.635070
Bazyleu, A., & Kumar, A. (2014). Incubation temperature, osmolarity, and salicylate affect the expression of resistance-nodulation-division efflux pumps and outer membrane porins in *Acinetobacter baumannii* ATCC19606T. *FEMS Microbiology Letters*, *357*(2), 136–143. https://doi.org/10.1111/1574-6968.12530
Beyer, D., Skripkin, E., Wadzack, J., & Nierhaus, K. H. (1994). How the ribosome moves along the mRNA during protein synthesis. *Journal of Biological Chemistry*, *269*(48), 30713–30717. https://doi.org/10.1016/s0021-9258(18)43872-0
Bhuiyan, M. S., Ellett, F., Murray, G. L., Kostoulias, X., Cerqueira, G. M., Schulze, K. E., Maifiah, M. H. M., Li, J., Creek, D. J., Lieschke, G. J., & Peleg, A. Y. (2016). *Acinetobacter baumannii* phenylacetic acid metabolism influences infection outcome through a direct effect on neutrophil chemotaxis. *Proceedings of the National Academy of Sciences of the United States of America*, *113*(34), 9599–9604. https://doi.org/10.1073/pnas.1523116113
Boll, J. M., Tucker, A. T., Klein, D. R., Beltran, A. M., Brodbelt, J. S., Davies, B. W., & Trent, M. S. (2015). Reinforcing lipid A acylation on the cell surface of *Acinetobacter baumannii* promotes cationic antimicrobial peptide resistance and desiccation survival. *MBio*, *6*(3), 1–11. https://doi.org/10.1128/mBio.00478-15
Borgeaud, S., Metzger, L. C., Scrignari, T., & Blokesch, M. (2015). The type VI secretion system of *Vibrio cholerae* fosters horizontal gene. *Science*, *347*(6217), 63–67.
Bouvet, P. J. M., & Grimont, P. a D. (1986). Taxonomy of the Genus *Acinetobacter* with the Recognition of nov . and Emended Descriptions of *Acinetobacter calcoaceticus* and *Acinetobacter lwofii*. *International Journal of Systematic Bacteriology*, *36*(2), 228–240. https://doi.org/10.1099/00207713-36-2-228
Bouvier, M., Sharma, C. M., Mika, F., Nierhaus, K. H., & Vogel, J. (2008). Small RNA Binding to 5′ mRNA Coding Region Inhibits Translational Initiation. *Molecular Cell*, *32*(6), 827–837. https://doi.org/10.1016/j.molcel.2008.10.027
Busch, A., Richter, A. S., & Backofen, R. (2008). IntaRNA: Efficient prediction of bacterial sRNA targets incorporating target site accessibility and seed regions. *Bioinformatics*, *24*(24), 2849–2856. https://doi.org/10.1093/bioinformatics/btn544
Butler, D. A., Biagi, M., Tan, X., Qasmieh, S., Bulman, Z. P., & Wenzler, E. (2019). Multidrug Resistant *Acinetobacter baumannii*: Resistance by Any Other Name Would Still be Hard to Treat. *Current Infectious Disease Reports*, *21*(12). https://doi.org/10.1007/s11908-019-0706-5
Cabral, M. P., Soares, N. C., Aranda, J., Parreira, J. R., Rumbo, C., Poza, M., Valle, J., Calamia, V., Lasa, Í., & Bou, G. (2011). Proteomic and functional analyses reveal a unique lifestyle for *Acinetobacter baumannii* biofilms and a key role for histidine metabolism. *Journal of Proteome Research*, *10*(8), 3399–3417. https://doi.org/10.1021/pr101299j
Cafiso, V., Stracquadanio, S., Lo Verde, F., Dovere, V., Zega, A., Pigola, G., Aranda, J., & Stefani, S. (2020). COLR *Acinetobacter baumannii* sRNA Signatures: Computational Comparative Identification and Biological Targets. *Frontiers in Microbiology*, *10*(January), 1–9. https://doi.org/10.3389/fmicb.2019.03075
Camacho, C., Coulouris, G., Avagyan, V., Ma, N., Papadopoulos, J., Bealer, K., & Madden, T. L. (2009). BLAST+: Architecture and applications. *BMC Bioinformatics*, *10*, 1–9. https://doi.org/10.1186/1471-2105-10-421

Carrier, M. C., Lalaouna, D., & Massé, E. (2016). A game of tag: MAPS catches up on RNA interactomes. *RNA Biology*, *13*(5), 473–476. https://doi.org/10.1080/15476286.2016.1156830

Casella, L. G., Weiss, A., Pérez-Rueda, E., Antonio Ibarra, J., & Shaw, L. N. (2017). Towards the complete proteinaceous regulome of *Acinetobacter baumannii*. *Microbial Genomics*, *3*(3). https://doi.org/10.1099/mgen.0.000107

Catel-Ferreira, M., Marti, S., Guillon, L., Jara, L., Coadou, G., Molle, V., Bouffartigues, E., Bou, G., Shalk, I., Jouenne, T., Vila-Farrés, X., & Dé, E. (2016). The outer membrane porin OmpW of *Acinetobacter baumannii* is involved in iron uptake and colistin binding. *FEBS Letters*, *590*(2), 224–231. https://doi.org/10.1002/1873-3468.12050

Cayô, R., Rodríguez, M. C., Espinal, P., Fernández-Cuenca, F., Ocampo-Sosa, A. A., Pascual, Á., Ayala, J. A., Vila, J., & Martínez-Martínez, L. (2011). Analysis of genes encoding penicillin-binding proteins in clinical isolates of *Acinetobacter baumannii*. *Antimicrobial Agents and Chemotherapy*, *55*(12), 5907–5913. https://doi.org/10.1128/AAC.00459-11

Centers for Disease Control and Prevention. (2019). *Antibiotic resistance threats in the United States*. *fcimb-07-00055.pdf*, 114. https://doi.org/CS239559-B

Cerqueira, G. M., Kostoulias, X., Khoo, C., Aibinu, I., Qu, Y., Traven, A., & Peleg, A. Y. (2014). A global virulence regulator in *Acinetobacter baumannii* and its control of the phenylacetic acid catabolic pathway. *Journal of Infectious Diseases*, *210*(1), 46–55. https://doi.org/10.1093/infdis/jiu024

Chen, M. Z., Hsueh, P. R., Lee, L. N., Yu, C. J., Yang, P. C., & Luh, K. T. (2001). Severe community-acquired pneumonia due to *Acinetobacter baumannii*. *Chest*, *120*(4), 1072–1077. https://doi.org/10.1378/chest.120.4.1072

Chen, W. (2020). Host Innate Immune Responses to *Acinetobacter baumannii* Infection. *Frontiers in Cellular and Infection Microbiology*, *10*(September), 1–16. https://doi.org/10.3389/fcimb.2020.00486

Chin, C. Y., Tipton, K. A., Farokhyfar, M., Burd, E. M., Weiss, D. S., & Rather, P. N. (2018). A high-frequency phenotypic switch links bacterial virulence and environmental survival in *Acinetobacter baumannii*. *Nature Microbiology*, *3*((5)), 563–569. https://doi.org/10.1177/0022146515594631.Marriage

Choi, C. H., Lee, J. S., Lee, Y. C., Park, T. I., & Lee, J. C. (2008). *Acinetobacter baumannii* invades epithelial cells and outer membrane protein A mediates interactions with epithelial cells. *BMC Microbiology*, *8*, 1–11. https://doi.org/10.1186/1471-2180-8-216

Chukwudi, C. U. (2016). rRNA Binding Sites and the Molecular Mechanism of Action of the Tetracyclines. *Antimicrobial Agents and Chemotherapy*, *60*(8), 4433–4441. https://doi.org/10.1128/AAC.00594-16.Address

Cook-Libin, S., Sykes, E. M. E., Kornelsen, V., & Kumar, A. (2022). Iron Acquisition Mechanisms and Their Role in the Virulence of *Acinetobacter baumannii*. *Infection and Immunity*, *90*(10). https://doi.org/10.1128/iai.00223-22

Cooper, R. M., Tsimring, L., & Hasty, J. (2017). Inter-species population dynamics enhance microbial horizontal gene transfer and spread of antibiotic resistance. *ELife*, *6*(Cdc), 1–26. https://doi.org/10.7554/eLife.25950

Corcoran, C. P., Podkaminski, D., Papenfort, K., Urban, J. H., Hinton, J. C. D., & Vogel, J. (2012). Superfolder GFP reporters validate diverse new mRNA targets of the classic porin regulator, MicF RNA. *Molecular Microbiology*, *84*(3), 428–445. https://doi.org/10.1111/j.1365-2958.2012.08031.x

Cornejo-Juárez, P., Cevallos, M. A., Castro-Jaimes, S., Castillo-Ramírez, S.,

Velázquez-Acosta, C., Martínez-Oliva, D., Pérez-Oseguera, A., Rivera-Buendía, F., & Volkow-Fernández, P. (2020). High mortality in an outbreak of multidrug resistant *Acinetobacter baumannii* infection introduced to an oncological hospital by a patient transferred from a general hospital. *PloS One*, *15*(7), e0234684. https://doi.org/10.1371/journal.pone.0234684

Correia, S., Poeta, P., Hébraud, M., Capelo, J. L., & Igrejas, G. (2017). Mechanisms of quinolone action and resistance: where do we stand? *Journal of Medical Microbiology*, *66*(5), 551–559. https://doi.org/10.1099/jmm.0.000475

Correia Santos, S., Bischler, T., Westermann, A. J., & Vogel, J. (2021). MAPS integrates regulation of actin-targeting effector SteC into the virulence control network of *Salmonella* small RNA PinT. *Cell Reports*, *34*(5). https://doi.org/10.1016/j.celrep.2021.108722

Cosgaya, C., Marí-Almirall, M., Van Assche, A., Fernández-Orth, D., Mosqueda, N., Telli, M., Huys, G., Higgins, P. G., Seifert, H., Lievens, B., Roca, I., & Vila, J. (2016). Acinetobacter dijkshoorniae sp. Nov., a member of the *Acinetobacter calcoaceticus–Acinetobacter baumannii* complex mainly recovered from clinical samples in different countries. *International Journal of Systematic and Evolutionary Microbiology*, *66*(10), 4105–4111. https://doi.org/10.1099/ijsem.0.001318

Coyne, S., Courvalin, P., & Périchon, B. (2011). Efflux-mediated antibiotic resistance in *Acinetobacter spp*. *Antimicrobial Agents and Chemotherapy*, *55*(3), 947–953. https://doi.org/10.1128/AAC.01388-10

Darty, K., Denise, A., & Ponty, Y. (2009). VARNA: Interactive drawing and editing of the RNA secondary structure. *BIOINFORMATICS*, *25*(15), 1974–1975. https://doi.org/10.1109/TCBB.2008.28

De Silva, P. M., & Kumar, A. (2019). Signal transduction proteins in *Acinetobacter baumannii*: Role in antibiotic resistance, virulence, and potential as drug targets. *Frontiers in Microbiology*, *10*(JAN), 1–12. https://doi.org/10.3389/fmicb.2019.00049

Dersch, P., Khan, M. A., Mühlen, S., & Görke, B. (2017). Roles of regulatory RNAs for antibiotic resistance in bacteria and their potential value as novel drug targets. *Frontiers in Microbiology*, *8*(MAY), 1–12. https://doi.org/10.3389/fmicb.2017.00803

Dexter, C., Murray, G. L., Paulsen, I. T., & Peleg, A. Y. (2015). Community-acquired *Acinetobacter baumannii*: clinical characteristics, epidemiology and pathogenesis. *Expert Review of Anti-Infective Therapy*, *13*(5), 567–573. https://doi.org/10.1586/14787210.2015.1025055

Diancourt, L., Passet, V., Nemec, A., Dijkshoorn, L., & Brisse, S. (2010). The population structure of *Acinetobacter baumannii*: Expanding multiresistant clones from an ancestral susceptible genetic pool. *PLoS ONE*, *5*(4). https://doi.org/10.1371/journal.pone.0010034

Diesh, C., Stevens, G. J., Xie, P., De Jesus Martinez, T., Hershberg, E. A., Leung, A., Guo, E., Dider, S., Zhang, J., Bridge, C., Hogue, G., Duncan, A., Morgan, M., Flores, T., Bimber, B. N., Haw, R., Cain, S., Buels, R. M., Stein, L. D., & Holmes, I. H. (2023). JBrowse 2: a modular genome browser with views of synteny and structural variation. *Genome Biology*, *24*(1), 1–21. https://doi.org/10.1186/s13059-023-02914-z

Distel, J. S., Di Venanzio, G., Mackel, J. J., Rosen, D. A., & Feldman, M. F. (2023). Replicative *Acinetobacter baumannii* strains interfere with phagosomal maturation by modulating the vacuolar pH. *PLoS Pathogens*, *19*(6 June), 1–24.

https://doi.org/10.1371/journal.ppat.1011173
Dönhöfer, A., Franckenberg, S., Wickles, S., Berninghausen, O., Beckmann, R., & Wilson, D. N. (2012). Structural basis for TetM-mediated tetracycline resistance. *Proceedings of the National Academy of Sciences of the United States of America*, *109*(42), 16900–16905. https://doi.org/10.1073/pnas.1208037109
Douchin, V., Bohn, C., & Bouloc, P. (2006). Down-regulation of porins by a small RNA bypasses the essentiality of the regulated intramembrane proteolysis protease RseP in *Escherichia coli*. *Journal of Biological Chemistry*, *281*(18), 12253–12259. https://doi.org/10.1074/jbc.M600819200
Dunham, D. T., Angermeyer, A., & Seed, K. D. (2023). The RNA-RNA interactome between a phage and its satellite virus reveals a small RNA that differentially regulates gene expression across both genomes. *Molecular Microbiology*, *119*(4), 515–533. https://doi.org/10.1111/mmi.15046.The
Eijkelkamp, B. A., Hassan, K. A., Paulsen, I. T., & Brown, M. H. (2011). Investigation of the human pathogen *Acinetobacter baumannii* under iron limiting conditions. *BMC Genomics*, *12*. https://doi.org/10.1186/1471-2164-12-126
Espinal, P., Martí, S., & Vila, J. (2012). Effect of biofilm formation on the survival of *Acinetobacter baumannii* on dry surfaces. *Journal of Hospital Infection*, *80*(1), 56–60. https://doi.org/10.1016/j.jhin.2011.08.013
Farrow, J. M., Wells, G., Palethorpe, S., Adams, M. D., & Pesci, E. C. (2020). CsrA supports both environmental persistence and host-associated growth of *Acinetobacter baumannii*. *Infection and Immunity*, IAI.00259-20. https://doi.org/10.1128/IAI.00259-20
Farrow, J. M., Wells, G., & Pesci, E. C. (2018). Desiccation tolerance in *Acinetobacter baumannii* is mediated by the two-component response regulator BfmR. *PLoS ONE*, *13*(10), 1–25. https://doi.org/10.1371/journal.pone.0205638
Fishbain, J., & Peleg, A. Y. (2010). Treatment of *Acinetobacter* infections. *Clinical Infectious Diseases*, *51*(1), 79–84. https://doi.org/10.1086/653120
Fröhlich, K. S., & Gottesman, S. (2018). Small Regulatory RNAs in the Enterobacterial Response to Envelope Damage and Oxidative Stress. *Microbiology Spectrum*, *6*(4), 1–25. https://doi.org/10.1128/microbiolspec.rwr-0022-2018
Fuchs, M., Lamm-Schmidt, V., Sulzer, J., Ponath, F., Jenniches, L., Kirk, J. A., Fagan, R. P., Barquist, L., Vogel, J., & Faber, F. (2021). An RNA-centric global view of *Clostridioides difficile* reveals broad activity of Hfq in a clinically important gram-positive bacterium. *Proceedings of the National Academy of Sciences of the United States of America*, *118*(25), 1–11. https://doi.org/10.1073/pnas.2103579118
Fuchs, M., Lamm-Schmidt, V., Lenče, T., Sulzer, J., Bublitz, A., Wackenreuter, J., Gerovac, M., Strowig, T., & Faber, F. (2023). A network of small RNAs regulates sporulation initiation in *Clostridioides difficile* . *The EMBO Journal*, *42*(12), 1–22. https://doi.org/10.15252/embj.2022112858
Gaddy, J. A., Actis, L. A., Arivett, B. A., Mcconnell, M. J., Rafael, L. R., & Pachón, J. (2012). Role of Acinetobactin-mediated iron acquisition functions in the interaction of *Acinetobacter baumannii* strain ATCC 19606T with human lung epithelial cells, *Galleria mellonella* caterpillars, and mice. *Infection and Immunity*, *80*(3), 1015–1024. https://doi.org/10.1128/IAI.06279-11
Gebhardt, M. J., Farland, E. A., Basu, P., Macarenoa, K., Melamed, S., & Dove, S. L. (2023). Hfq-licensed RNA–RNA interactome in *Pseudomonas aeruginosa* reveals a keystone sRNA. *Proceedings of the National Academy of Sciences*, *120*(21). https://doi.org/10.1073/pnas
Geisinger, E., Huo, W., Hernandez-Bird, J., & Isberg, R. R. (2019). *Acinetobacter*

baumannii: Envelope determinants that control drug resistance, virulence, and surface variability. *Annual Review of Microbiology*, *73*, 481–506. https://doi.org/10.1146/annurev-micro-020518-115714

Geisinger, E., Mortman, N. J., Dai, Y., Cokol, M., Syal, S., Farinha, A., Fisher, D. G., Tang, A. Y., Lazinski, D. W., Wood, S., Anthony, J., Van Opijnen, T., & Isberg, R. R. (2020). Antibiotic susceptibility signatures identify potential antimicrobial targets in the *Acinetobacter baumannii* cell envelope. *Nature Communications 2020 11:1*, *11*(1), 1–16. https://doi.org/10.1038/s41467-020-18301-2

Geisinger, E., Mortman, N. J., Vargas-Cuebas, G., Tai, A. K., & Isberg, R. R. (2018). A global regulatory system links virulence and antibiotic resistance to envelope homeostasis in *Acinetobacter baumannii*. *PLoS Pathogens*, *14*(5), 1–28. https://doi.org/10.1371/journal.ppat.1007030

Georg, J., Lalaouna, D., Hou, S., Lott, S. C., Caldelari, I., Marzi, S., Hess, W. R., & Romby, P. (2020). The power of cooperation: Experimental and computational approaches in the functional characterization of bacterial sRNAs. *Molecular Microbiology*, *113*(3), 603–612. https://doi.org/10.1111/mmi.14420

Godeux, A. S., Svedholm, E., Lupo, A., Haenni, M., Venner, S., Laaberki, M. H., & Charpentier, X. (2020). Scarless removal of large resistance island abar results in antibiotic susceptibility and increased natural transformability in *Acinetobacter baumannii*. *Antimicrobial Agents and Chemotherapy*, *64*(10), 1–9. https://doi.org/10.1128/AAC.00951-20

Gottesman, S., Mccullen, C., Guillier, M., Vanderpool, C., Benhammou, J., Thompson, K., Fitzgerald, P., Sowa, N., & Fitzgerald, D. (2006). Small RNA Regulators and the Bacterial Response to Stress. *Cold Spring Harbor Symposia on Quantitative Biology*, *71*, 1–11. https://doi.org/10.1101/sqb.2006.71.016.Small

Green, D. W. (2002). The bacterial cell wall as a source of antibacterial targets. *Expert Opinion on Therapeutic Targets*, *6*(1), 1–20. https://doi.org/10.1517/14728222.6.1.1

Green, E. R., Fakhoury, J. N., Monteith, A. J., Pi, H., Giedroc, D. P., & Skaar, E. P. (2022). Bacterial hydrophilins promote pathogen desiccation tolerance. *Cell Host and Microbe*, *30*(7), 975-987.e7. https://doi.org/10.1016/j.chom.2022.03.019

Grüll, M. P., & Massé, E. (2019). Mimicry, deception and competition: The life of competing endogenous RNAs. *Wiley Interdisciplinary Reviews: RNA*, *10*(3), 1–10. https://doi.org/10.1002/wrna.1525

Gu, Z., Gu, L., Eils, R., Schlesner, M., & Brors, B. (2014). Circlize implements and enhances circular visualization in R. *Bioinformatics*, *30*(19), 2811–2812. https://doi.org/10.1093/bioinformatics/btu393

Guillier, M., Gottesman, S., & Storz, G. (2006). Modulating the outer membrane with small RNAs. *Genes and Development*, *20*(17), 2338–2348. https://doi.org/10.1101/gad.1457506

Hamidian, M., & Nigro, S. J. (2019). Emergence, molecular mechanisms and global spread of carbapenem-resistant *Acinetobacter baumannii*. *Microbial Genomics*, *5*(10). https://doi.org/10.1099/mgen.0.000306

Hamrock, F. (2021). *Functional characterisation of small RNAs in Acinetobacter baumannii using Hi-GRIL-seq*. http://www.tara.tcd.ie/bitstream/handle/2262/96143/Fergal_Hamrock_MSc_Thesis_Corrected (1).pdf?sequence=1

Hamrock, F. J., Ryan, D., Ershova, A. S., Mogre, A., Sulimani, M. M., Ben Taarit, S., Hokamp, K., Westermann, A. J., & Kröger, C. (2024). Global analysis of the RNA–RNA interactome in *Acinetobacter baumannii* AB5075 uncovers a small

regulatory RNA repressing the virulence-related outer membrane protein CarO. *Nucleic Acids Research*, 1–18. https://doi.org/https://doi.org/10.1093/nar/gkae668
Han, K., Tjaden, B., & Lory, S. (2016). GRIL-seq provides a method for identifying direct targets of bacterial small regulatory RNA by in vivo proximity ligation. *Nature Microbiology*, *2*(0), 1–10. https://doi.org/10.1038/nmicrobiol.2016.239
Harding, C. M., Hennon, S. W., & Feldman, M. F. (2018). Uncovering the mechanisms of *Acinetobacter baumannii* virulence. *Nature Reviews Microbiology*, *16*(2), 91–102. https://doi.org/10.1038/nrmicro.2017.148
Harding, C. M., Pulido, M. R., Di Venanzio, G., Kinsella, R. L., Webb, A. I., Scott, N. E., Pachón, J., & Feldman, M. F. (2017). Pathogenic *Acinetobacter* species have a functional type I secretion system and contact-dependent inhibition systems. *Journal of Biological Chemistry*, *292*(22), 9075–9087. https://doi.org/10.1074/jbc.M117.781575
Harding, C. M., Tracy, E. N., Carruthers, M. D., Rather, P. N., Actis, L. A., & Munson, R. S. (2013). *Acinetobacter baumannii* strain M2 produces type IV Pili which play a role in natural transformation and twitching motility but not surface-associated motility. *MBio*, *4*(4), 1–10. https://doi.org/10.1128/mBio.00360-13
Hassan, K. A., Jackson, S. M., Penesyan, A., Patching, S. G., Tetu, S. G., Eijkelkamp, B. A., Brown, M. H., Henderson, P. J. F., & Paulsen, I. T. (2013). Transcriptomic and biochemical analyses identify a family of chlorhexidine efflux proteins. *Proceedings of the National Academy of Sciences of the United States of America*, *110*(50), 20254–20259. https://doi.org/10.1073/pnas.1317052110
Hawkey, J., Ascher, D. B., Judd, L. M., Wick, R. R., Kostoulias, X., Cleland, H., Spelman, D. W., Padiglione, A., Peleg, A. Y., & Holt, K. E. (2018). Evolution of carbapenem resistance in *Acinetobacter baumannii* during a prolonged infection. *Microbial Genomics*, *4*(3). https://doi.org/10.1099/mgen.0.000165
He, T., Wang, R., Liu, D., Walsh, T. R., Zhang, R., Lv, Y., Ke, Y., Ji, Q., Wei, R., Liu, Z., Shen, Y., Wang, G., Sun, L., Lei, L., Lv, Z., Li, Y., Pang, M., Wang, L., Sun, Q., … Wang, Y. (2019). Emergence of plasmid-mediated high-level tigecycline resistance genes in animals and humans. *Nature Microbiology*, *4*(9), 1450–1456. https://doi.org/10.1038/s41564-019-0445-2
Heimann, J. D. (2002). The extracytoplasmic function (ECF) sigma factors. In *Advances in Microbial Physiology* (Vol. 46). https://doi.org/10.1016/S0065-2911(02)46002-X
Hews, C. L., Cho, T., Rowley, G., & Raivio, T. L. (2019). Maintaining Integrity Under Stress: Envelope Stress Response Regulation of Pathogenesis in Gram-Negative Bacteria. *Frontiers in Cellular and Infection Microbiology*, *9*(September), 1–25. https://doi.org/10.3389/fcimb.2019.00313
Hoekzema, M., Romilly, C., Holmqvist, E., & Wagner, E. G. H. (2019). Hfq-dependent mRNA unfolding promotes sRNA -based inhibition of translation . *The EMBO Journal*, *38*(7), 1–14. https://doi.org/10.15252/embj.2018101199
Holmqvist, E., & Vogel, J. (2018). RNA-binding proteins in bacteria. *Nature Reviews Microbiology*, *16*(10), 601–615. https://doi.org/10.1038/s41579-018-0049-5
Holmqvist, E., & Wagner, G. H. (2017). Impact of bacterial sRNAs in stress responses. *Biochemical Society Transactions*, *45*(6), 1203–1212. https://doi.org/10.1042/BST20160363
Holmqvist, E., Wright, P. R., Li, L., Bischler, T., Barquist, L., Reinhardt, R., Backofen, R., & Vogel, J. (2016). Global RNA recognition patterns of post-transcriptional regulators Hfq and CsrA revealed by UV crosslinking in vivo . *The EMBO Journal*, *35*(9), 991–1011. https://doi.org/10.15252/embj.201593360

Hood, M. I., Becker, K. W., Roux, C. M., Dunman, P. M., & Skaar, E. P. (2013). Genetic determinants of intrinsic colistin tolerance in *Acinetobacter baumannii*. *Infection and Immunity*, *81*(2), 542–551. https://doi.org/10.1128/IAI.00704-12

Hood, M. I., Jacobs, A. C., Sayood, K., Dunman, P. M., & Skaar, E. P. (2010). *Acinetobacter baumannii* increases tolerance to antibiotics in response to monovalent cations. *Antimicrobial Agents and Chemotherapy*, *54*(3), 1029–1041. https://doi.org/10.1128/AAC.00963-09

Hood, M. I., Mortensen, B. L., Moore, J. L., Zhang, Y., Kehl-Fie, T. E., Sugitani, N., Chazin, W. J., Caprioli, R. M., & Skaar, E. P. (2012). Identification of an *Acinetobacter baumannii* Zinc Acquisition System that Facilitates Resistance to Calprotectin-mediated Zinc Sequestration. *PLoS Pathogens*, *8*(12), 20–24. https://doi.org/10.1371/journal.ppat.1003068

Hör, J., Garriss, G., Di Giorgio, S., Hack, L., Vanselow, J. T., Förstner, K. U., Schlosser, A., Henriques-Normark, B., & Vogel, J. (2020). Grad-seq in a Gram-positive bacterium reveals exonucleolytic sRNA activation in competence control . *The EMBO Journal*, *39*(9), 1–19. https://doi.org/10.15252/embj.2019103852

Hör, J., Gorski, S. A., & Vogel, J. (2018). Bacterial RNA Biology on a Genome Scale. *Molecular Cell*, *70*(5), 785–799. https://doi.org/10.1016/j.molcel.2017.12.023

Howden, B. P., Beaume, M., Harrison, P. F., Hernandez, D., Schrenzel, J., Seemann, T., Francois, P., & Stinear, T. P. (2013). Analysis of the small RNA transcriptional response in multidrug-resistant *Staphylococcus aureus* after antimicrobial exposure. *Antimicrobial Agents and Chemotherapy*, *57*(8), 3864–3874. https://doi.org/10.1128/AAC.00263-13

Huang, L., Sun, L., Xu, G., & Xia, T. (2008). Differential susceptibility to carbapenems due to the AdeABC efflux pump among nosocomial outbreak isolates of *Acinetobacter baumannii* in a Chinese hospital. *Diagnostic Microbiology and Infectious Disease*, *62*(3), 326–332. https://doi.org/10.1016/j.diagmicrobio.2008.06.008

Huber, M., Lippegaus, A., Melamed, S., Siemers, M., Wucher, B. R., Hoyos, M., Nadell, C., Storz, G., & Papenfort, K. (2022). An RNA sponge controls quorum sensing dynamics and biofilm formation in *Vibrio cholerae*. *Nature Communications*, *13*(1), 1–14. https://doi.org/10.1038/s41467-022-35261-x

Hubloher, J. J., Schabacker, K., Müller, V., & Averhoff, B. (2021). CsrA Coordinates Compatible Solute Synthesis in *Acinetobacter baumannii* and Facilitates Growth in Human Urine. *Microbiology Spectrum*, *9*(3), 1–12. https://doi.org/10.1128/spectrum.01296-21

Hubloher, J. J., Zeidler, S., Lamosa, P., Santos, H., Averhoff, B., & Müller, V. (2020). Trehalose-6-phosphate-mediated phenotypic change in *Acinetobacter baumannii*. *Environmental Microbiology*, *22*(12), 5156–5166. https://doi.org/10.1111/1462-2920.15148

Hunger, M., Schmucker, R., Kishan, V., & Hillen, W. (1990). Analysis and nucleotide sequence of an origin of an origin of DNA replication in *Acinetobacter calcoaceticus* and its use for *Escherichia coli* shuttle plasmids. *Gene*, *87*(1), 45–51. https://doi.org/10.1016/0378-1119(90)90494-C

Huo, W., Busch, L. M., Hernandez-Bird, J., Hamami, E., Marshall, C. W., Geisinger, E., Cooper, V. S., van Opijnen, T., Rosch, J. W., & Isberg, R. R. (2022). Immunosuppression broadens evolutionary pathways to drug resistance and treatment failure during *Acinetobacter baumannii* pneumonia in mice. *Nature Microbiology*, *7*(6), 796–809. https://doi.org/10.1038/s41564-022-01126-8

Huys, G., Cnockaert, M., Vaneechoutte, M., Woodford, N., Nemec, A., Dijkshoorn, L.,

& Swings, J. (2005). Distribution of tetracycline resistance genes in genotypically related and unrelated multiresistant *Acinetobacter baumannii* strains from different European hospitals. *Research in Microbiology*, *156*(3), 348–355. https://doi.org/10.1016/j.resmic.2004.10.008

Intorcia, V., Sava, R. L., Schroeder, G. P., & Gebhardt, M. J. (2024). A series of vectors for inducible gene expression in multidrug- resistant *Acinetobacter baumannii*. *Applied and Environmental Microbiology*, *0*(0).

Iosub, I. A., Marchioretto, M., Sy, B., McKellar, S., Nieken, K. J., van Nues, R. W., Tree, J. J., Viero, G., & Granneman, S. (2020). Hfq CLASH uncovers sRNA-target interaction networks enhancing adaptation to nutrient availability. *ELife*, *9*(e54655), 1–33.

Iyer, R., Moussa, S. H., Durand-Réville, T. F., Tommasi, R., & Miller, A. (2018). *Acinetobacter baumannii* OmpA Is a Selective Antibiotic Permeant Porin. *ACS Infectious Diseases*, *4*(3), 373–381. https://doi.org/10.1021/acsinfecdis.7b00168

Jacobs, A. C., Thompson, M. G., Black, C. C., Kessler, J. L., Clark, L. P., McQueary, C. N., Gancz, H. Y., Corey, B. W., Moon, J. K., Si, Y., Owen, M. T., Hallock, J. D., Kwak, Y. I., Summers, A., Li, C. Z., Rasko, D. A., Penwell, W. F., Honnold, C. L., Wise, M. C., … Zurawskia, D. V. (2014). AB5075, a Highly Virulent Isolate of *Acinetobacter baumannii*,as a Model Strain for the Evaluation of Pathogenesis and Antimicrobial Treatments. *Mbio*, *5*(3), 1–10. https://doi.org/10.1128/mBio.01076-14.Editor

Janssen, K. H., Diaz, M. R., Golden, M., Graham, J. W., Sanders, W., Wolfgang, M. C., & Yahr, T. L. (2018). Functional analyses of the RsmY and RsmZ small noncoding regulatory RNAs in *Pseudomonas aeruginosa*. *Journal of Bacteriology*, *200*(11), 1–15. https://doi.org/10.1128/JB.00736-17

Jaruratanasirikul, S., Nitchot, W., Wongpoowarak, W., Samaeng, M., & Nawakitrangsan, M. (2019). Population pharmacokinetics and Monte Carlo simulations of sulbactam to optimize dosage regimens in patients with ventilator-associated pneumonia caused by *Acinetobacter baumannii*. *European Journal of Pharmaceutical Sciences*, *136*(June 2018), 104940. https://doi.org/10.1016/j.ejps.2019.05.018

Jawad, A., Heritage, J., Snelling, A. M., Gascoyne-Binzi, D. M., & Hawkey, P. M. (1996). Influence of relative humidity and suspending menstrua on survival of *Acinetobacter spp.* on dry surfaces. *Journal of Clinical Microbiology*, *34*(12), 2881–2887. https://doi.org/10.1128/jcm.34.12.2881-2887.1996

Jayalath, K., Frisbie, S., To, M., & Abeysirigunawardena, S. (2020). Pseudouridine synthase rsua captures an assembly intermediate that is stabilized by ribosomal protein S17. *Biomolecules*, *10*(6). https://doi.org/10.3390/biom10060841

Johnson, E. N., Burns, T. C., Hayda, R. A., Hospenthal, D. R., & Murray, C. K. (2007). Infectious complications of open type III tibial fractures among combat casualties. *Clinical Infectious Diseases*, *45*(4), 409–415. https://doi.org/10.1086/520029

Jung, J., & Park, W. (2015). *Acinetobacter* species as model microorganisms in environmental microbiology: current state and perspectives. *Applied Microbiology and Biotechnology*, *99*(6), 2533–2548. https://doi.org/10.1007/s00253-015-6439-y

Juttukonda, L. J., Green, E. R., Lonergan, Z. R., Heffern, M. C., Chang, C. J., & Skaara, E. P. (2019). *Acinetobacter baumannii* OxyR Regulates the Transcriptional Response to Hydrogen Peroxide. *Infection and Immunity*, *87*(1). https://doi.org/10.1128/IAI.00413-18

Kamoshida, G., Tansho-Nagakawa, S., Kikuchi-Ueda, T., Nakano, R., Hikosaka, K., Nishida, S., Ubagai, T., Higashi, S., & Ono, Y. (2016). A novel bacterial transport

mechanism of *Acinetobacter baumannii* via activated human neutrophils through interleukin-8 . *Journal of Leukocyte Biology*, *100*(6), 1405–1412. https://doi.org/10.1189/jlb.4ab0116-023rr

Kamuyu, G., Ercoli, G., Ramos-Sevillano, E., Willcocks, S., Kewcharoenwong, C., Kiratisin, P., Taylor, P. W., Wren, B. W., Lertmemongkolchai, G., Stabler, R. A., & Brown, J. S. (2022). Strain Specific Variations in *Acinetobacter baumannii* Complement Sensitivity. *Frontiers in Immunology*, *13*(June), 1–15. https://doi.org/10.3389/fimmu.2022.853690

Karah, N., Sundsfjord, A., Towner, K., & Samuelsen, Ø. (2012). Insights into the global molecular epidemiology of carbapenem non-susceptible clones of *Acinetobacter baumannii*. *Drug Resistance Updates*, *15*(4), 237–247. https://doi.org/10.1016/j.drup.2012.06.001

Keen, E. F., Murray, C. K., Robinson, B. J., Hospenthal, D. R., A. Co, E.-M., & Aldous, W. K. (2010). Changes in the Incidences of Multidrug-Resistant and Extensively Drug-Resistant Organisms Isolated in a Military Medical Center. *Infection Control & Hospital Epidemiology*, *31*(7), 728–732. https://doi.org/10.1086/653617

Kempf, M., & Rolain, J. M. (2012). Emergence of resistance to carbapenems in *Acinetobacter baumannii* in Europe: Clinical impact and therapeutic options. *International Journal of Antimicrobial Agents*, *39*(2), 105–114. https://doi.org/10.1016/j.ijantimicag.2011.10.004

Kim, T., Bak, G., Lee, J., & Kim, K. sun. (2015). Systematic analysis of the role of bacterial Hfq-interacting sRNAs in the response to antibiotics. *Journal of Antimicrobial Chemotherapy*, *70*(6), 1659–1668. https://doi.org/10.1093/jac/dkv042

König, P., Wilhelm, A., Schaudinn, C., Poehlein, A., Daniel, R., Widera, M., Averhoff, B., & Müller, V. (2023). The VBNC state: a fundamental survival strategy of *Acinetobacter baumannii*. *MBio*, *14*(5). https://doi.org/10.1016/j.tim.2021.11.008

Krause, K. M., Serio, A. W., Kane, T. R., & Connolly, L. E. (2016). Aminoglycosides: An overview. *Cold Spring Harbor Perspectives in Medicine*, *6*(6), 1–18. https://doi.org/10.1101/cshperspect.a027029

Kröger, C., Colgan, A., Srikumar, S., Händler, K., Sivasankaran, S. K., Hammarlöf, D. L., Canals, R., Grissom, J. E., Conway, T., Hokamp, K., & Hinton, J. C. D. (2013). An infection-relevant transcriptomic compendium for *Salmonella enterica* serovar Typhimurium. *Cell Host and Microbe*, *14*(6), 683–695. https://doi.org/10.1016/j.chom.2013.11.010

Kröger, C., Kary, S. C., Schauer, K., & Cameron, A. D. S. (2017). Genetic regulation of virulence and antibiotic resistance in *Acinetobacter baumannii*. *Genes*, *8*(1). https://doi.org/10.3390/genes8010012

Kröger, C., MacKenzie, K. D., Alshabib, E. Y., Kirzinger, M. W. B., Suchan, D. M., Chao, T. C., Akulova, V., Miranda-CasoLuengo, A. A., Monzon, V. A., Conway, T., Sivasankaran, S. K., Hinton, J. C. D., Hokamp, K., & Cameron, A. D. S. (2018). The primary transcriptome, small RNAs and regulation of antimicrobial resistance in *Acinetobacter baumannii* ATCC 17978. *Nucleic Acids Research*, *46*(18), 9684–9698. https://doi.org/10.1093/nar/gky603

Krüger, J., & Rehmsmeier, M. (2006). RNAhybrid: MicroRNA target prediction easy, fast and flexible. *Nucleic Acids Research*, *34*(WEB. SERV. ISS.), 451–454. https://doi.org/10.1093/nar/gkl243

Kuo, H. Y., Chao, H. H., Liao, P. C., Hsu, L., Chang, K. C., Tung, C. H., Chen, C. H., & Liou, M. L. (2017). Functional characterization of *Acinetobacter baumannii*

Lacking the RNA chaperone Hfq. *Frontiers in Microbiology*, *8*(OCT), 1–12. https://doi.org/10.3389/fmicb.2017.02068

Kyriakidis, I., Vasileiou, E., Pana, Z. D., & Tragiannidis, A. (2021). *Acinetobacter baumannii* antibiotic resistance mechanisms. *Pathogens*, *10*(3), 1–31. https://doi.org/10.3390/pathogens10030373

Labrador-Herrera, G., Pérez-Pulido, A. J., Álvarez-Marín, R., Casimiro-Soriguer, C. S., Cebrero-Cangueiro, T., Morán-Barrio, J., Pachón, J., Viale, A. M., & Pachón-Ibáñez, M. E. (2020). Virulence role of the outer membrane protein CarO in carbapenem-resistant *Acinetobacter baumannii*. *Virulence*, *11*(1), 1727–1737. https://doi.org/10.1080/21505594.2020.1855912

Lalaouna, D., & Massé, E. (2015). Identification of sRNA interacting with a transcript of interest using MS2-affinity purification coupled with RNA sequencing (MAPS) technology. *Genomics Data*, *5*, 136–138. https://doi.org/10.1016/j.gdata.2015.05.033

Lamm-Schmidt, V., Fuchs, M., Sulzer, J., Gerovac, M., Hör, J., Dersch, P., Vogel, J., & Faber, F. (2021). Grad-seq identifies KhpB as a global RNA-binding protein in *Clostridioides difficile* that regulates toxin production. *MicroLife*, *2*(April), 1–21. https://doi.org/10.1093/femsml/uqab004

Langmead, B., & Salzberg, S. L. (2012). Fast gapped-read alignment with Bowtie 2. *Nature Methods*, *9*(4), 357–359. https://doi.org/10.1038/nmeth.1923

Leung, W. S., Chu, C. M., Tsang, K. Y., Lo, F. H., Lo, K. F., & Ho, P. L. (2006). Fulminant community-acquired *Acinetobacter baumannii* pneumonia as a distinct clinical syndrome. *Chest*, *129*(1), 102–109. https://doi.org/10.1378/chest.129.1.102

Leus, I. V., Weeks, J. W., Bonifay, V., Smith, L., Richardson, S., & Zgurskayaa, H. I. (2018). Substrate Specificities and Efflux Efficiencies of RND Efflux Pumps. *Journal of Bacteriology*, *200*(13).

Li, B., Ruotti, V., Stewart, R. M., Thomson, J. A., & Dewey, C. N. (2010). RNA-Seq gene expression estimation with read mapping uncertainty. *Bioinformatics*, *26*(4), 493–500. https://doi.org/10.1093/bioinformatics/btp692

Liao, Z., & Smirnov, A. (2023). *FinO / ProQ-family proteins : an evolutionary perspective*. *0*(March), 1–21.

Limansky, A. S., Mussi, M. A., & Viale, A. M. (2002). Loss of a 29-kilodalton outer membrane protein in *Acinetobacter baumannii* is associated with imipenem resistance. *Journal of Clinical Microbiology*, *40*(12), 4776–4778. https://doi.org/10.1128/JCM.40.12.4776-4778.2002

Lin, M. F., Lin, Y. Y., Yeh, H. W., & Lan, C. Y. (2014). Role of the BaeSR two-component system in the regulation of *Acinetobacter baumannii* adeAB genes and its correlation with tigecycline susceptibility. *BMC Microbiology*, *14*(1), 1–12. https://doi.org/10.1186/1471-2180-14-119

Liu, F., Chen, Z., Zhang, S., Wu, K., Bei, C., Wang, C., & Chao, Y. (2023). In vivo RNA interactome profiling reveals 3'UTR-processed small RNA targeting a central regulatory hub. *Nature Communications*, *14*(1), 1–15. https://doi.org/10.1038/s41467-023-43632-1

Loehfelm, T. W., Luke, N. R., & Campagnari, A. A. (2008). Identification and characterization of an *Acinetobacter baumannii* biofilm-associated protein. *Journal of Bacteriology*, *190*(3), 1036–1044. https://doi.org/10.1128/JB.01416-07

Lorenz, R., Bernhart, S. H., Siederdissen, C. H. zu, Tafer, H., Flamm, C., Stadler, P. F., & Hofacker, I. L. (2011). ViennaRNA Package 2.0. *Algorithms for Molecular Biology*, *6*(26). http://www.tbi.univie.ac.at/RNA.

Lucidi, M., Runci, F., Rampioni, G., Frangipani, E., Leoni, L., & Visca, P. (2018). New Shuttle Vectors for Gene Cloning and Expression in. *Antimicrobial Agents and Chemotherapy*, *62*(4), 1–19.

Ma, C., & McClean, S. (2021). Mapping global prevalence of *Acinetobacter baumannii* and recent vaccine development to tackle it. *Vaccines*, *9*(6). https://doi.org/10.3390/vaccines9060570

Magda, M., Bettoni, S., Laabei, M., Fairley, D., Russo, T. A., Riesbeck, K., & Blom, A. M. (2022). Clinical Isolates of *Acinetobacter spp.* Are Highly Serum Resistant Despite Efficient Recognition by the Complement System. *Frontiers in Immunology*, *13*(January), 1–16. https://doi.org/10.3389/fimmu.2022.814193

Mahgoub, S., Ahmed, J., & Glatt, A. E. (2002). Underlying characteristics of patients harboring highly resistant *Acinetobacter baumannii*. *American Journal of Infection Control*, *30*(7), 386–390. https://doi.org/10.1067/mic.2002.122648

Marchand, I., Damier-piolle, L., Courvalin, P., & Lambert, T. (2004). Expression of the RND-Type Efflux Pump AdeABC in *Acinetobacter baumannii* is regulated by the AdeRS two-component system. *Antimicrobial Agents and Chemotherapy*, *48*(9), 3298–3304. https://doi.org/10.1128/AAC.48.9.3298

Marchand, I., Marchand, I., Damier-piolle, L., Damier-piolle, L., Courvalin, P., Courvalin, P., Lambert, T., & Lambert, T. (2004). Expression of the RND-Type Ef ux Pump AdeABC in. *Society*, *48*(9), 3298–3304. https://doi.org/10.1128/AAC.48.9.3298

Marchetti, M., De Bei, O., Bettati, S., Campanini, B., Kovachka, S., Gianquinto, E., Spyrakis, F., & Ronda, L. (2020). Iron metabolism at the interface between host and pathogen: From nutritional immunity to antibacterial development. *International Journal of Molecular Sciences*, *21*(6). https://doi.org/10.3390/ijms21062145

Marie, L., Rapisarda, C., Morales, V., Bergé, M., Perry, T., Soulet, A. L., Gruget, C., Remaut, H., Fronzes, R., & Polard, P. (2017). Bacterial RadA is a DnaB-Type helicase interacting with RecA to promote bidirectional D-loop extension. *Nature Communications*, *8*(May), 1–14. https://doi.org/10.1038/ncomms15638

Massé, E., & Gottesman, S. (2002). A small RNA regulates the expression of genes involved in iron metabolism in *Escherichia coli*. *Proceedings of the National Academy of Sciences of the United States of America*, *99*(7), 4620–4625. https://doi.org/10.1073/pnas.032066599

Massé, E., Vanderpool, C. K., & Gottesman, S. (2005). Effect of RyhB Small RNA on Global Iron Use in *Escherichia coli*. *Journal of Bacteriology*, *187*(20), 6962 LP – 6971. https://doi.org/10.1128/JB.187.20.6962-6971.2005

Matera, G., Altuvia, Y., Gerovac, M., El Mouali, Y., Margalit, H., & Vogel, J. (2022). Global RNA interactome of *Salmonella* discovers a 5′ UTR sponge for the MicF small RNA that connects membrane permeability to transport capacity. *Molecular Cell*, *82*(3), 629-644.e4. https://doi.org/10.1016/j.molcel.2021.12.030

Maure, A., Robino, E., & Van der Henst, C. (2023). The intracellular life of *Acinetobacter baumannii*. *Trends in Microbiology*, *31*(12), 1238–1250. https://doi.org/10.1016/j.tim.2023.06.007

McDonnell, G., & Russell, A. D. (1999). Antiseptics and Disinfectants: Activity, Action, and Resistance. *Clinical Microbiology Reviews*, *12*(1).

Melamed, S., Faigenbaum-Romm, R., Peer, A., Reiss, N., Shechter, O., Bar, A., Altuvia, Y., Argaman, L., & Margalit, H. (2018). Mapping the small RNA interactome in bacteria using RIL-seq. *Nature Protocols*, *13*(1), 1–33. https://doi.org/10.1038/nprot.2017.115

Melamed, S., Peer, A., Faigenbaum-Romm, R., Gatt, Y. E., Reiss, N., Bar, A., Altuvia, Y., Argaman, L., & Margalit, H. (2016). Global Mapping of Small RNA-Target Interactions in Bacteria. *Molecular Cell*, *63*(5), 884–897. https://doi.org/10.1016/j.molcel.2016.07.026

Michaux, C., Verneuil, N., Hartke, A., & Giard, J. C. (2014). Physiological roles of small RNA molecules. *Microbiology (United Kingdom)*, *160*(PART 6), 1007–1019. https://doi.org/10.1099/mic.0.076208-0

Moffatt, J. H., Harper, M., Harrison, P., Hale, J. D. F., Vinogradov, E., Seemann, T., Henry, R., Crane, B., St. Michael, F., Cox, A. D., Adler, B., Nation, R. L., Li, J., & Boyce, J. D. (2010). Colistin resistance in *Acinetobacter baumannii* is mediated by complete loss of lipopolysaccharide production. *Antimicrobial Agents and Chemotherapy*, *54*(12), 4971–4977. https://doi.org/10.1128/AAC.00834-10

Mohapatra, S. S., Dwibedy, S. K., & Padhy, I. (2021). Polymyxins, the last-resort antibiotics: Mode of action, resistance emergence, and potential solutions. *Journal of Biosciences*, *46*(3). https://doi.org/10.1007/s12038-021-00209-8

Møller, T., Franch, T., Udesen, C., Gerdes, K., & Valentin-Hansen, P. (2002). Spot 42 RNA mediates discoordinate expression of the *E. coli* galactose operon. *Genes and Development*, *16*(13), 1696–1706. https://doi.org/10.1101/gad.231702

Monem, S., Furmanek-Blaszk, B., Łupkowska, A., Kuczyńska-Wiśnik, D., Stojowska-Swędrzyńska, K., & Laskowska, E. (2020). Mechanisms protecting *Acinetobacter baumannii* against multiple stresses triggered by the host immune response, antibiotics, and outside host environment. *International Journal of Molecular Sciences*, *21*(15), 1–30. https://doi.org/10.3390/ijms21155498

Moon, K., & Gottesman, S. (2009). A PhoQ/P-regulated small RNA regulates sensitivity of *Escherichia coli* to antimicrobial peptides. *Molecular Microbiology*, *74*(6), 1314–1330. https://doi.org/10.1111/j.1365-2958.2009.06944.x

Moore, J. L., Becker, K. W., Nicklay, J. J., Boyd, K. L., Skaar, E. P., & Caprioli, R. M. (2014). Imaging mass spectrometry for assessing temporal proteomics: Analysis of calprotectin in *Acinetobacter baumannii* pulmonary infection. *Proteomics*, *14*(7–8), 820–828. https://doi.org/10.1002/pmic.201300046

Morita, T., Mochizuki, Y., & Aiba, H. (2006). Translational repression is sufficient for gene silencing by bacterial small noncoding RNAs in the absence of mRNA destruction. *Proceedings of the National Academy of Sciences of the United States of America*, *103*(13), 4858–4863. https://doi.org/10.1073/pnas.0509638103

Mortensen, B. L., Rathi, S., Chazin, W. J., & Skaar, E. P. (2014). *Acinetobacter baumannii* response to host-mediated zinc limitation requires the transcriptional regulator zur. *Journal of Bacteriology*, *196*(14), 2616–2626. https://doi.org/10.1128/JB.01650-14

Moubareck, C. A., & Halat, D. H. (2020). Insights into *Acinetobacter baumannii*: A review of microbiological, virulence, and resistance traits in a threatening nosocomial pathogen. *Antibiotics*, *9*(3). https://doi.org/10.3390/antibiotics9030119

Mulvey, M. R., Switala, J., Borys, A., & Loewen, P. C. (1990). Regulation of transcription of *katE* and *katF* in *Escherichia coli*. *Journal of Bacteriology*, *172*(12), 6713–6720. https://doi.org/10.1128/jb.172.12.6713-6720.1990

Murdoch, C. C., & Skaar, E. P. (2022). Nutritional immunity: the battle for nutrient metals at the host–pathogen interface. *Nature Reviews Microbiology*, *20*(11), 657–670. https://doi.org/10.1038/s41579-022-00745-6

Mussi, M. A., Limansky, A. S., & Viale, A. M. (2005). Acquisition of resistance to carbapenems in multidrug-resistant clinical strains of *Acinetobacter baumannii*: Natural insertional inactivation of a gene encoding a member of a novel family of

β-barrel outer membrane proteins. *Antimicrobial Agents and Chemotherapy*, *49*(4), 1432–1440. https://doi.org/10.1128/AAC.49.4.1432-1440.2005

Mussi, M. A., Relling, V. M., Limansky, A. S., & Viale, A. M. (2007). CarO, an *Acinetobacter baumannii* outer membrane protein involved in carbapenem resistance, is essential for l-ornithine uptake. *FEBS Letters*, *581*(29), 5573–5578. https://doi.org/10.1016/j.febslet.2007.10.063

Naville, M., Ghuillot-Gaudeffroy, A., Marchais, A., & Gautheret, D. (2011). ARNold: A web tool for the prediction of Rho-independent transcription terminators. *RNA Biology*, *8*(1), 11–13. https://doi.org/10.4161/rna.8.1.13346

Nelson, R. E., Schweizer, M. L., Perencevich, E. N., Nelson, S. D., Khader, K., Chiang, H. Y., Chorazy, M. L., Blevins, A., Ward, M. A., & Samore, M. H. (2016). Costs and mortality associated with multidrug-resistant healthcare-associated *Acinetobacter* infections. *Infection Control and Hospital Epidemiology*, *37*(10), 1212–1218. https://doi.org/10.1017/ice.2016.145

Nemec, A., Krizova, L., Maixnerova, M., Sedo, O., Brisse, S., & Higgins, P. G. (2015). *Acinetobacter seifertii* sp. nov., a member of the *Acinetobacter calcoaceticus-Acinetobacter baumannii* complex isolated from human clinical specimens. *International Journal of Systematic and Evolutionary Microbiology*, *65*(3), 934–942. https://doi.org/10.1099/ijs.0.000043

Nemec, A., Krizova, L., Maixnerova, M., van der Reijden, T. J. K., Deschaght, P., Passet, V., Vaneechoutte, M., Brisse, S., & Dijkshoorn, L. (2011). Genotypic and phenotypic characterization of the *Acinetobacter calcoaceticus-Acinetobacter baumannii* complex with the proposal of *Acinetobacter pittii* sp. nov. (formerly *Acinetobacter* genomic species 3) and *Acinetobacter nosocomialis* sp. nov. (formerly Ac. *Research in Microbiology*, *162*(4), 393–404. https://doi.org/10.1016/j.resmic.2011.02.006

Nero, T. M., Dalia, T. N., Wang, J. C. Y., Kysela, D. T., Bochman, M. L., & Dalia, A. B. (2018). ComM is a hexameric helicase that promotes branch migration during natural transformation in diverse Gram-negative species. *Nucleic Acids Research*, *46*(12), 6099–6111. https://doi.org/10.1093/nar/gky343

Ng Kwan Lim, E., Sasseville, C., Carrier, M. C., & Massé, E. (2021). Keeping Up with RNA-Based Regulation in Bacteria: New Roles for RNA Binding Proteins. *Trends in Genetics*, *37*(1), 86–97. https://doi.org/10.1016/j.tig.2020.09.014

Nielsen, J. S., Lei, L. K., Ebersbach, T., Olsen, A. S., Klitgaard, J. K., Valentin-Hansen, P., & Kallipolitis, B. H. (2009). Defining a role for Hfq in Gram-positive bacteria: Evidence for Hfq-dependent antisense regulation in *Listeria monocytogenes*. *Nucleic Acids Research*, *38*(3), 907–919. https://doi.org/10.1093/nar/gkp1081

Nishino, K., Yamasaki, S., Hayashi-Nishino, M., & Yamaguchi, A. (2011). Effect of overexpression of small non-coding DsrA RNA on multidrug efflux in *Escherichia coli*. *Journal of Antimicrobial Chemotherapy*, *66*(2), 291–296. https://doi.org/10.1093/jac/dkq420

Nitzan, M., Rehani, R., & Margalit, H. (2017). Integration of Bacterial Small RNAs in Regulatory Networks. *Annual Review of Biophysics*, *46*(1), 131–148. https://doi.org/10.1146/annurev-biophys-070816-034058

Norton, M. D., Spilkia, A. J., & Godoy, V. G. (2013). Antibiotic resistance acquired through a DNA damage-inducible response in *Acinetobacter baumannii*. *Journal of Bacteriology*, *195*(6), 1335–1345. https://doi.org/10.1128/JB.02176-12

Nwugo, C. C., Gaddy, J. A., Zimbler, D. L., & Actis, L. A. (2011). Deciphering the iron response in *Acinetobacter baumannii*: A proteomics approach. *Journal of Proteomics*, *74*(1), 44–58. https://doi.org/10.1016/j.jprot.2010.07.010

Oda, Y., Shapiro, M. M., Lewis, N. M., Zhong, X., Huse, H. K., Zhong, W., Bruce, J. E., Manoil, C., & Harwood, C. S. (2022). CsrA-Controlled Proteins Reveal New Dimensions of *Acinetobacter baumannii* Desiccation Tolerance. *Journal of Bacteriology*, *204*(4), 1–12. https://doi.org/10.1128/jb.00479-21

Pakharukova, N., Tuittila, M., Paavilainen, S., Malmi, H., Parilova, O., Teneberg, S., Knight, S. D., & Zavialov, A. V. (2018). Structural basis for *Acinetobacter baumannii* biofilm formation. *Proceedings of the National Academy of Sciences of the United States of America*, *115*(21), 5558–5563. https://doi.org/10.1073/pnas.1800961115

Papenfort, K., Pfeiffer, V., Lucchini, S., Sonawane, A., Hinton, J. C. D., & Vogel, J. (2008). Systematic deletion of *Salmonella* small RNA genes identifies CyaR, a conserved CRP-dependent riboregulator of OmpX synthesis. *Molecular Microbiology*, *68*(4), 890–906. https://doi.org/10.1111/j.1365-2958.2008.06189.x

Papenfort, K., Pfeiffer, V., Mika, F., Lucchini, S., Hinton, J. C. D., & Vogel, J. (2006). σE-dependent small RNAs of *Salmonella* respond to membrane stress by accelerating global omp mRNA decay. *Molecular Microbiology*, *62*(6), 1674–1688. https://doi.org/10.1111/j.1365-2958.2006.05524.x

Papenfort, K., Said, N., Welsink, T., Lucchini, S., Hinton, J. C. D., & Vogel, J. (2009). Specific and pleiotropic patterns of mRNA regulation by ArcZ, a conserved, Hfq-dependent small RNA. *Molecular Microbiology*, *74*(1), 139–158. https://doi.org/10.1111/j.1365-2958.2009.06857.x

Parker, A., & Gottesman, S. (2016). Small RNA regulation of TolC, the outer membrane component of bacterial multidrug transporters. *Journal of Bacteriology*, *198*(7), 1101–1113. https://doi.org/10.1128/JB.00971-15

Peleg, A. Y., Seifert, H., & Paterson, D. L. (2008). *Acinetobacter baumannii*: Emergence of a successful pathogen. *Clinical Microbiology Reviews*, *21*(3), 538–582. https://doi.org/10.1128/CMR.00058-07

Penwell, W. F., Degrace, N., Tentarelli, S., Gauthier, L., Gilbert, C. M., Arivett, B. A., Miller, A. A., Durand-Reville, T. F., Joubran, C., & Actis, L. A. (2015). Discovery and Characterization of New Hydroxamate Siderophores, Baumannoferrin A and B, produced by *Acinetobacter baumannii*. *ChemBioChem*, *16*(13), 1896–1904. https://doi.org/10.1002/cbic.201500147

Pérez-Varela, M., Tierney, A. R. P., Dawson, E., Hutcheson, A. R., Tipton, K. A., Anderson, S. E., Haldopoulos, M. E., Song, S., Tomlinson, B. R., Shaw, L. N., Weiss, D. S., Kim, M., & Rather, P. N. (2022). Stochastic activation of a family of TetR type transcriptional regulators controls phenotypic heterogeneity in *Acinetobacter baumannii*. *PNAS Nexus*, *1*(5), 1–12. https://doi.org/10.1093/pnasnexus/pgac231

Perez, F., Hujer, A. M., Hujer, K. M., Decker, B. K., Rather, P. N., & Bonomo, R. A. (2007). Global challenge of multidrug-resistant *Acinetobacter baumannii*. *Antimicrobial Agents and Chemotherapy*, *51*(10), 3471–3484. https://doi.org/10.1128/AAC.01464-06

Pichon, C., & Felden, B. (2007). Proteins that interact with bacterial small RNA regulators. *FEMS Microbiology Reviews*, *31*(5), 614–625. https://doi.org/10.1111/j.1574-6976.2007.00079.x

Potts, A. H., Vakulskas, C. A., Pannuri, A., Yakhnin, H., Babitzke, P., & Romeo, T. (2017). Global role of the bacterial post-transcriptional regulator CsrA revealed by integrated transcriptomics. *Nature Communications*, *8*(1). https://doi.org/10.1038/s41467-017-01613-1

Proschak, A., Lubuta, P., Grün, P., Löhr, F., Wilharm, G., De Berardinis, V., & Bode,

H. B. (2013). Structure and Biosynthesis of Fimsbactins A-F, Siderophores from *Acinetobacter baumannii* and *Acinetobacter baylyi*. *ChemBioChem*, *14*(5), 633–638. https://doi.org/10.1002/cbic.201200764

Qin, Q. M., Pei, J., Gomez, G., Rice-Ficht, A., Ficht, T. A., & de Figueiredo, P. (2020). A Tractable Drosophila Cell System Enables Rapid Identification of *Acinetobacter baumannii* Host Factors. *Frontiers in Cellular and Infection Microbiology*, *10*(May), 1–10. https://doi.org/10.3389/fcimb.2020.00240

Quendera, A. P., Seixas, A. F., dos Santos, R. F., Santos, I., Silva, J. P. N., Arraiano, C. M., & Andrade, J. M. (2020). RNA-Binding Proteins Driving the Regulatory Activity of Small Non-coding RNAs in Bacteria. *Frontiers in Molecular Biosciences*, *7*(May), 1–9. https://doi.org/10.3389/fmolb.2020.00078

Ramirez, M. S., Don, M., Merkier, A. K., Bistué, A. J. S., Zorreguieta, A., Centrón, D., & Tolmasky, M. E. (2010). Naturally competent *Acinetobacter baumannii* clinical isolate as a convenient model for genetic studies. *Journal of Clinical Microbiology*, *48*(4), 1488–1490. https://doi.org/10.1128/JCM.01264-09

Rangel, K., Chagas, T. P. G., & De-Simone, S. G. (2021). *Acinetobacter baumannii* infections in times of COVID-19 pandemic. *Pathogens*, *10*(8), 1–13. https://doi.org/10.3390/pathogens10081006

Rice, J. B., & Vanderpool, C. K. (2011). The small RNA SgrS controls sugar-phosphate accumulation by regulating multiple PTS genes. *Nucleic Acids Research*, *39*(9), 3806–3819. https://doi.org/10.1093/nar/gkq1219

Richards, G. R., & Vanderpool, C. K. (2011). Molecular call and response: The physiology of bacterial small RNAs. *Biochimica et Biophysica Acta - Gene Regulatory Mechanisms*, *1809*(10), 525–531. https://doi.org/10.1016/j.bbagrm.2011.07.013

Robicsek, A., Jacoby, G. A., & Hooper, D. C. (2006). The worldwide emergence of plasmid-mediated quinolone resistance. *Lancet Infectious Diseases*, *6*(10), 629–640. https://doi.org/10.1016/S1473-3099(06)70599-0

Robinson, J. T., Thorvaldsdóttir, H., Winckler, W., Guttman, M., Lander, E. S., Getz, G., & Mesirov, J. P. (2011). Integrative Genome Viewer. *Nature Biotechnology*, *29*(1), 24–26. https://doi.org/10.1038/nbt.1754.Integrative

Ronish, L. A., Lillehoj, E., Fields, J. K., Sundberg, E. J., & Piepenbrink, K. H. (2019). The structure of PilA from Acinetobacter baumannii AB5075 suggests a mechanism for functional specialization in *Acinetobacter* type IV pili. *Journal of Biological Chemistry*, *294*(1), 218–230. https://doi.org/10.1074/jbc.RA118.005814

Rubio, T., Gagné, S., Debruyne, C., Dias, C., Cluzel, C., Mongellaz, D., Rousselle, P., Göttig, S., Seifert, H., Higgins, P. G., & Salcedo, S. P. (2022). Incidence of an Intracellular Multiplication Niche among *Acinetobacter baumannii* Clinical Isolates. *MSystems*, *7*(1). https://doi.org/10.1128/msystems.00488-21

Ruhland, E., Siemers, M., Gerst, R., Späth, F., Vogt, L. N., Figge, M. T., Papenfort, K., & Fröhlich, and K. S. (2024). The global RNA–RNA interactome of *Klebsiella pneumoniae* unveils a small RNA regulator of cell division. *Proceedings of the National Academy of Sciences*, *121*. https://doi.org/10.1073/pnas

Ryan, D., Jenniches, L., Reichardt, S., Barquist, L., & Westermann, A. J. (2020). A high-resolution transcriptome map identifies small RNA regulation of metabolism in the gut microbe *Bacteroides thetaiotaomicron*. *Nature Communications*, *11*(1). https://doi.org/10.1038/s41467-020-17348-5

Sahr, T., Escoll, P., Rusniok, C., Bui, S., Pehau-Arnaudet, G., Lavieu, G., & Buchrieser, C. (2022). Translocated *Legionella pneumophila* small RNAs mimic eukaryotic microRNAs targeting the host immune response. *Nature*

Communications, *13*(1). https://doi.org/10.1038/s41467-022-28454-x
Salah Ud-Din, A. I. M., & Roujeinikova, A. (2017). Methyl-accepting chemotaxis proteins: a core sensing element in prokaryotes and archaea. *Cellular and Molecular Life Sciences*, *74*(18), 3293–3303. https://doi.org/10.1007/s00018-017-2514-0
Salvail, H., Caron, M. P., Bélanger, J., & Massé, E. (2013). Antagonistic functions between the RNA chaperone Hfq and an sRNA regulate sensitivity to the antibiotic colicin. *EMBO Journal*, *32*(20), 2764–2778. https://doi.org/10.1038/emboj.2013.205
Santiago-Frangos, A., Jeliazkov, J. R., Gray, J. J., & Woodson, S. A. (2017). Acidic C-terminal domains autoregulate the RNA chaperone Hfq. *ELife*, *6*, 1–25. https://doi.org/10.7554/eLife.27049
Santiago-Frangos, A., & Woodson, S. A. (2018). Hfq chaperone brings speed dating to bacterial sRNA. *Wiley Interdisciplinary Reviews: RNA*, *9*(4), 1–16. https://doi.org/10.1002/wrna.1475
Sarshar, M., Scribano, D., Palamara, A. T., Ambrosi, C., & Masotti, A. (2022). The *Acinetobacter baumannii* model can explain the role of small non-coding RNAs as potential mediators of host-pathogen interactions. *Frontiers in Molecular Biosciences*, *9*(December), 1–9. https://doi.org/10.3389/fmolb.2022.1088783
Satchell, K. J. F. (2011). Structure and function of MARTX toxins and other large repetitive RTX proteins. *Annual Review of Microbiology*, *65*, 71–90. https://doi.org/10.1146/annurev-micro-090110-102943
Schilling, D., Findei, S., Richter, A. S., Taylor, J. A., & Gerischer, U. (2010). The small RNA Aar in Acinetobacter baylyi: A putative regulator of amino acid metabolism. *Archives of Microbiology*, *192*(9), 691–702. https://doi.org/10.1007/s00203-010-0592-6
Schilling, D., & Gerischer, U. (2009). The *Acinetobacter baylyi hfq* gene encodes a large protein with an unusual C terminus. *Journal of Bacteriology*, *191*(17), 5553–5562. https://doi.org/10.1128/JB.00490-09
Schneider, C. A., Rasband, W. S., & Eliceiri, K. W. (2012). NIH Image to ImageJ: 25 years of image analysis. *Nature Methods*, *9*(7), 671–675. https://doi.org/10.1038/nmeth.2089
Schu, D. J., Zhang, A., Gottesman, S., & Storz, G. (2015). Alternative Hfq-sRNA interaction modes dictate alternative mRNA recognition. *The EMBO Journal*, *34*(20), 2557–2573. https://doi.org/10.15252/embj.201591569
Schwarz, S., Hood, R. D., & Mougous, J. D. (2010). What is type VI secretion doing in all those bugs? *Trends in Microbiology*, *18*(12), 531–537. https://doi.org/10.1016/j.tim.2010.09.001
Scott, N. E., Kinsella, R. L., Edwards, A. V. G., Larsen, M. R., Dutta, S., Saba, J., Foster, L. J., & Feldman, M. F. (2014). Diversity within the O-linked protein glycosylation systems of *Acinetobacter* species. *Molecular and Cellular Proteomics*, *13*(9), 2354–2370. https://doi.org/10.1074/mcp.M114.038315
Sharma, A., Dubey, V., Sharma, R., Devnath, K., Gupta, V. K., Akhter, J., Bhando, T., Verma, A., Ambatipudi, K., Sarkar, M., & Pathania, R. (2018). The unusual glycine-rich C terminus of the *Acinetobacter baumannii* RNA chaperone Hfq plays an important role in bacterial physiology. *Journal of Biological Chemistry*, *293*(35), 13377–13388. https://doi.org/10.1074/jbc.RA118.002921
Sharma, C. M., Darfeuille, F., Plantinga, T. H., & Vogel, J. (2007). A small RNA regulates multiple ABC transporter mRNAs by targeting C/A-rich elements inside and upstream of ribosome-binding sites. *Genes and Development*, *21*(21), 2804–

2817. https://doi.org/10.1101/gad.447207
Sharma, C. M., Hoffmann, S., Darfeuille, F., Reignier, J., Findeiß, S., Sittka, A., Chabas, S., Reiche, K., Hackermüller, J., Reinhardt, R., Stadler, P. F., & Vogel, J. (2010). The primary transcriptome of the major human pathogen *Helicobacter pylori*. *Nature*, *464*(7286), 250–255. https://doi.org/10.1038/nature08756
Sharma, C. M., Papenfort, K., Pernitzsch, S. R., Mollenkopf, H. J., Hinton, J. C. D., & Vogel, J. (2011). Pervasive post-transcriptional control of genes involved in amino acid metabolism by the Hfq-dependent GcvB small RNA. *Molecular Microbiology*, *81*(5), 1144–1165. https://doi.org/10.1111/j.1365-2958.2011.07751.x
Sharma, R., Arya, S., Patil, S. D., Sharma, A., Jain, P. K., Navani, N. K., & Pathania, R. (2014). Identification of novel regulatory small RNAs in *Acinetobacter baumannii*. *PLoS ONE*, *9*(4). https://doi.org/10.1371/journal.pone.0093833
Sheldon, J. R., & Skaar, E. P. (2020). *Acinetobacter baumannii* can use multiple siderophores for iron acquisition, but only acinetobactin is required for virulence. In *PLoS Pathogens* (Vol. 16, Issue 10). https://doi.org/10.1371/journal.ppat.1008995
Shenkutie, A. M., Gebrelibanos, D., Yao, M., Bedada Hundie, G., Chow, F. W. N., & Leung, P. H. M. (2023). Impairment of novel non-coding small RNA00203 inhibits biofilm formation and reduces biofilm-specific antibiotic resistance in *Acinetobacter baumannii*. *International Journal of Antimicrobial Agents*, *62*(3), 106889. https://doi.org/10.1016/j.ijantimicag.2023.106889
Siroy, A., Molle, V., Lemaître-Guillier, C., Vallenet, D., Pestel-Caron, M., Cozzone, A. J., Jouenne, T., & Dé, E. (2005). Channel formation by CarO, the carbapenem resistance-associated outer membrane protein of *Acinetobacter baumannii*. *Antimicrobial Agents and Chemotherapy*, *49*(12), 4876–4883. https://doi.org/10.1128/AAC.49.12.4876-4883.2005
Smirnov, A., Förstner, K. U., Holmqvist, E., Otto, A., Günster, R., Becher, D., Reinhardt, R., & Vogel, J. (2016). Grad-seq guides the discovery of ProQ as a major small RNA-binding protein. *Proceedings of the National Academy of Sciences*, *113*(41), 11591 LP – 11596. https://doi.org/10.1073/pnas.1609981113
Smirnov, A., Wang, C., Drewry, L. L., & Vogel, J. (2017). Molecular mechanism of mRNA repression in trans by a ProQ-dependent small RNA . *The EMBO Journal*, *36*(8), 1029–1045. https://doi.org/10.15252/embj.201696127
Soukup, G. A., & Breaker, R. R. (1999). Relationship between internucleotide linkage geometry and the stability of RNA. *Rna*, *5*(10), 1308–1325. https://doi.org/10.1017/S1355838299990891
Spellberg, B., & Rex, J. H. (2013). The value of single-pathogen antibacterial agents. *Nature Reviews Drug Discovery*, *12*(12), 963–964. https://doi.org/10.1038/nrd3957-c1
Srinivasan, V. B., Vaidyanathan, V., & Rajamohan, G. (2015). AbuO, a TolC-like outer membrane protein of *Acinetobacter baumannii*, is involved in antimicrobial and oxidative stress resistance. *Antimicrobial Agents and Chemotherapy*, *59*(2), 1236–1245. https://doi.org/10.1128/AAC.03626-14
Storz, G., Vogel, J., & Wassarman, K. M. (2011). Regulation by Small RNAs in Bacteria: Expanding Frontiers. *Molecular Cell*, *43*(6), 880–891. https://doi.org/10.1016/j.molcel.2011.08.022.Regulation
Sun, B., Liu, H., Jiang, Y., Shao, L., Yang, S., & Chen, D. (2020). New Mutations Involved in Colistin Resistance in *Acinetobacter baumannii*. *MSphere*, *5*(2). https://doi.org/10.1128/msphere.00895-19

Sycz, G., Venanzio, G. Di, Distel, J. S., Sartorio, M. G., Le, N. H., Scott, N. E., Beatty, W. L., & Feldman, M. F. (2021). Modern *Acinetobacter baumannii* clinical isolates replicate inside spacious vacuoles and egress from macrophages. *PLoS Pathogens*, *17*(8), 1–19. https://doi.org/10.1371/journal.ppat.1009802

Tacconelli, E., Carrara, E., Savoldi, A., Harbarth, S., Mendelson, M., Monnet, D. L., Pulcini, C., Kahlmeter, G., Kluytmans, J., Carmeli, Y., Ouellette, M., Outterson, K., Patel, J., Cavaleri, M., Cox, E. M., Houchens, C. R., Grayson, M. L., Hansen, P., Singh, N., … Zorzet, A. (2018). Discovery, research, and development of new antibiotics: the WHO priority list of antibiotic-resistant bacteria and tuberculosis. *The Lancet Infectious Diseases*, *18*(3), 318–327. https://doi.org/10.1016/S1473-3099(17)30753-3

Tedin, K., & Bläsi, U. (1996). The RNA chain elongation rate of the λ late mRNA is unaffected by high levels of ppGpp in the absence of amino acid starvation. *Journal of Biological Chemistry*, *271*(30), 17675–17686. https://doi.org/10.1074/jbc.271.30.17675

Tomaras, A. P., Flagler, M. J., Dorsey, C. W., Gaddy, J. A., & Actis, L. A. (2008). Characterization of a two-component regulatory system from *Acinetobacter baumannii* that controls biofilm formation and cellular morphology. *Microbiology*, *154*(11), 3398–3409. https://doi.org/10.1099/mic.0.2008/019471-0

Tomás, M. D. M., Beceiro, A., Pérez, A., Velasco, D., Moure, R., Villanueva, R., Martínez-Beltrán, J., & Bou, G. (2005). Cloning and functional analysis of the gene encoding the 33- to 36-kilodalton outer membrane protein associated with carbapenem resistance in *Acinetobacter baumannii*. *Antimicrobial Agents and Chemotherapy*, *49*(12), 5172–5175. https://doi.org/10.1128/AAC.49.12.5172-5175.2005

Tomlinson, B. R., Denham, G. A., Torres, N. J., Brzozowski, R. S., Allen, J. L., Jackson, J. K., Eswara, P. J., & Shaw, L. N. (2022). Assessing the Role of Cold-Shock Protein C: a Novel Regulator of *Acinetobacter baumannii* Biofilm Formation and Virulence. *Infection and Immunity*, *90*(10), 1–21. https://doi.org/10.1128/iai.00376-22

Tooke, C. L., Hinchliffe, P., Bragginton, E. C., Colenso, C. K., Hirvonen, V. H. A., Takebayashi, Y., & Spencer, J. (2019). β-Lactamases and β-Lactamase Inhibitors in the 21st Century. *Journal of Molecular Biology*, *431*(18), 3472–3500. https://doi.org/10.1016/j.jmb.2019.04.002

Touchon, M., Cury, J., Yoon, E. J., Krizova, L., Cerqueira, G. C., Murphy, C., Feldgarden, M., Wortman, J., Clermont, D., Lambert, T., Grillot-Courvalin, C., Nemec, A., Courvalin, P., & Rocha, E. P. C. (2014). The genomic diversification of the whole *Acinetobacter* genus: Origins, mechanisms, and consequences. *Genome Biology and Evolution*, *6*(10), 2866–2882. https://doi.org/10.1093/gbe/evu225

Towner, K. J. (2009). *Acinetobacter*: an old friend, but a new enemy. *Journal of Hospital Infection*, *73*(4), 355–363. https://doi.org/10.1016/j.jhin.2009.03.032

Uppalapati, S. R., Sett, A., & Pathania, R. (2020). The Outer Membrane Proteins OmpA, CarO, and OprD of *Acinetobacter baumannii* Confer a Two-Pronged Defense in Facilitating Its Success as a Potent Human Pathogen. *Frontiers in Microbiology*, *11*(October), 1–12. https://doi.org/10.3389/fmicb.2020.589234

Urban, J. H., & Vogel, J. (2007). Translational control and target recognition by *Escherichia coli* small RNAs in vivo. *Nucleic Acids Research*, *35*(3), 1018–1037. https://doi.org/10.1093/nar/gkl1040

Vesel, N., & Blokesch, M. (2021). Pilus production in *Acinetobacter baumannii* is

growth phase dependent and essential for natural transformation. *Journal of Bacteriology*, *203*(8). https://doi.org/10.1128/JB.00034-21
Vogel, J., & Papenfort, K. (2006). Small non-coding RNAs and the bacterial outer membrane. *Current Opinion in Microbiology*, *9*(6), 605–611. https://doi.org/10.1016/j.mib.2006.10.006
Wagner, E. G. H., & Romby, P. (2015). Small RNAs in Bacteria and Archaea: Who They Are, What They Do, and How They Do It. In *Advances in Genetics* (Vol. 90). Elsevier Ltd. https://doi.org/10.1016/bs.adgen.2015.05.001
Wang, J. T., McDonald, L. C., Chang, S. C., & Ho, M. (2002). Community-acquired *Acinetobacter baumannii* bacteremia in adult patients in Taiwan. *Journal of Clinical Microbiology*, *40*(4), 1526–1529. https://doi.org/10.1128/JCM.40.4.1526-1529.2002
Wang, L., Liu, D., Lv, Y., Cui, L., Li, Y., Li, T., Song, H., Hao, Y., Shen, J., Yang Wang, B., & Timothy R. Walshb, C. (2020). Novel Plasmid-Mediated tet(X5) Gene Conferring Resistance to Tigecycline, Eravacycline, and Omadacycline in a Clinical Acinetobacter baumannii Isolate. *Antimicrobial Agents and Chemotherapy*, *64*(1), 1–5.
Waters, L. S., & Storz, G. (2009). Regulatory RNAs in Bacteria. *Cell*, *136*(4), 615–628. https://doi.org/10.1016/j.cell.2009.01.043
Waters, S. A., McAteer, S. P., Kudla, G., Pang, I., Deshpande, N. P., Amos, T. G., Leong, K. W., Wilkins, M. R., Strugnell, R., Gally, D. L., Tollervey, D., & Tree, J. J. (2017). Small RNA interactome of pathogenic *E. coli* revealed through crosslinking of RNase E. *The EMBO Journal*, *36*(3), 374–387. https://doi.org/10.15252/embj.201694639
Weiner, L. M., Webb, A. K., Limbago, B., Dudeck, M. A., Patel, J., Kallen, A. J., Edwards, J. R., & Sievert, D. M. (2016). Antimicrobial-Resistant Pathogens Associated With Healthcare-Associated Infections: Summary of Data Reported to the National Healthcare Safety Network at the Centers for Disease Control and Prevention, 2011-2014. *Infection Control and Hospital Epidemiology*, *37*(11), 1288–1301. https://doi.org/10.1016/j.physbeh.2017.03.040
Weiss, A., Broach, W. H., Lee, M. C., & Shaw, L. N. (2016). Towards the complete small RNome of *Acinetobacter baumannii*. *Microbial Genomics*, *2*(3), 1–18. https://doi.org/10.1099/mgen.0.000045
Wendt, C., Dietze, B., Dietz, E., & Rüden, H. (1997). Survival of *Acinetobacter baumannii* on dry surfaces. *Journal of Clinical Microbiology*, *35*(6), 1394–1397. https://doi.org/10.1128/jcm.35.6.1394-1397.1997
Westermann, A. J., Förstner, K. U., Amman, F., Barquist, L., Chao, Y., Schulte, L. N., Müller, L., Reinhardt, R., Stadler, P. F., & Vogel, J. (2016). Dual RNA-seq unveils noncoding RNA functions in host-pathogen interactions. *Nature*, *529*(7587), 496–501. https://doi.org/10.1038/nature16547
Wilharm, G., Piesker, J., Laue, M., & Skiebe, E. (2013). DNA Uptake by the nosocomial pathogen *Acinetobacter baumannii* occurs during movement along wet surfaces. *Journal of Bacteriology*, *195*(18), 4146–4153. https://doi.org/10.1128/JB.00754-13
Wilharm, G., Skiebe, E., Łopińska, A., Higgins, P. G., Weber, K., Neugebauer, C., Görlitz, K., Meimers, G., Rizova, Y., Blaschke, U., Heider, C., Cuny, C., Drewes, S., Heuser, E., Jeske, K., & Jacob, J. (2024). On the ecology of *Acinetobacter baumannii* – jet stream rider and opportunist by nature. *BioRxiv*.
Wisplinghoff, H., Paulus, T., Lugenheim, M., Stefanik, D., Higgins, P. G., Edmond, M. B., Wenzel, R. P., & Seifert, H. (2012). Nosocomial bloodstream infections due to

Acinetobacter baumannii, *Acinetobacter pittii* and *Acinetobacter nosocomialis* in the United States. *Journal of Infection*, *64*(3), 282–290. https://doi.org/10.1016/j.jinf.2011.12.008

Wong, D., Nielsen, T. B., Bonomo, R. A., Pantapalangkoor, P., Luna, B., & Spellberg, B. (2017). Clinical and pathophysiological overview of *Acinetobacter* infections: A century of challenges. *Clinical Microbiology Reviews*, *30*(1), 409–447. https://doi.org/10.1128/CMR.00058-16

Wright, P. R., Georg, J., Mann, M., Sorescu, D. A., Richter, A. S., Lott, S., Kleinkauf, R., Hess, W. R., & Backofen, R. (2014). CopraRNA and IntaRNA: Predicting small RNA targets, networks and interaction domains. *Nucleic Acids Research*, *42*(W1), 119–123. https://doi.org/10.1093/nar/gku359

Wright, P. R., Richter, A. S., Papenfort, K., Mann, M., Vogel, J., Hess, W. R., Backofen, R., & Georg, J. (2013). Comparative genomics boosts target prediction for bacterial small RNAs. *Proceedings of the National Academy of Sciences*, *110*(37), E3487 LP-E3496. https://doi.org/10.1073/pnas.1303248110

Wu, K., Lin, X., Lu, Y., Dong, R., Jiang, H., Svensson, S. L., Zheng, J., Shen, N., Camilli, A., & Chao, Y. (2024). RNA interactome of hypervirulent *Klebsiella pneumoniae* reveals a small RNA inhibitor of capsular mucoviscosity and virulence. *BioRxiv*. https://doi.org/10.1038/s41467-024-51213-z

Xu, C., Bilya, S. R., & Xu, W. (2019). AdeABC efflux gene in *Acinetobacter baumannii*. *New Microbes and New Infections*, *30*. https://doi.org/10.1016/j.nmni.2019.100549

Yuhan, Y., Ziyun, Y., Yongbo, Z., Fuqiang, L., & Qinghua, Z. (2016). Over expression of AdeABC and AcrAB-TolC efflux systems confers tigecycline resistance in clinical isolates of *Acinetobacter baumannii* and *Klebsiella pneumoniae*. *Revista Da Sociedade Brasileira de Medicina Tropical*, *49*(2), 165–171. https://doi.org/10.1590/0037-8682-0411-2015

Zahn, M., D'Agostino, T., Eren, E., Baslé, A., Ceccarelli, M., & Van Berg, B. Den. (2015). Small-molecule transport by CarO, an abundant eight-stranded β-barrel outer membrane protein from *Acinetobacter baumannii*. *Journal of Molecular Biology*, *427*(14), 2329–2339. https://doi.org/10.1016/j.jmb.2015.03.016

Zarrilli, R., Pournaras, S., Giannouli, M., & Tsakris, A. (2013). Global evolution of multidrug-resistant *Acinetobacter baumannii* clonal lineages. *International Journal of Antimicrobial Agents*, *41*(1), 11–19. https://doi.org/10.1016/j.ijantimicag.2012.09.008

Zeidler, S., Hubloher, J., Schabacker, K., Lamosa, P., Santos, H., & Müller, V. (2017). Trehalose, a temperature- and salt-induced solute with implications in pathobiology of *Acinetobacter baumannii*. *Environmental Microbiology*, *19*(12), 5088–5099. https://doi.org/10.1111/1462-2920.13987

Zhang, B., Liu, Z., Lin, Z., Zhang, X., & Fu, W. (2012). Microbiologic characteristics of pathogenic bacteria from hospitalized trauma patients who survived Wenchuan earthquake. *European Journal of Clinical Microbiology and Infectious Diseases*, *31*(10), 2529–2535. https://doi.org/10.1007/s10096-012-1591-0

Zhang, W., Yao, Y., Zhou, H., He, J., Wang, J., Li, L., Gao, M., Liu, X., Shi, Y., Lin, J., Liu, J., Chen, H., Feng, Y., Zhou, Z., Yu, Y., & Hua, X. (2022). Interactions between host epithelial cells and *Acinetobacter baumannii* promote the emergence of highly antibiotic resistant and highly mucoid strains. *Emerging Microbes and Infections*, *11*(1), 2556–2569. https://doi.org/10.1080/22221751.2022.2136534

Zhang, Y. F., Han, K., Chandler, C. E., Tjaden, B., Ernst, R. K., & Lory, S. (2017). Probing the sRNA regulatory landscape of *P. aeruginosa*: post-transcriptional

control of determinants of pathogenicity and antibiotic susceptibility. *Molecular Microbiology*, *106*(6), 919–937. https://doi.org/10.1111/mmi.13857

Zhang, Y., Werling, U., & Edelmann, W. (2012). SLiCE: A novel bacterial cell extract-based DNA cloning method. *Nucleic Acids Research*, *40*(8), 1–10. https://doi.org/10.1093/nar/gkr1288

Zhang, Y., Werling, U., & Edelmann, W. (2014). Seamless Ligation Cloning Extract (SLiCE) Cloning Method. *Methods in Molecular Biology*, *1116*(January), 1–24. https://doi.org/10.1007/978-1-62703-764-8

Zhong, X., Wu, X., Schweppe, D. K., Chavez, J. D., Mathay, M., Eng, J. K., Keller, A., & Bruce, J. E. (2020). In Vivo Cross-Linking MS Reveals Conservation in OmpA Linkage to Different Classes of β-Lactamase Enzymes. *Journal of the American Society for Mass Spectrometry*, *31*(2), 190–195. https://doi.org/10.1021/jasms.9b00021

Chapter 8 – Appendices

Appendix I – Oligonucleotides used in the study

Name	Sequence (5′-3′)	Purpose
Aar_P1	AACTGCAATAATGCTGAGG	Deletion of Aar in *A. baumannii*
Aar_P2	GGCCCAATTCGCCCTATAGTGAGTCGTGTTCATTAAGCTTCACG	Deletion of Aar in *A. baumannii*
Aar_P3	GGGTTTGCTCGGGTCGGTGGCATATGTGTCTATAATAATGTTGGC	Deletion of Aar in *A. baumannii*
Aar_P4	ATTTCTGGTGGTCAAGG	Deletion of Aar in *A. baumannii*
Aar_P5	CGACTCACTATAGGGCGAATTGGGCC GCTTTCCAGTCGGGAAACCTG	Deletion of Aar in *A. baumannii*
Aar_P6	CATATGCCACCGACCCGAGCAAACCC CGCCAGGGTTTTCCCAGTCACGAC	Deletion of Aar in *A. baumannii*
Aar_P7	CGTGAAGCTTAATGAACATGTCTATAATAATGTTGGC	Deletion of Aar in *A. baumannii*
Aar_P8	TGTTCATTAAGCTTCACG	Deletion of Aar in *A. baumannii*
Aar_del_test_F	TGAGTGATAGTGTAACGCG	Testing deletion of Aar in *A. baumannii*
Aar_del_test_R	CGAAGTTAAAGATGGTTTAGGC	Testing deletion of Aar in *A. baumannii*
Arp_P1	CTTGTTGTTGCATGATTTCACC	Deletion of Arp in A. baumannii
Arp_P2	GGCCCAATTCGCCCTATAGTGAGTCG TTAACCTCTAATAACTTAAATGC	Deletion of Arp in A. baumannii
Arp_P3	GGGTTTGCTCGGGTCGGTGGCATATG ACTTATTAAATGGCTTTGTTGC	Deletion of Arp in A. baumannii
Arp_P4	GTCAATGACAAAGAAGTATGC	Deletion of Arp in A. baumannii
Arp_P7	TTAACCTCTAATAACTTAAATGC	Deletion of Arp in A. baumannii
Arp_P8	GCATTTAAGTTATTAGAGGTTAA ACTTATTAAATGGCTTTGTTGC	Deletion of Arp in A. baumannii
Aar*_overlap_up_R	GGCTTAACCACAAATGTCGTGAGG	Generating Aar seed region mutation (Aar*)
Aar*_overlap_down_F	CACGACATTTGTGGTTAAGCCG	Generating Aar seed region mutation (Aar*)
pMHL2_FLAG_F	GCGAATTCACTAGTGATTCGACTACAAAGACCATGACGG	Construct pMHL2-3×FLAG
pMHL2_FLAG_R	GTTTCCCGACTGGAAAGCACTTCGAAGCAGCTCCAGC	Construct pMHL2-3×FLAG
pMHL2_bb_F	GCTTTCCAGTCGGGAAACCTG	Amplification of pMHL2 backbone
pMHL2_bb_R	GAATCACTAGTGAATTCGCG	Amplification of pMHL2 backbone
CarO_FLAG_up_F	ACGAATAAATACAGTCGG	Construction of *carO:: 3×FLAG*
CarO_FLAG_up_R	CCGTCATGGTCTTTGTAGTCCCAGAAGAAGTTCACACC	Construction of *carO:: 3×FLAG*
CarO_FLAG_down_F	GGGTTTGCTCGGGTCGGTGGCATATGTAAAGCATAAAAACGAGCTTCGG	Construction of *carO:: 3×FLAG*
CarO_FLAG_down_R	TACTTCGTATTATTGCGGG	Construction of *carO:: 3×FLAG*
FLAG_apra_sacB_F	GACTACAAAGACCATGACGG	Amplify *3×FLAG-sacB-aacC4*
T4_SalI_F_2	CGGAGGTCGACATGCAAGAACTTTTTAAC	Amplification of *t4rnlI* gene
T4_HindIII_R_2	CGGAGAAGCTTTTAGTATCCTTCTGGG	Amplification of *t4rnlI* gene
pVRL2Z_sfGFP_Aar_F	CAATTGTCTGATTCGTTACCAAAAGTTAAAGATGGTTTAGGC	Cloning Aar promoter into pVRL2Z-sfGFP
pVRL2Z_sfGFP_Aar_R	GGTTAGCCCAAAAAAACGGGTTCAAGTTATATTAGTGATGC	Cloning Aar promoter into pVRL2Z-sfGFP
pVRL2Z_sfGFP_BB_F	ATGAAAGTATTACGTGTTTTAGTGA	Amplification of the pVRL2Z-sfGFP backbone
pVRL2Z_sfGFP_BB_R	ATGAAAGTATTACGTGTTTTAGTGA	Amplification of the pVRL2Z-sfGFP backbone
Aar_pP$_L$_F	GTGAGCGGATAACAAGATACTGAGCACGTAGGTTGATATGAACC	Cloning Aar into pP$_L$
Aar_pP$_L$_R	GCCTTTCGTTTTATTTGATGCCTCTAGAAGTTATCAAACAAAGGCGC	Cloning Aar into pP$_L$
Arp_pPL_F	GTGAGCGGATAACAAGATACTGAGCAC ATCAAAAAGGATATATAATTCC	Cloning Arp into pPL
Arp_pPL_R	GCCTTTCGTTTTATTTGATGCCTCTAGA TTTGAGTAGATATGAGAAGTC	Cloning Arp into pPL
BB_pP$_L$_F	GTGCTCAGTATCTTGTTATCCGCTCAC	Amplification of pP$_L$ backbone
BB_pP$_L$_R	TCTAGAGGCATCAAATAAAACGAAAGGC	Amplification of pP$_L$ backbone
Aar*_overlap_up_F	GACGAAGTTAAAGATGGTTTAGGC	Generating Aar seed region mutation (Aar*)
CarO_pXG10_F	ACTGAGCACATGCATATGCTCTTGAATATAATTTTTGTC	Cloning CarO into pXG10sf
CarO_pXG10_R	AGCGGATCCGCTAGCAAGTAAAGCTGTAGTTGTCAC	Cloning CarO into pXG10sf
BfnH_pXG10_F	ACTGAGCACATGCATGCCTCTTGAAAAATCGTTGAG	Cloning BfnH into pXG10sf
BfnH_pXG10_R	AGCGGATCCGCTAGCGTGATTACGTGATTTAACCCC	Cloning BfnH into pXG10sf
ABUW_RS07310_pXG10_F	ACTGAGCACATGCATTTTCTTAATTAAAAATTAACATG	Cloning ABUW_RS07310 into pXG10sf
ABUW_RS07310_pXG10_R	AGCGGATCCGCTAGCTAAATGATGATCATCCACG	Cloning ABUW_RS07310 into pXG10sf
PilA_pXG10_F	ACTGAGCACATGCAT AGCTGAAAAAGCTTATATAAAAAC	Cloning PilA into pXG10sf
PilA_pXG10_R	AGCGGATCCGCTAGC GGCAACTACGATCATGAGTTCG	Cloning PilA into pXG10sf
BB_pXG10sf_F	GCTAGCGGATCCGCTGGCTCCGCTGC	Amplification of pXG10sf backbone
BB_pXG10_R	ATGCATGTGCTCAGTATCTCTATCAC	Amplification of pXG10sf backbone
CarO*_overlap_up_F	AAACGTGTTACGTTTAATTGAGG	Generating carO Aar binding site mutation (carO*)
CarO*_overlap_up_R	ATCGTTTTGTGGTTAAGAAAAGGCTCTG	Generating carO Aar binding site mutation (carO*)
CarO*_overlap_down_F	CTTAACCACAAAACGATGAAAGTATTACG	Generating carO Aar binding site mutation (carO*)
CarO*_overlap_down_R	CTGGAATTAATTGGTTTTTATCG	Generating carO Aar binding site mutation (carO*)
pWH1266_CarO_GFP F	AATATTGAAAAAGGAAGAGTATGCTCTTGAATATAATTTTTGTC	Cloning CarO-sfGFP into pWH1266
pWH1266_BfnH_GFP F	AATATTGAAAAAGGAAGAGTGCCTCTTGAAAAATCGTTGAG	Cloning BfnH-sfGFP into pWH1266
pWH1266_PilA_GFP F	AATATTGAAAAAGGAAGAGT AGCTGAAAAAGCTTATATAAAAAC	Cloning PilA-sfGFP into pWH1266
pWH1266_GFP_R	GAGTAAACTTGGTCTGACAGTTATTTGTAGAGCTCATCCATGC	Cloning target-sfGFP into pWH1266
pWH1266 B-lactam promoter bb F	ACTCTTCCTTTTTCAATATTATTGAAGC	Amplification of pWH1266 backbone
pWH1266 B-lactam promoter bb F	CTGTCAGACCAAGTTTACTC	Amplification of pWH1266 backbone
cAar_F	CCCTGATAAATGCTTCAATAGAAGTTAAAGATGGTTTAGGC	Cloning Aar locus into pWH1266
cAar_R	CCAATGCTTAATCAGTGAGGAGTTATCAAACAAAGGCGC	Cloning Aar locus into pWH1266
cAar_BB_F	TATTGAAGCATTTATCAGGG	Amplification of pWH1266 backbone
cAar_BB_R	CCTCACTGATTAAGCATTGG	Amplification of pWH1266 backbone
carO::3×FLAG_F	GCAACTCTCTACTGTTTCTCCATATGCTCTTGAATATAATTTTTGTC	Cloning carO::3×FLAG_F into pVRL2Z
carO::3×FLAG_R	CCGTCGACCTCGAGATTCTTCGAAGCAGCTCCAGC	Cloning carO::3×FLAG_F into pVRL2Z
pVRL2Z_BB_F	ATGGAGAAACAGTAGAGAGTTGC	Amplification of pVRL2Z backbone
pVRL2Z_BB_R	GAATCTCGAGGTCGACGG	Amplification of pVRL2Z backbone
pVRL2Z_carO:: 3×FLAG_Aar_F	TCCGCCGGGAGCGGATTTGAGTCAGGTGGCACTTTTCG	Cloning Aar into pVRL2Z_*carO:: 3×FLAG*
pVRL2Z_carO:: 3×FLAG_Aar_R	GGAAACGCAAAAAGGCCATCAACATTATTATAGACAAAAAAATACG	Cloning Aar into pVRL2Z_*carO:: 3×FLAG*
pVRL2Z_carO:: 3×FLAG_BB_F	TCAAATCCGCTCCCGGC	Amplification of pVRL2Z_*carO:: 3×FLAG* backbone
pVRL2Z_carO:: 3×FLAG_BB_R	ATGGCCTTTTTGCGTTTCC	Amplification of pVRL2Z_*carO:: 3×FLAG* backbone
Aar_rp_F	GTAGGTTGATATGAACCTCACG	Generating Aar riboprobe
Aar_rp_R	GAATTAATACGACTCACTATAAAAAAAAATACGCAATGATTGGG	Generating Aar riboprobe
Aar_in_vitro_F	GTTTTTTTTAATACGACTCACTATAGGGTAGGTTGATATGAACC	*In vitro* transcription of Aar
Aar_in_vitro_R	AAATACGCAATGATTGGG	*In vitro* transcription of Aar
CarO_in_vitro_F	GTTTTTTTTAATACGACTCACTATAGGATGCTCTTGAATATAATTTTTGTC	*In vitro* transcription of carO
CarO_in_vitro_R	CAGCAGCAAGTAAAGCTG	*In vitro* transcription of carO
BfnH_in_vitro_F	GTTTTTTTTAATACGACTCACTATAGGGCCTCTTGAAAAATCGTTGAG	*In vitro* transcription of bfnH
BfnH_in_vitro_R	GTGATTACGTGATTTAACCCC	*In vitro* transcription of bfnH
ABUW_RS07310_in_vitro_F	GTTTTTTTTAATACGACTCACTATAGGTTAGACTGAAAACTCACG	*In vitro* transcription of ABUW_RS07310
ABUW_RS07310_in_vitro_R	TCCCTGAAAGCAGCATGG	*In vitro* transcription of ABUW_RS07310
ABUW_RS04325_in_vitro_F	GTTTTTTTTAATACGACTCACTATAGGCTTGATACAAAAAATGTGGCC	*In vitro* transcription of ABUW_RS04325
ABUW_RS04325_in_vitro_R	AATACTAATACCACCTGCCC	*In vitro* transcription of ABUW_RS04325

Appendix II – Filtered Hi-GRIL-seq chimeric reads

Chromosomal interactions							
sRNA	**Interaction partner**	**Product**	**Total Chimeric Reads**	**NI Chimeric Reads**	**IND Chimeric Reads**	**DIP Chimeric Reads**	**IMIP Chimeric Reads**
sRNA99	sRNA102	sRNA102	4457	88	1336	1154	1879
sRNA99	sRNA21	sRNA21	461	22	94	150	195
sRNA99	ABUW_RS06260	hypothetical protein	936	20	234	253	429
sRNA99	ABUW_RS12995	hypothetical protein	251	9	67	61	114
sRNA99	sRNA38	sRNA38	164	9	45	54	56
sRNA99	ABUW_RS10585	acetyltransferase	82	6	0	75	1
sRNA99	ABUW_RS05800	acinetobactin biosynthesis isochorismate synthase BasJ	40	4	1	35	0
sRNA99	ABUW_RS14740	bacteriohemerythrin	81	3	27	18	33
sRNA99	ABUW_RS14880	protoporphyrinogen oxidase HemJ	27	1	11	10	5
sRNA99	ABUW_RS07835	type II toxin-antitoxin system RelB/DinJ family antitoxin	12	1	9	1	1
sRNA99	ABUW_RS18655	low molecular weight phosphotyrosine protein phosphatase	12	1	4	1	6
sRNA99	ABUW_RS09005	acyl-CoA dehydrogenase	10	1	3	1	5
sRNA99	sRNA86	sRNA86	12	1	2	4	5
sRNA99	ABUW_RS19810	hypothetical protein	11	1	1	6	3
sRNA99	ABUW_RS10640	siderophore biosynthesis protein	15	1	0	14	0
sRNA99	ABUW_RS01510	regulatory or redox protein complexing with Bfr in iron storage and mobility (BFD)	14	1	0	10	3
sRNA99	ABUW_RS10635	lysine/ornithine N-monooxygenase	11	1	0	10	0
sRNA99	ABUW_RS06690	peroxide stress protein YaaA	25	0	1	7	17
sRNA94	ABUW_RS19895	hypothetical protein	46	2	16	15	13
sRNA94	ABUW_RS10005	hypothetical protein	37	2	14	14	7
sRNA94	ABUW_RS12975	hypothetical protein	40	1	18	15	6
sRNA94	sRNA92	sRNA92	32	1	17	9	5
sRNA94	sRNA15	sRNA15	25	1	11	7	6
sRNA94	ABUW_RS08695	hypothetical protein	23	1	10	7	5
sRNA94	sRNA21	sRNA21	16	1	6	6	3
sRNA94	rna-ABUW_RS04565	tRNA-Ser	14	1	2	9	2
sRNA94	6S RNA	6S RNA	89	0	40	27	22
sRNA94	ABUW_RS19855	hypothetical protein	41	0	12	19	10
sRNA94	sRNA101	sRNA101	24	0	10	8	6
sRNA94	rna-ABUW_RS13710	tRNA-Ser	21	0	5	13	3
sRNA94	rna-ABUW_RS15625	tRNA-His	18	0	4	11	3
sRNA93	ABUW_RS12975	hypothetical protein	20	1	10	7	2
sRNA93	ABUW_RS00325	4-hydroxyphenylpyruvate dioxygenase	13	1	8	4	0
sRNA93	sRNA89	sRNA89	13	1	8	2	2
sRNA93	ABUW_RS12330	phenylacetic acid degradation bifunctional protein PaaZ	10	1	7	2	0
sRNA93	ABUW_RS00690	DUF2147 domain-containing protein	10	1	2	3	4
sRNA93	rna-ABUW_RS01360	tRNA-Ala	44	0	19	19	6
sRNA93	6S RNA	6S RNA	44	0	19	13	12
sRNA93	ABUW_RS12325	1%2C2-phenylacetyl-CoA epoxidase subunit A	11	0	9	1	1
sRNA93	ABUW_RS10005	hypothetical protein	16	0	6	7	3
sRNA93	ABUW_RS04845	RNA polymerase sigma factor	10	0	6	1	3
sRNA93	sRNA76	sRNA76	13	0	6	0	7
sRNA93	rna-ABUW_RS15625	tRNA-His	13	0	5	7	1
sRNA93	ABUW_RS12990	hypothetical protein	10	0	5	1	4
sRNA93	rna-ABUW_RS04565	tRNA-Ser	20	0	4	13	3
sRNA93	rna-ABUW_RS17530	tRNA-Tyr	11	0	4	4	3
sRNA93	rna-ABUW_RS13710	tRNA-Ser	16	0	3	11	2
sRNA92	sRNA84	sRNA84	102	4	45	30	23
sRNA92	ABUW_RS12975	hypothetical protein	60	2	24	22	12
sRNA92	ABUW_RS10005	hypothetical protein	38	2	21	10	5
sRNA92	sRNA26	sRNA26	39	2	20	5	12
sRNA92	sRNA94	sRNA94	20	2	7	6	5
sRNA92	ABUW_RS19895	hypothetical protein	89	1	42	17	29
sRNA92	sRNA76	sRNA76	22	1	8	5	8
sRNA92	ABUW_RS07500	hypothetical protein	12	1	7	4	0
sRNA92	sRNA21	sRNA21	11	1	5	2	3
sRNA92	ABUW_RS11840	stress-induced protein	14	1	4	2	7
sRNA92	sRNA62	sRNA62	61	0	29	13	19
sRNA92	sRNA24	sRNA24	33	0	21	7	5
sRNA92	sRNA101	sRNA101	28	0	9	7	12
sRNA92	ABUW_RS08695	hypothetical protein	14	0	8	3	3
sRNA92	rna-ABUW_RS15625	tRNA-His	11	0	7	2	2
sRNA92	rna-ABUW_RS00085	tRNA-Ala	12	0	6	3	3
sRNA90	ABUW_RS18870	hypothetical protein	8705	204	3188	2675	2638
sRNA90	ABUW_RS13220	hypothetical protein	969	30	292	443	204
sRNA90	ABUW_RS15920	hypothetical protein	360	8	120	149	83
sRNA90	ABUW_RS13040	hypothetical protein	80	7	22	26	25
sRNA90	ABUW_RS00325	4-hydroxyphenylpyruvate dioxygenase	43	4	15	19	5
sRNA90	ABUW_RS11885	hypothetical protein	23	2	6	12	3
sRNA90	ABUW_RS12300	enoyl-CoA hydratase	35	1	19	11	4
sRNA90	ABUW_RS10425	hypothetical protein	27	1	13	8	5
sRNA90	ABUW_RS04130	multidrug efflux RND transporter permease subunit AdeJ	19	1	9	8	1
sRNA90	ABUW_RS17120	30S ribosomal protein S15	11	1	6	2	2
sRNA90	ABUW_RS20405	hypothetical protein	31	1	5	17	8
sRNA90	ABUW_RS16815	DUF1311 domain-containing protein	18	1	4	7	6
sRNA90	ABUW_RS08245	hypothetical protein	10	1	4	2	3
sRNA90	ABUW_RS10185	CoA transferase subunit B	10	1	2	4	3
sRNA90	ABUW_RS02710	hypothetical protein	13	1	1	6	5
sRNA90	ABUW_RS06610	hemin uptake protein HemP	20	1	0	19	0
sRNA90	ABUW_RS00045	hypothetical protein	81	0	30	35	16
sRNA90	ABUW_RS12290	3-hydroxyacyl-CoA dehydrogenase	10	0	10	0	0
sRNA90	ABUW_RS11925	TetR/AcrR family transcriptional regulator	16	0	8	8	0
sRNA90	ABUW_RS10010	hypothetical protein	13	0	7	3	3
sRNA90	ABUW_RS04410	ATP-dependent metallopeptidase FtsH/Yme1/Tma family protein	10	0	4	5	1
sRNA90	ABUW_RS00260	DUF1328 domain-containing protein	13	0	4	2	7
sRNA90	ABUW_RS15335	hypothetical protein	11	0	3	6	2
sRNA90	ABUW_RS17690	ferrous iron transport protein A	34	0	0	31	3
sRNA90	ABUW_RS05800	acinetobactin biosynthesis isochorismate synthase BasJ	29	0	0	29	0
sRNA90	ABUW_RS10585	acetyltransferase	18	0	0	18	0
sRNA9	ABUW_RS12975	hypothetical protein	30	3	15	6	6
sRNA9	rna-ABUW_RS19905	6S RNA	71	2	42	18	9
sRNA9	ABUW_RS00325	4-hydroxyphenylpyruvate dioxygenase	13	1	8	4	0
sRNA9	rna-ABUW_RS13710	tRNA-Ser	13	1	7	4	1
sRNA9	rna-ABUW_RS04565	tRNA-Ser	16	0	10	4	2
sRNA9	ABUW_RS17440	membrane protein	11	0	10	1	0
sRNA9	rna-ABUW_RS19930	transfer-messenger RNA	13	0	9	1	3
sRNA9	ABUW_RS14685	VOC family protein	11	0	3	2	6

sRNA9	ABUW_RS12615	TetR/AcrR family transcriptional regulator	29	2	4	10	13
sRNA88	rna-ABUW_RS19780	signal recognition particle sRNA small type	14	1	5	4	4
sRNA88	ABUW_RS12975	hypothetical protein	11	0	8	2	1
sRNA88	6S RNA	6S RNA	13	0	6	4	3
sRNA88	sRNA1	sRNA1	12	0	3	5	4
sRNA87	rna-ABUW_RS17525	tRNA-Gly	38	3	20	9	6
sRNA87	rna-ABUW_RS15620	tRNA-Pro	21	2	12	3	4
sRNA87	ABUW_RS14610	hypothetical protein	22	2	12	0	8
sRNA87	rna-ABUW_RS15625	tRNA-His	25	2	9	3	11
sRNA87	ABUW_RS08695	hypothetical protein	13	1	8	2	2
sRNA87	rna-ABUW_RS02515	5S ribosomal RNA	12	1	7	1	3
sRNA87	sRNA76	sRNA76	12	1	6	2	3
sRNA87	rna-ABUW_RS02185	tRNA-Ser	13	1	5	4	3
sRNA87	ABUW_RS00325	4-hydroxyphenylpyruvate dioxygenase	12	1	4	2	5
sRNA87	ABUW_RS05445	alpha-keto acid decarboxylase family protein	11	1	4	1	5
sRNA87	rna-ABUW_RS18075	tRNA-Ile	10	1	3	5	1
sRNA87	ABUW_RS03380	entericidin A/B family lipoprotein	10	1	2	2	5
sRNA87	rna-ABUW_RS14950	tRNA-Met	29	0	15	8	6
sRNA87	rna-ABUW_RS14905	tRNA-Met	14	0	9	3	2
sRNA87	rna-ABUW_RS02640	tRNA-Leu	13	0	8	2	3
sRNA87	ABUW_RS13040	hypothetical protein	12	0	4	2	6
sRNA87	rna-ABUW_RS15820	16S ribosomal RNA	10	0	3	3	4
sRNA87	ABUW_RS06610	hemin uptake protein HemP	10	0	0	10	0
sRNA86	ABUW_RS11875	hypothetical protein	57	3	30	11	13
sRNA86	ABUW_RS00260	DUF1328 domain-containing protein	28	1	15	9	3
sRNA86	rna-ABUW_RS17255	tRNA-Leu	28	1	10	6	11
sRNA86	ABUW_RS17440	membrane protein	42	0	19	8	15
sRNA86	rna-ABUW_RS15625	tRNA-His	17	0	7	5	5
sRNA86	ABUW_RS08700	hypothetical protein	11	0	7	3	1
sRNA86	ABUW_RS10585	acetyltransferase	14	0	0	14	0
sRNA85	ABUW_RS11875	hypothetical protein	196	3	51	56	86
sRNA85	ABUW_RS11870	hypothetical protein	60	2	16	21	21
sRNA85	sRNA70	sRNA70	37	1	20	11	5
sRNA85	ABUW_RS11840	stress-induced protein	19	1	7	5	6
sRNA85	ABUW_RS07145	DUF2171 domain-containing protein	14	1	7	2	4
sRNA85	ABUW_RS00260	DUF1328 domain-containing protein	16	1	6	5	4
sRNA85	ABUW_RS12285	3-oxoadipyl-CoA thiolase	11	1	4	3	3
sRNA85	ABUW_RS06720	cold-shock protein	44	0	22	13	9
sRNA85	ABUW_RS12290	3-hydroxyacyl-CoA dehydrogenase	24	0	19	2	3
sRNA85	ABUW_RS10005	hypothetical protein	35	0	12	17	6
sRNA85	ABUW_RS16350	enoyl-ACP reductase	26	0	12	13	1
sRNA85	ABUW_RS00325	4-hydroxyphenylpyruvate dioxygenase	27	0	9	16	2
sRNA85	ABUW_RS19720	Ig-like domain-containing protein	24	0	8	8	8
sRNA85	ABUW_RS00010	DNA polymerase III subunit beta	10	0	8	1	1
sRNA85	ABUW_RS15330	hypothetical protein	14	0	7	4	3
sRNA85	ABUW_RS07590	phosphoenolpyruvate synthase	17	0	6	9	2
sRNA85	ABUW_RS20195	hypothetical protein	12	0	6	5	1
sRNA85	ABUW_RS09040	amidase	10	0	5	5	0
sRNA85	ABUW_RS01615	hemerythrin	11	0	5	4	2
sRNA85	ABUW_RS12725	hypothetical protein	12	0	5	1	6
sRNA85	ABUW_RS03195	OmpA family protein	14	0	4	3	7
sRNA85	ABUW_RS13805	LysM peptidoglycan-binding domain-containing protein	11	0	2	5	4
sRNA85	ABUW_RS10585	acetyltransferase	56	0	0	56	0
sRNA81	6S RNA	6S RNA	130	2	73	33	22
sRNA81	ABUW_RS20195	hypothetical protein	24	2	10	7	5
sRNA81	rna-ABUW_RS13710	tRNA-Ser	29	1	12	9	7
sRNA81	rna-ABUW_RS04565	tRNA-Ser	30	1	8	16	5
sRNA81	ABUW_RS05820	DUF3015 domain-containing protein	10	1	8	0	1
sRNA81	sRNA87	sRNA87	14	1	7	5	1
sRNA81	rna-ABUW_RS17530	tRNA-Tyr	12	1	4	5	2
sRNA81	ABUW_RS10005	hypothetical protein	52	0	13	26	13
sRNA81	sRNA46	sRNA46	13	0	7	3	3
sRNA81	sRNA76	sRNA76	16	0	6	7	3
sRNA81	ABUW_RS12975	hypothetical protein	20	0	6	5	9
sRNA81	rna-ABUW_RS02185	tRNA-Ser	15	0	5	8	2
sRNA81	rna-ABUW_RS14950	tRNA-Met	11	0	3	5	3
sRNA81	ABUW_RS08695	hypothetical protein	10	0	3	5	2
sRNA77	ABUW_RS00325	4-hydroxyphenylpyruvate dioxygenase	11	1	8	2	0
sRNA77	ABUW_RS09995	hypothetical protein	13	1	2	7	3
sRNA77	ABUW_RS07145	DUF2171 domain-containing protein	10	0	6	2	2
sRNA76	ABUW_RS11470	dicarboxylate/amino acid:cation symporter	1633	46	686	474	427
sRNA76	ABUW_RS00325	4-hydroxyphenylpyruvate dioxygenase	427	35	190	132	70
sRNA76	ABUW_RS13220	hypothetical protein	779	19	285	161	314
sRNA76	ABUW_RS02300	DUF2789 domain-containing protein	333	11	127	119	76
sRNA76	ABUW_RS04480	phosphoenolpyruvate carboxykinase (GTP)	209	10	74	43	82
sRNA76	ABUW_RS12305	phenylacetate-CoA oxygenase/reductase subunit PaaK	126	9	54	21	42
sRNA76	rna-ABUW_RS17530	tRNA-Tyr	112	9	52	24	27
sRNA76	sRNA99	sRNAA99	156	9	39	49	59
sRNA76	rna-ABUW_RS01045	tRNA-Thr	98	8	38	30	22
sRNA76	ABUW_RS00790	TonB-dependent siderophore receptor	110	8	22	65	15
sRNA76	ABUW_RS07925	iron-containing alcohol dehydrogenase	111	7	39	29	36
sRNA76	rna-ABUW_RS04565	tRNA-Ser	70	7	30	15	18
sRNA76	ABUW_RS14610	hypothetical protein	1925	6	552	597	770
sRNA76	sRNA21	sRNA21	290	6	133	56	95
sRNA76	ABUW_RS16240	hypothetical protein	100	6	49	15	30
sRNA76	ABUW_RS00020	DNA topoisomerase (ATP-hydrolyzing) subunit B	140	6	42	49	43
sRNA76	rna-ABUW_RS13710	tRNA-Ser	79	6	35	21	17
sRNA76	rna-ABUW_RS18330	tRNA-Gly	68	6	23	25	14
sRNA76	rna-ABUW_RS17535	tRNA-Thr	94	5	38	29	22
sRNA76	rna-ABUW_RS17525	tRNA-Gly	77	5	33	19	20
sRNA76	ABUW_RS12335	L-serine ammonia-lyase	74	5	27	20	22
sRNA76	ABUW_RS11475	type II asparaginase	211	4	96	64	47
sRNA76	ABUW_RS05865	anthranilate phosphoribosyltransferase	250	4	91	58	97
sRNA76	ABUW_RS06560	U32 family peptidase	115	4	45	27	39
sRNA76	ABUW_RS12310	phenylacetate-CoA oxygenase subunit PaaJ	52	4	30	8	10
sRNA76	ABUW_RS00335	VOC family protein	54	4	26	17	7
sRNA76	ABUW_RS15615	adenosine deaminase	79	4	19	22	34
sRNA76	ABUW_RS14255	glutaminase	42	4	11	10	17
sRNA76	ABUW_RS10520	TonB-dependent siderophore receptor	106	4	4	97	1
sRNA76	ABUW_RS08695	hypothetical protein	88	3	34	29	22

sRNA76	ABUW_RS00170	efflux RND transporter permease subunit	51	3	26	10	12
sRNA76	rna-ABUW_RS15620	tRNA-Pro	46	3	24	9	10
sRNA76	ABUW_RS16320	leucine--tRNA ligase	47	3	21	11	12
sRNA76	ABUW_RS07835	type II toxin-antitoxin system RelB/DinJ family antitoxin	38	3	20	6	9
sRNA76	ABUW_RS04920	Bcr/CflA family efflux MFS transporter	67	3	19	20	25
sRNA76	ABUW_RS13040	hypothetical protein	30	3	19	2	6
sRNA76	ABUW_RS06670	hypothetical protein	48	3	15	16	14
sRNA76	ABUW_RS00470	bifunctional 3%2C4-dihydroxy-2-butanone-4-phosphate synthase/GTP cyclohydrolase II	45	3	15	16	11
sRNA76	ABUW_RS05230	hypothetical protein	30	3	14	7	6
sRNA76	ABUW_RS08085	hypothetical protein	36	3	10	18	5
sRNA76	ABUW_RS05220	hypothetical protein	54	2	24	18	10
sRNA76	ABUW_RS08975	hypothetical protein	60	2	19	14	25
sRNA76	ABUW_RS07970	fimbrial biogenesis outer membrane usher protein	29	2	18	2	7
sRNA76	ABUW_RS13780	NADH:flavin oxidoreductase/NADH oxidase family protein	46	2	17	11	16
sRNA76	ABUW_RS12290	3-hydroxyacyl-CoA dehydrogenase	24	2	17	2	3
sRNA76	ABUW_RS16955	multidrug efflux MATE transporter AbeM	45	2	16	9	18
sRNA76	ABUW_RS03230	large conductance mechanosensitive channel protein MscL	31	2	15	8	6
sRNA76	rna-ABUW_RS02185	tRNA-Ser	40	2	14	12	12
sRNA76	ABUW_RS17420	hypothetical protein	28	2	13	8	5
sRNA76	ABUW_RS06070	septal ring lytic transglycosylase RlpA family protein	20	2	13	2	3
sRNA76	ABUW_RS02710	hypothetical protein	24	2	11	7	4
sRNA76	rna-ABUW_RS01235	tRNA-Phe	20	2	10	6	2
sRNA76	ABUW_RS01265	RNA-binding transcriptional accessory protein	22	2	10	3	7
sRNA76	rna-ABUW_RS12865	tRNA-Gly	45	2	9	14	20
sRNA76	ABUW_RS18435	amino acid permease	26	2	9	8	7
sRNA76	rna-ABUW_RS18325	tRNA-Gly	42	2	8	16	16
sRNA76	ABUW_RS06690	peroxide stress protein YaaA	30	2	8	9	11
sRNA76	ABUW_RS17715	D-alanyl-D-alanine endopeptidase PBP7/8	27	2	7	9	9
sRNA76	ABUW_RS10790	hypothetical protein	29	2	7	8	12
sRNA76	ABUW_RS14860	30S ribosomal protein S7	20	2	7	3	8
sRNA76	ABUW_RS17290	DMT family transporter	21	2	6	6	7
sRNA76	ABUW_RS18255	OsmC family peroxiredoxin	92	1	36	31	24
sRNA76	ABUW_RS01775	EamA family transporter	98	1	32	28	37
sRNA76	ABUW_RS00895	hypothetical protein	43	1	24	10	8
sRNA76	ABUW_RS01245	GNAT family acetyltransferase	55	1	22	13	19
sRNA76	ABUW_RS08375	sulfurtransferase complex subunit TusD	34	1	19	5	9
sRNA76	ABUW_RS11065	TetR/AcrR family transcriptional regulator	44	1	18	7	18
sRNA76	rna-ABUW_RS15625	tRNA-His	76	1	17	25	33
sRNA76	ABUW_RS03005	acyl-CoA desaturase	49	1	15	16	17
sRNA76	ABUW_RS15215	signal recognition particle protein	74	1	14	23	36
sRNA76	ABUW_RS04845	RNA polymerase sigma factor	35	1	14	7	13
sRNA76	ABUW_RS18195	F0F1 ATP synthase subunit A	22	1	14	3	4
sRNA76	ABUW_RS12320	1%2C2-phenylacetyl-CoA epoxidase subunit B	18	1	14	0	3
sRNA76	ABUW_RS08405	D-amino acid dehydrogenase	15	1	11	1	2
sRNA76	ABUW_RS16420	type IV pilus biogenesis/stability protein PilW	13	1	11	0	1
sRNA76	ABUW_RS01260	two-component system response regulator OmpR	34	1	10	9	14
sRNA76	ABUW_RS15905	exopolyphosphatase	26	1	10	9	6
sRNA76	ABUW_RS15550	amidohydrolase	17	1	10	3	3
sRNA76	ABUW_RS10485	YARHG domain-containing protein	15	1	10	3	1
sRNA76	ABUW_RS04965	7-cyano-7-deazaguanine synthase QueC	17	1	9	5	2
sRNA76	ABUW_RS10890	DUF1049 domain-containing protein	20	1	9	4	6
sRNA76	ABUW_RS15910	thioredoxin	17	1	9	1	6
sRNA76	ABUW_RS11165	transketolase	18	1	8	3	6
sRNA76	rna-ABUW_RS15630	tRNA-Arg	17	1	8	3	5
sRNA76	ABUW_RS07785	hypothetical protein	12	1	8	3	0
sRNA76	ABUW_RS10740	HIT domain-containing protein	15	1	8	1	5
sRNA76	ABUW_RS00860	DUF805 domain-containing protein	12	1	8	1	2
sRNA76	ABUW_RS16655	energy transducer TonB	22	1	7	12	2
sRNA76	ABUW_RS13450	GMC family oxidoreductase	21	1	7	8	5
sRNA76	rna-ABUW_RS15805	23S ribosomal RNA	16	1	7	6	2
sRNA76	ABUW_RS17100	DNA-binding protein	22	1	7	5	9
sRNA76	rna-ABUW_RS01355	tRNA-Glu	17	1	7	5	4
sRNA76	ABUW_RS17195	monovalent cation/H+ antiporter subunit A	15	1	7	3	4
sRNA76	rna-ABUW_RS18845	tRNA-Ile	13	1	7	2	3
sRNA76	ABUW_RS11690	MFS transporter	14	1	7	1	5
sRNA76	ABUW_RS04825	rhombotarget A	11	1	7	1	2
sRNA76	ABUW_RS12530	type VI secretion system contractile sheath large subunit	10	1	7	1	1
sRNA76	ABUW_RS18610	sugar transferase	20	1	6	8	5
sRNA76	ABUW_RS14565	helicase	19	1	6	6	6
sRNA76	ABUW_RS09690	zonular occludens toxin	19	1	6	6	6
sRNA76	ABUW_RS03470	alpha/beta hydrolase	13	1	6	3	3
sRNA76	ABUW_RS15260	multidrug transporter MatE	10	1	6	3	0
sRNA76	rna-ABUW_RS05930	tRNA-Asn	11	1	6	2	2
sRNA76	ABUW_RS05535	LysM peptidoglycan-binding domain-containing protein	11	1	6	2	2
sRNA76	rna-ABUW_RS17245	tRNA-Met	13	1	6	1	5
sRNA76	ABUW_RS05980	adenosylhomocysteinase	11	1	6	0	4
sRNA76	ABUW_RS03095	preprotein translocase subunit SecA	10	1	6	0	3
sRNA76	ABUW_RS17725	PAS domain-containing sensor histidine kinase	11	1	5	5	0
sRNA76	ABUW_RS15245	hypothetical protein	20	1	5	4	10
sRNA76	ABUW_RS15000	tetratricopeptide repeat protein	10	1	5	2	2
sRNA76	rna-ABUW_RS02350	5S ribosomal RNA	11	1	5	1	4
sRNA76	ABUW_RS02875	HAMP domain-containing histidine kinase	11	1	5	1	4
sRNA76	ABUW_RS11020	phosphotransferase	20	1	4	8	7
sRNA76	ABUW_RS02130	NAD(P)/FAD-dependent oxidoreductase	17	1	4	7	5
sRNA76	rna-ABUW_RS07120	tRNA-Trp	19	1	4	5	9
sRNA76	ABUW_RS05400	ferredoxin reductase	14	1	4	5	4
sRNA76	rna-ABUW_RS02335	tRNA-Ile	13	1	4	5	3
sRNA76	sRNA90	sRNA90	13	1	4	4	4
sRNA76	ABUW_RS08415	2-C-methyl-D-erythritol 2%2C4-cyclodiphosphate synthase	12	1	4	4	3
sRNA76	rna-ABUW_RS15810	tRNA-Ala	11	1	4	4	2
sRNA76	ABUW_RS08175	TetR family transcriptional regulator	15	1	4	3	7
sRNA76	rna-ABUW_RS01240	tRNA-Phe	11	1	4	3	3
sRNA76	ABUW_RS18630	polysaccharide biosynthesis protein	15	1	4	2	8
sRNA76	ABUW_RS16295	bifunctional diguanylate cyclase/phosphodiesterase	10	1	4	2	3
sRNA76	ABUW_RS10190	short-chain fatty acid transporter	10	1	4	2	3
sRNA76	ABUW_RS02705	Rha family transcriptional regulator	10	1	4	2	3
sRNA76	ABUW_RS07465	methionine ABC transporter ATP-binding protein	11	1	4	0	6
sRNA76	ABUW_RS15705	methyltransferase	10	1	4	0	5
sRNA76	ABUW_RS17485	50S ribosomal protein L10	10	1	4	0	5
sRNA76	ABUW_RS05540	LysR family transcriptional regulator	10	1	4	0	5

sRNA76	ABUW_RS05160	hypothetical protein	12	1	3	7	1
sRNA76	ABUW_RS15440	hypothetical protein	10	1	3	4	2
sRNA76	ABUW_RS07195	alpha/beta fold hydrolase	14	1	3	3	7
sRNA76	ABUW_RS00910	cation acetate symporter	12	1	3	3	5
sRNA76	ABUW_RS11950	hydroxymethylglutaryl-CoA lyase	10	1	3	3	3
sRNA76	rna-ABUW_RS02340	tRNA-Ala	10	1	3	2	4
sRNA76	ABUW_RS10120	AraC family transcriptional regulator	12	1	3	1	7
sRNA76	rna-ABUW_RS05935	tRNA-Asn	13	1	2	5	5
sRNA76	rna-ABUW_RS07110	tRNA-Trp	10	1	2	5	2
sRNA76	ABUW_RS11115	sodium/proline symporter PutP	17	1	2	4	10
sRNA76	ABUW_RS06405	hypothetical protein	12	1	2	3	6
sRNA76	ABUW_RS04540	lytic transglycosylase domain-containing protein	12	1	2	2	7
sRNA76	ABUW_RS10640	siderophore biosynthesis protein	25	1	1	22	1
sRNA76	ABUW_RS18960	aromatic ring-hydroxylating dioxygenase subunit alpha	22	1	1	8	12
sRNA76	ABUW_RS12260	DUF2813 domain-containing protein	12	1	1	5	5
sRNA76	ABUW_RS16665	TetR/AcrR family transcriptional regulator	12	1	1	4	6
sRNA76	ABUW_RS14415	BCCT family transporter	10	1	1	1	7
sRNA76	ABUW_RS10585	acetyltransferase	36	1	0	33	2
sRNA76	ABUW_RS05710	siderophore-interacting protein	10	1	0	9	0
sRNA76	ABUW_RS17685	ferrous iron transporter B	197	0	36	143	18
sRNA76	ABUW_RS08745	hypothetical protein	70	0	24	25	21
sRNA76	ABUW_RS17650	NUDIX hydrolase	91	0	22	35	34
sRNA76	ABUW_RS16740	zinc-binding alcohol dehydrogenase family protein	43	0	22	10	11
sRNA76	ABUW_RS18250	glutathione S-transferase	71	0	20	23	28
sRNA76	ABUW_RS07310	DMT family transporter	29	0	15	5	9
sRNA76	ABUW_RS07570	cytochrome o ubiquinol oxidase subunit III	15	0	13	1	1
sRNA76	rna-ABUW_RS07115	tRNA-Leu	28	0	12	7	9
sRNA76	ABUW_RS18015	DUF2726 domain-containing protein	18	0	11	3	4
sRNA76	ABUW_RS05095	SDR family oxidoreductase	36	0	10	17	9
sRNA76	ABUW_RS07025	general secretion pathway protein GspL	12	0	10	1	1
sRNA76	ABUW_RS02150	hypothetical protein	23	0	9	9	5
sRNA76	ABUW_RS16920	long-chain-acyl-CoA synthetase	17	0	9	6	2
sRNA76	rna-ABUW_RS02515	5S ribosomal RNA	19	0	9	4	6
sRNA76	rna-ABUW_RS07105	tRNA-Leu	17	0	9	2	6
sRNA76	ABUW_RS11310	acyltransferase	16	0	9	1	6
sRNA76	ABUW_RS03480	peptide antibiotic transporter SbmA	22	0	8	5	9
sRNA76	ABUW_RS06035	30S ribosomal protein S2	11	0	8	1	2
sRNA76	ABUW_RS02115	30S ribosomal protein S4	10	0	8	0	2
sRNA76	ABUW_RS09960	hypothetical protein	15	0	7	6	2
sRNA76	rna-ABUW_RS18840	tRNA-Ala	15	0	7	5	3
sRNA76	ABUW_RS00160	TetR/AcrR family transcriptional regulator	12	0	7	1	4
sRNA76	ABUW_RS00765	M23 family metallopeptidase	12	0	7	0	5
sRNA76	ABUW_RS11315	YebC/PmpR family DNA-binding transcriptional regulator	32	0	6	9	17
sRNA76	ABUW_RS08210	low molecular weight phosphotyrosine protein phosphatase	15	0	6	7	2
sRNA76	rna-ABUW_RS13740	tRNA-Glu	14	0	6	6	2
sRNA76	ABUW_RS01710	amino acid permease	12	0	6	4	2
sRNA76	ABUW_RS05995	acyl-CoA dehydrogenase	14	0	6	3	5
sRNA76	rna-ABUW_RS03410	tRNA-Asp	11	0	6	3	2
sRNA76	rna-ABUW_RS00085	tRNA-Ala	10	0	6	2	2
sRNA76	rna-ABUW_RS02495	16S ribosomal RNA	11	0	6	1	4
sRNA76	ABUW_RS03910	hypothetical protein	10	0	6	0	4
sRNA76	ABUW_RS10205	LysR family transcriptional regulator	19	0	5	11	3
sRNA76	rna-ABUW_RS16925	tRNA-Lys	13	0	5	5	3
sRNA76	ABUW_RS05310	insulinase family protein	13	0	5	5	3
sRNA76	ABUW_RS03110	hemolysin III	11	0	5	4	2
sRNA76	ABUW_RS03280	folate-binding protein YgfZ	11	0	5	4	2
sRNA76	ABUW_RS02925	UDP-N-acetylglucosamine 2-epimerase (non-hydrolyzing)	11	0	5	3	3
sRNA76	ABUW_RS01380	16S rRNA (cytosine(1402)-N(4))-methyltransferase RsmH	11	0	5	2	4
sRNA76	ABUW_RS12755	TetR family transcriptional regulator	10	0	5	1	4
sRNA76	rna-ABUW_RS02210	tRNA-Arg	13	0	4	8	1
sRNA76	rna-ABUW_RS17520	tRNA-Thr	17	0	4	5	8
sRNA76	ABUW_RS03150	CoA transferase	10	0	4	5	1
sRNA76	ABUW_RS04485	diacylglycerol kinase	11	0	4	3	4
sRNA76	ABUW_RS11425	tautomerase family protein	10	0	4	3	3
sRNA76	ABUW_RS00135	hypothetical protein	11	0	4	2	5
sRNA76	ABUW_RS02025	30S ribosomal protein S3	10	0	4	1	5
sRNA76	rna-ABUW_RS18060	5S ribosomal RNA	10	0	3	3	4
sRNA76	ABUW_RS08030	TetR/AcrR family transcriptional regulator	10	0	3	2	5
sRNA76	ABUW_RS06655	alpha/beta hydrolase	10	0	2	7	1
sRNA76	ABUW_RS11275	cytosine permease	11	0	2	4	5
sRNA76	ABUW_RS05760	(2%2C3-dihydroxybenzoyl)adenylate synthase	58	0	1	56	1
sRNA76	ABUW_RS05770	histidine decarboxylase	10	0	1	9	0
sRNA76	ABUW_RS05800	acinetobactin biosynthesis isochorismate synthase BasJ	48	0	0	48	0
sRNA76	ABUW_RS03435	membrane protein	19	0	0	18	1
sRNA76	ABUW_RS10070	Fur family transcriptional regulator	15	0	0	14	1
sRNA76	ABUW_RS00710	TonB-dependent siderophore receptor	11	0	0	10	1
sRNA75	ABUW_RS12325	1%2C2-phenylacetyl-CoA epoxidase subunit A	11	1	9	1	0
sRNA74	ABUW_RS20195	hypothetical protein	294	6	78	97	113
sRNA7	ABUW_RS17415	DsbA family oxidoreductase	66	0	22	17	27
sRNA62	ABUW_RS11870	hypothetical protein	53	16	19	12	6
sRNA62	ABUW_RS11875	hypothetical protein	32	10	12	9	1
sRNA62	ABUW_RS12975	hypothetical protein	27	3	12	7	5
sRNA62	ABUW_RS17440	membrane protein	16	1	9	5	1
sRNA62	sRNA26	sRNA26	13	1	6	2	4
sRNA62	ABUW_RS07500	hypothetical protein	5	1	4	0	0
sRNA62	ABUW_RS20195	hypothetical protein	10	1	3	3	3
sRNA62	rna-ABUW_RS13710	tRNA-Ser	10	1	3	3	3
sRNA62	6S RNA	6S RNA	29	0	15	10	4
sRNA62	sRNA76	sRNA76	16	0	7	2	7
sRNA62	rna-ABUW_RS15625	tRNA-His	22	0	5	8	9
sRNA62	rna-ABUW_RS04565	tRNA-Ser	13	0	4	7	2
sRNA56	ABUW_RS20195	hypothetical protein	24	0	11	6	7
sRNA54	ABUW_RS17440	membrane protein	10	1	6	2	1
sRNA54	sRNA103	sRNA103	17	1	5	1	10
sRNA54	sRNA39	sRNA39	73	0	36	21	16
sRNA54	ABUW_RS06260	hypothetical protein	26	0	10	7	9
sRNA54	ABUW_RS02485	diguanylate cyclase	24	0	9	8	7
sRNA54	ABUW_RS18745	hypothetical protein	10	0	4	5	1
sRNA46	rna-ABUW_RS19905	6S RNA	91	1	40	38	12
sRNA46	sRNA101	sRNA101	53	1	29	12	11

sRNA46	rna-ABUW_RS17255	tRNA-Leu	14	1	4	6	3
sRNA46	sRNA90	sRNA90	12	1	4	4	3
sRNA46	ABUW_RS12975	hypothetical protein	39	0	20	13	6
sRNA46	rna-ABUW_RS18845	tRNA-Ile	20	0	12	3	5
sRNA46	rna-ABUW_RS18075	tRNA-Ile	17	0	11	1	5
sRNA46	rna-ABUW_RS02335	tRNA-Ile	12	0	9	2	1
sRNA46	rna-ABUW_RS15815	tRNA-Ile	12	0	9	1	2
sRNA46	rna-ABUW_RS02500	tRNA-Ile	14	0	6	3	5
sRNA46	ABUW_RS00325	4-hydroxyphenylpyruvate dioxygenase	11	0	5	3	3
sRNA46	ABUW_RS08695	hypothetical protein	14	0	4	6	4
sRNA46	rna-ABUW_RS04565	tRNA-Ser	10	0	3	7	0
sRNA46	ABUW_RS10005	hypothetical protein	13	0	3	3	7
sRNA44	ABUW_RS20195	hypothetical protein	22	0	12	4	6
sRNA44	ABUW_RS19720	Ig-like domain-containing protein	28	0	8	14	6
sRNA44	ABUW_RS05340	type I-F CRISPR-associated helicase Cas3	11	0	3	6	2
sRNA42	ABUW_RS08705	hypothetical protein	15	0	8	4	3
sRNA40	ABUW_RS01495	pilin	119	1	40	50	28
sRNA40	rna-ABUW_RS18070	tRNA-Ala	10	1	3	2	4
sRNA40	ABUW_RS10585	acetyltransferase	11	0	0	11	0
sRNA39	sRNA54	sRNA54	89	0	30	32	27
sRNA39	ABUW_RS07145	DUF2171 domain-containing protein	22	0	10	9	3
sRNA39	ABUW_RS10005	hypothetical protein	12	0	8	3	1
sRNA27	ABUW_RS10025	hypothetical protein	11	1	6	3	1
sRNA27	ABUW_RS03195	OmpA family protein	13	0	8	5	0
sRNA27	ABUW_RS05910	hypothetical protein	22	0	6	9	7
sRNA26	6S RNA	6S RNA	95	4	45	27	19
sRNA26	sRNA24	sRNA24	47	4	19	14	10
sRNA26	ABUW_RS03195	OmpA family protein	17	1	13	2	1
sRNA26	sRNA89	sRNA89	11	1	6	4	0
sRNA26	sRNA76	sRNA76	12	1	2	4	5
sRNA26	ABUW_RS12975	hypothetical protein	43	0	19	14	10
sRNA26	sRNA62	sRNA62	26	0	14	7	5
sRNA26	ABUW_RS10005	hypothetical protein	12	0	9	2	1
sRNA26	ABUW_RS06720	cold-shock protein	14	0	8	3	3
sRNA26	rna-ABUW_RS13710	tRNA-Ser	17	0	6	9	2
sRNA26	rna-ABUW_RS04565	tRNA-Ser	15	0	3	10	2
sRNA26	rna-ABUW_RS15625	tRNA-His	10	0	1	3	6
sRNA25	ABUW_RS10005	hypothetical protein	50	0	13	26	11
sRNA24	ABUW_RS17440	membrane protein	11	1	6	3	1
sRNA24	6S RNA	6S RNA	71	0	29	24	18
sRNA24	ABUW_RS12975	hypothetical protein	14	0	7	5	2
sRNA24	ABUW_RS20195	hypothetical protein	10	0	6	1	3
sRNA24	ABUW_RS10005	hypothetical protein	14	0	5	5	4
Aar	ABUW_RS07145	DUF2171 domain-containing protein	1002	19	493	201	289
Aar	rna-ABUW_RS17255	tRNA-Leu	133	10	42	34	47
Aar	ABUW_RS10005	hypothetical protein	916	6	282	383	245
Aar	ABUW_RS10425	hypothetical protein	419	4	244	80	91
Aar	ABUW_RS04980	ornithine uptake porin CarO type 3	283	4	69	140	70
Aar	ABUW_RS12975	hypothetical protein	53	4	29	11	9
Aar	ABUW_RS00325	4-hydroxyphenylpyruvate dioxygenase	29	2	18	6	3
Aar	ABUW_RS12330	phenylacetic acid degradation bifunctional protein PaaZ	21	2	13	3	3
Aar	ABUW_RS04045	porin	28	2	9	14	3
Aar	ABUW_RS15275	iron-sulfur cluster carrier protein ApbC	20	2	4	6	8
Aar	ABUW_RS17440	Outer membrane protein W	141	1	52	39	49
Aar	ABUW_RS07825	rRNA pseudouridine synthase	161	1	40	66	54
Aar	ABUW_RS07310	DMT family transporter	36	1	19	10	6
Aar	rna-ABUW_RS13710	tRNA-Ser	28	1	18	3	6
Aar	ABUW_RS13040	hypothetical protein	38	1	16	11	10
Aar	ABUW_RS08645	hypothetical protein	39	1	15	15	8
Aar	rna-ABUW_RS01045	tRNA-Thr	31	1	15	13	2
Aar	ABUW_RS16465	alpha/beta hydrolase	52	1	14	15	22
Aar	rna-ABUW_RS15625	tRNA-His	52	1	13	24	14
Aar	ABUW_RS11850	glucose 1-dehydrogenase	26	1	12	8	5
Aar	rna-ABUW_RS17530	tRNA-Tyr	23	1	11	7	4
Aar	ABUW_RS02710	hypothetical protein	19	1	10	5	3
Aar	sRNA100	sRNA100	17	1	10	3	3
Aar	rna-ABUW_RS02500	tRNA-Ile	21	1	9	7	4
Aar	rna-ABUW_RS04565	tRNA-Ser	16	1	9	4	2
Aar	ABUW_RS11860	iron-containing redox enzyme family protein	13	1	9	2	1
Aar	rna-ABUW_RS18075	tRNA-Ile	30	1	8	12	9
Aar	ABUW_RS03310	DUF1508 domain-containing protein	17	1	8	6	2
Aar	ABUW_RS05445	alpha-keto acid decarboxylase family protein	18	1	8	5	4
Aar	ABUW_RS00260	DUF1328 domain-containing protein	12	1	7	3	1
Aar	ABUW_RS13350	carbon storage regulator CsrA	24	1	6	7	10
Aar	rna-ABUW_RS15635	tRNA-Pro	22	1	6	7	8
Aar	ABUW_RS13010	DUF4142 domain-containing protein	16	1	6	5	4
Aar	rna-ABUW_RS02185	tRNA-Ser	14	1	6	3	4
Aar	rna-ABUW_RS17525	tRNA-Gly	13	1	6	1	5
Aar	ABUW_RS11960	indolepyruvate ferredoxin oxidoreductase family protein	11	1	5	4	1
Aar	ABUW_RS13220	hypothetical protein	15	1	5	1	8
Aar	ABUW_RS13120	four-helix bundle copper-binding protein	10	1	4	4	1
Aar	ABUW_RS06610	hemin uptake protein HemP	11	1	1	9	0
Aar	ABUW_RS18200	ATP synthase subunit I	12	1	1	1	9
Aar	ABUW_RS04930	NIF3 1	87	0	41	46	0
Aar	ABUW_RS11010	16S rRNA (guanine(527)-N(7))-methyltransferase RsmG	86	0	39	15	32
Aar	ABUW_RS13380	hypothetical protein	74	0	26	23	25
Aar	ABUW_RS04000	amino acid permease	39	0	24	11	4
Aar	ABUW_RS06065	DUF962 domain-containing protein	22	0	14	5	3
Aar	ABUW_RS19340	hypothetical protein	29	0	13	8	8
Aar	rna-ABUW_RS18845	tRNA-Ile	27	0	13	7	7
Aar	ABUW_RS12725	hypothetical protein	22	0	13	3	6
Aar	rna-ABUW_RS00080	tRNA-Ile	34	0	12	15	7
Aar	rna-ABUW_RS02335	tRNA-Ile	25	0	12	6	7
Aar	ABUW_RS05820	DUF3015 domain-containing protein	16	0	12	1	3
Aar	ABUW_RS15085	acyl carrier protein	40	0	10	15	15
Aar	ABUW_RS13035	hypothetical protein	19	0	10	2	7
Aar	rna-ABUW_RS15815	tRNA-Ile	26	0	9	10	7
Aar	ABUW_RS08835	3-deoxy-7-phosphoheptulonate synthase	12	0	9	0	3
Aar	ABUW_RS08695	hypothetical protein	24	0	8	10	6
Aar	rna-ABUW_RS17535	tRNA-Thr	20	0	8	9	3

Aar	ABUW_RS19585	hypothetical protein	15	0	8	5	2
Aar	sRNA103	sRNA103	16	0	8	4	4
Aar	ABUW_RS02150	hypothetical protein	14	0	8	4	2
Aar	ABUW_RS02765	carbapenem-hydrolyzing class D beta-lactamase OXA-23	14	0	8	3	3
Aar	sRNA102	sRNA102	13	0	8	3	2
Aar	sRNA81	sRNA81	13	0	7	3	3
Aar	ABUW_RS07820	hypothetical protein	12	0	7	0	5
Aar	ABUW_RS15450	response regulator BfmR	23	0	6	10	7
Aar	rna-ABUW_RS17520	tRNA-Thr	16	0	6	9	1
Aar	ABUW_RS05200	VIT family protein	20	0	6	5	9
Aar	ABUW_RS06165	hypothetical protein	13	0	6	4	3
Aar	rna-ABUW_RS14905	tRNA-Met	10	0	6	1	3
Aar	ABUW_RS03285	toxin	13	0	6	0	7
Aar	ABUW_RS03565	long-chain fatty acid transporter	20	0	5	8	7
Aar	ABUW_RS10925	uracil-DNA glycosylase	12	0	5	7	0
Aar	ABUW_RS16485	permease	16	0	5	6	5
Aar	ABUW_RS14610	hypothetical protein	14	0	5	6	3
Aar	ABUW_RS15160	trehalose-phosphatase	10	0	5	3	2
Aar	ABUW_RS07860	RNA chaperone Hfq	11	0	5	2	4
Aar	ABUW_RS15515	flavin reductase	10	0	5	2	3
Aar	ABUW_RS04170	outer membrane lipoprotein chaperone LolA	10	0	5	2	3
Aar	ABUW_RS04325	neutral zinc metallopeptidase	13	0	4	6	3
Aar	ABUW_RS00190	4-hydroxy-tetrahydrodipicolinate reductase	15	0	3	10	2
Aar	ABUW_RS10605	TonB-dependent receptor	28	0	2	25	1
Aar	ABUW_RS08700	hypothetical protein	13	0	2	6	5
Aar	ABUW_RS13760	RHS repeat protein	10	0	1	6	3
Aar	ABUW_RS12700	hypothetical protein	10	0	1	5	4
Aar	ABUW_RS10585	acetyltransferase	99	0	0	99	0
Aar	ABUW_RS05745	TonB-dependent siderophore receptor	46	0	0	46	0
Aar	ABUW_RS05710	siderophore-interacting protein BauF	33	0	0	33	0
Aar	ABUW_RS17685	ferrous iron transporter B	11	0	0	11	0
sRNA15	sRNA76	sRNA76	44	4	11	19	10
sRNA15	rna-ABUW_RS13710	tRNA-Ser	40	2	15	18	5
sRNA15	rna-ABUW_RS19930	transfer-messenger RNA	27	2	13	9	3
sRNA15	rna-ABUW_RS14905	tRNA-Met	26	2	10	6	8
sRNA15	ABUW_RS17440	membrane protein	24	2	6	11	5
sRNA15	sRNA90	sRNA90	20	2	3	5	10
sRNA15	6S RNA	6S RNA	124	1	50	42	31
sRNA15	ABUW_RS12975	hypothetical protein	n	1	43	33	22
sRNA15	ABUW_RS08700	hypothetical protein	11	1	9	0	1
sRNA15	ABUW_RS12335	L-serine ammonia-lyase	13	1	8	3	1
sRNA15	ABUW_RS17120	30S ribosomal protein S15	10	1	7	1	1
sRNA15	sRNA103	sRNA103	13	1	5	4	3
sRNA15	rna-ABUW_RS02335	tRNA-Ile	14	1	4	6	3
sRNA15	rna-ABUW_RS17530	tRNA-Tyr	12	1	4	5	2
sRNA15	ABUW_RS06475	DUF4760 domain-containing protein	11	1	4	5	1
sRNA15	rna-ABUW_RS02505	tRNA-Ala	10	1	3	6	0
sRNA15	rna-ABUW_RS02185	tRNA-Ser	11	1	3	4	3
sRNA15	sRNA1	sRNA1	72	0	45	9	18
sRNA15	rna-ABUW_RS04565	tRNA-Ser	28	0	9	15	4
sRNA15	rna-ABUW_RS15625	tRNA-His	23	0	8	9	6
sRNA15	ABUW_RS13040	hypothetical protein	11	0	8	2	1
sRNA15	ABUW_RS08695	hypothetical protein	32	0	7	14	11
sRNA15	rna-ABUW_RS00080	tRNA-Ile	10	0	6	4	0
sRNA15	rna-ABUW_RS18070	tRNA-Ala	13	0	3	6	4
sRNA15	rna-ABUW_RS18840	tRNA-Ala	13	0	3	6	4
sRNA15	rna-ABUW_RS00085	tRNA-Ala	11	0	1	6	4
sRNA15	ABUW_RS10585	acetyltransferase	10	0	0	10	0
sRNA105	ABUW_RS07145	DUF2171 domain-containing protein	12	0	8	0	4
sRNA103	ABUW_RS07145	DUF2171 domain-containing protein	226	12	103	50	61
sRNA103	ABUW_RS01615	hemerythrin	142	7	63	37	35
sRNA103	ABUW_RS10425	hypothetical protein	278	4	158	57	59
sRNA103	rna-ABUW_RS15625	tRNA-His	49	2	20	20	7
sRNA103	ABUW_RS07965	molecular chaperone	23	2	12	5	4
sRNA103	ABUW_RS18015	DUF2726 domain-containing protein	21	2	10	6	3
sRNA103	ABUW_RS14740	bacteriohemerythrin	21	2	9	9	1
sRNA103	sRNA87	sRNA87	22	2	8	4	8
sRNA103	rna-ABUW_RS01045	tRNA-Thr	18	1	9	5	3
sRNA103	rna-ABUW_RS15620	tRNA-Pro	18	1	6	5	6
sRNA103	rna-ABUW_RS15635	tRNA-Pro	16	1	3	7	5
sRNA103	ABUW_RS05720	acinetobactin non-ribosomal peptide synthetase subunit BasB	12	1	0	11	0
sRNA103	ABUW_RS17960	long-chain-fatty-acid--CoA ligase	55	0	16	21	18
sRNA103	rna-ABUW_RS02185	tRNA-Ser	38	0	14	13	11
sRNA103	rna-ABUW_RS17520	tRNA-Thr	25	0	12	9	4
sRNA103	rna-ABUW_RS02500	tRNA-Ile	21	0	11	7	3
sRNA103	rna-ABUW_RS00080	tRNA-Ile	12	0	8	1	3
sRNA103	ABUW_RS07570	cytochrome o ubiquinol oxidase subunit III	18	0	7	9	2
sRNA103	rna-ABUW_RS01240	tRNA-Phe	13	0	6	4	3
sRNA103	rna-ABUW_RS15815	tRNA-Ile	12	0	6	3	3
sRNA103	rna-ABUW_RS18845	tRNA-Ile	15	0	5	6	4
sRNA103	sRNA21	sRNA21	11	0	5	5	1
sRNA103	ABUW_RS02765	carbapenem-hydrolyzing class D beta-lactamase OXA-23	14	0	5	4	5
sRNA103	rna-ABUW_RS01235	tRNA-Phe	10	0	5	3	2
sRNA103	ABUW_RS03980	hypothetical protein	10	0	4	3	3
sRNA103	rna-ABUW_RS04565	tRNA-Ser	11	0	4	1	6
sRNA103	ABUW_RS10585	acetyltransferase	27	0	0	27	0
sRNA102	sRNA99	sRNA99	1849	51	457	740	601
sRNA102	ABUW_RS07500	hypothetical protein	11	1	8	2	0
sRNA102	ABUW_RS06040	elongation factor Ts	10	1	6	0	3
sRNA102	ABUW_RS15080	peptidoglycan-binding protein LysM	10	1	5	4	0
sRNA102	rna-ABUW_RS17255	tRNA-Leu	17	1	4	7	5
sRNA102	ABUW_RS14025	copper resistance protein NlpE	10	1	4	3	2
sRNA102	ABUW_RS12325	1%2C2-phenylacetyl-CoA epoxidase subunit A	15	0	15	0	0
sRNA102	ABUW_RS09695	hypothetical protein	21	0	8	9	4
sRNA102	ABUW_RS07855	tRNA (adenosine(37)-N6)-dimethylallyltransferase MiaA	22	0	8	3	11
sRNA102	ABUW_RS00325	4-hydroxyphenylpyruvate dioxygenase	12	0	7	5	0
sRNA102	rna-ABUW_RS17530	tRNA-Tyr	13	0	6	2	5
sRNA102	ABUW_RS00260	DUF1328 domain-containing protein	10	0	6	2	2
sRNA102	ABUW_RS00045	hypothetical protein	18	0	3	8	7
sRNA102	ABUW_RS10585	acetyltransferase	72	0	0	71	1

sRNA101	sRNA76	sRNA76	878	3	237	266	372
sRNA101	sRNA94	sRNA94	127	3	41	37	46
sRNA101	ABUW_RS11875	hypothetical protein	65	3	24	14	24
sRNA101	ABUW_RS07965	molecular chaperone	19	2	2	9	6
sRNA101	ABUW_RS06610	hemin uptake protein HemP	30	2	0	28	0
sRNA101	ABUW_RS01495	pilin	52	1	19	24	8
sRNA101	ABUW_RS13350	carbon storage regulator CsrA	22	1	9	9	3
sRNA101	ABUW_RS18195	F0F1 ATP synthase subunit A	15	1	9	1	4
sRNA101	rna-ABUW_RS15625	tRNA-His	10	1	6	2	1
sRNA101	ABUW_RS11960	indolepyruvate ferredoxin oxidoreductase family protein	13	1	5	5	2
sRNA101	ABUW_RS08050	hypothetical protein	12	1	5	1	5
sRNA101	ABUW_RS08835	3-deoxy-7-phosphoheptulonate synthase	16	0	9	5	2
sRNA101	ABUW_RS18650	membrane protein	11	0	7	2	2
sRNA101	ABUW_RS18190	F0F1 ATP synthase subunit C	15	0	6	6	3
sRNA101	ABUW_RS13030	head morphogenesis protein	16	0	6	5	5
sRNA101	ABUW_RS00325	4-hydroxyphenylpyruvate dioxygenase	21	0	5	12	4
sRNA101	sRNA62	sRNA62	14	0	5	3	6
sRNA101	ABUW_RS08085	hypothetical protein	10	0	5	2	3
sRNA101	ABUW_RS15525	DUF1852 domain-containing protein	20	0	4	13	3
sRNA101	ABUW_RS07565	cytochrome o ubiquinol oxidase subunit IV	12	0	4	6	2
sRNA101	ABUW_RS01035	class I SAM-dependent methyltransferase	10	0	4	6	0
sRNA101	ABUW_RS17105	MerR family transcriptional regulator	11	0	3	3	5
sRNA101	ABUW_RS12975	hypothetical protein	13	0	2	10	1
sRNA101	ABUW_RS12280	phenylacetate--CoA ligase	11	0	1	7	3
sRNA101	ABUW_RS10585	acetyltransferase	10	0	0	10	0
sRNA100	ABUW_RS11470	dicarboxylate/amino acid:cation symporter	1016	50	380	290	296
sRNA100	sRNA102	sRNA102	712	15	218	209	270
sRNA100	ABUW_RS13040	hypothetical protein	186	13	70	47	56
sRNA100	ABUW_RS15155	alpha/beta fold hydrolase	11	1	1	3	6
sRNA100	sRNA105	sRNA105	16	0	4	4	8
sRNA1	6S RNA	6S RNA	23	2	14	5	2
sRNA1	sRNA87	sRNA87	17	1	9	2	5
sRNA1	sRNA15	sRNA15	16	1	7	4	4
sRNA1	ABUW_RS10005	hypothetical protein	10	1	5	3	1
sRNA1	ABUW_RS12975	hypothetical protein	16	0	8	4	4

NZ_CP008707.1 plasmid filtered							
sRNA	**Interaction partner**	**Product**	**Total Chimeric Reads**	**NI Chimeric Reads**	**IND Chimeric Reads**	**DIP Chimeric Reads**	**IMIP Chimeric Reads**
sRNA94	ABUW_RS19310	CmlA family chloramphenicol efflux MFS transporter	175	0	75	54	46
sRNA76	ABUW_RS19580	hypothetical protein	174	11	69	48	46
sRNA89	ABUW_RS19315	aminoglycoside nucleotidyltransferase ANT(2")-Ia	143	12	73	39	19
sRNA92	ABUW_RS19310	CmlA family chloramphenicol efflux MFS transporter	137	1	66	40	30
sRNA37	ABUW_RS19315	aminoglycoside nucleotidyltransferase ANT(2")-Ia	65	1	22	25	17
sRNA76	ABUW_RS19280	class A extended-spectrum beta-lactamase GES-11	56	4	30	11	11
sRNA84	ABUW_RS19575	hypothetical protein	55	3	27	10	15
sRNA37	ABUW_RS19575	hypothetical protein	46	2	30	8	6
sRNA84	ABUW_RS19585	hypothetical protein	45	4	23	11	7
sRNA88	ABUW_RS19280	class A extended-spectrum beta-lactamase GES-11	42	0	17	15	10
sRNA37	ABUW_RS19585	hypothetical protein	42	3	15	9	15
sRNA76	ABUW_RS19315	aminoglycoside nucleotidyltransferase ANT(2")-Ia	40	3	17	9	11
sRNA93	ABUW_RS19270	trimethoprim-resistant dihydrofolate reductase DfrA7	34	3	12	9	10
sRNA37	ABUW_RS19280	class A extended-spectrum beta-lactamase GES-11	30	2	9	13	6
sRNA90	ABUW_RS19270	trimethoprim-resistant dihydrofolate reductase DfrA7	27	0	13	10	4
sRNA92	ABUW_RS19315	aminoglycoside nucleotidyltransferase ANT(2")-Ia	22	1	6	9	6
sRNA94	ABUW_RS19315	aminoglycoside nucleotidyltransferase ANT(2")-Ia	22	0	9	5	8
sRNA84	ABUW_RS19315	aminoglycoside nucleotidyltransferase ANT(2")-Ia	22	1	13	7	1
sRNA21	ABUW_RS19315	aminoglycoside nucleotidyltransferase ANT(2")-Ia	22	0	10	7	5
sRNA21	ABUW_RS19280	class A extended-spectrum beta-lactamase GES-11	21	1	11	6	3
sRNA21	ABUW_RS19155	hypothetical protein	21	0	6	4	11
sRNA103	ABUW_RS19280	class A extended-spectrum beta-lactamase GES-11	20	2	6	9	3
sRNA84	ABUW_RS19280	class A extended-spectrum beta-lactamase GES-11	20	1	9	6	4
sRNA103	ABUW_RS19175	hypothetical protein	18	0	7	5	6
sRNA21	ABUW_RS19175	hypothetical protein	17	0	8	7	2
sRNA81	ABUW_RS19315	aminoglycoside nucleotidyltransferase ANT(2")-Ia	17	0	8	9	0
sRNA26	ABUW_RS19315	aminoglycoside nucleotidyltransferase ANT(2")-Ia	16	1	3	7	5
sRNA103	ABUW_RS19155	hypothetical protein	15	1	4	2	8
sRNA21	ABUW_RS19585	hypothetical protein	15	0	8	5	2
sRNA103	ABUW_RS19340	hypothetical protein	15	0	10	1	4
sRNA84	ABUW_RS19310	CmlA family chloramphenicol efflux MFS transporter	14	0	9	1	4
sRNA26	ABUW_RS19575	hypothetical protein	14	0	10	2	2
sRNA90	ABUW_RS19215	type II toxin-antitoxin system RelE/ParE family toxin	13	0	2	8	3
sRNA92	ABUW_RS19280	class A extended-spectrum beta-lactamase GES-11	13	0	2	6	5
sRNA81	ABUW_RS19280	class A extended-spectrum beta-lactamase GES-11	12	0	6	3	3
sRNA101	ABUW_RS19280	class A extended-spectrum beta-lactamase GES-11	12	0	4	6	2
sRNA21	ABUW_RS19575	hypothetical protein	12	1	5	3	3
sRNA76	ABUW_RS19210	helix-turn-helix transcriptional regulator	12	1	9	1	1
sRNA15	ABUW_RS19280	class A extended-spectrum beta-lactamase GES-11	12	1	8	1	2
sRNA89	ABUW_RS19085	H-NS histone family protein	11	0	1	3	7
sRNA103	ABUW_RS19315	aminoglycoside nucleotidyltransferase ANT(2")-Ia	11	0	5	3	3
sRNA9	ABUW_RS19315	aminoglycoside nucleotidyltransferase ANT(2")-Ia	11	1	5	3	2
sRNA93	ABUW_RS19280	class A extended-spectrum beta-lactamase GES-11	11	0	5	4	2
sRNA76	ABUW_RS20385	hypothetical protein	11	0	3	3	5
sRNA37	ABUW_RS19275	aminoglycoside N-acetyltransferase AAC(6')-Ib3	10	1	7	1	1
sRNA65	ABUW_RS19585	hypothetical protein	10	1	2	4	3
sRNA24	ABUW_RS19575	hypothetical protein	10	0	7	1	2
sRNA9	ABUW_RS19280	class A extended-spectrum beta-lactamase GES-11	10	0	6	1	3

NZ_CP008708.1 plasmid filtered							
sRNA	**Interaction partner**	**Product**	**Total Chimeric Reads**	**NI Chimeric Reads**	**IND Chimeric Reads**	**DIP Chimeric Reads**	**IMIP Chimeric Reads**
sRNA76	ABUW_RS19620	DIP1984 family protein	4587	104	1704	1664	1115
sRNA99	ABUW_RS19600	sel1 repeat family protein	952	55	170	222	505
sRNA84	ABUW_RS19620	DIP1984 family protein	752	25	347	190	190
sRNA21	ABUW_RS19620	DIP1984 family protein	519	6	219	161	133
sRNA101	ABUW_RS19620	DIP1984 family protein	291	12	127	96	56
sRNA76	ABUW_RS19600	sel1 repeat family protein	214	18	85	68	43
sRNA87	ABUW_RS19620	DIP1984 family protein	58	4	31	12	11
sRNA21	ABUW_RS19600	sel1 repeat family protein	56	3	12	30	11
sRNA1	ABUW_RS19620	DIP1984 family protein	44	1	24	11	8
sRNA92	ABUW_RS19620	DIP1984 family protein	40	2	19	9	10
sRNA84	ABUW_RS20495	hypothetical protein	39	2	16	15	6
sRNA86	ABUW_RS19620	DIP1984 family protein	39	2	14	11	12
sRNA21	ABUW_RS19590	replication initiation protein	36	1	15	15	5
sRNA46	ABUW_RS19620	DIP1984 family protein	33	2	16	9	6
sRNA84	ABUW_RS19600	sel1 repeat family protein	31	3	12	14	2
sRNA75	ABUW_RS19620	DIP1984 family protein	27	0	24	3	0
sRNA93	ABUW_RS19620	DIP1984 family protein	25	1	10	7	7
sRNA81	ABUW_RS19620	DIP1984 family protein	20	2	5	5	8
sRNA24	ABUW_RS19620	DIP1984 family protein	20	1	8	9	2
sRNA27	ABUW_RS19620	DIP1984 family protein	18	0	14	1	3
sRNA88	ABUW_RS19620	DIP1984 family protein	13	0	10	2	1
sRNA87	ABUW_RS19615	TonB-dependent receptor	11	1	6	1	3
sRNA9	ABUW_RS19600	sel1 repeat family protein	10	1	3	3	3

NZ_CP008709.1 plasmid filtered							
sRNA	**Interaction partner**	**Product**	**Total Chimeric Reads**	**NI Chimeric Reads**	**IND Chimeric Reads**	**DIP Chimeric Reads**	**IMIP Chimeric Reads**
sRNA84	ABUW_RS19635	protein rep	18	10	4	4	0
sRNA21	ABUW_RS19645	hypothetical protein	13	6	3	3	1
sRNA9	ABUW_RS19635	protein rep	12	4	8	0	0

Appendix III – Targets shared by Hi-GRIL-seq and CopraRNA

sRNA	Interaction partner	Product	No. of ligations
sRNA21	ABUW_RS04980	ornithine uptake porin CarO type 3	283
sRNA21	ABUW_RS15085	acyl carrier protein	40
sRNA21	ABUW_RS04000	amino acid permease	39
sRNA21	ABUW_RS08645	hypothetical protein	39
sRNA21	ABUW_RS13040	hypothetical protein	38
sRNA21	ABUW_RS07310	DMT family transporter	36
sRNA21	ABUW_RS10605	TonB-dependent receptor BfnH	28
sRNA21	ABUW_RS15450	response regulator BfmR	23
sRNA21	ABUW_RS16485	permease	16
sRNA21	ABUW_RS03285	toxin	13
sRNA26	ABUW_RS06720	cold-shock protein	44
sRNA40	ABUW_RS01495	pilin	119
sRNA54	ABUW_RS06260	hypothetical protein	26
sRNA76	ABUW_RS05865	anthranilate phosphoribosyltransferase	250
sRNA76	ABUW_RS10520	TonB-dependent siderophore receptor	106
sRNA76	ABUW_RS16240	hypothetical protein	100
sRNA76	ABUW_RS15615	adenosine deaminase	79
sRNA76	ABUW_RS16320	leucine--tRNA ligase	47
sRNA76	ABUW_RS08375	sulfurtransferase complex subunit TusD	34
sRNA76	ABUW_RS16655	energy transducer TonB	22
sRNA76	ABUW_RS10205	LysR family transcriptional regulator	19
sRNA76	ABUW_RS03435	membrane protein	19
sRNA76	ABUW_RS15910	thioredoxin	17
sRNA76	ABUW_RS11310	acyltransferase	16
sRNA76	ABUW_RS03150	CoA transferase	10
sRNA76	ABUW_RS14415	BCCT family transporter	10
sRNA85	ABUW_RS12290	3-hydroxyacyl-CoA dehydrogenase	24
sRNA86	ABUW_RS08700	hypothetical protein	11
sRNA90	ABUW_RS18870	hypothetical protein	8705
sRNA90	ABUW_RS12300	enoyl-CoA hydratase	35
sRNA90	ABUW_RS16815	DUF1311 domain-containing protein	18
sRNA90	ABUW_RS10185	CoA transferase subunit B	10
sRNA99	ABUW_RS14880	protoporphyrinogen oxidase HemJ	27
sRNA101	ABUW_RS13030	head morphogenesis protein	16
sRNA101	ABUW_RS18195	F0F1 ATP synthase subunit A	15
sRNA101	ABUW_RS11960	indolepyruvate ferredoxin oxidoreductase family protein	13
sRNA101	ABUW_RS08050	hypothetical protein	12
sRNA101	ABUW_RS10585	acetyltransferase	10
sRNA102	ABUW_RS07500	hypothetical protein	11
sRNA103	ABUW_RS07145	DUF2171 domain-containing protein	226
sRNA103	ABUW_RS01615	hemerythrin	142
sRNA103	ABUW_RS07570	cytochrome o ubiquinol oxidase subunit III	18

Appendix IV – Differentially expressed genes following Aar overexpression

Downregulated			
Gene	Product	log2FoldChange	Adjusted p-value
ABUW_RS00355	hypothetical protein	-1.000211069	0.00892569
ABUW_RS08280	ABC transporter substrate-binding protein	-1.001239473	0.00448924
ABUW_RS19485	conjugal transfer protein TraB	-1.002918638	0.000349089
ABUW_RS02375	DUF1446 domain-containing protein	-1.003171327	0.002055414
ABUW_RS04825	rhombotarget A	-1.004526896	0.029562252
ABUW_RS13600	aspartate aminotransferase family protein	-1.005985127	0.051900836
ABUW_RS01160	aquaporin Z	-1.007105714	0.054595065
ABUW_RS17790	transcriptional repressor NrdR	-1.007256199	0.037112226
ABUW_RS08120	MgtC/SapB family protein	-1.007888562	0.00739108
ABUW_RS19570	Y-family DNA polymerase	-1.008272478	8.99E-05
ABUW_RS00935	excinuclease ABC subunit UvrA	-1.012766849	0.004743056
ABUW_RS11700	FMN-binding negative transcriptional regulator	-1.013578871	0.003307113
ABUW_RS08560	amino acid permease	-1.016042678	0.031523497
ABUW_RS02825	DUF3380 domain-containing protein	-1.017543505	0.005200804
ABUW_RS06250	hypothetical protein	-1.017702195	0.018267135
ABUW_RS18105	DUF2946 family protein	-1.017803591	0.051677008
ABUW_RS14265	MFS transporter	-1.018253368	0.138917095
ABUW_RS18185	F0F1 ATP synthase subunit B	-1.018284844	0.32676538
ABUW_RS02330	16S ribosomal RNA	-1.018838754	0.188054117
ABUW_RS12190	MFS transporter	-1.019214564	0.041272955
ABUW_RS05720	acinetobactin non-ribosomal peptide synthetase subunit BasB	-1.019953072	0.264867038
ABUW_RS17330	DUF1656 domain-containing protein	-1.02103794	0.000705513
ABUW_RS18280	glutamine-hydrolyzing GMP synthase	-1.02192596	0.026731469
sRNA37	no	-1.022739222	0.165788583
ABUW_RS02870	phage portal protein	-1.023767416	0.011401671
ABUW_RS19405	hypothetical protein	-1.025523601	0.048059345
ABUW_RS19060	hypothetical protein	-1.025951613	0.021335589
ABUW_RS08070	TonB-dependent siderophore receptor	-1.02675143	0.107453481
ABUW_RS04720	GtrA family protein	-1.02991668	0.061101862
ABUW_RS13445	alpha/beta hydrolase	-1.031014722	0.020524204
ABUW_RS13370	adenosine deaminase	-1.031189819	0.027499387
ABUW_RS16580	Sec-independent protein translocase subunit TatA	-1.03216821	0.000789028
ABUW_RS11815	hypothetical protein	-1.03620609	0.001484157
ABUW_RS12230	hypothetical protein	-1.037750999	0.386798781
ABUW_RS20510	hypothetical protein	-1.037825832	0.044356073
ABUW_RS05840	xanthine dehydrogenase small subunit	-1.038092537	0.000603999
ABUW_RS12125	carboxymuconolactone decarboxylase family protein	-1.0390616	0.120213062
ABUW_RS17845	Cd(II)/Pb(II)-responsive transcriptional regulator	-1.039450408	0.022712804
ABUW_RS04970	7-carboxy-7-deazaguanine synthase QueE	-1.040227982	0.180036757
ABUW_RS12200	CoA transferase	-1.042201405	0.176870301
ABUW_RS02020	50S ribosomal protein L22	-1.042709206	0.217865598
ABUW_RS01025	pirin family protein	-1.045600689	0.051678043
ABUW_RS15820	16S ribosomal RNA	-1.046482685	0.17630669
ABUW_RS14495	TonB-dependent receptor	-1.048449051	0.144782812
ABUW_RS00865	acetate--CoA ligase	-1.048708654	0.114640853
ABUW_RS10345	2-oxo acid dehydrogenase subunit E2	-1.049105549	0.030403066
ABUW_RS12130	NAD-dependent succinate-semialdehyde dehydrogenase	-1.05115705	0.042367972
sRNA44	no	-1.052052431	0.470108999
ABUW_RS07685	acyl-CoA dehydrogenase family protein	-1.052615617	0.074573285
ABUW_RS09390	DMT family transporter	-1.0529853	0.018737783
ABUW_RS12965	transposase	-1.053543415	0.095325274
ABUW_RS07015	hypothetical protein	-1.056230479	0.019415957
ABUW_RS19790	helix-turn-helix transcriptional regulator	-1.056973934	0.07462813
ABUW_RS19780	signal recognition particle sRNA small type	-1.057541534	0.154252017
ABUW_RS09025	OprD family outer membrane porin	-1.058513183	0.019665469
ABUW_RS11365	LLM class flavin-dependent oxidoreductase	-1.058613722	0.001123006
ABUW_RS11470	dicarboxylate/amino acid:cation symporter	-1.059676565	0.08593369
ABUW_RS00655	allantoinase PuuE	-1.059811344	2.57E-06
ABUW_RS01995	50S ribosomal protein L3	-1.059871958	0.19810001
ABUW_RS12915	fibronectin type III domain-containing protein	-1.060211763	0.004990961
ABUW_RS17600	response regulator transcription factor	-1.060611677	0.000237449
ABUW_RS02850	terminase	-1.06128995	0.003659777
ABUW_RS10260	ferredoxin family protein	-1.064506501	0.040779345
ABUW_RS13930	dioxygenase	-1.064535871	0.00692906
ABUW_RS05650	hypothetical protein	-1.065758945	0.003748572
ABUW_RS09530	TetR/AcrR family transcriptional regulator	-1.065878585	0.019567248
ABUW_RS19455	lytic transglycosylase domain-containing protein	-1.065956401	0.001881292
ABUW_RS10835	energy transducer TonB	-1.066162758	0.010403774
ABUW_RS06375	hypothetical protein	-1.069192031	0.04134821
ABUW_RS09485	DHA2 family efflux MFS transporter permease subunit	-1.069564897	0.039907908
ABUW_RS16185	hypothetical protein	-1.070757709	0.001752881
sRNA70	no	-1.070897161	0.022576237
ABUW_RS14490	transferrin-binding protein-like solute binding protein	-1.071651347	0.212932753
ABUW_RS13170	benzoate/H(+) symporter BenE	-1.073962155	0.011422775
ABUW_RS06445	DUF1833 family protein	-1.073968841	0.002730537
ABUW_RS14225	SDR family oxidoreductase	-1.074393477	0.004119203
ABUW_RS14750	GNAT family N-acetyltransferase	-1.07475534	0.003934041
ABUW_RS05175	glutamate 5-kinase	-1.07674298	0.011163857
ABUW_RS00985	AzlC family ABC transporter permease	-1.076970195	0.014535819
ABUW_RS15605	LysR family transcriptional regulator	-1.078278465	0.002638061
ABUW_RS15755	hypothetical protein	-1.079742762	0.102382403
ABUW_RS09505	hypothetical protein	-1.08101387	0.004874582
ABUW_RS11370	methionine transporter	-1.081173693	0.017496349
ABUW_RS12615	TetR/AcrR family transcriptional regulator	-1.081331547	0.040516058
ABUW_RS10230	MFS transporter	-1.083289039	0.187747829
ABUW_RS07300	ADP-ribose pyrophosphatase	-1.084892652	0.372940358
ABUW_RS04725	glycosyltransferase family 2 protein	-1.085657967	0.034032893
ABUW_RS14935	tartrate dehydrogenase	-1.087794713	0.001785854
ABUW_RS02645	site-specific integrase	-1.089837036	0.0231046
ABUW_RS09085	transcriptional regulator FeaR	-1.090665856	0.087530403
ABUW_RS06290	hypothetical protein	-1.090863721	0.011079238
ABUW_RS07220	SDR family oxidoreductase	-1.092987478	0.05254232
ABUW_RS19395	hypothetical protein	-1.093601017	0.000645294
ABUW_RS06530	ABC transporter substrate-binding protein	-1.095833331	0.005216713
ABUW_RS18345	hypothetical protein	-1.096658255	0.000213215
ABUW_RS19475	conjugal transfer protein TraE	-1.097571899	1.81E-05

ABUW_RS08960	right-handed parallel beta-helix repeat-containing protein	-1.098216332	0.000231827
ABUW_RS06980	hypothetical protein	-1.098799705	0.002204836
ABUW_RS10350	alpha-ketoacid dehydrogenase subunit beta	-1.099247104	0.086014946
ABUW_RS04195	helix-turn-helix transcriptional regulator	-1.101497494	0.111362115
ABUW_RS04625	glycerate kinase	-1.102158075	0.004119203
ABUW_RS04070	ammonium transporter	-1.102174336	0.002455048
ABUW_RS05445	alpha-keto acid decarboxylase family protein	-1.102976398	0.11569741
ABUW_RS06545	ATP-binding cassette domain-containing protein	-1.104647193	0.000250842
ABUW_RS15250	hypothetical protein	-1.105608081	0.008513149
sRNA60	no	-1.107703238	0.011422775
ABUW_RS19490	DsbC family protein	-1.110682894	0.001597096
ABUW_RS18100	TonB-dependent copper receptor	-1.111347343	0.109156923
ABUW_RS09565	SDR family NAD(P)-dependent oxidoreductase	-1.111842127	0.007289865
ABUW_RS13410	metal-dependent hydrolase	-1.112184118	0.02713537
ABUW_RS17920	PLP-dependent aminotransferase family protein	-1.112843449	0.000129407
ABUW_RS16180	hypothetical protein	-1.113475596	0.000129407
ABUW_RS03505	Asp-tRNA(Asn)/Glu-tRNA(Gln) amidotransferase subunit GatB	-1.114084267	0.00027044
ABUW_RS18425	LysR family transcriptional regulator	-1.114859286	0.005262179
ABUW_RS11745	rhodanese-like domain-containing protein	-1.115208274	0.015440727
ABUW_RS19515	signal peptidase I	-1.116260426	0.000836419
ABUW_RS09630	FAD-binding oxidoreductase	-1.117501843	0.007008883
ABUW_RS18455	Lrp/AsnC ligand binding domain-containing protein	-1.118184529	0.005658766
ABUW_RS18705	acyl-CoA desaturase	-1.118771406	0.001051069
ABUW_RS05690	TetR/AcrR family transcriptional regulator	-1.11937084	0.014418568
ABUW_RS12195	hydroxymethylglutaryl-CoA lyase	-1.120418505	0.028832474
ABUW_RS09110	3-oxoadipate enol-lactonase	-1.121443245	0.001204237
ABUW_RS09490	hypothetical protein	-1.122757786	0.01189
ABUW_RS10365	transcriptional regulator	-1.123573336	0.10327742
ABUW_RS10270	GntR family transcriptional regulator	-1.125443995	0.009378482
ABUW_RS02830	phage holin family protein	-1.128333547	0.014501294
ABUW_RS17120	30S ribosomal protein S15	-1.131948345	0.02033135
ABUW_RS19520	type-F conjugative transfer system protein TraW	-1.134041915	0.000201774
ABUW_RS13715	NADPH-dependent 2,4-dienoyl-CoA reductase	-1.134640572	4.36E-05
ABUW_RS09855	hypothetical protein	-1.136962549	0.044116633
ABUW_RS10795	SOS response-associated peptidase family protein	-1.137520709	0.000640491
ABUW_RS15165	trehalose-6-phosphate synthase	-1.140743802	0.122682549
ABUW_RS13385	NAD(P)/FAD-dependent oxidoreductase	-1.141972059	0.008103519
ABUW_RS12360	fosfomycin efflux MFS transporter AbaF	-1.142075518	0.000584124
ABUW_RS12440	nucleoside deaminase	-1.143130992	0.003652743
ABUW_RS09670	hypothetical protein	-1.14398082	0.138917095
ABUW_RS12290	3-hydroxyacyl-CoA dehydrogenase	-1.144216818	0.065289288
ABUW_RS15510	TetR/AcrR family transcriptional regulator	-1.145643002	0.031117869
ABUW_RS07335	hydroxyisourate hydrolase	-1.147782043	0.000179947
ABUW_RS17935	hypothetical protein	-1.147877325	4.44E-09
ABUW_RS02710	hypothetical protein	-1.149827664	0.084855184
ABUW_RS17835	signal peptidase II	-1.150686802	0.047527244
ABUW_RS18025	esterase-like activity of phytase family protein	-1.151561415	0.006406039
ABUW_RS06285	hypothetical protein	-1.153208536	0.093104471
ABUW_RS06365	hypothetical protein	-1.153978803	0.005658766
ABUW_RS11970	acyl-CoA dehydrogenase C-terminal domain-containing protein	-1.154225927	0.000327943
ABUW_RS16885	DUF1345 domain-containing protein	-1.154255641	1.97E-07
ABUW_RS14485	DUF560 domain-containing protein	-1.156078052	0.143811
ABUW_RS10250	ABC transporter permease	-1.158695531	1.10E-06
ABUW_RS14385	C4-dicarboxylate transporter DctA	-1.158851676	0.00171028
ABUW_RS12120	LysR family transcriptional regulator	-1.16026978	0.001827148
ABUW_RS16965	SfnB family sulfur acquisition oxidoreductase	-1.160977725	0.000699682
ABUW_RS03960	hypothetical protein	-1.161322261	0.003104469
ABUW_RS01080	AraC family transcriptional regulator	-1.161703716	0.019665469
ABUW_RS01895	ABC transporter substrate-binding protein	-1.162359463	1.84E-06
ABUW_RS07670	aliphatic sulfonate ABC transporter substrate-binding protein	-1.162629696	0.001406094
ABUW_RS13120	four-helix bundle copper-binding protein	-1.162670957	0.111096171
ABUW_RS14625	DNA-binding protein	-1.164397621	0.007818315
ABUW_RS19530	type-F conjugative transfer system pilin assembly protein TrbC	-1.164941816	0.000780172
ABUW_RS11715	CidA/LrgA family protein	-1.166371797	0.010495501
ABUW_RS12210	TetR/AcrR family transcriptional regulator	-1.166643238	0.205934792
ABUW_RS13545	glucarate dehydratase	-1.167199168	8.25E-05
ABUW_RS07225	SRPBCC family protein	-1.168630559	0.035914079
ABUW_RS09445	NAD(P)-dependent oxidoreductase	-1.169055325	0.071905873
ABUW_RS11655	malonate decarboxylase subunit epsilon	-1.171805798	0.010670975
ABUW_RS16195	hypothetical protein	-1.173833108	3.95E-05
ABUW_RS11650	malonate transporter subunit MadL	-1.173996744	0.061067699
ABUW_RS09510	acid phosphatase	-1.174657984	0.009104123
ABUW_RS19495	hypothetical protein	-1.175325427	0.110109934
ABUW_RS11380	ATP-binding cassette domain-containing protein	-1.176771558	7.03E-06
ABUW_RS04605	helix-turn-helix transcriptional regulator	-1.177179811	0.021763438
ABUW_RS00775	2-oxo acid dehydrogenase subunit E2	-1.179073608	0.01222998
ABUW_RS05645	ethanolamine utilization protein EutQ	-1.179846869	0.000250917
ABUW_RS01735	N-succinylarginine dihydrolase	-1.180247362	0.111362115
ABUW_RS19070	hypothetical protein	-1.180749512	0.015523221
ABUW_RS04080	AEC family transporter	-1.18220679	4.06E-05
ABUW_RS09080	flavin reductase family protein	-1.182464237	0.003799915
ABUW_RS06465	hypothetical protein	-1.183764323	0.056376397
ABUW_RS11865	CinA family protein	-1.184010277	0.226732987
ABUW_RS09140	muconate cycloisomerase	-1.184762136	0.004893099
ABUW_RS12095	putative 2-aminoethylphosphonate ABC transporter substrate-binding protein	-1.185159654	0.000975773
ABUW_RS20230	hypothetical protein	-1.18531397	0.291253478
ABUW_RS19605	BrnT family toxin	-1.185461476	0.002241072
ABUW_RS07615	poly-beta-1,6-N-acetyl-D-glucosamine biosynthesis protein PgaD	-1.187920123	0.004111795
ABUW_RS13635	FAD-binding oxidoreductase	-1.190667343	0.000602844
ABUW_RS12550	ABC transporter permease	-1.190850669	0.000204176
ABUW_RS12045	enoyl-CoA hydratase	-1.191139844	0.000390132
ABUW_RS06500	alpha/beta fold hydrolase	-1.192518065	0.062292396
ABUW_RS09360	amidohydrolase family protein	-1.192643225	0.003394334
ABUW_RS16445	glycosyltransferase family 1 protein	-1.196686327	0.000877928
ABUW_RS15600	acyl-CoA dehydrogenase	-1.196895964	0.003394449
ABUW_RS00640	purine permease	-1.197082475	1.55E-05
ABUW_RS12020	3-hydroxyacyl-CoA dehydrogenase	-1.197476157	0.002075519
ABUW_RS13230	ExeM/NucH family extracellular endonuclease	-1.197790853	0.002246659
ABUW_RS00970	MFS transporter	-1.199033258	0.002452426
ABUW_RS02855	phage major capsid protein, P2 family	-1.199674111	0.000231827

sRNA88	no	-1.200015384	0.07076901
ABUW_RS19525	TraU family protein	-1.200890938	7.61E-06
ABUW_RS14605	hypothetical protein	-1.203046195	0.011318841
ABUW_RS15240	hypothetical protein	-1.203934054	0.016995743
ABUW_RS01740	succinylglutamate desuccinylase	-1.205512364	0.053385356
ABUW_RS19190	hypothetical protein	-1.205871352	0.010933897
ABUW_RS05005	alpha/beta hydrolase	-1.209656577	0.343384542
ABUW_RS11510	chromate transporter	-1.210004611	0.013631769
ABUW_RS06535	histidine ABC transporter permease HisQ	-1.211916425	0.000661933
ABUW_RS09705	hypothetical protein	-1.212650673	0.026547673
ABUW_RS20215	hypothetical protein	-1.215594606	0.030540297
ABUW_RS10265	fumarate reductase/succinate dehydrogenase flavoprotein subunit	-1.21708231	0.000325257
ABUW_RS03935	tape measure protein	-1.21775466	2.22E-06
ABUW_RS02640	tRNA-Leu	-1.219047365	0.17630669
ABUW_RS14560	DUF4391 domain-containing protein	-1.220205312	0.001657812
ABUW_RS09805	hypothetical protein	-1.220311478	0.034881695
ABUW_RS09755	hypothetical protein	-1.221159015	0.042615815
ABUW_RS20150	hypothetical protein	-1.224575966	0.026510892
ABUW_RS00645	hydroxyisourate hydrolase	-1.22567739	1.17E-05
ABUW_RS11785	amino acid ABC transporter ATP-binding protein	-1.227460267	0.121133959
ABUW_RS12385	4-hydroxyproline epimerase	-1.229377655	1.71E-05
ABUW_RS14500	FecR domain-containing protein	-1.231563175	0.056689486
ABUW_RS05290	YbfB/YjiJ family MFS transporter	-1.231765625	2.97E-05
ABUW_RS13540	5-dehydro-4-deoxyglucarate dehydratase	-1.232183092	0.002131975
ABUW_RS17475	DNA-directed RNA polymerase subunit beta	-1.232860387	0.031240017
ABUW_RS07340	heme-binding protein	-1.234093844	0.000172532
ABUW_RS05680	hypothetical protein	-1.236628656	4.28E-05
ABUW_RS14615	hypothetical protein	-1.238070724	0.00393348
ABUW_RS18350	outer membrane lipoprotein-sorting protein	-1.238713543	4.22E-09
ABUW_RS11325	hypothetical protein	-1.240829618	0.003211492
ABUW_RS11810	response regulator	-1.240908104	0.000133961
ABUW_RS15160	trehalose-phosphatase	-1.241504245	0.136747625
ABUW_RS11530	metalloregulator ArsR/SmtB family transcription factor	-1.243329468	0.024825045
ABUW_RS00630	FAD-dependent urate hydroxylase HpxO	-1.243621707	5.34E-07
ABUW_RS08910	3-oxoacid CoA-transferase subunit A	-1.244173094	0.01546749
ABUW_RS00650	2-oxo-4-hydroxy-4-carboxy-5-ureidoimidazoline decarboxylase	-1.244459736	0.000249031
ABUW_RS14410	choline transporter	-1.244918508	0.015523221
ABUW_RS11565	NCS1 family nucleobase:cation symporter-1	-1.247155656	0.001402419
ABUW_RS05335	type I-F CRISPR-associated endonuclease Cas1	-1.247869541	0.015536103
ABUW_RS19065	hypothetical protein	-1.248075019	0.00051314
ABUW_RS12040	nitronate monooxygenase	-1.248198209	0.021387655
ABUW_RS00880	dimethyl sulfone monooxygenase SfnG	-1.249965981	4.54E-07
ABUW_RS16175	hypothetical protein	-1.252877016	0.000550688
ABUW_RS12110	IclR family transcriptional regulator PobR	-1.253393779	0.000500039
ABUW_RS09425	fumarylacetoacetate hydrolase family protein	-1.254200855	0.011381273
ABUW_RS06360	hypothetical protein	-1.254256821	0.000364947
ABUW_RS19610	BrnA antitoxin family protein	-1.254333857	0.000517814
ABUW_RS16160	copper resistance protein CopC	-1.254410537	0.000177749
ABUW_RS12215	hypothetical protein	-1.256362966	0.064471308
ABUW_RS17830	ISL3-like element ISPpu12 family transposase	-1.256680989	0.003097139
ABUW_RS00605	hypothetical protein	-1.257296136	2.30E-07
ABUW_RS12560	ABC transporter substrate-binding protein	-1.257451947	0.000672666
ABUW_RS15470	ribonucleotide-diphosphate reductase subunit beta	-1.257572311	0.001484157
ABUW_RS10150	MFS transporter	-1.257773588	0.010691495
ABUW_RS20380	hypothetical protein	-1.259023019	2.03E-11
ABUW_RS01165	AraC family transcriptional regulator	-1.260681227	1.38E-05
ABUW_RS14160	TonB-dependent siderophore receptor	-1.261745253	0.030403066
ABUW_RS12165	amino acid synthesis family protein	-1.262117112	0.109787378
ABUW_RS19275	aminoglycoside N-acetyltransferase AAC(6')-Ib3	-1.262699396	0.024061289
ABUW_RS09890	hypothetical protein	-1.26422055	0.014680447
ABUW_RS13435	NAD(P)/FAD-dependent oxidoreductase	-1.265749118	0.006778139
ABUW_RS17850	universal stress protein	-1.266008355	6.96E-05
ABUW_RS19500	type IV conjugative transfer system lipoprotein TraV	-1.266718428	0.002730537
ABUW_RS11705	PLP-dependent aminotransferase family protein	-1.272552621	0.0004866
ABUW_RS05710	acinetobactin utilization protein BauF	-1.27325864	0.116151203
ABUW_RS09090	primary-amine oxidase	-1.273335228	0.000988708
ABUW_RS01730	succinylglutamate-semialdehyde dehydrogenase	-1.274143313	0.075599258
ABUW_RS15245	hypothetical protein	-1.274528597	0.009172829
ABUW_RS11670	biotin-independent malonate decarboxylase subunit beta	-1.276416949	0.009914261
ABUW_RS11665	biotin-independent malonate decarboxylase subunit gamma	-1.276710171	0.001564244
sRNA63	no	-1.277278758	0.004352329
sRNA56	no	-1.279703313	0.216168041
ABUW_RS12145	aldehyde dehydrogenase	-1.279776027	0.0002055
ABUW_RS09105	penicillin acylase family protein	-1.279954368	3.87E-05
ABUW_RS18035	DUF2938 domain-containing protein	-1.280622972	0.000172103
ABUW_RS09380	MFS transporter	-1.28090762	0.030403066
ABUW_RS14600	DUF927 domain-containing protein	-1.281751727	3.41E-05
ABUW_RS12895	hypothetical protein	-1.284550416	0.028314368
ABUW_RS10340	dihydrolipoyl dehydrogenase	-1.285127427	0.00133761
ABUW_RS09605	multidrug efflux RND transporter permease subunit AdeB	-1.285832789	0.003086915
ABUW_RS17125	EstA family serine hydrolase	-1.288502979	2.27E-08
ABUW_RS01370	hypothetical protein	-1.289051901	0.001727772
ABUW_RS16960	acyl-CoA dehydrogenase family protein	-1.289398221	5.16E-05
sRNA7	no	-1.291554461	0.137689612
ABUW_RS16465	alpha/beta hydrolase	-1.292153063	0.00731336
ABUW_RS18365	acyl-CoA dehydrogenase	-1.295197084	0.001219482
ABUW_RS12055	CoA transferase	-1.295959351	0.002759195
ABUW_RS05635	FAD-dependent oxidoreductase	-1.29647513	8.37E-06
ABUW_RS02150	hypothetical protein	-1.296497165	0.051273097
ABUW_RS16585	twin-arginine translocase subunit TatB	-1.298070272	3.44E-05
ABUW_RS19480	type-F conjugative transfer system secretin TraK	-1.29973972	0.000147891
ABUW_RS09810	replication initiation factor domain-containing protein	-1.30049481	0.015707051
ABUW_RS05760	(2,3-dihydroxybenzoyl)adenylate synthase BasE	-1.300497909	0.216114744
ABUW_RS08965	carbohydrate porin	-1.300901486	0.004489387
ABUW_RS15540	fatty acid desaturase	-1.301159451	3.91E-06
ABUW_RS14175	arylsulfatase	-1.302257067	2.60E-05
ABUW_RS09440	MFS transporter	-1.303347876	0.06551713
ABUW_RS04575	non-ribosomal peptide synthetase	-1.303763406	0.000491331
ABUW_RS09710	replication initiation factor domain-containing protein	-1.305258551	0.016995743
ABUW_RS13455	OprD family outer membrane porin	-1.305610754	0.016556633

ABUW_RS09365	SLC13 family permease	-1.306882371	0.005031563
ABUW_RS12005	acyl-CoA dehydrogenase family protein	-1.307224283	0.002598792
sRNA22	no	-1.307567842	0.023432628
ABUW_RS07375	class I SAM-dependent methyltransferase	-1.311417675	0.001564244
ABUW_RS09135	muconolactone Delta-isomerase	-1.312348829	0.002535125
ABUW_RS09860	replication initiation factor domain-containing protein	-1.313178857	0.016146774
ABUW_RS02395	enoyl-CoA hydratase/isomerase family protein	-1.313283821	3.31E-05
ABUW_RS12875	site-specific integrase	-1.314684739	0.006092155
ABUW_RS19240	hypothetical protein	-1.320342513	0.044201273
ABUW_RS09760	replication initiation factor domain-containing protein	-1.323942918	0.011142904
ABUW_RS09495	GH3 auxin-responsive promoter family protein	-1.327061886	1.20E-05
ABUW_RS06960	hypothetical protein	-1.328167412	5.11E-05
ABUW_RS00980	AzlD domain-containing protein	-1.330345039	5.07E-05
ABUW_RS18110	peptide deformylase	-1.332692683	0.000697876
ABUW_RS14510	LysR family transcriptional regulator	-1.336025524	6.22E-05
ABUW_RS14925	alpha/beta hydrolase	-1.337903599	0.001437655
ABUW_RS13025	MFS transporter	-1.339286252	0.001458024
ABUW_RS18990	CDF family Co(II)/Ni(II) efflux transporter DmeF	-1.3396828	1.63E-06
ABUW_RS00885	FMN reductase	-1.340792315	0.001326146
ABUW_RS06955	hypothetical protein	-1.341771689	0.01445437
ABUW_RS01715	Glu/Leu/Phe/Val dehydrogenase	-1.341887596	0.008577947
ABUW_RS13535	aldehyde dehydrogenase (NADP(+))	-1.342140205	6.81E-09
ABUW_RS06540	ABC transporter permease	-1.345272659	0.000166411
ABUW_RS02800	baseplate J/gp47 family protein	-1.347890852	0.000912524
ABUW_RS16600	PhoX family phosphatase	-1.349245524	5.91E-08
ABUW_RS07360	acyl-CoA desaturase	-1.349331707	0.00061368
ABUW_RS02785	phage tail sheath protein	-1.351999984	0.000525053
ABUW_RS16595	DUF839 domain-containing protein	-1.352947071	8.05E-08
ABUW_RS11750	serine acetyltransferase	-1.354843798	0.004505636
ABUW_RS01600	lipase secretion chaperone	-1.355140358	0.026588444
ABUW_RS06295	DUF2280 domain-containing protein	-1.356599446	0.001027103
ABUW_RS09250	metal-dependent hydrolase	-1.357353235	0.000131959
ABUW_RS14315	VOC family protein	-1.359345044	1.06E-05
ABUW_RS06510	multidrug efflux RND transporter outer membrane subunit AdeH	-1.359533834	1.59E-05
ABUW_RS12370	NAD(P)/FAD-dependent oxidoreductase	-1.359827541	4.37E-05
ABUW_RS05730	ferric acinetobactin ABC transporter permease subunit BauC	-1.361775422	0.053999702
ABUW_RS19135	hypothetical protein	-1.362280823	NA
ABUW_RS07725	potassium-transporting ATPase subunit KdpB	-1.362486977	4.57E-08
ABUW_RS09940	hypothetical protein	-1.370116014	0.005658766
ABUW_RS11375	MetQ/NlpA family ABC transporter substrate-binding protein	-1.371648758	0.000159545
ABUW_RS07720	potassium-transporting ATPase subunit KdpA	-1.371757604	0.000277086
ABUW_RS13415	SDR family NAD(P)-dependent oxidoreductase	-1.372668386	0.000339058
ABUW_RS08955	type I 3-dehydroquinate dehydratase	-1.372833918	0.001045527
ABUW_RS14930	BCCT family carnitine transporter	-1.373341351	2.24E-07
ABUW_RS13395	metal-dependent hydrolase	-1.374735311	0.00018921
ABUW_RS01755	S8 family serine peptidase	-1.377536864	3.18E-06
ABUW_RS01725	arginine N-succinyltransferase	-1.380519238	0.053999702
ABUW_RS17915	ATP-binding protein	-1.381208427	3.14E-08
ABUW_RS12060	acyl-CoA dehydrogenase family protein	-1.381440946	0.000556034
ABUW_RS13165	1,6-dihydroxycyclohexa-2,4-diene-1-carboxylate dehydrogenase	-1.381597606	2.15E-05
ABUW_RS09100	NAD-dependent phenylacetaldehyde dehydrogenase	-1.383067259	5.17E-05
ABUW_RS12960	DUF2280 domain-containing protein	-1.384210897	0.010463041
ABUW_RS01710	amino acid permease	-1.386146057	0.085512941
ABUW_RS15535	LysE family translocator	-1.38996943	6.10E-05
ABUW_RS11755	hypothetical protein	-1.39162339	0.008290918
ABUW_RS08285	ANTAR domain-containing protein	-1.392745129	0.004147069
ABUW_RS12675	hypothetical protein	-1.393594678	0.002112465
ABUW_RS06520	multidrug efflux RND transporter periplasmic adaptor subunit AdeF	-1.393746843	0.000445785
ABUW_RS18450	D-amino acid dehydrogenase	-1.394740367	0.026248882
ABUW_RS06020	MFS transporter	-1.394995591	2.43E-05
ABUW_RS14415	BCCT family transporter	-1.395202214	0.000695521
ABUW_RS12105	4-hydroxybenzoate 3-monooxygenase	-1.39569346	0.004690736
ABUW_RS08290	hypothetical protein	-1.395718452	0.072799747
ABUW_RS13180	OprD family outer membrane porin	-1.397109228	2.59E-05
ABUW_RS02810	phage baseplate assembly protein V	-1.398731212	0.005200804
ABUW_RS19230	hypothetical protein	-1.399555385	1.35E-05
ABUW_RS09255	NADH:flavin oxidoreductase/NADH oxidase family protein	-1.400011854	6.96E-05
ABUW_RS02835	membrane protein	-1.400217018	0.001433924
ABUW_RS18495	IS256-like element ISAba26 family transposase	-1.401080052	1.42E-14
ABUW_RS11760	cysteine desulfurase	-1.401259857	6.84E-05
ABUW_RS08925	3-carboxy-cis,cis-muconate cycloisomerase	-1.406404035	3.92E-05
ABUW_RS10125	transporter	-1.408371064	0.002759195
ABUW_RS02865	terminase family protein	-1.414199971	0.007818315
ABUW_RS00040	RND transporter	-1.414264947	7.68E-09
ABUW_RS01170	hypothetical protein	-1.414291028	4.46E-05
ABUW_RS12350	APC family permease	-1.416573483	0.004874582
ABUW_RS02795	phage tail protein I	-1.418436567	0.007091467
ABUW_RS12140	cytosine permease	-1.430356643	0.000120507
ABUW_RS13160	ring-hydroxylating dioxygenase ferredoxin reductase family protein	-1.432297069	2.30E-07
ABUW_RS12085	putative 2-aminoethylphosphonate ABC transporter permease subunit	-1.437098663	5.60E-06
ABUW_RS08935	MFS transporter	-1.43761292	0.000175253
ABUW_RS12065	MFS transporter	-1.437621029	0.000435903
ABUW_RS09715	hypothetical protein	-1.437659246	0.062674565
ABUW_RS12070	phosphonoacetaldehyde hydrolase	-1.439196631	3.04E-07
ABUW_RS12295	2-(1,2-epoxy-1,2-dihydrophenyl)acetyl-CoA isomerase	-1.43967437	0.066262739
ABUW_RS02840	tail protein X	-1.445038492	0.000906592
ABUW_RS09095	hypothetical protein	-1.445491781	0.015440727
ABUW_RS14420	transcriptional regulator BetI	-1.445982157	0.003535308
ABUW_RS14245	MFS transporter	-1.446317883	5.48E-10
ABUW_RS12010	enoyl-CoA hydratase	-1.449411866	0.000596205
ABUW_RS14310	FAD-dependent oxidoreductase	-1.450088035	8.17E-05
ABUW_RS16215	inovirus-type Gp2 protein	-1.450395975	4.45E-06
ABUW_RS18040	flavodoxin family protein	-1.452785304	1.13E-07
ABUW_RS08125	benzoate/H(+) symporter BenE family transporter	-1.452846925	0.010324564
ABUW_RS06450	hypothetical protein	-1.454593287	0.00119624
ABUW_RS06305	DUF4055 domain-containing protein	-1.456750996	9.52E-05
ABUW_RS01900	STAS domain-containing protein	-1.457388216	1.13E-07
ABUW_RS14515	dihydrodipicolinate synthase family protein	-1.462821967	0.00015246
ABUW_RS09815	hypothetical protein	-1.465604978	0.026459426
ABUW_RS07380	DUF1295 domain-containing protein	-1.467501981	0.000100005

ABUW_RS09120	CoA transferase subunit B	-1.467882908	0.000562211
ABUW_RS19140	ParA family protein	-1.46797624	0.00494707
ABUW_RS07610	poly-beta-1,6 N-acetyl-D-glucosamine synthase	-1.468315372	2.64E-05
ABUW_RS12300	enoyl-CoA hydratase/isomerase family protein	-1.470461282	0.036478844
ABUW_RS12025	3-oxoadipyl-CoA thiolase	-1.471834316	0.001727772
ABUW_RS09435	SDR family oxidoreductase	-1.47253373	0.019665469
ABUW_RS15590	CoA transferase	-1.47276603	5.76E-07
ABUW_RS01085	TetR/AcrR family transcriptional regulator	-1.477311212	0.057554717
ABUW_RS07730	potassium-transporting ATPase subunit KdpC	-1.481828772	2.57E-06
ABUW_RS08940	4-carboxymuconolactone decarboxylase	-1.485433785	3.41E-05
ABUW_RS09165	multidrug efflux MFS transporter AbaQ	-1.487479618	4.36E-05
ABUW_RS11905	SGNH/GDSL hydrolase family protein	-1.491517212	0.001916509
ABUW_RS11515	chromate transporter	-1.492454107	0.003774325
ABUW_RS03870	hypothetical protein	-1.493640078	0.001190183
ABUW_RS11910	hypothetical protein	-1.494464937	0.071905873
ABUW_RS01595	triacylglycerol lipase	-1.495071445	0.021427664
ABUW_RS14335	non-heme iron oxygenase ferredoxin subunit	-1.496370277	0.002695462
ABUW_RS15465	hypothetical protein	-1.497547724	0.006161868
ABUW_RS02655	hypothetical protein	-1.499383412	3.01E-05
ABUW_RS18390	MHS family MFS transporter	-1.499408977	0.103630561
ABUW_RS12015	SDR family oxidoreductase	-1.49968445	1.59E-05
ABUW_RS14620	hypothetical protein	-1.501017379	3.44E-05
ABUW_RS02805	GPW/gp25 family protein	-1.502599549	0.001305964
sRNA5	no	-1.502990308	0.150278161
ABUW_RS00285	hypothetical protein	-1.506117702	0.019431279
ABUW_RS02845	head completion/stabilization protein	-1.508705469	0.00015246
ABUW_RS15610	zinc-binding dehydrogenase	-1.509239559	2.30E-08
ABUW_RS12355	aldehyde dehydrogenase (NADP(+))	-1.514664877	0.000308411
ABUW_RS11990	3-oxoacid CoA-transferase subunit B	-1.515453736	4.34E-07
ABUW_RS05630	aldehyde dehydrogenase family protein	-1.515883135	4.20E-08
ABUW_RS09070	SDR family oxidoreductase	-1.516361192	6.10E-05
ABUW_RS01720	aspartate aminotransferase family protein	-1.51762029	0.007165739
ABUW_RS18695	phospholipase C, phosphocholine-specific	-1.518950792	9.00E-11
ABUW_RS14405	MarC family protein	-1.519442576	0.000975773
ABUW_RS06460	hypothetical protein	-1.523396055	0.002414403
ABUW_RS00485	hypothetical protein	-1.523638777	2.04E-05
ABUW_RS06355	hypothetical protein	-1.525092588	0.000202833
ABUW_RS09130	catechol 1,2-dioxygenase	-1.528182379	0.000152358
ABUW_RS13175	aromatic acid/H+ symport family MFS transporter	-1.534139066	0.000145685
ABUW_RS19470	type IV conjugative transfer system protein TraL	-1.534236678	5.17E-08
ABUW_RS01750	hypothetical protein	-1.53663343	0.002217858
ABUW_RS20225	alpha/beta hydrolase	-1.537518187	0.001027103
ABUW_RS09420	dihydroxy-acid dehydratase family protein	-1.538143697	0.002691217
ABUW_RS12220	hypothetical protein	-1.54069807	0.16042716
ABUW_RS13440	SDR family oxidoreductase	-1.541332491	4.06E-05
ABUW_RS02155	rhombosortase	-1.54144157	0.010933897
ABUW_RS00975	single-stranded DNA-binding protein	-1.543277814	6.93E-06
ABUW_RS09600	multidrug efflux RND transporter periplasmic adaptor subunit AdeA	-1.547156008	0.058731259
ABUW_RS19270	trimethoprim-resistant dihydrofolate reductase DfrA7	-1.553132511	0.000997134
ABUW_RS07215	aldo/keto reductase	-1.554971812	0.004926172
ABUW_RS14210	transketolase	-1.558415572	0.000697876
ABUW_RS06965	lytic transglycosylase domain-containing protein	-1.559063351	5.64E-06
ABUW_RS09075	oxidoreductase	-1.559512813	0.000185104
ABUW_RS03770	RelA/SpoT domain-containing protein	-1.56443856	0.002804987
ABUW_RS20220	flavin reductase family protein	-1.569907932	3.49E-05
ABUW_RS03950	hypothetical protein	-1.569969001	0.000243449
ABUW_RS12380	FAD-binding oxidoreductase	-1.570033224	2.28E-05
ABUW_RS14610	hypothetical protein	-1.57051911	0.005272751
ABUW_RS16170	DUF932 domain-containing protein	-1.572068265	3.42E-07
ABUW_RS05625	aromatic ring-hydroxylating dioxygenase subunit alpha	-1.576751538	2.39E-05
ABUW_RS09125	3-oxoacid CoA-transferase subunit A	-1.579704998	9.19E-05
ABUW_RS15585	tricarballylate utilization 4Fe-4S protein TcuB	-1.581842942	0.169229985
ABUW_RS06945	carbohydrate-binding protein	-1.584184771	2.98E-05
ABUW_RS11985	hypothetical protein	-1.587249628	5.59E-06
ABUW_RS09115	3-oxoadipyl-CoA thiolase	-1.588919424	2.48E-05
ABUW_RS19220	hypothetical protein	-1.590299677	8.79E-05
ABUW_RS12945	minor capsid protein	-1.591714347	0.003549135
ABUW_RS19260	sulfonamide-resistant dihydropteroate synthase Sul1	-1.5918555	0.016110746
ABUW_RS00050	hypothetical protein	-1.592612266	0.004955773
ABUW_RS11940	enoyl-CoA hydratase/isomerase family protein	-1.598545823	0.03477033
ABUW_RS07605	poly-beta-1,6-N-acetyl-D-glucosamine N-deacetylase PgaB	-1.601234838	1.12E-06
ABUW_RS15565	MFS transporter	-1.603683631	0.082330204
ABUW_RS08950	protocatechuate 3,4-dioxygenase subunit alpha	-1.604157343	2.24E-05
ABUW_RS18360	acyl carrier protein	-1.60438771	1.54E-05
ABUW_RS20460	hypothetical protein	-1.60489541	0.000349089
ABUW_RS06350	hypothetical protein	-1.604962597	0.000105194
ABUW_RS12000	MFS transporter	-1.609437872	1.13E-05
ABUW_RS11600	MFS transporter	-1.613909385	0.000342514
ABUW_RS13555	galactarate dehydratase	-1.616518458	0.001610165
ABUW_RS19265	quaternary ammonium compound efflux SMR transporter QacE delta 1	-1.62508991	0.001637929
ABUW_RS08295	nitrite reductase large subunit	-1.625528055	2.80E-06
ABUW_RS08515	recombinase RecA	-1.627069983	5.50E-09
ABUW_RS08300	nitrite reductase small subunit NirD	-1.628317668	1.57E-06
ABUW_RS13265	hypothetical protein	-1.628781696	1.75E-05
ABUW_RS18775	aliphatic sulfonate ABC transporter permease SsuC	-1.62985268	5.20E-05
ABUW_RS14275	thiamine pyrophosphate-binding protein	-1.632119697	3.21E-08
ABUW_RS06950	GNAT family N-acetyltransferase	-1.634228589	0.011223725
ABUW_RS15475	hypothetical protein	-1.637192247	0.000117062
ABUW_RS17930	dihydrodipicolinate synthase family protein	-1.63884451	0.000647618
ABUW_RS12555	ABC transporter ATP-binding protein	-1.639180361	8.03E-08
ABUW_RS17925	aldolase	-1.640019648	0.007077656
ABUW_RS10145	dienelactone hydrolase family protein	-1.641342101	1.09E-05
ABUW_RS09065	aromatic-ring-hydroxylating dioxygenase subunit beta	-1.643266161	0.000290527
ABUW_RS16440	phosphatase PAP2 family protein	-1.644484579	7.99E-05
ABUW_RS13155	benzoate 1,2-dioxygenase small subunit	-1.644684462	3.85E-06
ABUW_RS18710	ferredoxin reductase	-1.644795221	1.83E-05
ABUW_RS01660	MFS transporter	-1.646644398	0.003457873
ABUW_RS18355	non-ribosomal peptide synthetase	-1.647701984	2.44E-08
ABUW_RS07900	ethanolamine ammonia-lyase subunit EutB	-1.647871322	0.000569204
ABUW_RS13500	AMP-binding protein	-1.655423731	0.002424305

ABUW_RS09500	TolC family protein	-1.657634663	0.000114163
ABUW_RS09765	hypothetical protein	-1.658069528	0.019003782
ABUW_RS15570	substrate-binding domain-containing protein	-1.659918368	0.006075247
ABUW_RS07370	DUF1365 domain-containing protein	-1.663321676	8.35E-06
ABUW_RS06515	multidrug efflux RND transporter permease subunit AdeG	-1.664318492	4.30E-08
ABUW_RS14270	hypothetical protein	-1.672782278	2.31E-06
ABUW_RS12590	urea carboxylase	-1.67921001	2.68E-07
ABUW_RS05725	ferric acinetobactin ABC transporter permease subunit BauD	-1.681204163	0.098557768
ABUW_RS06310	minor capsid protein	-1.68413161	5.22E-07
ABUW_RS13080	LexA family transcriptional regulator	-1.684276453	3.44E-09
ABUW_RS12150	LLM class flavin-dependent oxidoreductase	-1.685963626	2.17E-07
ABUW_RS19235	hypothetical protein	-1.689477541	0.001366789
ABUW_RS09415	aldehyde dehydrogenase (NADP(+))	-1.692243341	0.002533499
ABUW_RS13485	3-(3-hydroxy-phenyl)propionate transporter MhpT	-1.695201297	3.74E-09
ABUW_RS12375	(2Fe-2S)-binding protein	-1.695480725	1.88E-05
ABUW_RS09060	aromatic ring-hydroxylating dioxygenase subunit alpha	-1.698732183	5.47E-06
ABUW_RS09575	alpha/beta fold hydrolase	-1.699195803	0.000860462
ABUW_RS09240	SDR family oxidoreductase	-1.700696028	0.000663488
ABUW_RS13490	p-hydroxycinnamoyl CoA hydratase/lyase	-1.70076008	6.76E-05
ABUW_RS11685	malonate decarboxylase subunit alpha	-1.701506051	3.63E-05
ABUW_RS09030	MFS transporter	-1.702227174	0.000849597
ABUW_RS12135	hypothetical protein	-1.708154135	1.04E-05
ABUW_RS14280	aldehyde dehydrogenase	-1.714304747	5.70E-07
ABUW_RS14530	hypothetical protein	-1.715909368	0.010477396
ABUW_RS11360	SfnB family sulfur acquisition oxidoreductase	-1.716960853	2.62E-08
ABUW_RS18760	sulfonate ABC transporter substrate-binding protein	-1.719578573	1.97E-05
ABUW_RS06265	hypothetical protein	-1.727642685	0.00984931
ABUW_RS12075	2-aminoethylphosphonate--pyruvate transaminase	-1.730193379	3.42E-07
ABUW_RS06755	IS256-like element ISAba26 family transposase	-1.734396436	5.60E-28
ABUW_RS18560	transcriptional regulator LldR	-1.735931175	0.018149458
ABUW_RS03790	hypothetical protein	-1.736168702	2.22E-06
ABUW_RS13510	OprD family porin	-1.738081514	0.035591187
ABUW_RS08945	protocatechuate 3,4-dioxygenase subunit beta	-1.738438767	6.23E-07
ABUW_RS11935	methylcrotonoyl-CoA carboxylase	-1.738529442	0.041290872
ABUW_RS06325	hypothetical protein	-1.739648373	0.047831734
ABUW_RS02650	hypothetical protein	-1.743525729	1.82E-07
ABUW_RS13465	aromatic ring-hydroxylating dioxygenase subunit alpha	-1.743993658	2.08E-06
ABUW_RS09170	GguC protein	-1.745869695	6.76E-07
ABUW_RS13505	acyl-CoA dehydrogenase family protein	-1.748577645	0.004835951
ABUW_RS12090	ATP-binding cassette domain-containing protein	-1.753006264	0.000373431
ABUW_RS13515	DUF3237 domain-containing protein	-1.758233794	0.002667136
ABUW_RS15460	ribonucleoside-diphosphate reductase subunit alpha	-1.759286214	1.31E-05
ABUW_RS10115	anthranilate 1,2-dioxygenase electron transfer component AntC	-1.760344266	3.41E-05
ABUW_RS08915	CoA transferase subunit B	-1.760659812	8.00E-05
ABUW_RS18765	sulfonate ABC transporter substrate-binding protein	-1.76109694	2.41E-07
ABUW_RS14305	MFS transporter	-1.763238644	1.63E-08
ABUW_RS14295	alpha/beta hydrolase	-1.76542044	9.34E-06
ABUW_RS14290	SDR family oxidoreductase	-1.766153733	4.48E-09
ABUW_RS14215	transketolase	-1.766510733	0.001452105
ABUW_RS13520	PaaI family thioesterase	-1.769148976	0.007927221
ABUW_RS18960	aromatic ring-hydroxylating dioxygenase subunit alpha	-1.769566735	1.55E-12
ABUW_RS13525	tannase/feruloyl esterase family alpha/beta hydrolase	-1.769586734	0.000489592
ABUW_RS18780	ATP-binding cassette domain-containing protein	-1.77316564	5.64E-10
ABUW_RS07365	FAD-dependent oxidoreductase	-1.775595905	1.36E-05
ABUW_RS13390	SDR family NAD(P)-dependent oxidoreductase	-1.778274633	5.34E-07
ABUW_RS13550	MFS transporter	-1.779483533	1.06E-06
ABUW_RS10110	anthranilate 1,2-dioxygenase small subunit	-1.779574852	0.000444598
ABUW_RS13150	benzoate 1,2-dioxygenase large subunit	-1.780400677	1.21E-09
ABUW_RS18565	L-lactate permease	-1.784694296	0.036884165
ABUW_RS12600	DUF1989 domain-containing protein	-1.78924876	1.17E-05
ABUW_RS09865	hypothetical protein	-1.789812513	0.011422775
ABUW_RS12570	transcriptional regulator	-1.792224862	0.000131959
ABUW_RS19225	hypothetical protein	-1.792393192	0.002404932
ABUW_RS06380	hypothetical protein	-1.792661093	1.52E-05
ABUW_RS15580	FAD-dependent tricarballylate dehydrogenase TcuA	-1.801922039	0.162864812
ABUW_RS10120	AraC family transcriptional regulator	-1.802636645	0.003457873
ABUW_RS11995	3-oxoacid CoA-transferase subunit A	-1.80833647	3.64E-06
ABUW_RS03785	hypothetical protein	-1.808576184	5.76E-07
ABUW_RS12305	phenylacetate-CoA oxygenase/reductase subunit PaaK	-1.811387619	0.001466248
ABUW_RS12950	DUF1073 domain-containing protein	-1.816114669	4.37E-06
ABUW_RS14435	malate dehydrogenase (quinone)	-1.818976505	4.32E-06
ABUW_RS10190	short-chain fatty acid transporter	-1.823321848	0.014373925
ABUW_RS08920	3-oxoadipyl-CoA thiolase	-1.826142558	1.83E-05
ABUW_RS09245	acetoacetate decarboxylase family protein	-1.827013493	1.17E-05
ABUW_RS19355	hypothetical protein	-1.827170146	0.004993455
ABUW_RS06300	phage terminase large subunit	-1.827890684	7.76E-07
ABUW_RS14525	OprD family outer membrane porin	-1.828227527	6.94E-07
ABUW_RS12565	allophanate hydrolase	-1.83004569	1.19E-06
ABUW_RS11840	stress-induced protein	-1.832210274	0.028832474
ABUW_RS09175	aldehyde dehydrogenase (NADP(+))	-1.833103599	1.35E-05
ABUW_RS19255	GNAT family N-acetyltransferase	-1.834681799	0.071787618
ABUW_RS14320	SDR family oxidoreductase	-1.835524999	2.57E-06
ABUW_RS19345	molecular chaperone DnaJ	-1.842416446	0.031953197
ABUW_RS20245	hypothetical protein	-1.842999631	0.000398804
ABUW_RS09055	nuclear transport factor 2 family protein	-1.843153445	1.78E-06
ABUW_RS11680	triphosphoribosyl-dephospho-CoA synthase	-1.843763873	2.96E-06
ABUW_RS06455	hypothetical protein	-1.843975815	8.35E-09
ABUW_RS15595	MFS transporter	-1.84670677	6.41E-06
ABUW_RS11675	malonate decarboxylase subunit delta	-1.848886013	0.005132263
ABUW_RS07690	AMP-binding protein	-1.849676555	0.004317043
ABUW_RS14285	aspartate dehydrogenase	-1.85788143	1.69E-06
ABUW_RS14520	MFS transporter	-1.859935277	2.31E-06
ABUW_RS18770	FMNH2-dependent alkanesulfonate monooxygenase	-1.869257118	5.98E-08
ABUW_RS18410	AMP-binding protein	-1.869634889	0.033725935
ABUW_RS14300	cupin domain-containing protein	-1.870704214	5.22E-07
ABUW_RS12080	TIGR03364 family FAD-dependent oxidoreductase	-1.872002497	2.45E-06
ABUW_RS19340	hypothetical protein	-1.873429724	0.057127943
ABUW_RS19130	SAM-dependent DNA methyltransferase	-1.875050964	0.032232888
ABUW_RS11920	AMP-binding protein	-1.875561555	0.009839843
ABUW_RS09945	replication initiation factor domain-containing protein	-1.876426502	5.16E-06

ABUW_RS10130	flavin reductase family protein	-1.87816472	4.85E-05
ABUW_RS00360	zinc metallochaperone GTPase ZigA	-1.88126372	3.41E-08
ABUW_RS06345	hypothetical protein	-1.881868256	8.78E-06
ABUW_RS14330	hypothetical protein	-1.888291536	2.42E-06
ABUW_RS03760	DUF968 domain-containing protein	-1.888434372	0.000826214
ABUW_RS09950	hypothetical protein	-1.892013473	0.006602587
ABUW_RS12930	DUF2213 domain-containing protein	-1.892815387	6.79E-06
ABUW_RS12925	hypothetical protein	-1.894702836	0.000135591
ABUW_RS20440	hypothetical protein	-1.901691311	0.000168633
ABUW_RS19350	hypothetical protein	-1.907408475	4.23E-05
ABUW_RS13495	aldehyde dehydrogenase	-1.913385358	1.49E-05
ABUW_RS06930	hypothetical protein	-1.916236043	1.16E-06
ABUW_RS03955	hypothetical protein	-1.92425691	2.21E-08
ABUW_RS06925	hypothetical protein	-1.93020634	0.000809017
ABUW_RS20015	Mu transposase C-terminal domain-containing protein	-1.947362066	NA
ABUW_RS10140	SDR family oxidoreductase	-1.955943518	3.18E-05
ABUW_RS02660	3'-5' exonuclease	-1.957602493	8.85E-13
ABUW_RS11930	isovaleryl-CoA dehydrogenase	-1.961744679	0.02135762
ABUW_RS09675	hypothetical protein	-1.962141145	0.013050895
ABUW_RS02675	hypothetical protein	-1.964548118	4.07E-10
ABUW_RS11825	LysE family translocator	-1.965516059	0.004029676
ABUW_RS01810	putative DNA modification/repair radical SAM protein	-1.968331911	2.30E-08
ABUW_RS06935	hypothetical protein	-1.968795081	1.13E-05
ABUW_RS03945	DUF1833 family protein	-1.968886945	0.000501974
ABUW_RS02665	single-stranded DNA-binding protein	-1.970538011	2.37E-13
ABUW_RS11915	class I SAM-dependent methyltransferase	-1.974829891	0.002759195
ABUW_RS09040	amidase	-1.979446044	0.000589152
ABUW_RS09895	replication initiation factor domain-containing protein	-1.986063198	1.19E-06
ABUW_RS18420	CoA-acylating methylmalonate-semialdehyde dehydrogenase	-1.989131793	0.042182251
ABUW_RS19310	CmlA family chloramphenicol efflux MFS transporter	-1.994687881	0.000289324
ABUW_RS14220	MFS transporter	-2.003004875	0.000364947
ABUW_RS20420	hypothetical protein	-2.003445532	2.31E-08
ABUW_RS06940	hypothetical protein	-2.004123042	0.000123915
ABUW_RS02680	hypothetical protein	-2.005229627	2.37E-08
ABUW_RS12330	phenylacetic acid degradation bifunctional protein PaaZ	-2.006571396	0.000389465
ABUW_RS03775	hypothetical protein	-2.017022184	8.41E-06
ABUW_RS07600	poly-beta-1,6 N-acetyl-D-glucosamine exporter porin PgaA	-2.030619132	1.85E-06
ABUW_RS03930	hypothetical protein	-2.031690845	0.007850821
ABUW_RS12955	phage terminase large subunit	-2.034184985	1.97E-05
ABUW_RS10105	anthranilate 1,2-dioxygenase large subunit	-2.040611051	0.00257752
ABUW_RS03840	hypothetical protein	-2.052430157	9.75E-08
ABUW_RS03875	hypothetical protein	-2.056045146	3.70E-08
ABUW_RS18900	matrixin family metalloprotease	-2.058567294	5.67E-05
ABUW_RS09900	hypothetical protein	-2.060273752	0.001745464
ABUW_RS06910	hypothetical protein	-2.066001334	3.95E-05
ABUW_RS13460	MFS transporter	-2.082301654	0.001395399
ABUW_RS12755	TetR/AcrR family transcriptional regulator	-2.098366325	0.000449971
ABUW_RS19360	hypothetical protein	-2.10094835	0.000836419
ABUW_RS03765	hypothetical protein	-2.103646102	0.001139536
ABUW_RS03830	hypothetical protein	-2.105072778	5.59E-09
ABUW_RS03825	hypothetical protein	-2.105661982	9.25E-06
ABUW_RS03835	hypothetical protein	-2.110452152	1.93E-06
ABUW_RS02670	hypothetical protein	-2.115775441	2.40E-15
ABUW_RS09050	hypothetical protein	-2.119879793	2.03E-07
ABUW_RS14425	betaine-aldehyde dehydrogenase	-2.138458746	1.98E-05
ABUW_RS18415	3-hydroxyisobutyrate dehydrogenase	-2.143523046	0.031723618
ABUW_RS03845	hypothetical protein	-2.144816496	2.89E-08
ABUW_RS03800	terminase family protein	-2.145755886	1.90E-12
ABUW_RS13065	N-acetylmuramidase	-2.155033476	2.40E-11
ABUW_RS20525	hypothetical protein	-2.155138988	0.000133502
ABUW_RS11835	hypothetical protein	-2.155582729	9.94E-06
ABUW_RS12325	1,2-phenylacetyl-CoA epoxidase subunit A	-2.157923791	0.000836419
ABUW_RS06390	hypothetical protein	-2.159128118	0.005874658
ABUW_RS14325	aromatic ring-hydroxylating dioxygenase subunit alpha	-2.165669594	1.48E-09
ABUW_RS20105	hypothetical protein	-2.167474924	3.50E-05
ABUW_RS11830	translesion error-prone DNA polymerase V autoproteolytic subunit	-2.167876907	2.39E-13
ABUW_RS06340	stress-responsive nuclear envelope protein	-2.186184203	0.000265363
ABUW_RS09045	acyl-CoA dehydrogenase family protein	-2.186831712	0.000860462
ABUW_RS09570	SDR family NAD(P)-dependent oxidoreductase	-2.194292375	2.07E-05
ABUW_RS06915	hypothetical protein	-2.204654677	0.000783049
ABUW_RS10135	hypothetical protein	-2.206971283	1.32E-06
ABUW_RS12320	1,2-phenylacetyl-CoA epoxidase subunit B	-2.215366216	0.000101562
ABUW_RS20030	class 1 integron integrase IntI1	-2.223611982	1.13E-05
ABUW_RS03815	hypothetical protein	-2.252059467	5.50E-09
ABUW_RS19125	hypothetical protein	-2.258912459	3.15E-06
ABUW_RS03820	hypothetical protein	-2.264286534	1.05E-06
ABUW_RS12595	DUF1989 domain-containing protein	-2.264401302	8.19E-07
ABUW_RS12315	phenylacetate-CoA oxygenase subunit PaaC	-2.275380742	1.95E-05
ABUW_RS09985	DUF4882 family protein	-2.277537327	2.08E-10
ABUW_RS20020	TniB family NTP-binding protein	-2.310693388	0.058258152
ABUW_RS14430	choline dehydrogenase	-2.313920049	3.69E-13
ABUW_RS06920	head-tail connector protein	-2.323001386	4.64E-09
ABUW_RS09980	type 1 fimbrial protein	-2.333008214	1.17E-10
ABUW_RS03940	hypothetical protein	-2.337728505	0.000700337
ABUW_RS06330	hypothetical protein	-2.367117868	3.41E-05
ABUW_RS03810	minor capsid protein	-2.377998138	2.14E-13
ABUW_RS03795	DUF2280 domain-containing protein	-2.38478945	1.20E-08
ABUW_RS06335	hypothetical protein	-2.396930455	2.52E-08
ABUW_RS12310	phenylacetate-CoA oxygenase subunit PaaJ	-2.400944717	8.99E-05
ABUW_RS03755	tRNA-Arg	-2.406066857	0.008053493
sRNA4	no	-2.436801759	0.1054706
ABUW_RS06385	hypothetical protein	-2.460591503	2.53E-05
ABUW_RS09975	fimbrial biogenesis outer membrane usher protein	-2.478165012	1.24E-09
ABUW_RS06110	hypothetical protein	-2.493064457	1.60E-11
ABUW_RS02685	toprim domain-containing protein	-2.49323563	9.61E-13
ABUW_RS13070	hypothetical protein	-2.495092747	1.06E-11
ABUW_RS19305	ANT(3")-Ia family aminoglycoside nucleotidyltransferase AadA2	-2.538201787	1.33E-06
ABUW_RS03745	hypothetical protein	-2.538529155	1.25E-18
ABUW_RS03805	DUF4055 domain-containing protein	-2.542297919	1.42E-14
ABUW_RS03880	hypothetical protein	-2.561101926	2.77E-07

ABUW_RS02690	hypothetical protein	-2.57398624	3.60E-05
ABUW_RS08275	Y-family DNA polymerase	-2.578348887	2.44E-12
ABUW_RS03625	hypothetical protein	-2.588390507	1.13E-11
ABUW_RS09970	molecular chaperone	-2.597873807	0.000741955
ABUW_RS19295	APH(6)-I family aminoglycoside O-phosphotransferase	-2.619136163	3.85E-06
ABUW_RS06895	hypothetical protein	-2.622985534	4.83E-10
ABUW_RS03885	hypothetical protein	-2.64928406	8.35E-09
ABUW_RS19300	aminoglycoside O-phosphotransferase APH(3")-Ib	-2.651680225	1.72E-06
ABUW_RS03610	AlpA family phage regulatory protein	-2.764459448	1.04E-16
ABUW_RS06905	hypothetical protein	-2.787350741	3.91E-14
ABUW_RS03750	hypothetical protein	-2.789999922	2.31E-22
ABUW_RS06900	hypothetical protein	-2.794423342	1.78E-13
ABUW_RS06120	hypothetical protein	-2.796875729	1.06E-07
ABUW_RS16890	glutathione S-transferase family protein	-2.826280239	5.42E-11
ABUW_RS03630	hypothetical protein	-2.875175075	2.15E-13
ABUW_RS06245	DUF559 domain-containing protein	-2.890723999	3.69E-13
ABUW_RS06880	hypothetical protein	-2.987213195	2.02E-12
ABUW_RS03720	hypothetical protein	-2.99614922	8.46E-10
ABUW_RS06235	hypothetical protein	-2.998598314	6.41E-11
ABUW_RS03715	hypothetical protein	-3.046334655	1.80E-10
ABUW_RS06780	hypothetical protein	-3.05372336	1.80E-11
ABUW_RS20455	hypothetical protein	-3.055335718	6.07E-17
ABUW_RS06220	hypothetical protein	-3.060850798	1.35E-10
ABUW_RS06875	hypothetical protein	-3.07571657	2.37E-12
ABUW_RS03735	VRR-NUC domain-containing protein	-3.085923725	4.09E-19
ABUW_RS03620	hypothetical protein	-3.097636696	7.01E-19
sRNA73	no	-3.10712768	5.43E-08
ABUW_RS06115	hypothetical protein	-3.121855438	7.14E-10
ABUW_RS19690	hypothetical protein	-3.148138651	7.65E-17
ABUW_RS06835	hypothetical protein	-3.149385312	4.70E-20
ABUW_RS06855	hypothetical protein	-3.155817479	1.63E-26
ABUW_RS09965	type 1 fimbrial protein	-3.159304415	1.48E-05
ABUW_RS06230	hypothetical protein	-3.219660085	5.88E-34
ABUW_RS06760	hypothetical protein	-3.226584561	1.50E-18
ABUW_RS06890	hypothetical protein	-3.235659226	7.51E-27
ABUW_RS06885	hypothetical protein	-3.25127776	3.92E-21
ABUW_RS06215	hypothetical protein	-3.264779419	1.92E-20
ABUW_RS03615	hypothetical protein	-3.266019954	2.40E-19
ABUW_RS06840	ribbon-helix-helix protein, CopG family	-3.280261503	2.20E-19
ABUW_RS06240	hypothetical protein	-3.289883861	4.21E-16
ABUW_RS03710	hypothetical protein	-3.300339115	1.30E-15
ABUW_RS06225	hypothetical protein	-3.32929932	8.80E-32
ABUW_RS06845	hypothetical protein	-3.333273834	2.85E-20
ABUW_RS20435	hypothetical protein	-3.336206165	1.30E-13
ABUW_RS03665	hypothetical protein	-3.368289544	1.45E-11
ABUW_RS06190	hypothetical protein	-3.372251364	1.15E-17
ABUW_RS03740	metallophosphoesterase	-3.382240805	9.40E-42
ABUW_RS06765	hypothetical protein	-3.383062236	1.33E-18
ABUW_RS03730	hypothetical protein	-3.384210631	7.28E-22
ABUW_RS03725	hypothetical protein	-3.39174765	4.13E-18
ABUW_RS06860	hypothetical protein	-3.408097665	1.07E-23
ABUW_RS06195	hypothetical protein	-3.410719719	7.99E-16
ABUW_RS03695	AAA family ATPase	-3.453266123	2.08E-19
ABUW_RS06130	hypothetical protein	-3.458191923	2.14E-13
ABUW_RS06770	hypothetical protein	-3.459736875	3.85E-22
ABUW_RS06135	hypothetical protein	-3.459961184	4.78E-11
ABUW_RS03705	hypothetical protein	-3.46246535	5.34E-19
ABUW_RS03660	hypothetical protein	-3.487992382	2.33E-13
ABUW_RS06125	hypothetical protein	-3.512035143	1.06E-14
ABUW_RS06205	AAA family ATPase	-3.521557075	7.01E-19
ABUW_RS03685	hypothetical protein	-3.546549693	8.66E-19
ABUW_RS06775	hypothetical protein	-3.557498307	1.85E-18
ABUW_RS06795	hypothetical protein	-3.587651488	4.13E-18
ABUW_RS03635	hypothetical protein	-3.626665314	7.09E-25
ABUW_RS03655	hypothetical protein	-3.630446961	3.21E-16
ABUW_RS06850	hypothetical protein	-3.639898448	2.13E-22
ABUW_RS06820	hypothetical protein	-3.640819357	3.11E-10
ABUW_RS06200	replication protein	-3.661310661	3.71E-16
ABUW_RS06815	hypothetical protein	-3.719782543	1.21E-12
ABUW_RS03650	hypothetical protein	-3.72082905	5.86E-18
ABUW_RS06160	hypothetical protein	-3.732924292	9.74E-12
ABUW_RS20430	hypothetical protein	-3.741196717	6.91E-13
ABUW_RS06785	YqaJ viral recombinase family protein	-3.787480693	4.11E-19
ABUW_RS06140	hypothetical protein	-3.80952663	5.28E-19
ABUW_RS06870	hypothetical protein	-3.810253065	4.73E-38
ABUW_RS20450	hypothetical protein	-3.814346759	2.39E-14
ABUW_RS03690	GntR family transcriptional regulator	-3.81825851	1.64E-26
ABUW_RS03640	hypothetical protein	-3.837116636	2.32E-24
ABUW_RS06790	phage recombination protein Bet	-3.842778994	3.60E-23
ABUW_RS06865	hypothetical protein	-3.843512598	1.68E-34
ABUW_RS06155	hypothetical protein	-3.867433971	3.66E-12
ABUW_RS06810	hypothetical protein	-3.925664354	4.15E-18
ABUW_RS06805	hypothetical protein	-3.928559182	1.99E-20
ABUW_RS06150	hypothetical protein	-3.962823749	1.15E-18
ABUW_RS06800	hypothetical protein	-3.989052562	3.92E-21
ABUW_RS06145	PD-(D/E)XK nuclease-like domain-containing protein	-4.116960796	5.50E-18

Upregulated			
Gene	Product	log2FoldChange	Adjusted p-value
sRNA21	no	7.613986763	1.16E-28
ABUW_RS01495	pilin	4.91302525	2.67E-06
ABUW_RS20125	hypothetical protein	4.045843851	1.92E-20
ABUW_RS09960	hypothetical protein	3.86133612	2.89E-12
ABUW_RS00890	response regulator transcription factor	3.004075274	2.27E-17
ABUW_RS07305	TetR/AcrR family transcriptional regulator	2.724021469	0.005140569
ABUW_RS05570	EAL domain-containing protein	2.577214655	7.77E-08
sRNA19	no	2.466401273	0.003524913
ABUW_RS03350	methyl-accepting chemotaxis protein	2.457380584	0.003736154
ABUW_RS11240	fimbria/pilus periplasmic chaperone	2.421811643	4.56E-07
ABUW_RS17440	outer membrane beta-barrel protein	2.196720138	0.142129751
ABUW_RS03345	purine-binding chemotaxis protein CheW	2.191999953	0.015098395
ABUW_RS06430	hypothetical protein	2.187953013	6.92E-11
ABUW_RS07890	glutamine amidotransferase	2.108661139	3.89E-08
ABUW_RS03355	Hpt domain-containing protein	2.069385238	0.007765701
ABUW_RS02500	tRNA-Ile	2.040853303	0.002246105
ABUW_RS02505	tRNA-Ala	2.031515105	0.002988164
ABUW_RS00080	tRNA-Ile	2.009613069	0.003530158
ABUW_RS14950	tRNA-Met	2.006034047	0.002884378
ABUW_RS00085	tRNA-Ala	1.997810828	0.0041722
ABUW_RS02335	tRNA-Ile	1.997428667	0.002759195
ABUW_RS18845	tRNA-Ile	1.970121249	0.003535308
ABUW_RS18840	tRNA-Ala	1.962998199	0.004527734
ABUW_RS02340	tRNA-Ala	1.961290137	0.003648892
ABUW_RS06435	hypothetical protein	1.952252437	5.21E-07
ABUW_RS18075	tRNA-Ile	1.944435988	0.003932258
ABUW_RS08735	cytochrome d ubiquinol oxidase subunit II	1.943315167	0.014712139
sRNA14	no	1.940327114	0.003096182
ABUW_RS03360	hypothetical protein	1.935099545	0.004143152
ABUW_RS12420	epoxyqueuosine reductase QueH	1.923115602	2.63E-08
ABUW_RS01440	pilus assembly protein PilP	1.922260761	0.039104003
ABUW_RS14905	tRNA-Met	1.920581039	0.003086915
ABUW_RS06425	hypothetical protein	1.914059036	1.91E-08
ABUW_RS01430	PilN domain-containing protein	1.895497045	0.047664133
ABUW_RS14740	bacteriohemerythrin	1.893115359	0.175921238
ABUW_RS15815	tRNA-Ile	1.879705034	0.005899268
ABUW_RS18070	tRNA-Ala	1.877456897	0.006810549
ABUW_RS01435	type 4a pilus biogenesis protein PilO	1.872899487	0.063982278
ABUW_RS12415	hypothetical protein	1.872669464	0.005842813
ABUW_RS05525	hypothetical protein	1.869098778	0.020743834
ABUW_RS15810	tRNA-Ala	1.867183618	0.007320553
ABUW_RS07415	aspartate/glutamate racemase family protein	1.845896562	2.79E-10
ABUW_RS08605	hypothetical protein	1.842389214	7.88E-05
ABUW_RS06555	YfhL family 4Fe-4S dicluster ferredoxin	1.838924535	0.005282477
sRNA48	no	1.808761511	0.000411294
ABUW_RS08400	hypothetical protein	1.806966118	6.58E-07
ABUW_RS08730	cytochrome bd-I oxidase subunit CydX	1.783120206	0.015283092
sRNA40	no	1.777949151	0.389747623
ABUW_RS05825	DUF4105 domain-containing protein	1.751070835	0.004600693
ABUW_RS11310	1-acyl-sn-glycerol-3-phosphate acyltransferase	1.743922204	0.0233352
ABUW_RS08740	cytochrome ubiquinol oxidase subunit I	1.713973135	0.019660253
ABUW_RS10010	hypothetical protein	1.709816349	0.030426812
ABUW_RS13815	hypothetical protein	1.708481048	0.000312201
ABUW_RS03340	response regulator	1.70385647	0.018504588
ABUW_RS14715	PilT/PilU family type 4a pilus ATPase	1.691578995	0.013020322
ABUW_RS08725	cyd operon YbgE family protein	1.681651841	0.018600686
ABUW_RS13055	cold-shock protein	1.675811967	0.024240735
ABUW_RS03335	twitching motility response regulator PilG	1.6701084	0.025381949
ABUW_RS08270	type II 3-dehydroquinate dehydratase	1.66684109	0.000363096
ABUW_RS01445	type IV pilus secretin PilQ family protein	1.651454777	0.035881008
sRNA58	no	1.644497674	0.027491674
ABUW_RS08745	hypothetical protein	1.628539681	0.025062662
ABUW_RS16280	hypothetical protein	1.624818492	9.52E-05
ABUW_RS16790	hypothetical protein	1.611587066	0.078834024
ABUW_RS12255	ATP-dependent helicase	1.609568612	2.30E-05
ABUW_RS18295	DedA family protein	1.595450846	4.13E-10
ABUW_RS11135	tRNA (uridine(54)-C5)-methyltransferase TrmA	1.534613462	0.000550688
ABUW_RS02165	hypothetical protein	1.531026106	0.000160154
ABUW_RS02200	HAD-IB family hydrolase	1.520752501	0.015325884
ABUW_RS09350	DUF2314 domain-containing protein	1.49701234	0.003524913
ABUW_RS16210	hypothetical protein	1.496709459	0.00033514
ABUW_RS05915	hypothetical protein	1.490294974	0.010933897
ABUW_RS05395	HTH-type transcriptional repressor FabR	1.478380939	3.05E-05
ABUW_RS05795	acinetobactin biosynthesis phosphopantetheinyl transferase BasI	1.469953116	0.001047889
ABUW_RS09695	hypothetical protein	1.42920838	0.000221016
ABUW_RS02930	hypothetical protein	1.423527462	0.00027349
ABUW_RS12260	AAA family ATPase	1.423519866	0.000389269
ABUW_RS17275	type II secretion system F family protein	1.388464183	0.074708746
ABUW_RS06720	cold-shock protein	1.381782382	0.156289152
ABUW_RS03380	entericidin A/B family lipoprotein	1.377964196	0.031240017
ABUW_RS13825	alpha/beta hydrolase	1.375493048	1.99E-06
ABUW_RS09625	TetR/AcrR family transcriptional regulator	1.366612972	0.000132413
ABUW_RS08495	3-hydroxyacyl-ACP dehydratase FabZ	1.365754237	0.001810879
ABUW_RS14190	hypothetical protein	1.351073601	0.004600693
ABUW_RS06560	tRNA 5-hydroxyuridine modification protein YegQ	1.347528618	0.130182125
ABUW_RS03330	hypothetical protein	1.345054313	0.023117279
ABUW_RS18580	glucose-6-phosphate isomerase	1.338007588	0.000729391
ABUW_RS10430	HRDC domain-containing protein	1.33735349	8.19E-07
ABUW_RS17800	P-II family nitrogen regulator	1.336845008	0.021607238
ABUW_RS06735	nitroreductase	1.335181351	4.47E-08
ABUW_RS14080	esterase	1.327309264	0.089613456
ABUW_RS19420	APH(3')-VI family aminoglycoside O-phosphotransferase	1.3240863	4.35E-07
ABUW_RS02220	YcxB family protein	1.322139086	0.007471241
ABUW_RS00595	DUF1311 domain-containing protein	1.319807432	0.194944947
ABUW_RS10545	3-deoxy-7-phosphoheptulonate synthase	1.318206937	3.85E-06
ABUW_RS05790	acinetobactin biosynthesis thioesterase BasH	1.316675824	0.009890154

ABUW_RS02525	hypothetical protein	1.315011456	0.085373363
ABUW_RS07935	5-carboxymethyl-2-hydroxymuconate Delta-isomerase	1.313072283	2.39E-05
ABUW_RS02170	YheV family putative metal-binding protein	1.308924388	0.000556551
ABUW_RS10750	hypothetical protein	1.305722277	0.000138795
ABUW_RS10940	type II secretion system minor pseudopilin GspJ	1.305038607	8.06E-10
ABUW_RS18650	polysaccharide biosynthesis/export family protein	1.303262366	0.010020621
ABUW_RS05400	ferredoxin reductase	1.299705242	0.088414727
ABUW_RS05405	acyl-CoA desaturase	1.294394217	0.076008366
ABUW_RS06070	septal ring lytic transglycosylase RlpA family protein	1.291085989	0.025757624
ABUW_RS20145	hypothetical protein	1.290615527	0.087469111
ABUW_RS10970	DNA polymerase III subunit delta'	1.290441965	7.33E-06
ABUW_RS05255	D-alanyl-D-alanine carboxypeptidase PBP6B	1.288360939	0.004119203
ABUW_RS08490	UDP-3-O-(3-hydroxymyristoyl)glucosamine N-acyltransferase	1.28380046	0.000194218
ABUW_RS11440	succinyldiaminopimelate transaminase	1.28315348	0.010495501
ABUW_RS20505	hypothetical protein	1.276235786	0.011456113
ABUW_RS02935	hypothetical protein	1.271744022	0.000983218
ABUW_RS18655	low molecular weight phosphotyrosine protein phosphatase	1.267819504	0.017441836
ABUW_RS08500	acyl-ACP--UDP-N-acetylglucosamine O-acyltransferase	1.264884651	0.003653646
ABUW_RS17730	sigma-54-dependent Fis family transcriptional regulator	1.25992993	0.064232659
ABUW_RS05920	DUF2726 domain-containing protein	1.251218263	0.081453429
ABUW_RS07835	type II toxin-antitoxin system RelB/DinJ family antitoxin	1.241098434	0.071283698
ABUW_RS12700	hypothetical protein	1.239270849	3.91E-05
ABUW_RS05575	hypothetical protein	1.238518979	0.000521898
ABUW_RS10220	aspartate ammonia-lyase	1.23410853	0.127113056
ABUW_RS18645	Vi polysaccharide biosynthesis UDP-N-acetylglucosamine C-6 dehydrogenase TviB	1.233271226	4.32E-07
ABUW_RS06745	histidine phosphatase family protein	1.230960554	0.006469376
ABUW_RS05390	AI-2E family transporter	1.230286048	1.84E-06
ABUW_RS10995	MotA/TolQ/ExbB proton channel family protein	1.223302754	0.000121285
ABUW_RS00660	HPF/RaiA family ribosome-associated protein	1.218232797	0.074432726
ABUW_RS10755	Dyp-type peroxidase	1.216334472	8.37E-06
ABUW_RS11235	type 1 fimbrial protein	1.21593055	0.046853795
ABUW_RS11410	hypothetical protein	1.213264192	0.000124043
ABUW_RS05780	acinetobactin export ABC transporter permease/ATP-binding subunit BarA	1.213024274	0.043503242
ABUW_RS16720	hypothetical protein	1.209517589	0.020524204
ABUW_RS04855	class 1 fructose-bisphosphatase	1.204992198	0.03677524
ABUW_RS09345	hypothetical protein	1.2028186	0.010324564
ABUW_RS14790	septum site-determining protein MinC	1.199594779	4.61E-08
ABUW_RS02580	septation protein IspZ	1.197220167	0.018443451
ABUW_RS18585	UDP-glucose/GDP-mannose dehydrogenase family protein	1.196817743	0.002122513
ABUW_RS09700	hypothetical protein	1.195553004	0.072429764
ABUW_RS14535	hypothetical protein	1.194888898	0.001662816
ABUW_RS15255	dCTP deaminase	1.186249781	2.30E-05
ABUW_RS06740	NAD(P)H-dependent glycerol-3-phosphate dehydrogenase	1.185322686	6.09E-06
ABUW_RS07775	hypothetical protein	1.181200079	5.31E-05
ABUW_RS18660	polysaccharide biosynthesis tyrosine autokinase	1.178111412	0.010618544
ABUW_RS08785	TrkA family potassium uptake protein	1.177976938	1.66E-15
ABUW_RS03850	hypothetical protein	1.175421877	0.03923317
sRNA95	no	1.175093745	0.000200263
ABUW_RS04440	tRNA-Leu	1.173858468	0.346799722
ABUW_RS00435	hypothetical protein	1.171187061	0.032849995
ABUW_RS00425	DNA cytosine methyltransferase	1.166218654	0.014957795
ABUW_RS18440	RidA family protein	1.16416516	0.048411319
ABUW_RS06590	Flp pilus assembly complex ATPase component TadA	1.158087169	0.017412559
sRNA43_truncated	no	1.154618434	0.140127344
ABUW_RS10205	LysR family transcriptional regulator	1.153341425	3.23E-05
ABUW_RS18630	oligosaccharide flippase family protein	1.152198445	0.134048952
ABUW_RS13050	hypothetical protein	1.146335972	0.20611294
ABUW_RS15280	hypothetical protein	1.145079702	0.042364547
ABUW_RS06475	DUF4760 domain-containing protein	1.141534559	0.005606451
ABUW_RS14710	type IV pilus twitching motility protein PilT	1.141251689	0.127522565
ABUW_RS13820	NAD(+) diphosphatase	1.140867977	0.000500039
ABUW_RS17270	type IV-A pilus assembly ATPase PilB	1.138099052	0.049181803
ABUW_RS15080	peptidoglycan-binding protein LysM	1.134198794	0.003357509
ABUW_RS10385	50S ribosomal protein L3 N(5)-glutamine methyltransferase	1.133773149	0.107662266
ABUW_RS07960	spore coat protein U domain-containing protein	1.131156663	0.098146414
ABUW_RS04880	protein TolR	1.12678401	0.016531605
ABUW_RS02970	phosphate-starvation-inducible PsiE family protein	1.122997067	0.000168921
ABUW_RS00825	putative porin	1.122895051	0.023185684
ABUW_RS02265	energy transducer TonB	1.121035085	0.057127943
ABUW_RS04235	hypothetical protein	1.114067738	0.001326776
ABUW_RS01425	pilus assembly protein PilM	1.113193758	0.213637013
ABUW_RS10935	type II secretion system minor pseudopilin GspK	1.109561824	2.31E-05
ABUW_RS07535	alanine racemase	1.107706153	0.00039275
ABUW_RS18590	UTP--glucose-1-phosphate uridylyltransferase GalU	1.105473844	0.007818315
ABUW_RS03440	SdpI family protein	1.103417328	0.020591614
ABUW_RS18595	polysaccharide biosynthesis protein	1.103030461	0.013019828
ABUW_RS15900	acetyl-CoA carboxylase carboxyltransferase subunit alpha	1.100530811	1.55E-06
ABUW_RS14110	SPOR domain-containing protein	1.100045795	0.011904054
ABUW_RS06700	sulfur carrier protein ThiS	1.09995138	1.29E-05
ABUW_RS03990	integrase arm-type DNA-binding domain-containing protein	1.094774352	4.80E-05
ABUW_RS15295	LysE family translocator	1.091971308	0.01530165
ABUW_RS00510	phosphatidylserine decarboxylase	1.091514786	0.000596079
ABUW_RS05545	ATP-binding protein	1.089079571	0.045789634
ABUW_RS09995	hypothetical protein	1.085496541	0.000605706
ABUW_RS08505	tetratricopeptide repeat protein	1.084803459	1.89E-05
ABUW_RS02630	hypothetical protein	1.084224233	0.01838713
ABUW_RS15005	outer membrane lipoprotein LolB	1.082290705	0.000676272
ABUW_RS11885	hypothetical protein	1.082236692	0.187747829
ABUW_RS08140	transaldolase	1.080293431	0.0058359
ABUW_RS15065	3,4-dihydroxy-2-butanone-4-phosphate synthase	1.078405021	0.000397028
ABUW_RS12790	ferredoxin family protein	1.07216093	0.003658839
ABUW_RS10990	biopolymer transporter ExbD	1.071604689	0.00120565
ABUW_RS13830	BON domain-containing protein	1.071271247	0.000274187
ABUW_RS16785	hypothetical protein	1.068449048	0.078748048
ABUW_RS01845	shikimate dehydrogenase	1.064318747	0.029891806
ABUW_RS15990	ribosome-associated protein	1.063719011	1.07E-06
ABUW_RS10865	cell division protein ZapE	1.063098712	0.000737297
ABUW_RS10945	type II secretion system minor pseudopilin GspI	1.062301319	0.001002316
ABUW_RS00430	ATP-binding protein	1.060504224	0.009432759
ABUW_RS17415	DsbA family oxidoreductase	1.059093106	0.001406778

ABUW_RS06725	ATP-dependent RNA helicase RhlB	1.055955208	0.003304483
ABUW_RS03585	PaaX family transcriptional regulator	1.055589769	0.039023177
ABUW_RS15210	pantothenate kinase	1.054281287	0.0016317
ABUW_RS11065	TetR/AcrR family transcriptional regulator	1.052256119	0.03081449
ABUW_RS04885	protein TolQ	1.049309055	0.012832941
ABUW_RS10485	YARHG domain-containing protein	1.040961786	0.129341695
ABUW_RS00855	mechanosensitive ion channel family protein	1.038508097	4.56E-05
ABUW_RS02270	rRNA maturation RNase YbeY	1.037821284	0.013043678
ABUW_RS10880	lysine exporter LysO family protein	1.036277809	8.15E-05
ABUW_RS07785	hypothetical protein	1.030841935	0.027331912
ABUW_RS08780	potassium uptake protein (TrkH)	1.03056269	4.65E-10
ABUW_RS08265	acetyl-CoA carboxylase biotin carboxyl carrier protein	1.029729277	0.138699875
ABUW_RS18575	UDP-glucose 4-epimerase GalE	1.026235533	3.10E-05
ABUW_RS17565	type II secretion system protein N	1.024363246	0.016023907
ABUW_RS18670	FKBP-type peptidyl-prolyl cis-trans isomerase	1.022937927	0.001926446
ABUW_RS18620	oligosaccharide repeat unit polymerase	1.021823214	0.23924471
ABUW_RS13895	hypothetical protein	1.021460724	8.13E-08
ABUW_RS03325	efflux RND transporter periplasmic adaptor subunit	1.021020921	0.006075247
ABUW_RS01460	hypothetical protein	1.020310218	4.98E-05
ABUW_RS10625	siderophore achromobactin biosynthesis protein AcsC	1.01985456	0.209998156
ABUW_RS02920	glycosyltransferase family 25 protein	1.019373721	0.070725157
ABUW_RS17280	prepilin peptidase	1.016799407	0.038135218
ABUW_RS09690	zonular occludens toxin	1.014012728	0.000533224
ABUW_RS01450	shikimate kinase AroK	1.013114325	0.014418812
ABUW_RS00415	glutamate racemase	1.007075762	0.094320628
ABUW_RS04595	hypothetical protein	1.006566124	0.179643462
ABUW_RS19055	hypothetical protein	1.002630039	0.001261323